N° d'ordre : 747

THESE

présentée à

L'UNIVERSITE DES SCIENCES ET TECHNIQUES DE LILLE FLANDRES ARTOIS

pour obtenir le grade de

DOCTEUR ES SCIENCES PHYSIQUES

par

Michel FOULON

LES PHASES CRISTALLINES DES ADAMANTANES 1 SUBSTITUES (PLASTIQUES, ORDONNEES, VITREUSES) THERMODYNAMIQUE, STRUCTURES, MOUVEMENTS MOLECULAIRES

Soutenue le 25 Septembre 1987 devant la Commission d'Examen

M. R.	FOURET	Professeur, U.S.T.L.F.A.	Président et Rapporteur
M. H.A.J.	OONK	Professeur, Université UTRECHT (Pays-Bas)	Rapporteur
M. J.P.	AMOUREUX	Maître de conférences, U.S.T.L.F.A.	Rapporteur
M. H.	CAILLEAU	Professeur, Université de RENNES	Examinateur
M. A.	MIERZCEWSKI	Professeur, Université WROCLAW (Pologne)	Examinateur
M. H.	FONTAINE	Professeur, U.S.T.L.F.A.	Examinateur
M. H.	DUBOIS	Professeur, U.S.T.L.F.A.	Examinateur

TOME II

ANNEXES

CHAPITRE VI

ANNEXE A - VI - 1 : Les FONCTIONS de DISTRIBUTIONS

I -- INTRODUCTION [1] , [2] , [3] , [4] , [5]

Les temps de relaxation T_{1Z}, $T_{1\rho}$ en RMN, la permittivité diélectrique ε^* en relaxation diélrctrique et la loi de diffusion neutronique $S(\vec{Q},\omega)$ en IQNS sont des grandeurs physiques observables que nous noterons $M(\tau)$ et qui dépendent du (des) temps de corrélation τ_α caractérisant les mouvements moléculaires. Ceux-ci s'expriment généralement de façon simple en fonction des différents temps de résidence.

Nous ne considèrerons ici qu'un seul temps de corrélation (exemple du modèle de rotation diffusionnelle) dont la valeur peut être distribuée.

L'expérience donne accès à la grandeur M_{exp} qui tient compte de cette distribution. On peut écrire:

$$M_{exp} = \int_0^{\infty} M(\tau) \cdot G(\tau) \, d\tau \quad \text{avec} \int_0^{\infty} G(\tau) \, d\tau = 1 \qquad 1 - a$$

ou encore

$$M_{exp} = \int_{-\infty}^{+\infty} M(z) \, F(z) \, dz \quad \text{avec} \int_{-\infty}^{+\infty} F(z) \, dz = 1 \qquad 1 - b$$

et

$z = \text{Log}(\tau / \tau_m)$ où τ_m est le temps de corrélation pour lequel $F(z)$ est maximale.

Les caractéristiques des fonctions $G(\tau)$ (linéaires) et $F(z)$ (logarithmiques) doivent permettre de rendre compte d'une distribution continue des temps de résidence associés à un mouvement moléculaire.

L'introduction de cette distribution peut être physiquement justifiée en admettant que la dynamique de ce mouvement varie d'une molécule à l'autre parce que leur environnement local est différent.

II -- LES FONCTIONS DE DISTRIBUTION

Nous appellerons FWHM la largeur totale relative à mi hauteur de la distribution et $< \tau >$ le temps de corrélation moyen.

A) Distribution gaussienne(symétrique)

$$G(\tau) = (\alpha \sqrt{2\pi})^{-1} \exp(-(\tau - \tau_m)^2 / 2\alpha^2) \qquad 2$$

$\text{FWHM} = 2.35\alpha / \tau_m$ et $< \tau > = \tau_m$

$\alpha = 0$ pas de distribution

B) Log - gaussienne

$$F(z) = (\alpha' \sqrt{2\pi})^{-1} \exp(-z^2 / 2\alpha'^2) \qquad 3$$

FWHM = $2 \sinh (\alpha' \sqrt{2\mathrm{Log}(2)})$ et $\langle \tau \rangle = \tau_m \exp(\alpha'^2/2)$

$\alpha' = 0$ pas de distribution

C) Distribution de COLE et COLE (symétrique) [3]

$$F(z) = \frac{1}{2\pi} \frac{\sin \pi}{\cosh(\gamma z) + \cos \gamma \pi} \qquad (4)$$

FWHM = $2 \sinh \left[\gamma^{-1} \mathrm{Arg\ cosh}\ (2+\cos \gamma \pi) \right]$

$\gamma = 1$ pas de distribution

D) Distribution de FUOSS et KIRKWOOD (symétrique) [4]

$$F(z) = \frac{\beta}{\pi} \frac{\cos(\frac{\beta\pi}{2}) \cosh(\beta z)}{\cos^2(\frac{\beta\pi}{2}) + \sinh^2(\beta z)} \qquad (5)$$

FWHM = $2 \sinh \left[\beta^{-1} \mathrm{Arg\ cosh}\ (a) \right]$

avec $a = \cos^2(\frac{\beta\pi}{2}) + \sqrt{(\cos^2(\frac{\beta\pi}{2}) - \frac{1}{2})^2 + \frac{3}{4}}$

$\beta = 1$ pas de distribution

E) Distribution de COLE et DAVIDSON (asymétrique) [5]

$$\begin{cases} F(z) = \frac{\sin \delta\pi}{\pi} (e^{-z} - 1)^{\delta} & (z < 0) \\ F(z) = 0 \quad \text{pour} \quad z > 0 \end{cases} \qquad (6)$$

$\delta = 1$ pas de distribution

III -- INTRODUCTION DES FONCTIONS DE DISTRIBUTION POUR L'INTERPRETATION DES RESULTATS EXPERIMENTAUX

Pour le modèle de diffusion rotationnelle isotrope ou celui de Frenkel les grandeurs physiques observables $M(\tau)$ ou $M(z)$ sont des combinaisons linéaires de fonctions lorentziennes en RMN, en IQNS ou en relaxation diélectrique (ε'').

Pour cette technique, ε' s'exprime en fonction de $1/(1+\omega^2 \tau_m^2)$.

Dans les deux cas, il est possible de trouver une expression analytique des expressions 1 - a ou 1 - b permettant ainsi un calcul simple de M_{exp} [2]

A) En RMN

AMOUREUX et SAHOUR [1] cherchent à expliquer la dissymétrie de la courbe $T_{1Z} = f(10^3/T(K))$. Ils montrent que les distributions de COLE et COLE, de FUOSS et KIRKWOOD et de COLE et DAVIDSON rendent compte de cette anomalie et que la position du minimum de T_{1Z} n'est pas affectée par les distributions.

B) En relaxation diélectrique

La permittivité complexe calculée en introduisant les fonctions de

distribution de COLE et COLE (CC) ou de COLE et DAVIDSON (CD) a déjà été décrite en [VI - 35] et [VI - 36].

AMOUREUX et SAHOUR [1] montrent que si la distribution est symétrique, sa largeur n'influe pas sur la fréquence critique F_C, ce qui n'est pas le cas pour une distribution asymétrique. De plus, l'énergie d'activation mesurée en relaxation diélectrique est indépendante de l'existence d'une distribution symétrique. Pour une distribution asymétrique, l'énergie d'activation est différente mais sa variation est moins importante en relaxation diélectrique qu'en RMN.

C) IQNS [6]

Nous avons étudié l'influence de la distribution de FUOSS-KIRKWOOD sur la loi de diffusion théorique $S(\vec{Q},\omega)$. Soit $S^D_{exp}(\vec{Q},\omega)$ la loi de diffusion expérimentale tirée de VII-28. Les caractéristiques de $S^D_{exp}(\vec{Q},\omega)$ ont été étudiées dans le cas du modèle de rotation uniaxiale d'ordre 12 en tenant compte de la résolution instrumentale. On trouvera le détail du calcul dans l'annexe A-XI-5.

L'introduction de cette distribution permet de rendre compte de l'excès de diffusion élastique observé dans le cas du CNADM. On montre également que l'interprétation d'un spectre expérimental distribué par un modèle à un seul temps de résidence conduit à la surestimation de ce temps.

Finalement, on trouve que cet effet devient faible si la largeur (FWHM) de la première lorentzienne du modèle est au moins 3 fois supérieure à celle de la résolution instrumentale.

BIBLIOGRAPHIE - ANNEXE 1 AU CHAPITRE VI

[1] - SAHOUR M. - 1986 - Thèse ; Université Lille I.

[2] - CONNOR T.H. - 1964 - Trans. Faraday Soc.; 60, 1574.

[3] - COLE K.S. and COLE R.H. - 1941 - J. Chem. Phys.; 9, 341.

[4] - KIRKWOOD J.G. and FUOSS R.M. - 1941 - J. Chem. Phys.; 9, 329.

[5] - DAVIDSON D.W. and COLE R.H. - 1951 - J. Chem. Phys. ; 19, 1484.

[6] - BEE M., FOULON M., AMOUREUX J.P., CAUCHETEUX C. and POINSIGNON C. - 1987 - J. Phys. C., Solid state phys.; 20, 337 - 349.

ANNEXE A - VI - 2 :

RELATIONS entre les TEMPS de CORRELATION et les TEMPS de RESIDENCE en RMN

Pour le modèle de Frenkel et dans le cas où la molécule effectue une rotation autour de son axe ainsi qu'un basculement par rapport aux axes cristallins, la fonction d'autocorrélation est décrite par une somme de 6 exponentielles dont les temps de corrélation sont notés τ_α. Ceux-ci sont liés aux temps de résidence τ_{mp} et $\tau_{C\beta}$ par les expressions suivantes :

$$\tau_1^{-1} = \tau_{b1}^{-1}$$

$$\tau_2^{-1} = \tau_{b1}^{-1} + \tau_{r1}^{-1}$$

$$\tau_3^{-1} = \tau_{b1}^{-1} + \tau_{r2}^{-1}$$

$$\tau_4^{-1} = \tau_{b2}^{-1}$$

$$\tau_5^{-1} = \tau_{b2}^{-1} + \tau_{r1}^{-1}$$

$$\tau_6^{-1} = \tau_{b2}^{-1} + \tau_{r2}^{-1}$$

où τ_{b1}, τ_{b2}, τ_{r1}, et τ_{r2} s'expriment à partir des temps de résidence des mouvements de basculement et de rotation uniaxiale d'ordre p respectivement.

$$\tau_{b1}^{-1} = \frac{4}{3}\tau_{C4}^{-1} + \frac{2}{3}\tau_{C'2}^{-1} + \tau_{C3}^{-1} + \frac{4}{3}\tau_{C2}^{-1}$$

$$\tau_{b2}^{-1} = \tau_{C4}^{-1} + \tau_{C'2}^{-1} + \frac{3}{2}\tau_{C3}^{-1}$$

$$\tau_{r1}^{-1} = \frac{(2-\sqrt{3})}{2}\tau_{m12}^{-1} + \frac{1}{2}\tau_{m6}^{-1} + \tau_{m4}^{-1} + \frac{3}{2}\tau_{m3}^{-1} + 2\tau_{m2}^{-1}$$

$$\tau_{r2}^{-1} = \frac{1}{2}\tau_{m12}^{-1} + \frac{3}{2}\tau_{m6}^{-1} + 2\tau_{m4}^{-1} + \frac{3}{2}\tau_{m3}^{-1} + \tau_{m2}^{-1}$$

de façon générale :

$$\tau_{rq}^{-1} = 2\sum_{p} \frac{\sin^2(\pi q/p)}{\tau_{mp}}$$

Pour un échantillon de poudre, les vitesses de relaxation deviennent:

$$T_{1Z}^{-1} = \frac{2}{3}\Delta M_2 \sum_{\alpha=1}^{6} \Psi_\alpha \left[L(\omega_o, \tau_\alpha) + 4L(2\omega_o, \tau_\alpha) \right]$$

$$T_{1\rho}^{-1} = \frac{2}{3}\Delta M_2 \sum_{\alpha=1}^{6} \Psi_\alpha \left[\frac{3}{2} L(2\omega_1, \tau_\alpha) + \frac{5}{2} L(\omega_o, \tau_\alpha) + L(2\omega_o, \tau_\alpha) \right.$$

avec $\sum_{\alpha=1}^{6} \Psi_\alpha = 1$ et $\Psi_\alpha = \dfrac{\sum_{k \neq 1} A^m_{k1,\alpha} / r_{k1}^6}{\sum_{k \neq 1} r_{k1}^{-6}}$

FIGURES ET TABLEAUX

CHAPITRE VII

Figure VII - 1 a
d'après [1]

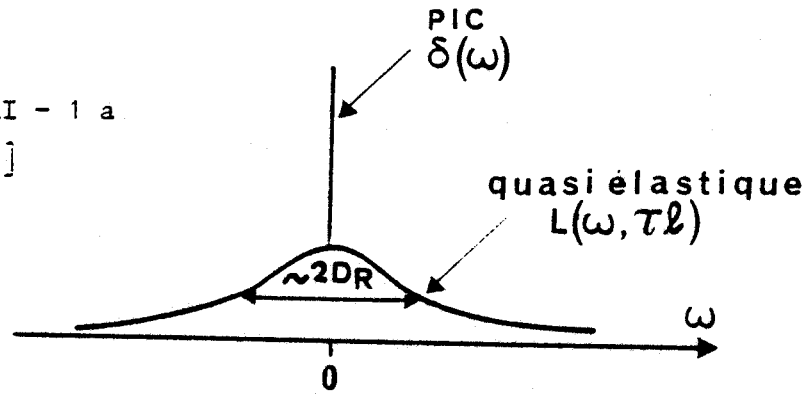

Loi de diffusion incohérente pour le modèle de diffusion rotationnelle isotrope.

Figure VII - 1 b
d'après [1]

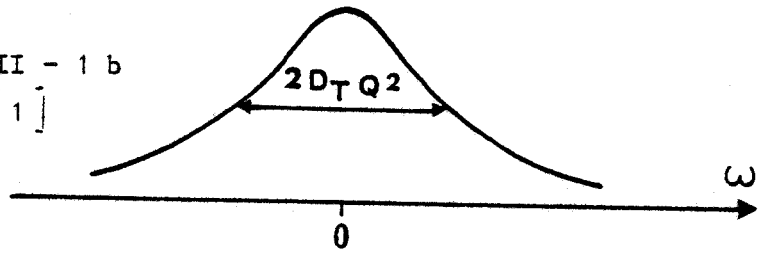

Loi de diffusion incohérente pour le modèle de diffusion translationnelle isotrope

Figure VII - 2
d'après [2]

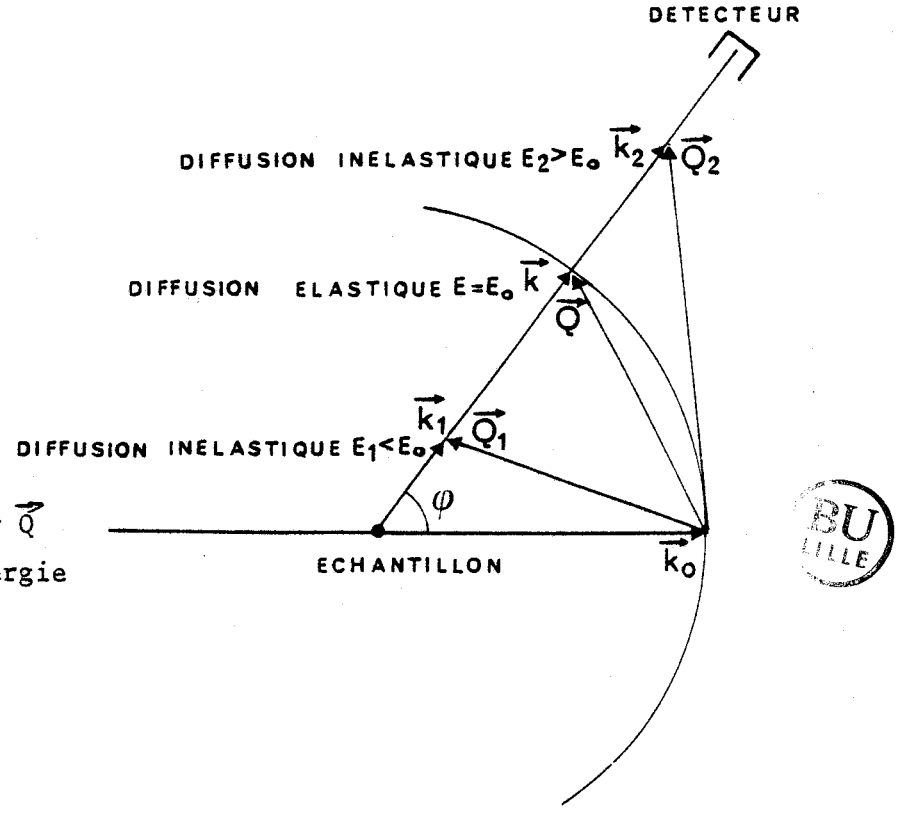

Variation du vecteur $\vec{Q}$ en fonction de l'énergie de transfert

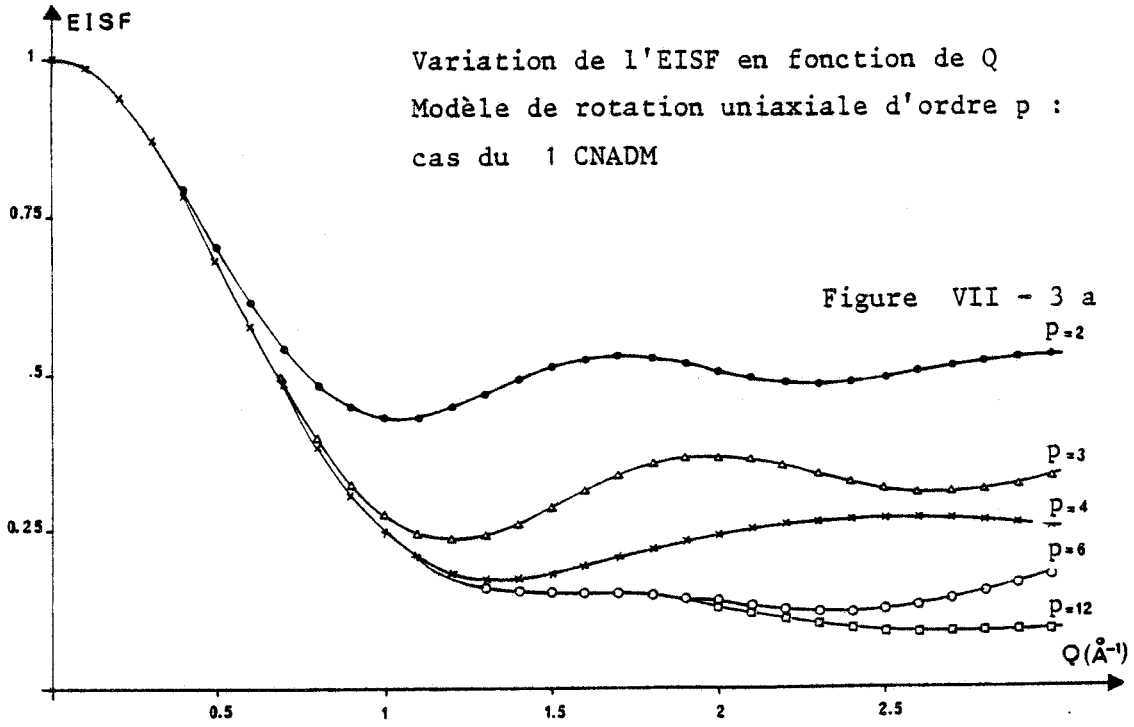

Variation de l'EISF en fonction de Q
Modèle de rotation uniaxiale d'ordre p :
cas du 1 CNADM

Figure VII - 3 a

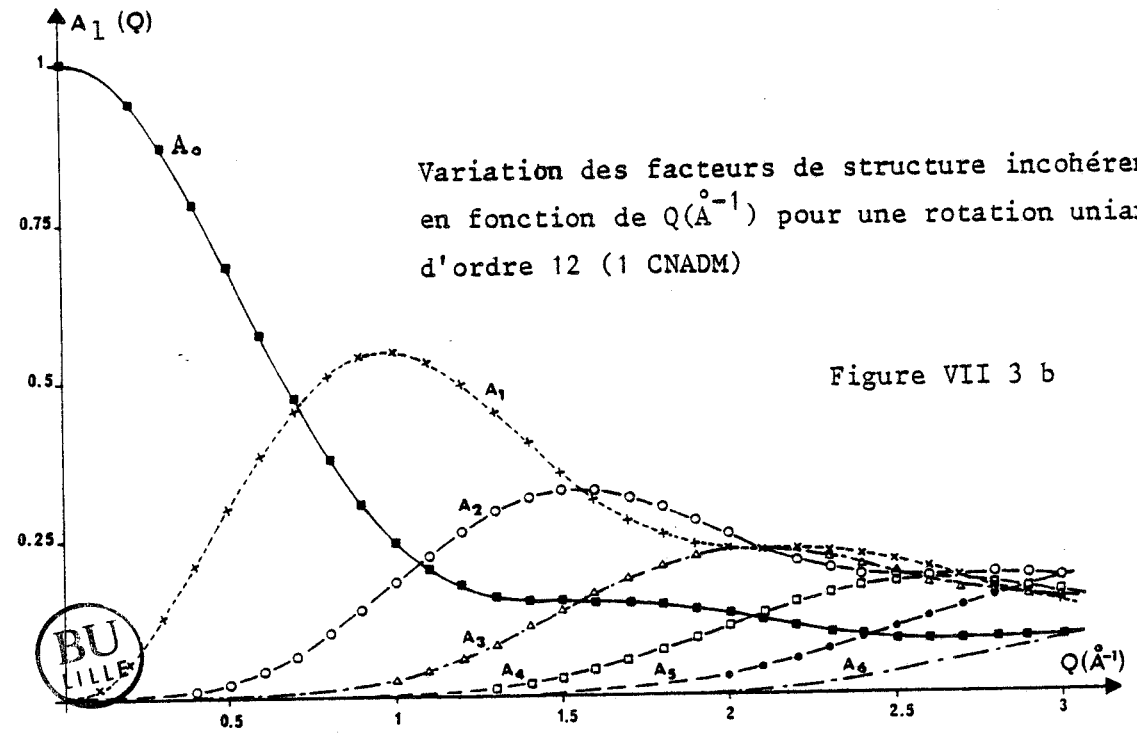

Variation des facteurs de structure incohérents en fonction de $Q(\mathring{A}^{-1})$ pour une rotation uniaxiale d'ordre 12 (1 CNADM)

Figure VII 3 b

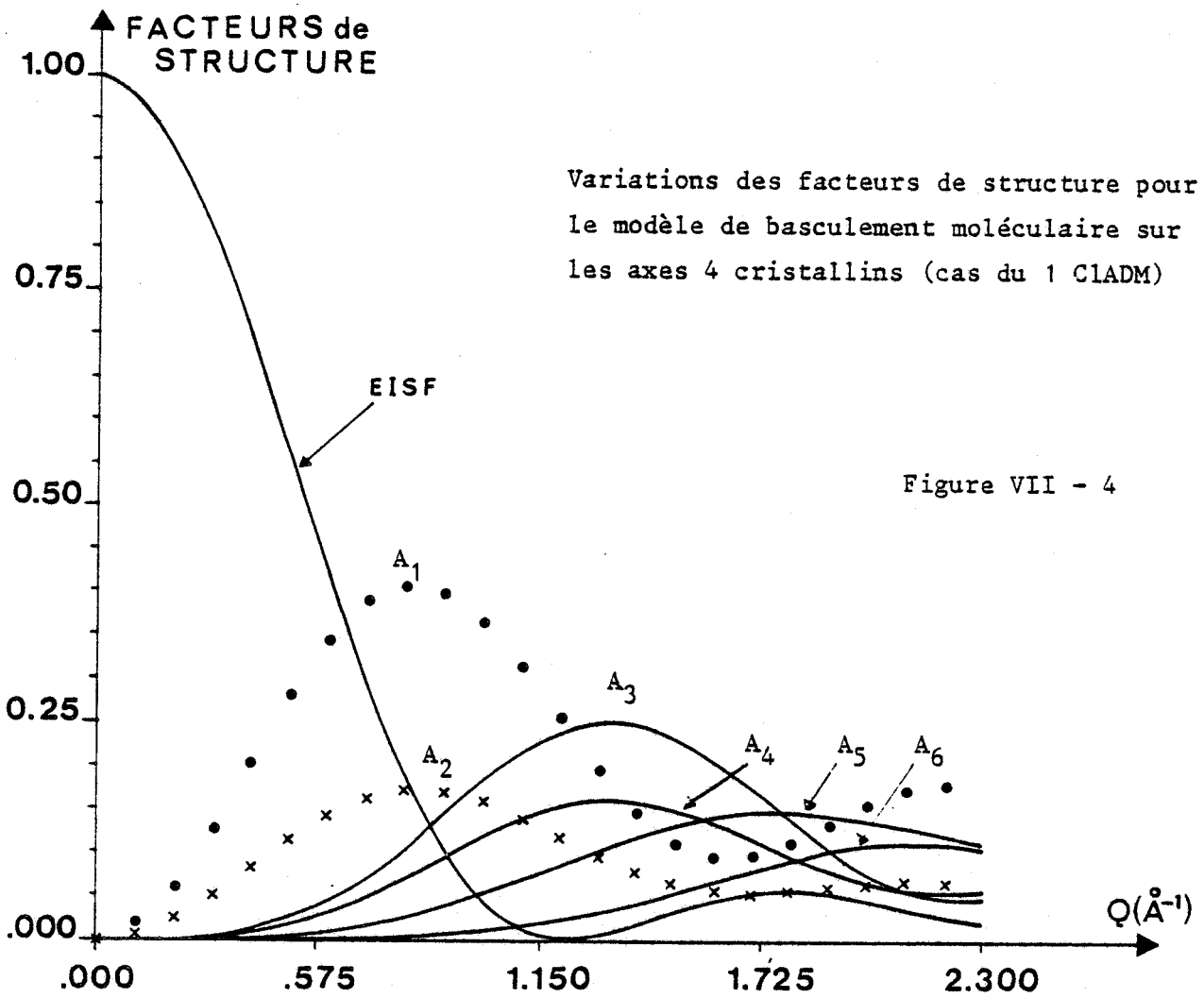

Variations des facteurs de structure pour le modèle de basculement moléculaire sur les axes 4 cristallins (cas du 1 ClADM)

Figure VII - 4

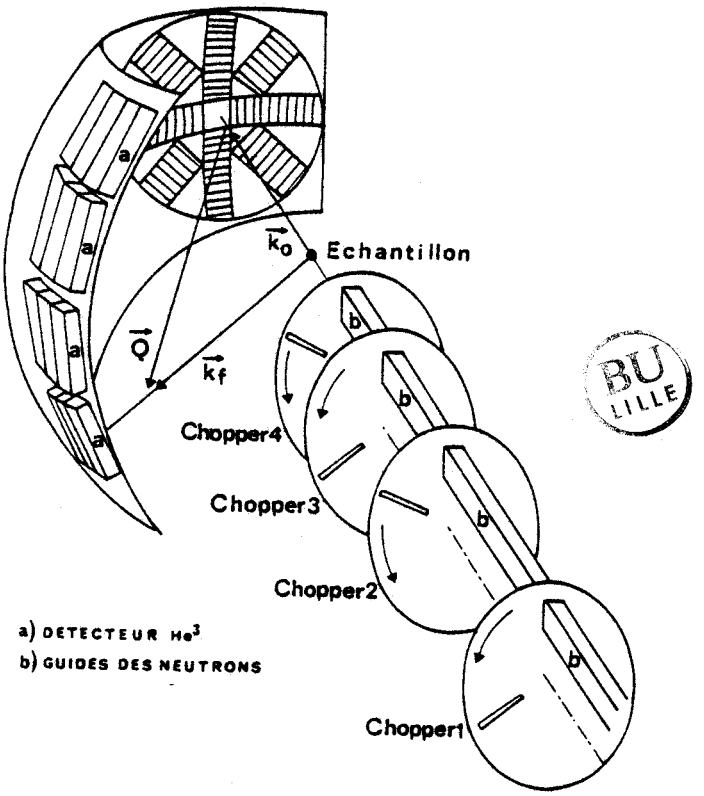

L'instrument IN5 (ILL)

Figure VII - 5
d'après [2]

Figure VII - 6
d'après [2]

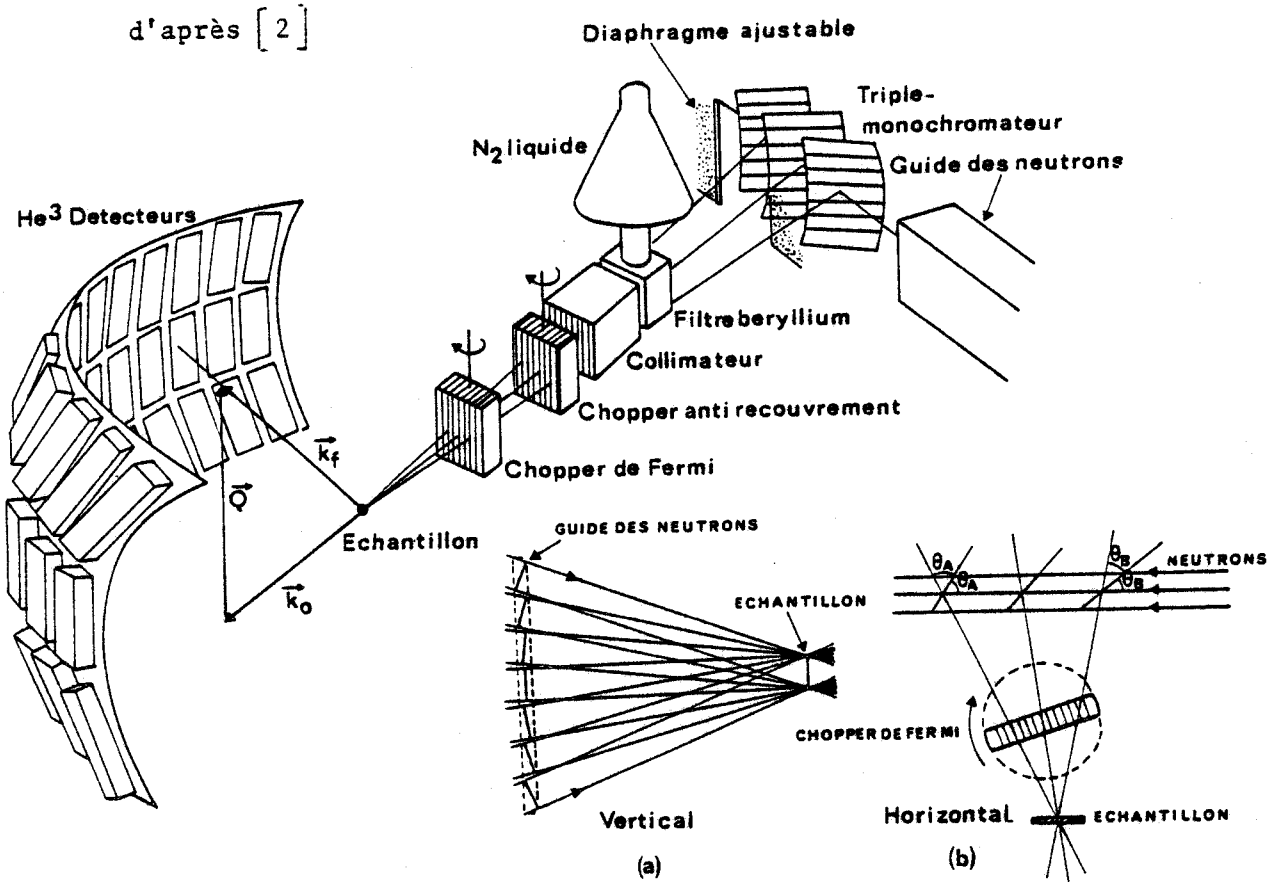

L'instrument IN6 (ILL)

Figure VII - 7
d'après [2]

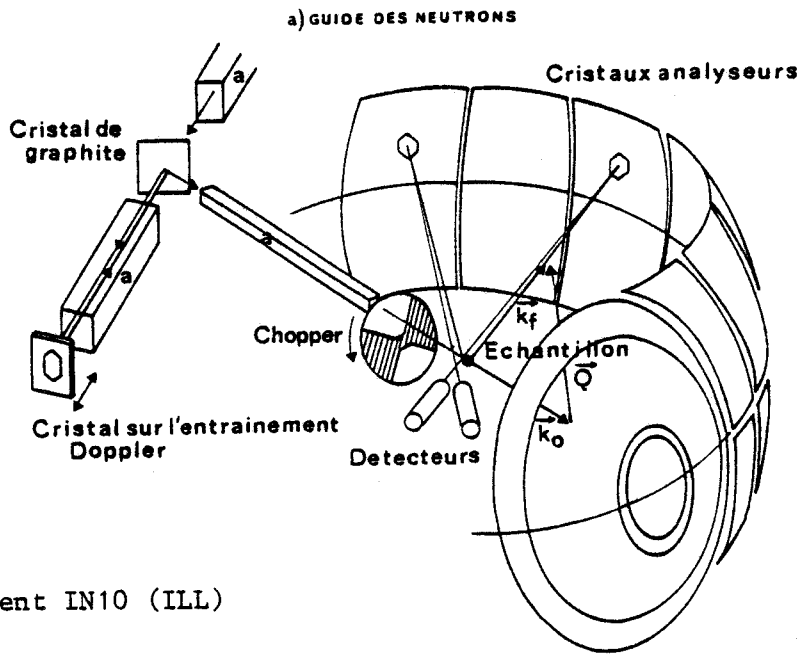

L'instrument IN10 (ILL)

ANNEXE

CHAPITRE VII

ANNEXE A - VII - 1

Modèle de rotation uniaxiale d'ordre N : expressions des τ_ℓ et A_ℓ

N	$1/\tau_\ell$	$A_\ell(\alpha)$
2	$1/\tau_0 = 0$ $1/\tau_1 = 2/\tau_{m2}$	$A_0(\alpha) = [1+J_0(2\alpha)]/2$ $A_1(\alpha) = [1-J_0(2\alpha)]/2$
3	$1/\tau_0 = 0$ $1/\tau_1 = 1/\tau_2 = 1.5/\tau_{m3}$	$A_0(\alpha) = [1+2J_0(\alpha\sqrt{3})]/3$ $A_1(\alpha) = A_2(\alpha) = [1-J_0(\alpha\sqrt{3})]/3$
4	$1/\tau_0 = 0$ $1/\tau_1 = 1/\tau_3 = 1/\tau_{m4}$ $1/\tau_2 = 2/\tau_{m4}$	$A_0(\alpha) = [1+2J_0(\alpha\sqrt{2})+J_0(2\alpha)]/4$ $A_1(\alpha) = A_3(\alpha) = [1 - J_0(2\alpha)]/4$ $A_2(\alpha) = [1-2J_0(\alpha\sqrt{2})+J_0(2\alpha)]/4$
6	$1/\tau_0 = 0$ $1/\tau_1 = 1/\tau_5 = 0.5/\tau_{m6}$ $1/\tau_2 = 1/\tau_4 = 1.5/\tau_{m6}$ $1/\tau_3 = 2/\tau_{m6}$	$A_0(\alpha) = [1+2J_0(\alpha)+2J_0(\alpha\sqrt{3})+J_0(2\alpha)]/6$ $A_1(\alpha) = A_5(\alpha) = [1+J_0(\alpha)-J_0(\alpha\sqrt{3})-J_0(2\alpha)]/6$ $A_2(\alpha) = A_4(\alpha) = [1-J_0(\alpha)-J_0(\alpha\sqrt{3})+J_0(2\alpha)]/6$ $A_3(\alpha) = [1-2J_0(\alpha)+2J_0(\alpha\sqrt{3})-J_0(2\alpha)]/6$
12	$1/\tau_0 = 0$ $1/\tau_1 = 1/\tau_{11} = 0.134/\tau_{m12}$ $1/\tau_2 = 1/\tau_{10} = 0.5/\tau_{m12}$ $1/\tau_3 = 1/\tau_9 = 1/\tau_{m12}$ $1/\tau_4 = 1/\tau_8 = 1.5/\tau_{m12}$ $1/\tau_5 = 1/\tau_7 = 1.866/\tau_{m12}$ $1/\tau_6 = 2/\tau_{m12}$ $A_i(\alpha) = A_{12-i}(\alpha)$	$\begin{bmatrix} A_0 \\ A_1 \\ A_2 \\ A_3 \\ A_4 \\ A_5 \\ A_6 \end{bmatrix} = \frac{1}{12} \begin{bmatrix} 1 & 2 & 2 & 2 & 2 & 2 & 1 \\ 1 & \sqrt{3} & 1 & 0 & -1 & -\sqrt{3} & -1 \\ 1 & 1 & -1 & -2 & -1 & 1 & 1 \\ 1 & 0 & -2 & 0 & 2 & 0 & -1 \\ 1 & -1 & -1 & 2 & -1 & -1 & 1 \\ 1 & -\sqrt{3} & 1 & 0 & -1 & \sqrt{3} & -1 \\ 1 & -2 & 2 & -2 & 2 & -2 & 1 \end{bmatrix} \begin{bmatrix} 1 \\ J_0(\alpha_1) \\ J_0(\alpha_2) \\ J_0(\alpha_3) \\ J_0(\alpha_4) \\ J_0(\alpha_5) \\ J_0(\alpha_6) \end{bmatrix}$ avec $\alpha_1 = 0.518\ rQ$ $\alpha_2 = Qr$ $\alpha_3 = Qr\sqrt{2}$ $\alpha_4 = Qr\sqrt{3}$ $\alpha_5 = 1.932\ Qr$ $\alpha_6 = 2r$

On note : $\alpha = Qr$ (Q = module du vecteur de diffusion)
(r = rayon du cercle sur lequel se déplace le proton)

FIGURES ET TABLEAUX

CHAPITRE VIII

	Z	groupe spatial	a Å	c Å	V Å^3	orientations moléculaires	$\langle u_i^2 \rangle$ ou $\langle u_{//}^2 \rangle$ Å^2	$\langle u_\perp^2 \rangle$ Å^2	$\langle \theta_i^2 \rangle^{1/2}$ ou $\langle \theta_{//}^2 \rangle^{1/2}$	$\langle \theta_\perp^2 \rangle^{1/2}$	R_w %	R %	Nbre de raies	Références
ADM 295 K Plastique	4	Fm3m	9.445	—	843	2	0.048(3)	—	9°(0.2)	—	14	11	66	[12]
ADM 173 K Basse Température	2	$P\bar{4}2_1c$	6.60	8.81	384	1	—	Facteur U_i atomique U_i = 0.046 Å^2		—	—	8	53	[8]
FADM 293 K Plastique	4	Fm3m	9.535	—	867	8	0.060(1)	—	11°(0.6)	6.5°(0.2)	8	—	52	[13]
FADM Basse Température	2	tétragonal	6.82	8.92	415	4	—	—	—	—	—	—	—	Notre étude

TABLEAU VIII-1

Structure des phases cristallines de ADM et FADM - paramètres cristallins - Résultats d'affinements

	τ_R, τ_{c4} τ_o (s)	E (K)	REFERENCES	TECHNIQUE
ADM Phase Plastique	9.4×10^{-14}	1548	[18]	RMN (^1H)
	18.9×10^{-14}	1395	[19], [23]	RMN (^1H)
	17.9×10^{-14}	1397	[20], [24]	IQNS
	18×10^{-14}	1587	[27]	simulation
ADM Phase BT	1.13×10^{-15}	3268	[18]	RMN (^1H)

TABLEAU VIII-2

ADAMANTANE : Temps de résidence τ_{c4}

$\tau_{c4} = \tau_o \exp(E/T)$ (E en (K))

	τ_{c4} τ_o	E (K)	REFERENCES	TECHNIQUE	τ_{m3} τ_o	E (K)	REFERENCES	TECHNIQUE
PHASE PLASTIQUE de FADM	9.3×10^{-15}	2960	[21]	IQNS	5.9×10^{-13}	1560	[21]	IQNS
	3.6×10^{-14}	2282	[22]	R.D(1)	Non mesurable			R.D
	3.6×10^{-14}	2282	[22]	R.D(1)	3.7×10^{-14}	2837	[32]	RMN
	4.0×10^{-14}	2282	[22]	R.D(2)	1.9×10^{-14}	2865	[32]	RMN
PHASE BASSE TEMPERATURE	9.73×10^{-16}	3502	[22]	R.D(1)	$5.3(\pm 4.7) \times 10^{-14}$	2420	[32]	RMN
	12.4×10^{-16}	3502	[32]	R.D(2)	$5.4(\pm 4.7) \times 10^{-14}$	2408	[32]	RMN

TABLEAU VIII-3

FLUOROADAMANTANE

RD (1) : hypothèse du champ interne de GLARUM et COLE

RD (2) : hypothèse du champ interne de FATUZZO et MASON

Caractéristiques des mouvements moléculaires pour FADM : $\tau = \tau_o \exp(E/T)$ (T en (K)

d_{min} \ T(K)	208.6 K	295 K	425 K	503 K
d^{+}_{min} A°	2.329	2.401	2.517	2.588
d^{-}_{min} (A°)	2.658	2.722	2.827	2.890

ADM : Distances minimums entre atomes d'Hydrogène de molécules proches voisines

Tableau VIII-4

ADAMANTANE T = 188 K

Tetragonal Z = 2

a = 6.639(7) Å c = 8.918(9) Å v = 393.1(1.2) Å^3

F(0,0,0) = 152

Space Group $P\bar{4}2_1C$

211 reflections as $I \geq 3\sigma(I)$

Phase basse température de l'ADM paramètres cristallins

Tableau VIII-5

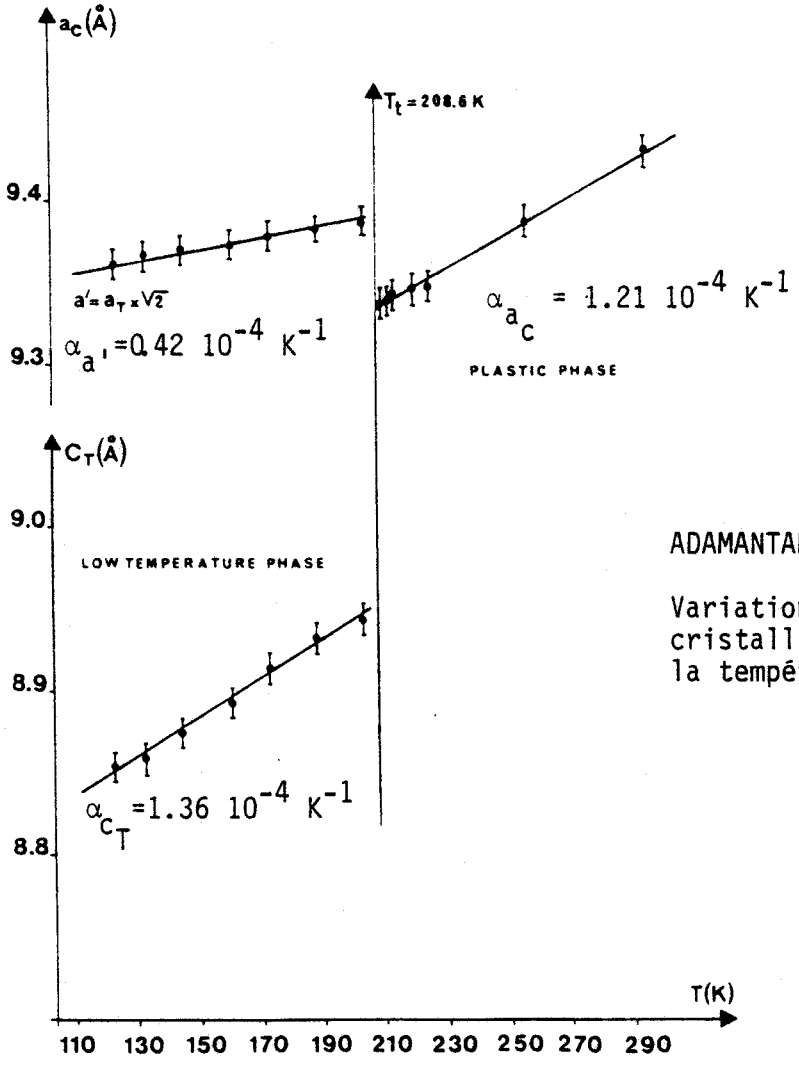

ADAMANTANE

Variations des paramètres cristallins en fonction de la température.

Figure VIII-1

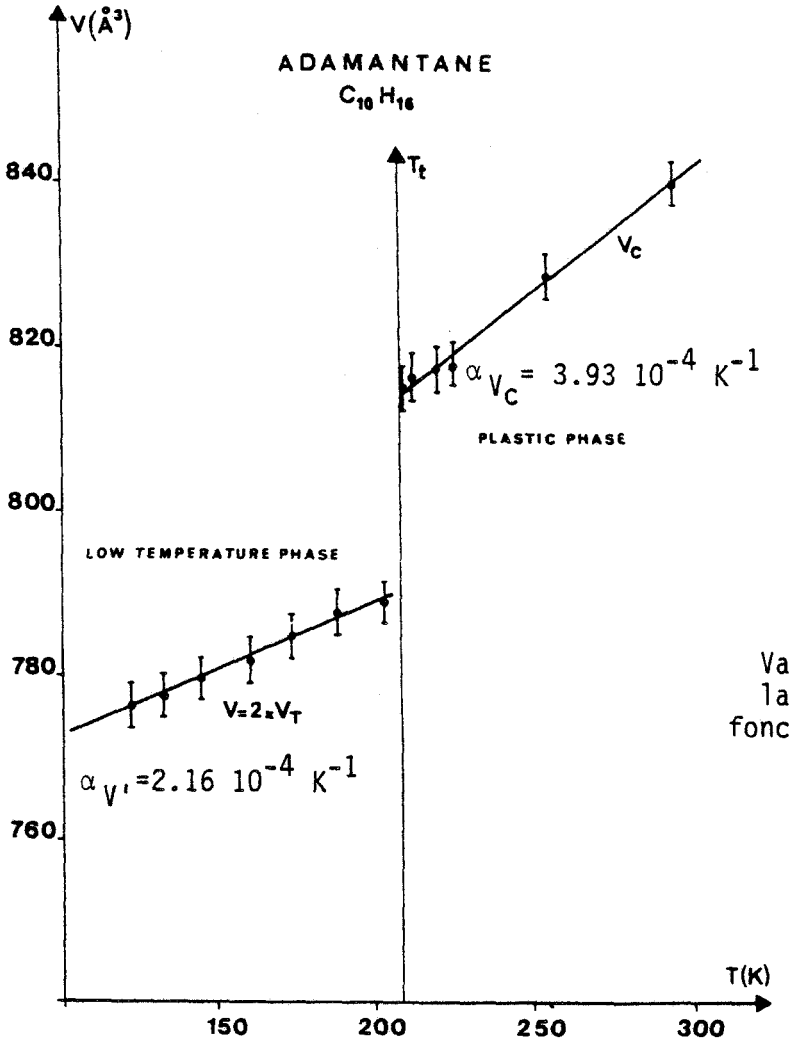

Variation du volume de la maille cristalline en fonction de la température.

Figure VIII-2

- Independent Atoms (Shelx)

	X/a	Y/b	Z/c	(U_{iso}) U_{11}	U_{22}	U_{33}	U_{12}	U_{13}	U_{23}
C(1)	0	0	0.1980(3)	0.0357(20)	0.0319(19)	0.0219(12)	-0.0009(23)	0	0
C(2)	- 0.0262(4)	0.1862(4)	0.0992(3)	0.0317(12)	0.0199(10)	0.0287(10)	0.0008(10)	0.0021(12)	-0.0063(10)
C(3)	0.1600(4)	0.2122(4)	0	0.0271(11)	0.0260(10)	0.0385(12)	-0.0078(8)	0.0003(14)	0.0001(14)
HC(1)	0.1156(40)	0.0099(73)	0.2688(27)	0.0428(40)					
HC(2)	-0.0355(50)	0.3016(46)	0.1590(32)	0.0428(40)					
HC(3)	0.2817(53)	0.2303(48)	0.0626(33)	0.0428(40)					
H'C(3)	0.1427(48)	0.3286(47)	-0.0570(33)	0.0428(40)					

$\langle d\ (c - c) \rangle = 1.529(3)$ Å

$\langle \widehat{c - c - c} \rangle = 109°5(4)$

R = 3.6 % Rw = 3.9 % WGHT = $0.54/(\sigma^2 + 8.4\times10^{-4}\ F^2)$

- Rigid Group (ORION) ($w^2 = 1/\sigma_c^2(F)$)

$T_{11} = T_{22} = 0.0183\,(12)$ Å^2 $T_{33} = 0.0211(12)$ Å^2

$\sqrt{L_{11}} = \sqrt{L_{22}} = 4°.3\,(0°.5)$ $\sqrt{L_{33}} = 3°7(0°.6)$

$S_{11} - S_{22} = -2(S_{22} - S_{33}) = -2(S_{33} - S_{11}) = 0.00106(101)$

R = 4.0% R_w = 2.4 %. $S_{12} = S_{21} = -0.00002(71)$

Tenseurs T.L.S déduits des U_{ij} affinés par atomes indépendants (SHELX) (symétrie $\bar{4}$)

$T_{11} = T_{22} = 0.0174(7)$ Å^2 $T_{33} = 0.0212(6)$ Å^2

$\sqrt{L_{11}} = \sqrt{L_{22}} = 4°34\ (0°12)$ $\sqrt{L_{33}} = 4°32(0°12)$

$S_{11} - S_{22} = -2\,(S_{22} - S_{33}) = -2\,(S_{33} - S_{11}) = 0.00071(79)$

$S_{12} = S_{21} = 0.00025(22)$

$\langle d_{c-c} \rangle_{corrigé} = 1.538(1)$ Å

Tableau VIII-6

Adamantane : résultats d'affinements : T = 188 K

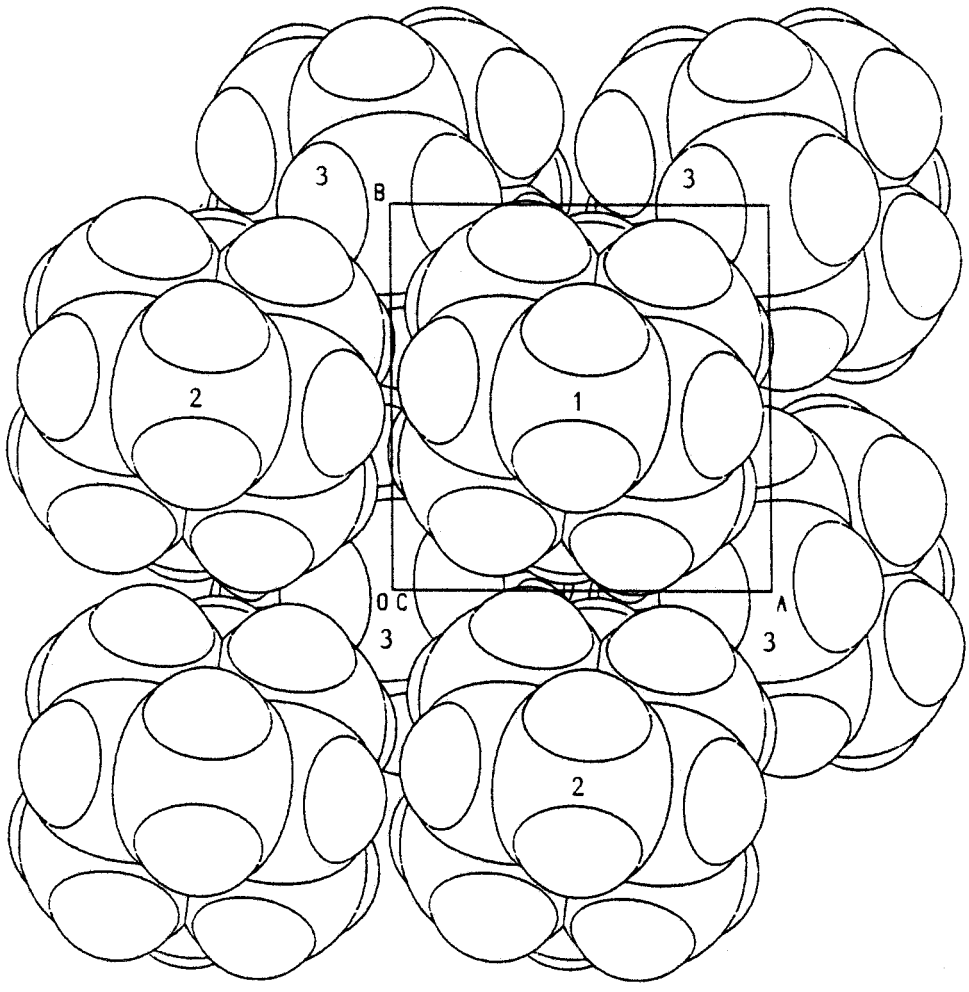

ADM : Phase basse température : Projection le long de $\vec{c}_T$

FIGURE VIII-3

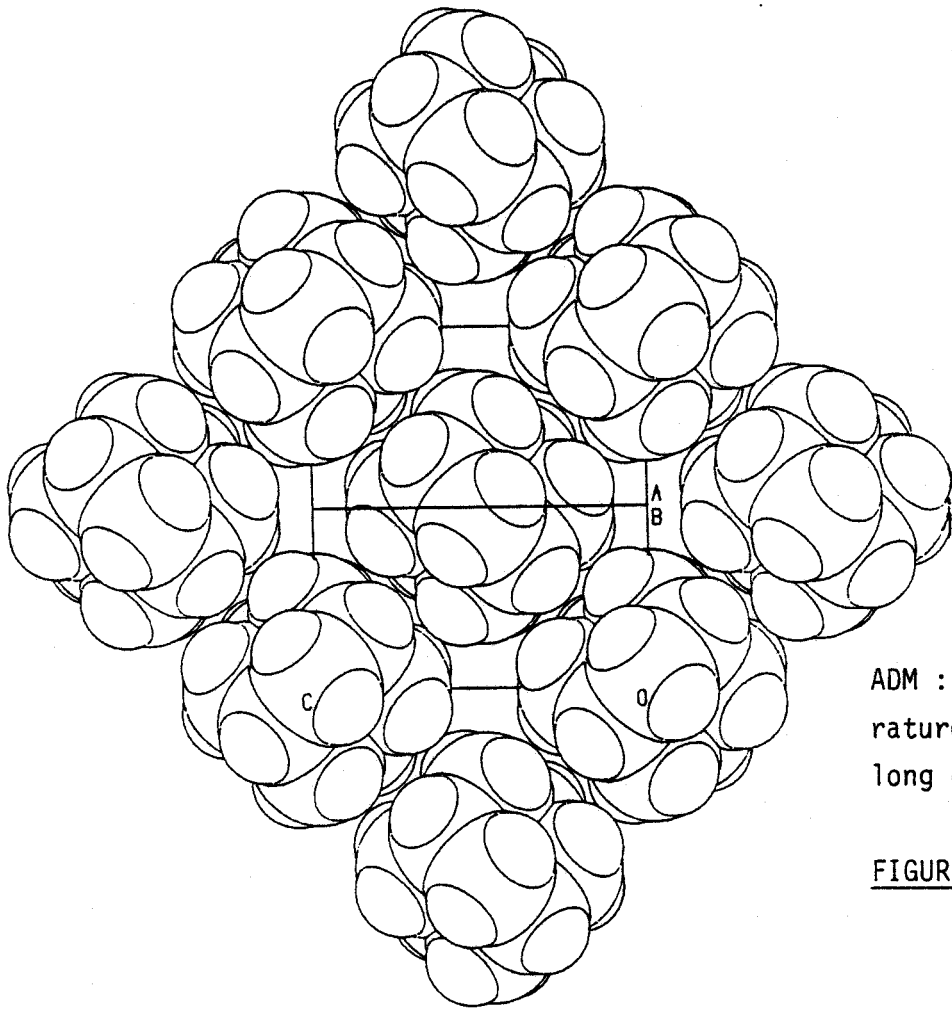

ADM : Phase basse température : Projection le long de <110>

FIGURE VIII-4

raie n°	d(h k l) mesurés Å	Intensités relatives %	Indices Miller	d(h k l)	h k l cubique
1	5.390	100	1 0 1	5.403	1 1 1
2	4.812	25	1 1 0	4.808	2 0 0
3	4.452	7	0 0 2	4.450	0 0 2
4	3.721	6	1 0 2	3.724	1 1 2
5	3.171	8	2 0 1	3.176	2 2 1
6	2.880	3	2 1 1	2.878	3 1 1
7	2.702	10	2 0 2	2.702	2 2 2
8	2.510	2.5	1 2 2	2.511	3 1 2
9	2.237	1	2 0 3	2.235	2 2 3
10	2.203	0.5	3 0 1	2.197	3 3 1
11	2.124	1	1 2 3	2.124	3 1 3
12	2.021	1	1 1 4	2.019	2 0 4
13	1.936	1.5	1 3 2	1.936	4 2 2
14	1.785	2	1 2 4	1.796	3 1 4
15	1.738	0.5	1 3 3	1.741	4 2 3

$$R = \sum_{1}^{15} \frac{|d_{mes} - d_{calc}|}{\sum d_{mes}} = 1.2 \times 10^{-3}$$

TABLEAU VIII-7

FADM Phase basse température 173 K

a = 6.80 Å , c = 8.90 Å

FLUOROADAMANTANE T = 217K

Tétragonal Z = 2

a = 6.810 (7) Å c = 8.979 (9) Å v = 416.4 Å^3

F (0, 0, 0) = 168

Space group $P\bar{4}2_1c$ ou $P4_2/nmc$

87 réflections telles que $I \geq 3\sigma(I)$

R = 3.8 % R_w = 3.78 %

Poids = $1.326/(\sigma_c^2 + 2.75 \times 10^{-4} F^2)$

TABLEAU VIII-8

Résultats cristallographiques

T = 0 K	a' (A°)	C_T (A°)	a_c (A°)	V_c (A°^{3})	$2V_T$(A°^{3})	ε_c (0 K)
ADM	9.311	8.704	9.104	755 (2)	756 (2)	0.77
FADM	9.468	8.593	9.198	782 (2)	780 (2)	0.76

TABLEAU VIII-9

Extrapolation à 0K des paramètres cristallins

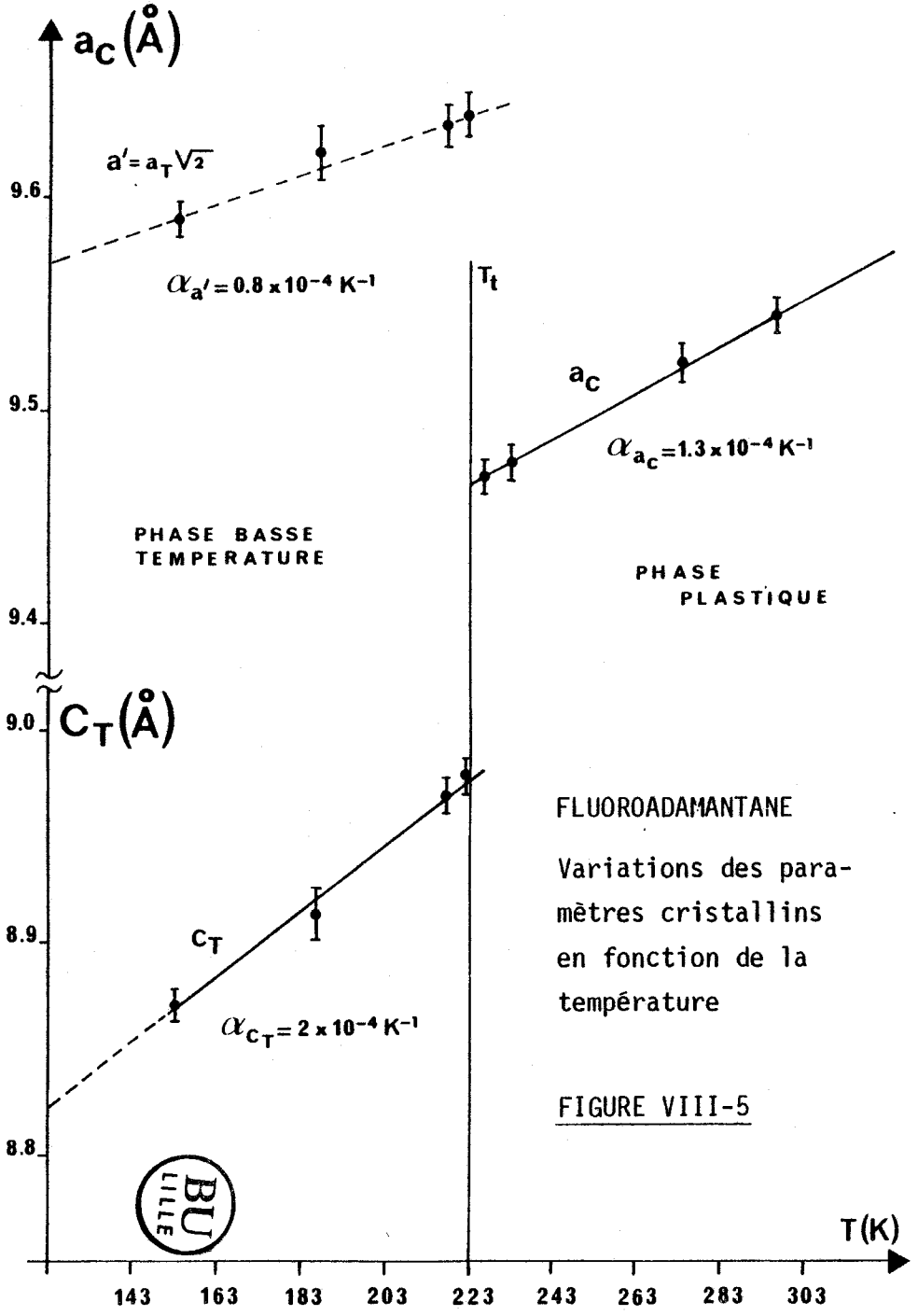

FLUOROADAMANTANE

Variations des paramètres cristallins en fonction de la température

FIGURE VIII-5

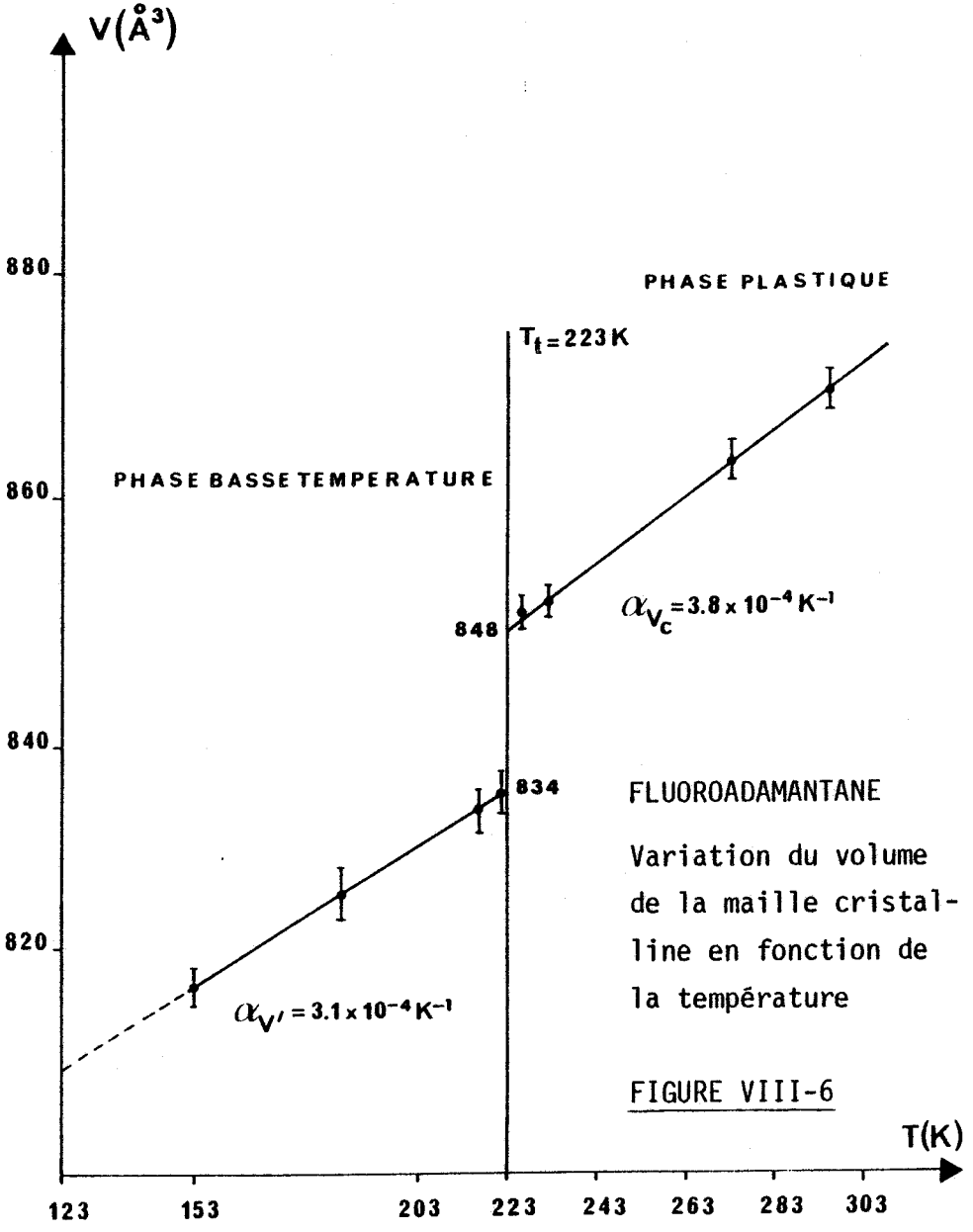

FLUOROADAMANTANE

Variation du volume de la maille cristalline en fonction de la température

FIGURE VIII-6

FIGURE VIII-7

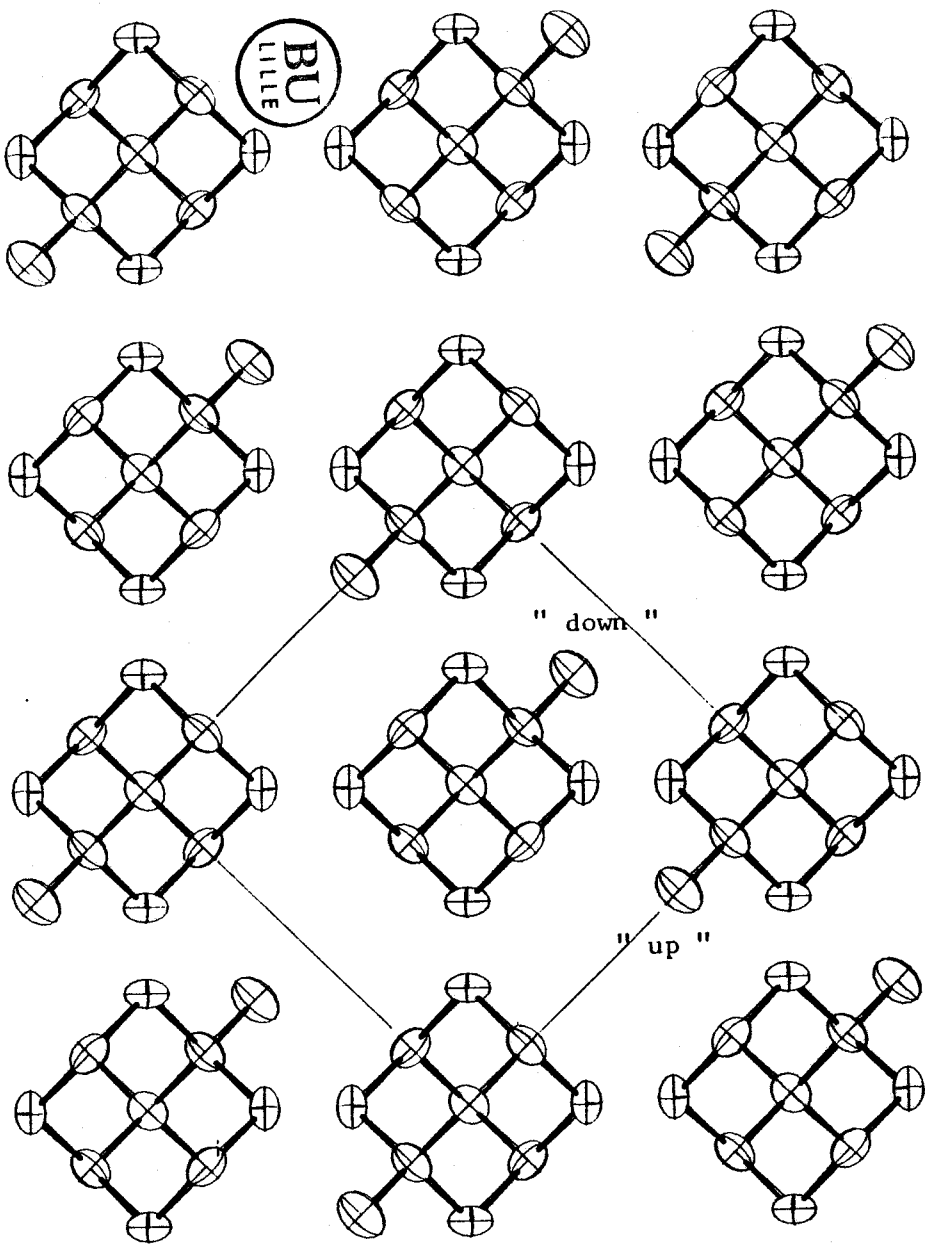

FADM : Phase basse température : Projection // à $\vec{c}_T$
Ordre local antiferroélectrique

	x	y	z	U
F	0 (1)	3393 (17)	1769 (13)	68 (15)
C1	0 (1)	0 (1)	1962 (8)	49 (7)
H11	1135 (54)	0 (1)	2624 (35)	63 (4)
C2	0 (1)	1797 (8)	972 (5)	49 (6)
H22	0 (1)	3027 (66)	1615 (49)	63 (4)
C3	1822 (5)	1822 (5)	0 (1)	45 (5)
H31	3115 (99)	1500 (71)	617 (20)	63 (4)
H32	2092 (69)	2922 (99)	-617 (20)	63 (4)

	U11	U22	U33	U23	U13	U12
F	996 (84)	491 (71)	739 (79)	-160 (73)	0 (1)	0 (1)
C1	617 (51)	427 (42)	435 (43)	0 (1)	0 (1)	0 (1)
H11	638 (49)					
C2	645 (39)	362 (32)	521 (24)	-92 (32)	0 (1)	0 (1)
H22	638 (49)					
C3	474 (20)	474 (20)	589 (28)	39 (21)	-39 (21)	-180 (26)
H31	638 (49)					
H32	638 (49)					

R = 3.80 % RW = 3.78 % Poids = $1.32/(\sigma_c^2 + 2.75 \times 10^{-4} F^2)$

F	- C2	1.302 (13)	C2	- C3	1.518 (4)
F	- H22	0.285 (46)	C3	- H31	1.063 (58)
C1	- H11	0.975 (35)	C3	- H32	0.950 (55)
C1	- C2	1.513 (7)			

C2	- F -	H22	4.3 (75)
H11	- C1 -	C2	111.0 (17)
F	- C2 -	C1	110.6 (5)
F	- C2 -	H22	1.2 (21)
F	- C2 -	C3	107.9 (5)
C1	- C2 -	H22	109.4 (21)
C1	- C2 -	C3	110.3 (3)
H22	- C2 -	C3	108.5 (21)
F	- H22 -	C2	174.4 (95)
C2	- C3 -	H31	112.0 (27)
C2	- C3 -	H32	120.2 (29)
H31	- C3 -	H32	107.9 (40)

Tableau VIII-10

Coordonnées atomiques, facteurs d'agitation, distances et angles intramoléculaires : Fluoroadamantane BT : T = 217 K

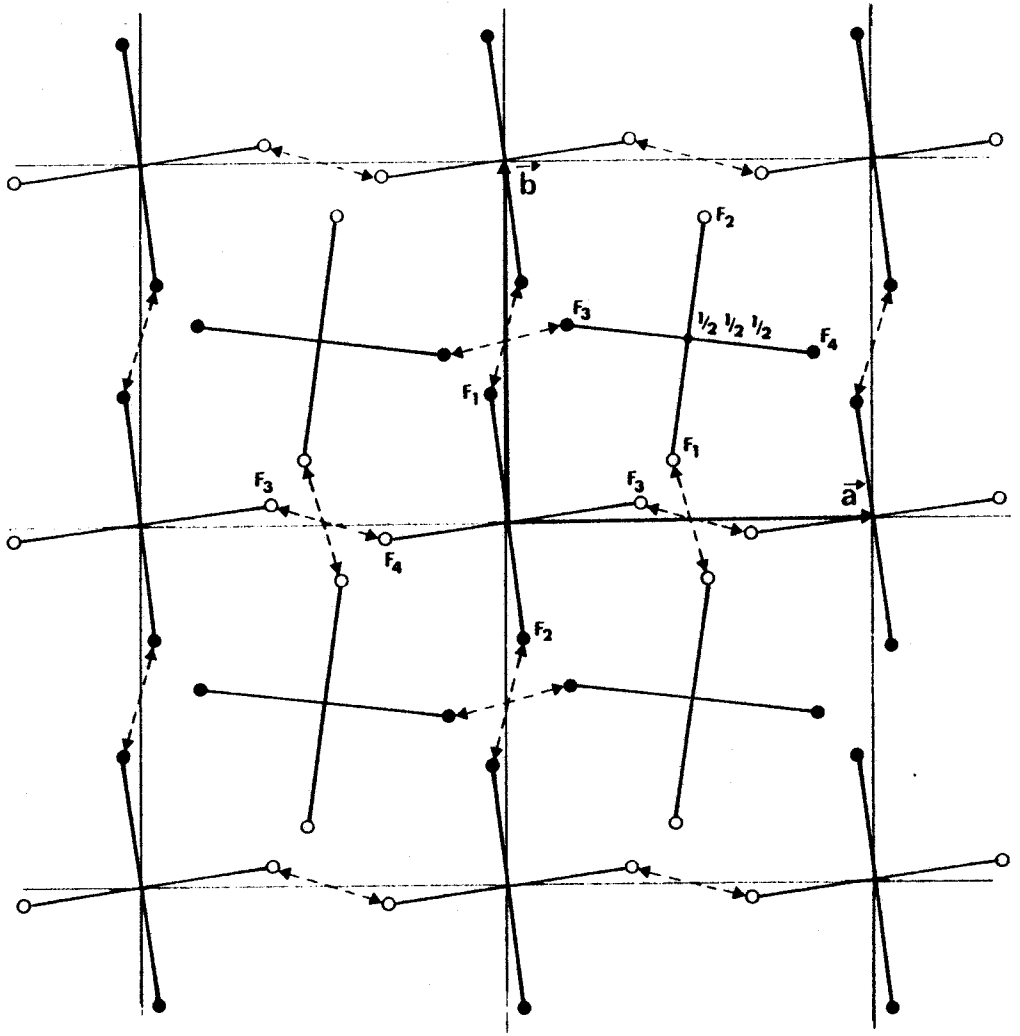

o F en-dessous du plan
● F au-dessus du plan
<---> d = 2.295 Å

FIGURE VIII-9

Projection dans le plan $(\vec{a}_T, \vec{b}_T)$ des atomes de Fluor des molécules moyennes : angle de "Tilt" = 8°

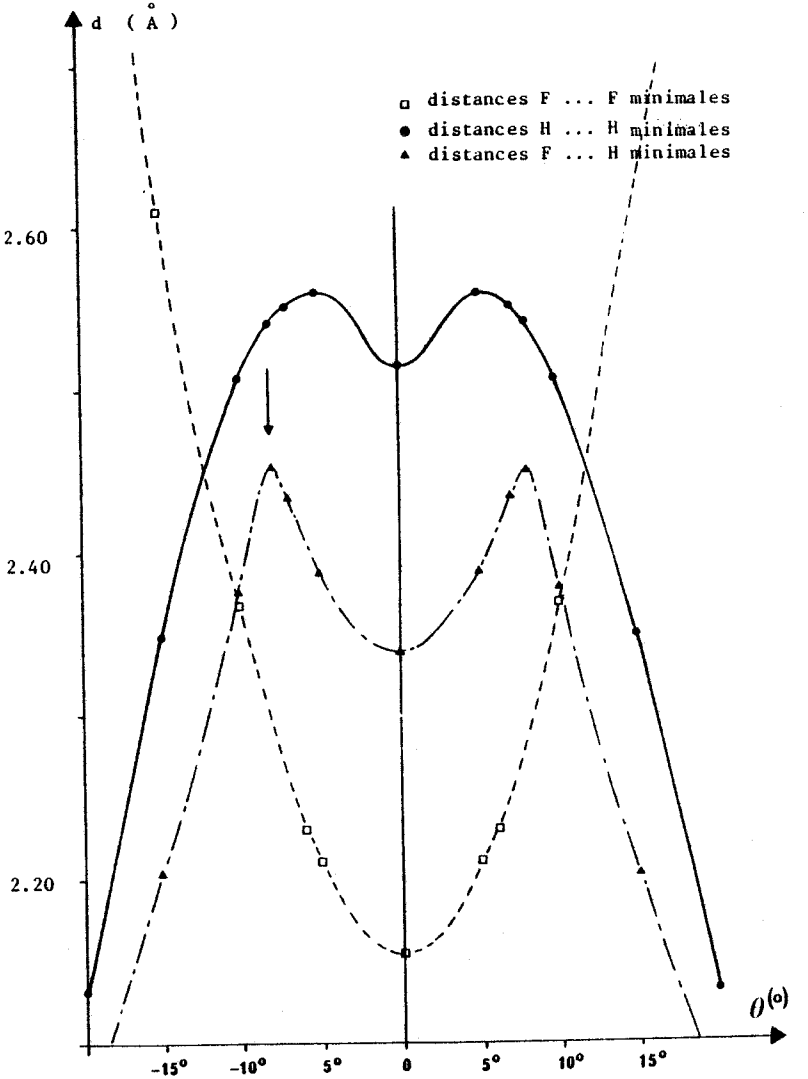

FIGURE VIII-8

FADM : Distances interatomiques en fonction de de l'angle de "Tilt"

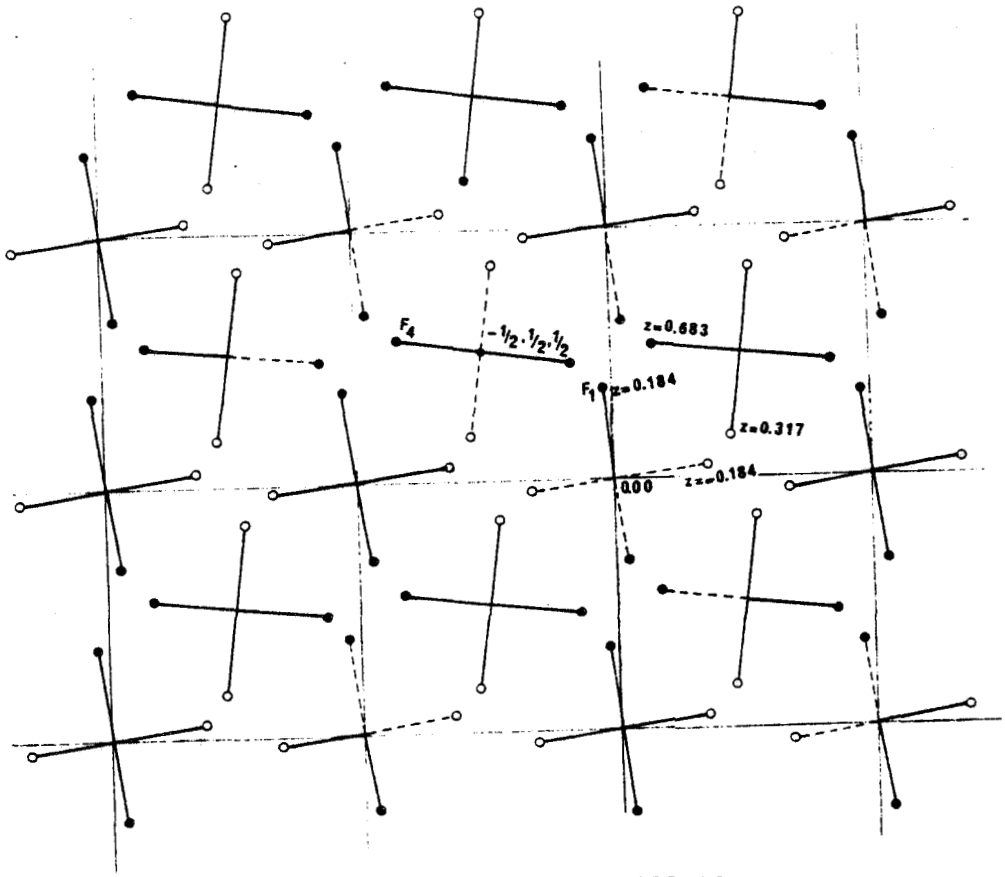

FIGURE VIII-10

FADM : Phase basse température : Exemple d'environnements locaux possibles

Compound	T(°K)	Rw(%)	R(%)	Ti(Å^2)	T_{11}(Å^2)	T_{33}(Å^2)	$\sqrt{L_I}$(°)	$\sqrt{L_1}$(°)	$\sqrt{L_{//}}$ (°)	NT
$C_{10}H_{16}$	223	4.9	4.9	. 037 (. 002)			7.8 (.2)			79
	295	8.0	7.7	. 049 (. 002)			9.2 (.2)			66
	188	2.4	4.0	. 019 (. 001)			4.1 (1.6)			211
$C_{10}H_{15}F$	229	7.9	10.1	. 038 (. 003)			6.5 (.2)			98
		7.3	8.9	. 038 (. 003)				5.6 (.3)	8.8 (.6)	
		7.1	8.8		. 045 (. 006)	. 028 (. 008)		5.5 (.3)	8.8 (.6)	
	295	7.2	5.0	. 061 (. 002)			8.1 (.2)			52
		6.2	4.5	. 060 (. 002)				6.8 (.3)	11.1 (.7)	
		6.0	4.4		. 070 (. 006)	. 048 (. 009)		6.8 (.3)	10.7 (.7)	

TABLEAU VIII-11

Résultats avec le modèle de FRENKEL : NT = Nombre de facteurs de structure observés ($F_o > 3\sigma$)

Compound	T(°K)	Rw (%)	R(%)	$T_i(\AA^2)$	$\hat{A}^4_{11}$	$\hat{A}^6_{11}$	$\hat{A}^8_{11}$	$\hat{A}^{10}_{11}$	$\hat{A}^{12}_{11}$	$\hat{A}^{12}_{22}$	$\hat{A}^{12}_{12}$	
$C_{10}H_{16}$	223	3.9	4.9	.034 2	.80 1	.67 1	.49 1	.37 3	.24 4	.27 4		79
	295	1.4	1.8	.047 1	.66 1	.57 1	.40 1	.26 2	.12 1	.16 2	- .43 3	66
$C_{10}H_{15}F$	229	12	11	.038 3	.81 2	.74 3	.58 3	.37 11	.30 9	.18 18		98
	295	4.9	4.8	.062 2	.75 1	.64 1	.49 2	.51 3	.30 3	.43 5		52

TABLEAU VIII-12

Résultats avec les harmoniques cubiques K^{ℓ}_m comme fonctions adaptées à la symétrie : pour FADM on considère une molécule moyenne de symétrie T_d

T(°K)	Rw %	R %	$T_i(\AA^2)$	$\hat{A}^4_{11}$	$\hat{A}^4_{12}$	$\hat{A}^6_{11}$	$\hat{A}^6_{13}$	$\hat{A}^8_{11}$	$\hat{A}^8_{13}$	$\hat{A}^{10}_{11}$	$\hat{A}^{10}_{14}$	$\hat{A}^{12}_{13}$	$\hat{A}^{12}_{15}$	$\hat{A}^{12}_{21}$	N_t
molecule fixed : A^{ℓ}_{mm}, (f)				- .51	.86	.63	.56	.21	.75	- .65	.60	- .53	.07	- .41	
229	6.7	6.9	.041 2	- .44 4	.78 4	.50 5	.52 6	.15 3	.71 3	- .38 5	.58 18	- .45 14	.98 25	- .23 5	66
	$A^{\ell}_{m1}/A^{\ell}_{m1}$ (f)			.86 8		.79 8		.71 14		.58 8				.56 12	
295	4.2	3.1	.060 2	- .34 3	.64 3	.43 4	.48 3	.11 3	.55 2	- .30 4	.54 16	- .40 8	.68 16	- .20 3	52
	$A^{\ell}_{m1}/A^{\ell}_{m1}$ (f)			.67 6		.68 6		.52 14		.46 6				.48 7	

TABLEAU VIII-13

Résultats de l'affinement par le modèle F.A.S. : $C_{10}H_{15}F$

Compound	$C_{10}H_{16}$				$C_{10}H_{15}F$	
atom μ	Ct		Cs		Δ	
T(k)	223	295	223	295	229	295
$\mathcal{P}_{FR}$	1.05 (6)	0.76 (3)	1.39 (7)	1.02 (4)	2.16 (19)	1.39 (11)
$\mathcal{P}_{CH}$	0.93 (4)	0.72 (3)	1.27 (6)	0.90 (3)	1.21 (15)	1.00 (11)

TABLEAU VIII-14

Probabilités maximums, $\mathcal{P}_{\mu,max}$, déduites du modèle de FRENKEL et de la description par les harmoniques cubiques

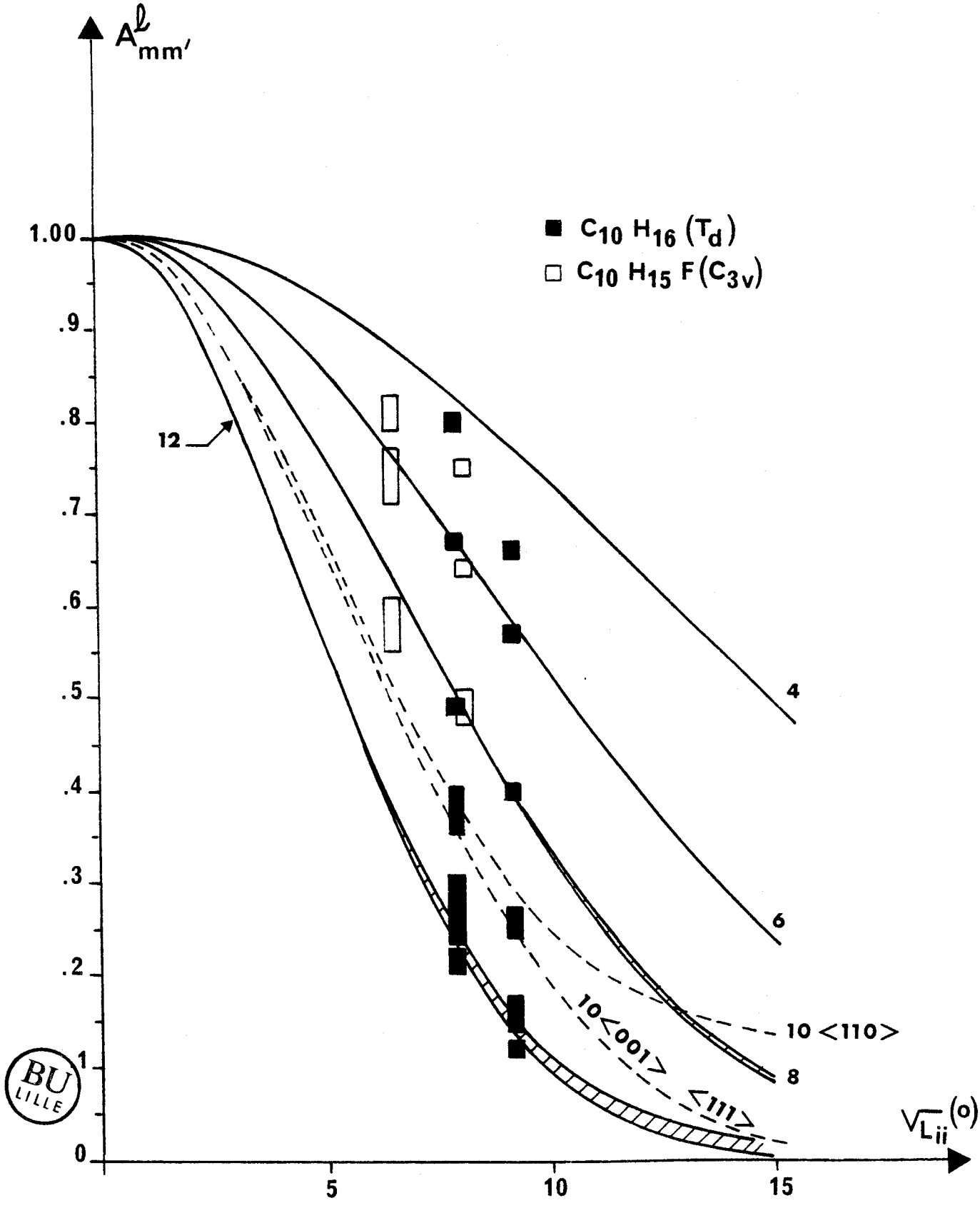

FIGURE VIII-11

Variations des coefficients A^{ℓ}_{mm}, calculés en fonction de $\sqrt{L_i}$

ANNEXE

CHAPITRE VIII

ANNEXE

CHAPITRE VIII

ANNEXE A - VIII - 1

I) FORMULATION GENERALE

Pour les librations isotropes, $\mathcal{C}_\mu^{HC}(\Omega)$ et $\mathcal{C}_\mu^{FR}(\Omega)$ ont la même symétrie et deviennent identiques :

$$\sum_{lmm'} A^l_{mm'} M^l_{m'} (\Omega^\mu_M) K^l_m (\Omega) = \frac{1}{2\pi NL} \sum_{j=1}^{N} \exp\left(-\frac{\theta'^2_{\mu j}}{2L}\right) \quad [A-1]$$

Ω^μ_M = angles polaires définissant l'atome μ dans la molécule.

N = nombre de positions d'équilibre

$\theta'_{\mu j}$ = angle de libration de l'atome μ dans la $j^{ième}$ position d'équilibre.

L = (L_i pour ADM ou $L_\perp$ pour l'axe Δ de FADM) est l'amplitude quadratique moyenne de libration.

Les propriétés d'orthonormalisation des fonctions K^l_m conduisent à :

$$\sum_{m'} A^l_{mm'} M^l_{m'} (\Omega^\mu_M) = \frac{1}{2\pi NL} \sum_{j=1}^{N} \int \exp\left(-\frac{\theta'^2_{\mu j}}{2L}\right) K^l_m (\Omega)\, d\Omega \quad [A-2]$$

Les positions d'équilibre et les fonctions K^l_m suivent la symétrie cubique. La valeur de l'intégrale dans [A - 2] est identique pour toutes les orientations j, d'où :

$$\sum_{m'} A^l_{mm'} M^l_{m'} (\Omega^\mu_M) = \frac{1}{2\pi L} \int \exp\left(-\frac{\theta'^2_\mu}{2L}\right) K^l_m (\Omega)\, d\Omega \quad [A-3]$$

II) MOLECULE FIXE : LIBRATION NULLE

Lorsque la molécule est fixe, l'atome est fixé par ses angles polaires dans le réseau (Ω^μ_R).

Dans ce cas, les coefficients $A^l_{mm'}(f)$ (f pour molécule fixe) sont donnés par :

$$\sum_{m'} A^l_{mm'}(f) M^l_{m'} (\Omega^\mu_M) = K^l_m (\Omega^\mu_R) \quad [A-4]$$

Pour une symétrie moléculaire T_d ou O_h [A - 4] devient :

$$\sum_{m'} A^l_{mm'}(f) K^l_{m'} (\Omega^\mu_M) = K^l_m (\Omega^\mu_R) \quad [A-5]$$

Cette relation se simplifie encore si les positions d'équilibre ont la symétrie du site ($\Omega^\mu_M = \Omega^\mu_R$).

$$\hat{A}^{1}_{mm'}(f) = \delta_{mm'} \qquad [A-6]$$

Pour l'axe C_3 (Δ) de FADM, les coefficients $\hat{\hat{A}}^{1}_{mm'}$ non nuls sont tels que m' = 1, et on trouve :

$$\hat{\hat{A}}^{1}_{m1}(f) = \sqrt{\frac{4\pi}{2l+1}}\, K^{1}_{m}(\Omega^{\Delta}_{R}) \qquad [A-7]$$

III) MOLECULES EFFECTUANT DES LIBRATIONS

Pour ADM, on obtient simplement les coefficients A^{1}_{mm} à partir de A - 3 :

$$\hat{A}^{1}_{mm} = \frac{1}{2\pi L_i K^{1}_{m}} \int \exp\left(-\frac{\theta'^{2}_{\mu}}{2 L_i}\right) K^{1}_{m}(\Omega)\, d\Omega \qquad [A-8]$$

De même, les termes $\hat{\hat{A}}^{1}_{m1}$ décrivant l'orientation de l'axe Δ de FADM s'écrivent :

$$\hat{\hat{A}}^{1}_{m1} = \frac{1}{2\pi L_\perp} \sqrt{\frac{4\pi}{2l+1}} \int_{\Omega} \exp\left(-\frac{\theta'^{2}}{2 L_\perp}\right) K^{1}_{m}(\Omega)\, d\Omega \qquad [A-9]$$

Dans les deux cas, les rapports $A^{1}/A^{1}(f)$ sont donnés par [A - 8]. Ils ne dépendent que des positions d'équilibre dans le réseau cubique de l'atome μ (ADM) ou de l'axe Δ (FADM).

L'équation [A - 8] a été programmée pour différentes valeurs de L et pour les orientations $<001>$, $<110>$ et $<111>$. Les courbes tracées sur la figure IX - 5 représentent les variations des coefficients A^{1}_{mm}, pour les ordres 4 à 12. Seuls les coefficients d'ordre 10 dépendent de l'orientation considérée et pour des angles de libration importants ($\geq 7°$).

FIGURES ET TABLEAUX

CHAPITRE IX

FIGURES ET TABLEAUX

CHAPITRE IX

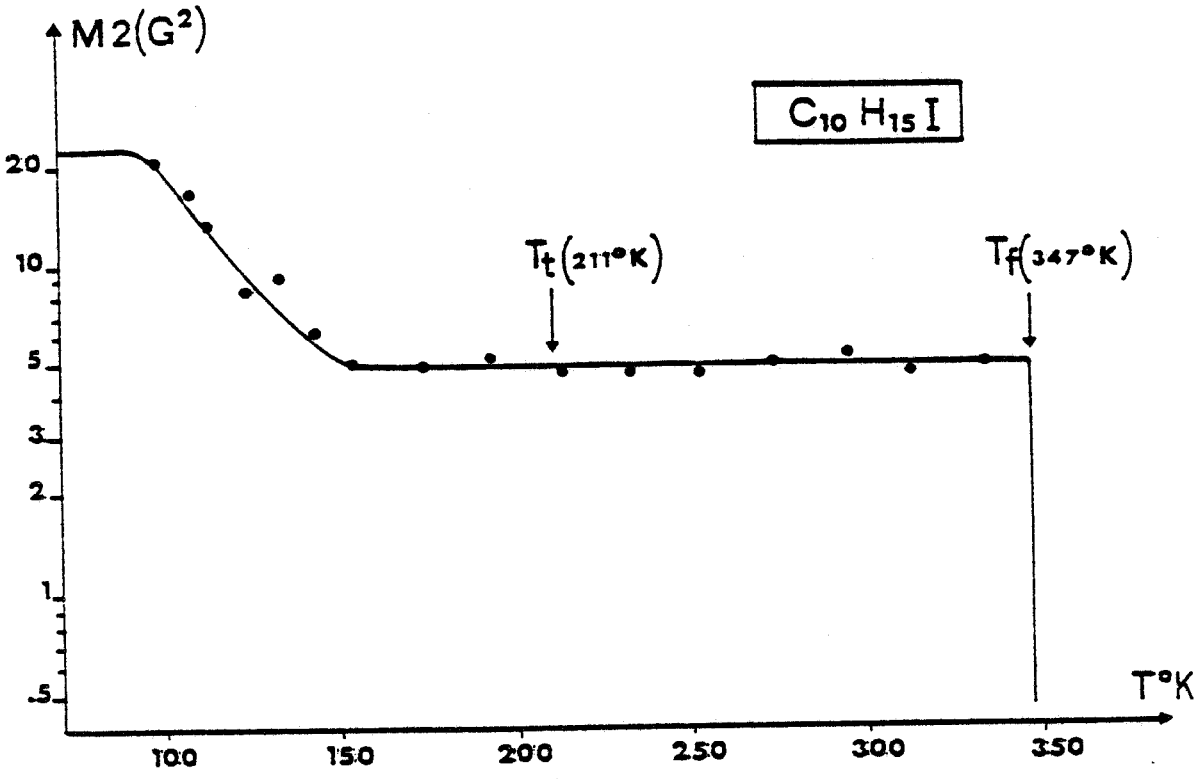

FIGURE IX-1a

Variation du second moment de la raie d'absorption en RMN ^{1}H

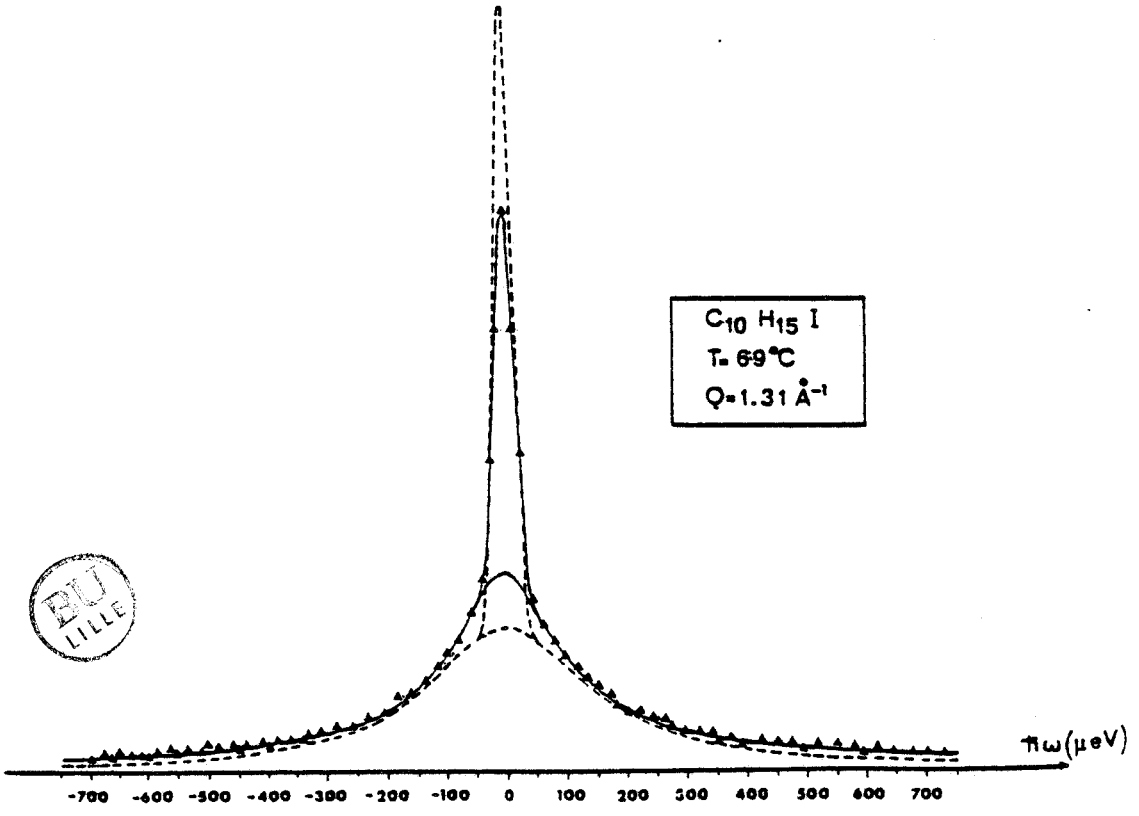

FIGURE IX-1b: Diffusion quasi-élastique incohérente des neutrons dans $C_{10}H_{15}I$. Ce spectre enregistré à 69°C correspond à un vecteur de diffusion Q = 1.31 $Å^{-1}$. Suivant l'ordre de la rotation uniaxiale, l'affinement correspondant est représenté par la courbe en pointillé : ordre 3, ou par la courbe continue : ordre 6.

	T = 295K	T = 256K
$\lambda_{MoK\bar{\alpha}}$	0.7107Å	0.7107Å
sin θ/λ	0.049 to 0.766 $Å^{-1}$	0.049 to 0.807 $Å^{-1}$
h	0 to 13	0 to 13
k	0 to 10	0 to 10
l	0 to 13	0 to 13
N_m	1813	1318
N_i	1120	1276
N	1060	1211
N_R	560	672
space group	P_{mmn}	P_{mmn}
a	8.676(17)Å	8.640(17)Å
b	6.703(13)Å	6.693(13)Å
c	8.860(17)Å	8.854(17)Å
Z	2	2
D_x	1.69g/cm^3	1.70g/cm^3
μ(cm^{-1})	30.85cm^{-1}	31.05cm^{-1}
F(000) =	256	256

(N_m, N_i, N, N_R) = number of intensities, measured, independant, non systematically absent, included in the refinement $F > 6\sigma(F)$)

TABLEAU IX-1

Collection des données de la Diffraction X
Paramètres cristallins : 1 IODOADAMANTANE : $C_{10}H_{15}I$

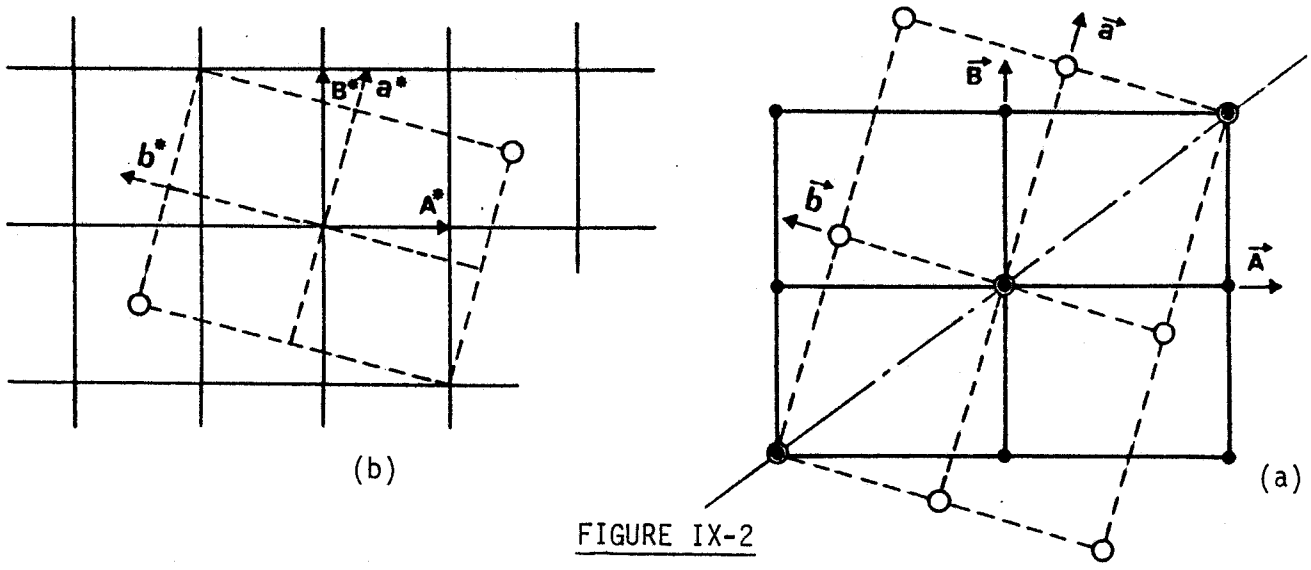

FIGURE IX-2

$\vec{A},\vec{B}$; $\vec{A}^*,\vec{B}^*$: vecteurs des réseaux direct et réciproque du gros individu
$\vec{a},\vec{b}$; $\vec{a}^*,\vec{b}^*$: vecteurs des réseaux direct et réciproque du petit individu

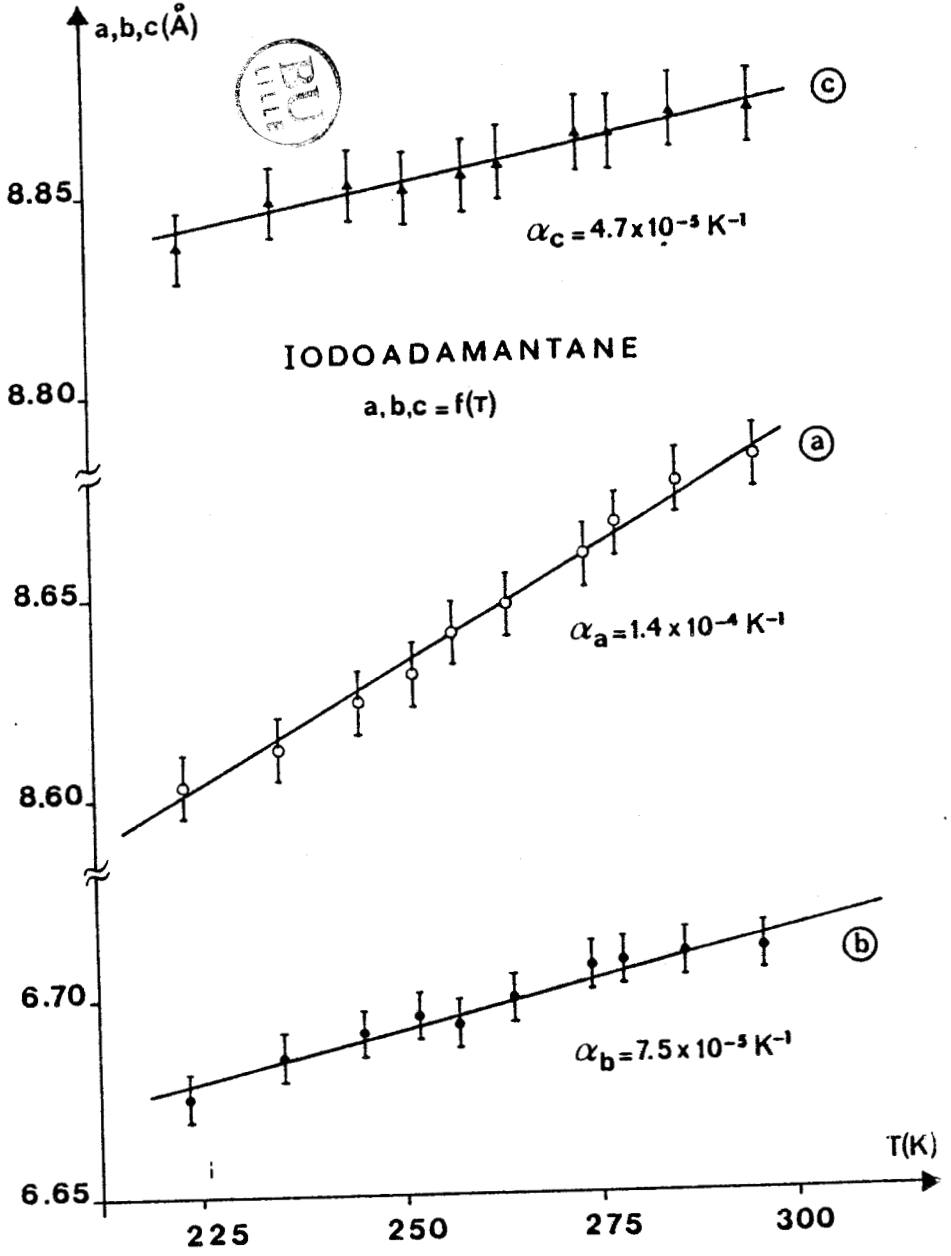

FIGURE IX-3

Variations des paramètres cristallins en fonction de la température : IADM

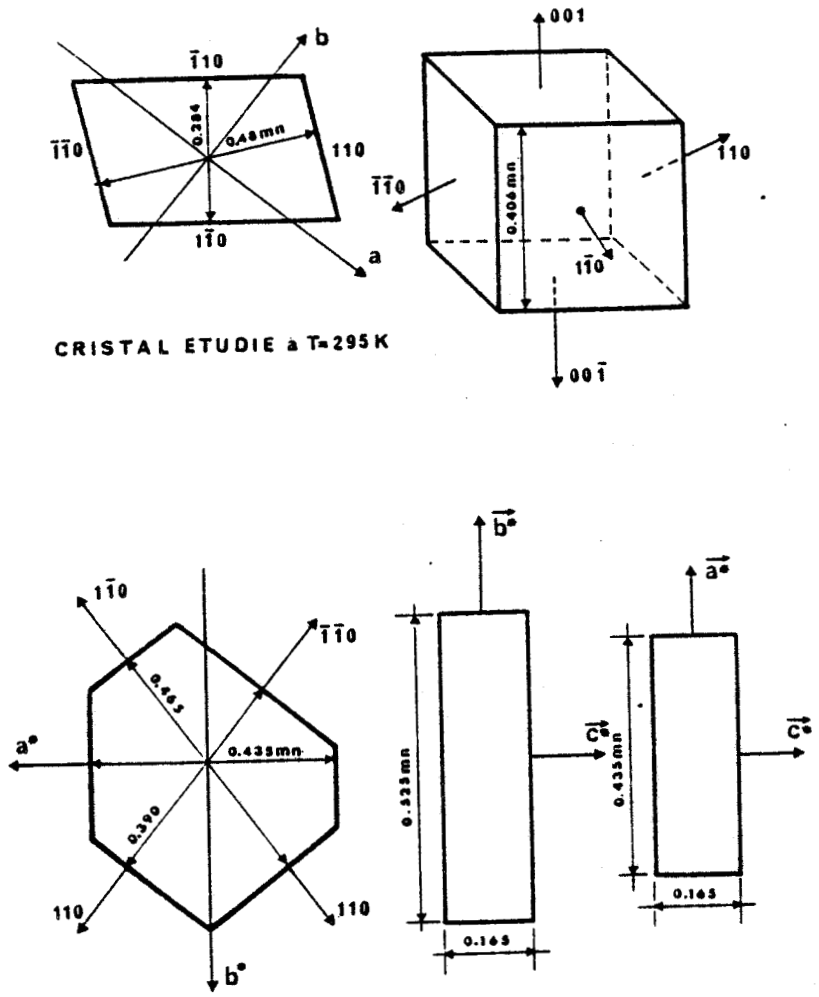

FIGURE IX-4

Formes et dimensions des deux cristaux étudiés : IADM

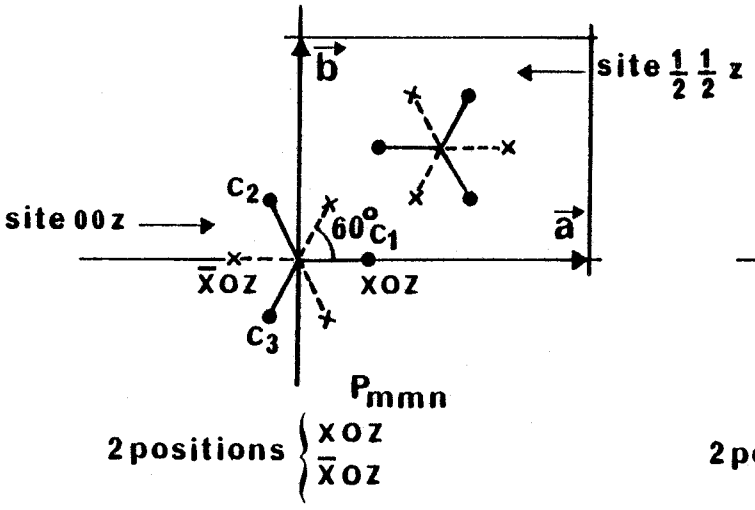

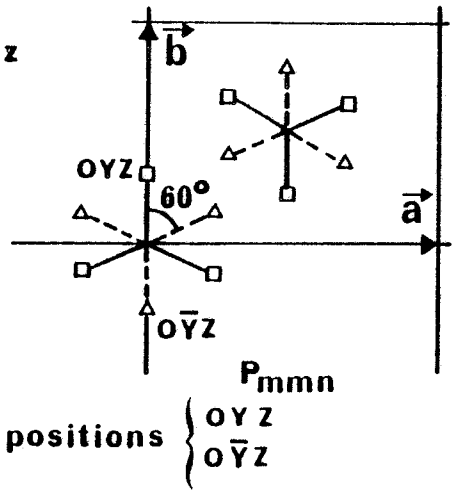

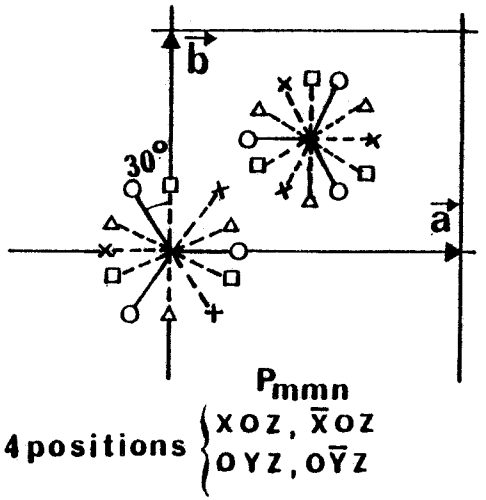

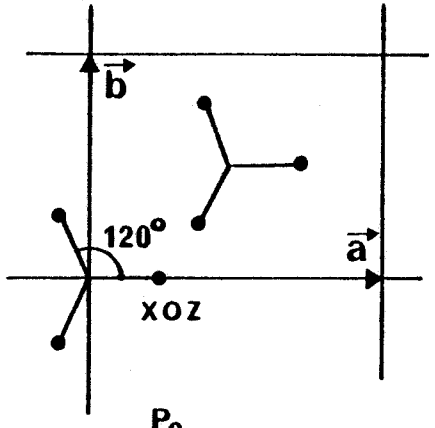

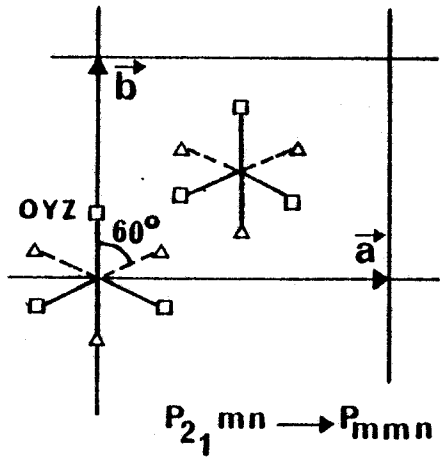

FIGURE IX-6

5 possibilités d'orientations et de désordre moléculaire autour de l'axe $\vec{c}$

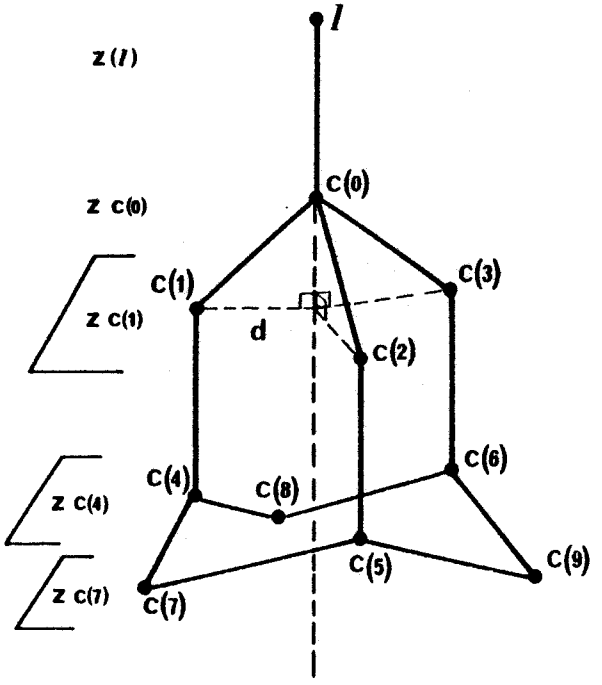

FIGURE IX-5

Numérotation atomique
Paramètres géométriques définissant la géométrie moléculaire

T = 256K

Positions of the molecule in 000 and 1/1 1/2 1/2 sites	Space group	R %	R_w %	N_T	ρ_{max} / ρ_{min} ($e/Å^3$)	d (QZ) Å	Refinement procedure	COMMENTS
I Iodine	P_{mmn} P_{2_1mn}	14.7	15.4	594	25.8 / -7.2	-	A	
XOZ (000) $\bar{X}OZ$(1/2 1/2 1/2)	$P_{2_1/m}$	6.8	7.5	675	2.4 / -3.0	1.434	A, distinct positions for the two sites	A.M.G. d(C(1) - C(4)) 1.74 Å
XOZ	P_{2_1mn}	4.1	4.4	672	3.4 / -2.5	1.425	A 1 orientation	H.R.E.D.
OYZ (1/2) $O\bar{Y}Z$ (1/2)	P_{mmn}	5.4	6	672	3.5 / -30	1.277	A 2 orientations	A.M.G. H.R.E.D. D.W.F. anomalies
$\bar{X}XZ$, $\bar{X}\bar{X}Z$, $X\bar{X}Z$, XXZ (1/4)	P_{mmn}	5.5	6	672	3.6 / -3.5	1.436	A 4 general orientations	H.R.E.D. σ high
XOZ, $\bar{X}OZ$ OYZ, $O\bar{Y}Z$ (1/4)	P_{mmn}	3.4	3.4	672	1.25 / -2.4	1.409	A 4 special orientations	A.M.G., D.W.F. anomalies; N_T of parameter x 2
XOZ, $\bar{X}OZ$ (0.95) OYZ, $O\bar{Y}Z$ (0.05)	P_{mmn}	13.1	13.5	672	17.4 / -8.		A for XOZ I for OYZ	Divergence
XOZ, $\bar{X}OZ$ (1/2)	P_{mmn}	3.5	3.8	672	1.3 / -2.5	1.425	A	Correct solution
T = 295K								
OYZ,$O\bar{Y}Z$ (1/2)	P_{mmn}	5.8	6.2	560	4.2 / -3.2	1.285	A	A.M.G. D.W.F. anomalies
XOZ, $\bar{X}OZ$ (1/2)	P_{mmn}	4.6	4.7	560	1.9 / -3.0	1.428	A	Correct solution

Abrevations for comments

A = Anisotropic Debye Waller factors

I = Isotropic Debye Waller factors

H.R.E.D. = high residual electronic density

D.W.F. = Debye Waller factors

A.M.G. = Anomalous molecular geometry

TABLEAU IX-2

Affinements par atomes indépendants

T = 256 K et T = 295 K

T = 256K

Positions in the 000 and 1/2 1/2 1/2 sites	Space group	RZ	R_wZ	$\sqrt{T_{11}}$ Å	$\sqrt{T_{22}}$ Å	$\sqrt{T_{33}}$ Å	$\sqrt{L_{11}}$(°)	$\sqrt{L_{22}}$(°)	$\sqrt{L_{33}}$(°)	$S_{12}\times10^{-4}$ (radxÅ)	$S_{21}\times10^{-4}$ (radxÅ)	N_T	Model
∞	P_{mmn}	5.8	10.0	0.219(7)	0.250(7)	0.186(1)	4.9(0.3)	3.9(0.4)	0	-149(7)	50(7)	674	C.E.D.
OYZ $O\bar{Y}Z$	P_{mmn}	6.4	12.3	0.217(10	0.273(10)	0.184(2)	3.9(0.6)	3.8(0.5)	27.5(1.5)	-114(11)	49(9)	674	Frenkel 2 positions
(XOZ-$\bar{X}$OZ)1/2 (OYZ-$O\bar{Y}Z$)1/2	P_{mmn}	6.5	6.7	0.232(14)	0.262(13)	0.182(2)	3.9(0.7)	2.6(1.0)	11.5(1.4)	-122(15)	30(14)	674	Frenkel 4 positions
XOZ-$\bar{X}$OZ	P_{mmn}	3.7	6.1	0.214(4)	0.265(4)	0.187(1)	4.5(0.2)	4.10(0.2)	12.4(0.3)	-124(4)	55(4)	674	Frenkel 2 positions
	T = 295K												
∞	P_{mmn}	6.2	10.8	0.247(9)	0.279(7)	0.199(1)	5.1(0.3)	4.3(0.5)	0	-175(80)	52(9)	557	C.E.D.
OYZ $O\bar{Y}Z$	P_{mmn}	7.8	14.6	0.255(12)	0.285(10)	0.198(2)	4.9(0.5)	4.0(0.7	25.7(1.4)	-159(11)	40(13)	557	Frenkel 2 positions
(XOZ-$\bar{X}$OZ)1/2 (OYZ-$O\bar{Y}Z$)1/2	P_{mmn}	6.3	10.9	0.243(8)	0.280(7)	0.199(1)	5.1(0.3)	4.6(0.4)	8.4(2.1)	-173(8)	57(8)	557	Frenkel 4 positions
XOZ $\bar{X}$OZ	P_{mmn}	4.5	7.5	0.238(5)	0.289(4)	0.199(1)	5.0(0.2)	4.6(0.3)	13.1(0.4)	-154(5)	64(5)	557	Frenkel 2 positions

TABLEAU IX-3

Affinements par groupe rigide

T = 256 K et T = 295 K

IODOADAMANTANE T=256K

	x	y	z	U
I	0 (1)	0 (1)	1565 (1)	73 (1)
C0	0 (1)	0 (1)	-927 (6)	43 (3)
C1	1649 (4)	0 (1)	-1441 (5)	77 (11)
C2	-828 (2)	-1849 (4)	-1441 (5)	61 (10)
C3	-829 (2)	1849 (4)	-1441 (5)	88 (10)
C4	1649 (4)	0 (1)	-3211 (7)	102 (18)
C5	-828 (2)	-1849 (4)	-3211 (7)	63 (11)
C6	-828 (2)	1849 (4)	-3211 (7)	83 (11)
C7	-1655 (4)	0 (1)	-3784 (7)	71 (13)
C8	823 (2)	1843 (4)	-3784 (7)	86 (15)
C9	823 (2)	-1843 (2)	-3784 (7)	116 (15)
H11	2236 (1)	1256 (1)	-1058 (1)	91 (9)
H12	2236 (1)	-1256 (1)	-1058 (1)	91 (9)
H21	-277 (1)	-3132 (1)	-1058 (1)	91 (9)
H22	-1963 (1)	-1874 (1)	-1058 (1)	91 (9)
H31	-277 (1)	3132 (1)	-1058 (1)	91 (9)
H32	-1963 (1)	1874 (1)	-1058 (1)	91 (9)
H4	2794 (1)	0 (1)	-3609 (1)	91 (9)
H5	-1309 (1)	-3128 (1)	-3610 (1)	91 (9)
H6	-1309 (1)	3128 (1)	-3610 (1)	91 (9)
H71	-2794 (1)	0 (1)	-3347 (1)	91 (9)
H72	-1706 (1)	0 (1)	-4919 (1)	91 (9)
H81	1397 (1)	3125 (1)	-3348 (1)	91 (9)
H82	849 (1)	1901 (1)	-4919 (1)	91 (9)
H91	1397 (1)	-3125 (1)	-3348 (1)	91 (9)
H92	849 (1)	-1901 (1)	-4919 (1)	91 (9)

Coordonnées atomiques

	U11	U22	U33	U23	U13	U12
I	704 (3)	1157 (5)	547 (2)	0 ( )	0 ( )	0 ( )
C0	428 (21)	515 (26)	358 (21)	0 ( )	0 ( )	0 ( )
C1	449 (36)	1395 (99)	451 (43)	0 ( )	17 (30)	0 ( )
C2	1184 (64)	731 (38)	479 (30)	51 (26)	-138 (30)	-464 (45)
C3	1184 (64)	731 (38)	479 (30)	-51 (26)	-138 (30)	464 (45)
C4	475 (47)	2016 (**)	442 (62)	0 (1)	145 (35)	0 (1)
C5	1255 (70)	525 (35)	599 (55)	-10 (27)	-161 (37)	-288 (40)
C6	1255 (70)	525 (35)	599 (55)	10 (27)	-161 (37)	288 (40)
C7	637 (60)	1242 (96)	479 (63)	0 (1)	-199 (41)	0 (1)
C8	1461 (87)	1095 (73)	472 (46)	113 (40)	8 (43)	-563 (67)
C9	1461 (87)	1095 (73)	472 (46)	-113 (40)	8 (43)	563 (67)
H11	917 (93)					
H12	917 (93)					
H21	917 (93)					
H22	917 (93)					
H31	917 (93)					
H32	917 (93)					
H4	917 (93)					
H5	917 (93)					
H6	917 (93)					
H71	917 (93)					
H72	917 (93)					
H81	917 (93)					
H82	917 (93)					
H91	917 (93)					
H92	917 (93)					

Tenseurs U_{ij} d'agitation thermique

I	- C0	2.207 (5)	C4	- C9	1.513 (4)	C2	- C5	- C7	109.5 (3)
C0	- C1	1.496 (4)	C4	- H4	1.051 (4)	C2	- C5	- C9	109.6 (3)
C0	- C2	1.500 (3)	C5	- C7	1.516 (4)	C2	- C5	- H5	110.4 (3)
C0	- C3	1.500 (3)	C5	- C9	1.514 (4)	C7	- C5	- C9	109.2 (3)
C1	- C4	1.567 (8)	C5	- H5	1.015 (3)	C7	- C5	- H5	112.3 (4)
C1	- H11	1.039 (2)	C6	- C7	1.516 (4)	C9	- C5	- H5	105.7 (3)
C1	- H12	1.039 (2)	C6	- C8	1.514 (4)	C3	- C6	- C7	109.5 (3)
C2	- C5	1.567 (8)	C6	- H6	1.015 (3)	C3	- C6	- C8	109.6 (3)
C2	- H21	1.038 (3)	C7	- H71	1.061 (4)	C3	- C6	- H6	110.4 (3)
C2	- H22	1.038 (2)	C7	- H72	1.006 (6)	C7	- C6	- C8	109.2 (3)
C3	- C6	1.567 (8)	C8	- H81	1.063 (3)	C7	- C6	- H6	112.3 (4)
C3	- H31	1.038 (3)	C8	- H82	1.006 (6)	C8	- C6	- H6	105.7 (3)
C3	- H32	1.038 (2)	C9	- H91	1.063 (3)	C5	- C7	- C6	109.4 (3)
C4	- C8	1.513 (4)	C9	- H92	1.006 (6)	C5	- C7	- H71	108.5 (3)
						C5	- C7	- H72	110.8 (4)
						C6	- C7	- H71	108.5 (3)
						C6	- C7	- H72	110.8 (4)
						H71	- C7	- H72	108.9 (4)
						C4	- C8	- C6	109.5 (3)
						C4	- C8	- H81	108.4 (3)
						C4	- C8	- H82	110.8 (4)
						C6	- C8	- H81	108.4 (3)
						C6	- C8	- H82	110.9 (4)
						H81	- C8	- H82	108.7 (4)
						C4	- C9	- C5	109.5 (3)
						C4	- C9	- H91	108.4 (3)
						C4	- C9	- H92	110.8 (4)
						C5	- C9	- H91	108.4 (3)
						C5	- C9	- H92	110.9 (4)
						H91	- C9	- H92	108.7 (4)

Distances intramoléculaires

I	- C0	- C1	107.7 (2)	C2	- C5	- C7	109.5 (3)
I	- C0	- C2	107.7 (2)	C2	- C5	- C9	109.6 (3)
I	- C0	- C3	107.7 (2)	C2	- C5	- H5	110.4 (3)
C1	- C0	- C2	111.2 (3)	C7	- C5	- C9	109.2 (3)
C1	- C0	- C3	111.2 (3)	C7	- C5	- H5	112.3 (4)
C2	- C0	- C3	111.2 (3)	C9	- C5	- H5	105.7 (3)
C0	- C1	- C4	107.7 (3)	C3	- C6	- C7	109.5 (3)
C0	- C1	- H11	111.4 (3)	C3	- C6	- C8	109.6 (3)
C0	- C1	- H12	111.4 (3)	C3	- C6	- H6	110.4 (3)
C4	- C1	- H11	109.1 (3)	C7	- C6	- C8	109.2 (3)
C4	- C1	- H12	109.1 (3)	C7	- C6	- H6	112.3 (4)
H11	- C1	- H12	108.1 (3)	C8	- C6	- H6	105.7 (3)
C0	- C2	- C5	107.7 (3)	C5	- C7	- C6	109.4 (3)
C0	- C2	- H21	111.4 (3)	C5	- C7	- H71	108.5 (3)
C0	- C2	- H22	111.4 (3)	C5	- C7	- H72	110.8 (4)
C5	- C2	- H21	109.1 (3)	C6	- C7	- H71	108.5 (3)
C5	- C2	- H22	109.1 (3)	C6	- C7	- H72	110.8 (4)
H21	- C2	- H22	108.2 (3)	H71	- C7	- H72	108.9 (4)
C0	- C3	- C6	107.7 (3)	C4	- C8	- C6	109.5 (3)
C0	- C3	- H31	111.4 (3)	C4	- C8	- H81	108.4 (3)
C0	- C3	- H32	111.4 (3)	C4	- C8	- H82	110.8 (4)
C6	- C3	- H31	109.1 (3)	C6	- C8	- H81	108.4 (3)
C6	- C3	- H32	109.1 (3)	C6	- C8	- H82	110.9 (4)
H31	- C3	- H32	108.2 (3)	H81	- C8	- H82	108.7 (4)
C1	- C4	- C8	109.6 (3)	C4	- C9	- C5	109.5 (3)
C1	- C4	- C9	109.6 (3)	C4	- C9	- H91	108.4 (3)
C1	- C4	- H4	109.6 (3)	C4	- C9	- H92	110.8 (4)
C8	- C4	- C9	109.3 (3)	C5	- C9	- H91	108.4 (3)
C8	- C4	- H4	109.4 (3)	C5	- C9	- H92	110.9 (4)
C9	- C4	- H4	109.4 (3)	H91	- C9	- H92	108.7 (4)

Angles intramoléculaires

Résultats cristallographiques

TABLEAU IX-4

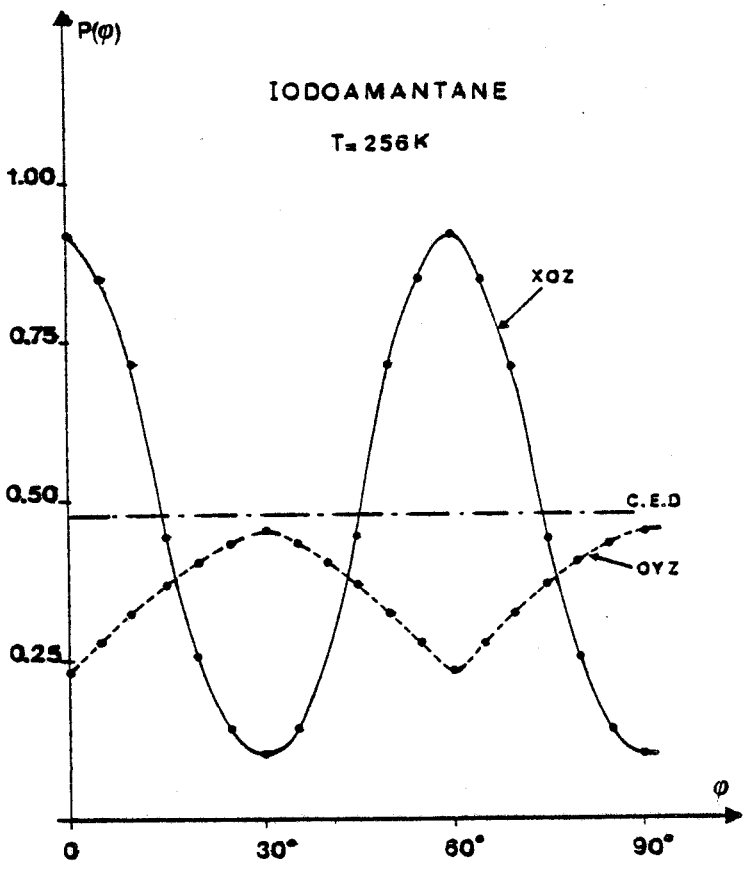

FIGURE IX-7

Probabilité rotationnelle pour 3 modèles : $P(\varphi)$

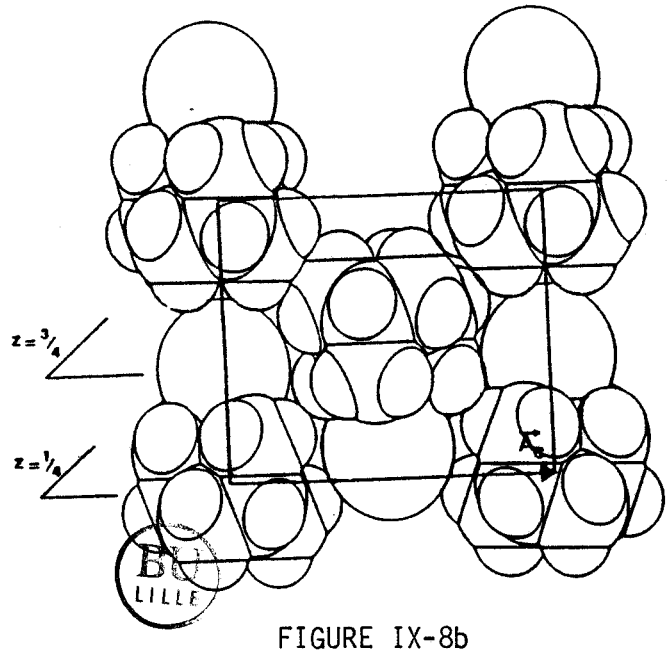

FIGURE IX-8b

Projection de la structure // $\vec{B}_c = (\vec{a}+\vec{b})/2$ qui montre l'ordre antiferroélectrique

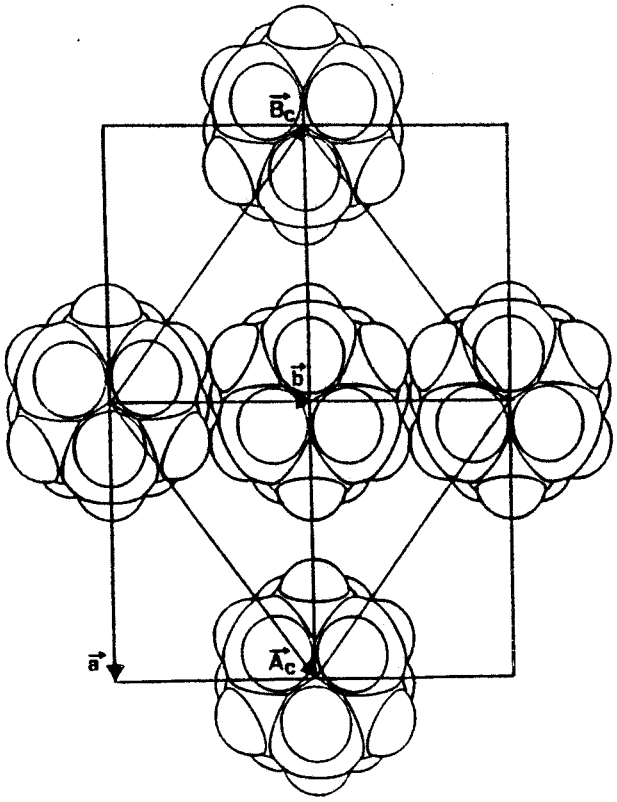

FIGURE IX-8a

Projection de la structure // $\vec{c}$

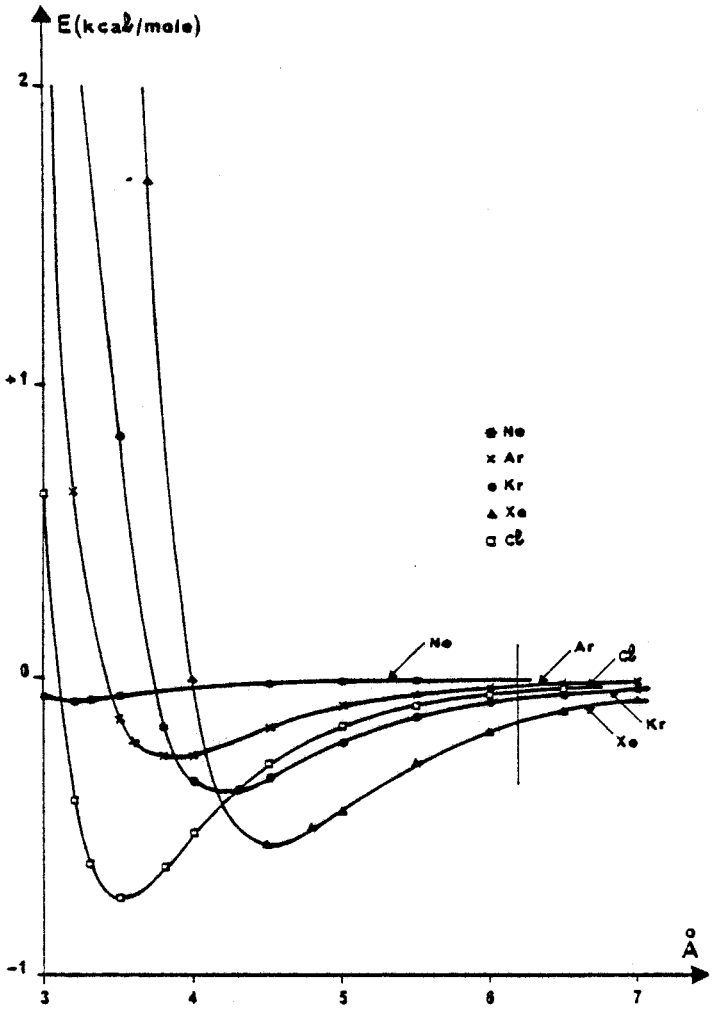

FIGURE IX-9

Potentiels atome-atome des gaz rares

E (kcal/mole) = f(r)

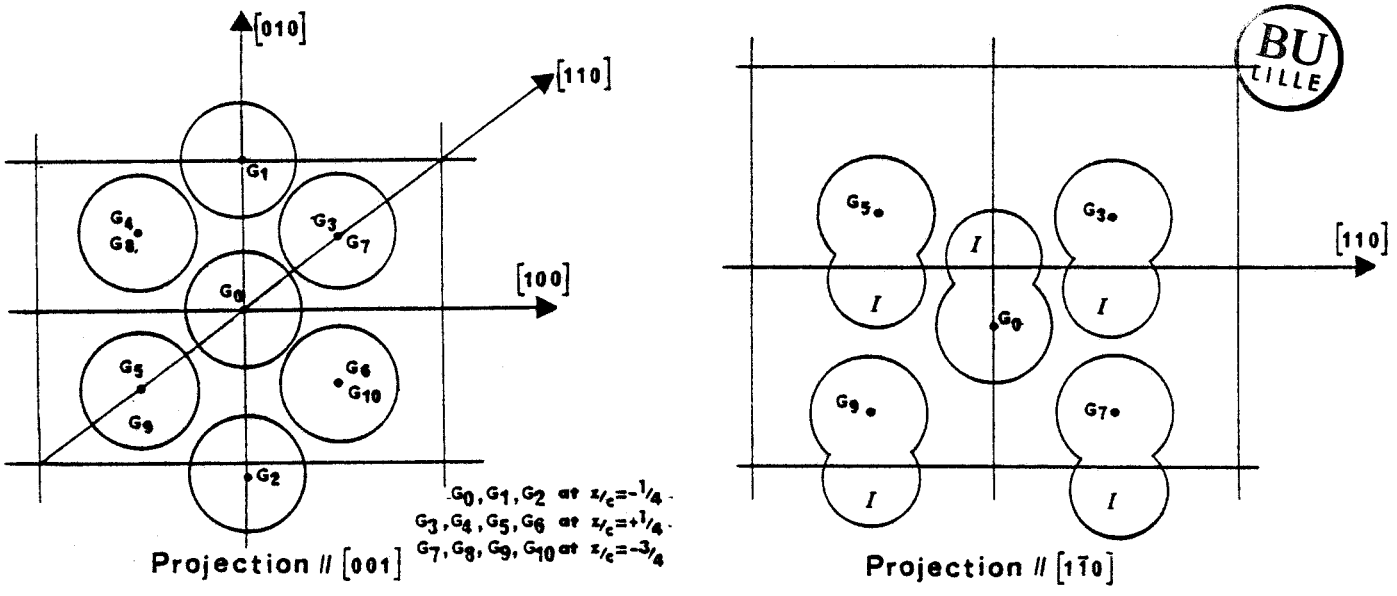

FIGURE IX-10

Projections schématisées des molécules

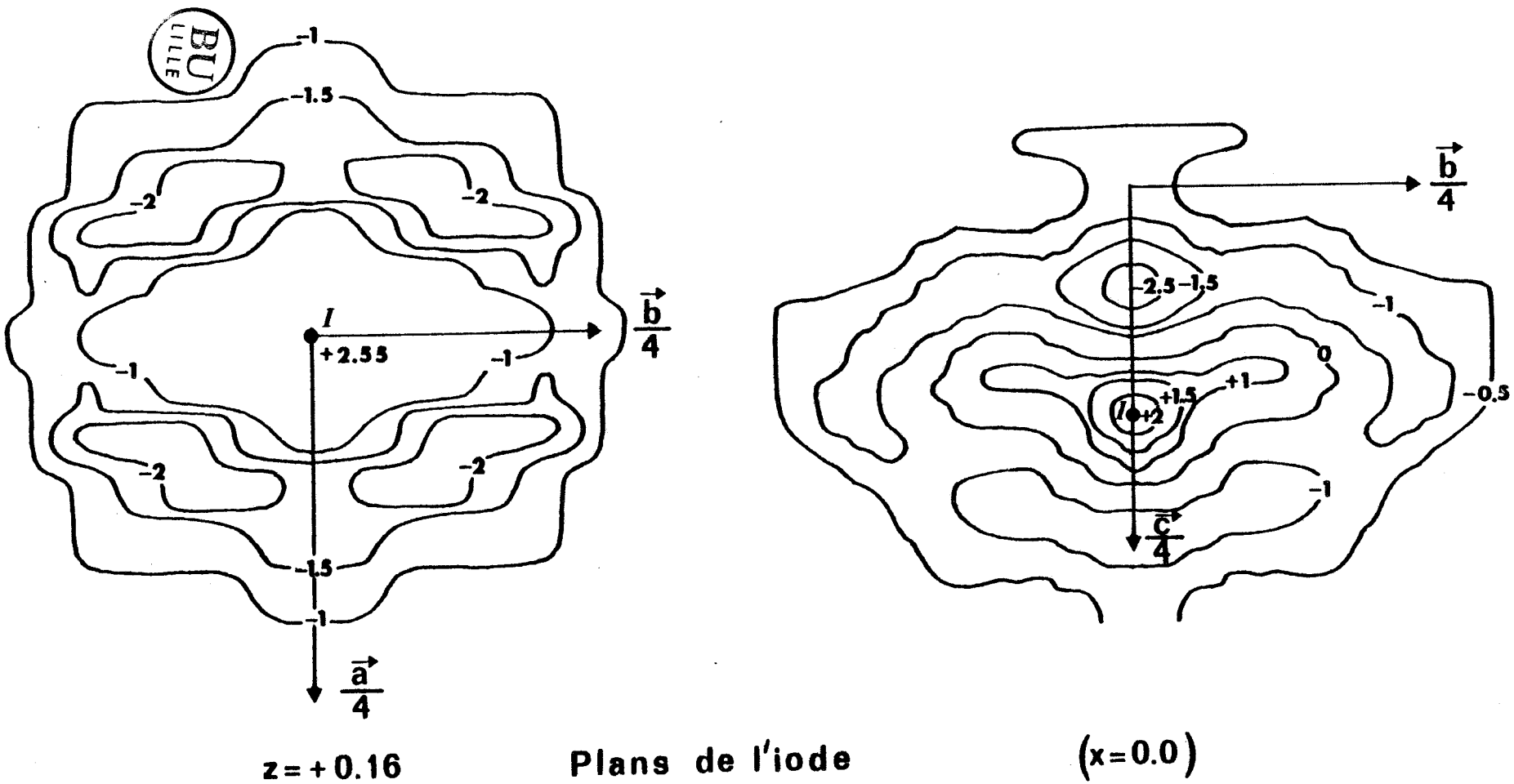

z = +0.16 **Plans de l'iode** (x=0.0)

FIGURE IX-11

Densité électronique résiduelle ($e/\mathring{A}^3$)

FIGURES ET TABLEAUX

CHAPITRE X

FIGURES ET TABLEAUX

CHAPITRE X

Modèle	RW %	R %	nombre de paramètres	N	$\sqrt{U_{//}^2}$ (Å)	$\sqrt{U_{\perp}^2}$ (Å)	$\sqrt{\Theta_{//}^2}$ °	$\sqrt{\Theta_{\perp}^2}$ °	Exentrement Å	Nbre de positions d'équilibre	Références	T(K)
FRENKEL	18.1	9	5	112	0.409 (0.017)	0.324 (0.017)	28.0 (2.0)	8.1 (0.3)	0	24 { 6 <001> 4 (C_3)	[2]	295
D.E.C.	22.0		4	112	0.391 (0.027)	0.295 (0.025)	fixé 0	8.6 (0.4)	0	6 6 <001>	[2]	295
F.A.S.	13.8		10	112	$\sqrt{<u^2x>}$ 0.41 (0.03)	—	—	7°	0	—	[2]	295

TABLEAU X-1

Chloroadamantane : phase plastique

			τ_o	E(kJ/mole)	τ	τ	Références
BROMOADAMANTANE	PHASE I	τ_D	5.4×10^{-16}	81.0	$T_f = 396.5$ 2.5×10^{-5}	$T_{t_2} = 310.5$ K 2.3×10^{-2}	[4]
		τ_{RE}	2.2×10^{-16}	32.0	3.6×10^{-12}	5.3×10^{-11}	
	PHASE II	τ_{M_6}	8.4×10^{-15}	21.4	$T_{t_2} = 310.5$ 3.34×10^{-11}	$T_{t_1} = 279$ K 8.5×10^{-11}	[4]
	PHASE III	τ_{M_3}	7.9×10^{-16}	31.0	$T_{t_1} = 279$ K 5.0×10^{-10}	T = 150 K 4.9×10^{-5}	
CHLOROADAMANTANE	PHASE I	τ_{C_3}	1.09×10^{-14}	10.28	$T_f = 442.5$ K 1.8×10^{-13}	$T_t = 244.2$ K 1.7×10^{-12}	[5]
		$\tau_{M_{12}}$	1.23×10^{-14}	21.41	4.1×10^{-12}	4.7×10^{-10}	
	PHASE III	τ_{M_3}	—	—	—	—	

τ_D : Diffusion translationnelle

$\tau_{R,E}$: Rotation endosphérique

τ_{C_3} : Réorientation autour des axes 3 cristallins

τ_{M_p} : Rotation d'ordre p autour de l'axe C_3 moléculaire

TABLEAU X-2

	Mode de scan	Domaine angulaire Θ°	Vitesse du balayage (°/s)	Largeur du balayage en °	N	N_{NE}	Nt ($F > 3\sigma$)
T = 295 K	Θ - 2Θ	0° - 30°	0.01	1°.2	121	103	34
T = 275 K	Θ - 2Θ	0° - 31°	0.02	1°.2	305	110	45

N : Nombre total de raies enregistrées

N_{NE} : Nombre de raies non équivalentes

N_t : Nombre de raies gardées pour l'affinement telles que $F_o > 3\sigma$

TABLEAU X-3

Chloroadamantane : phase plastique

conditions d'enregistrement de la diffraction

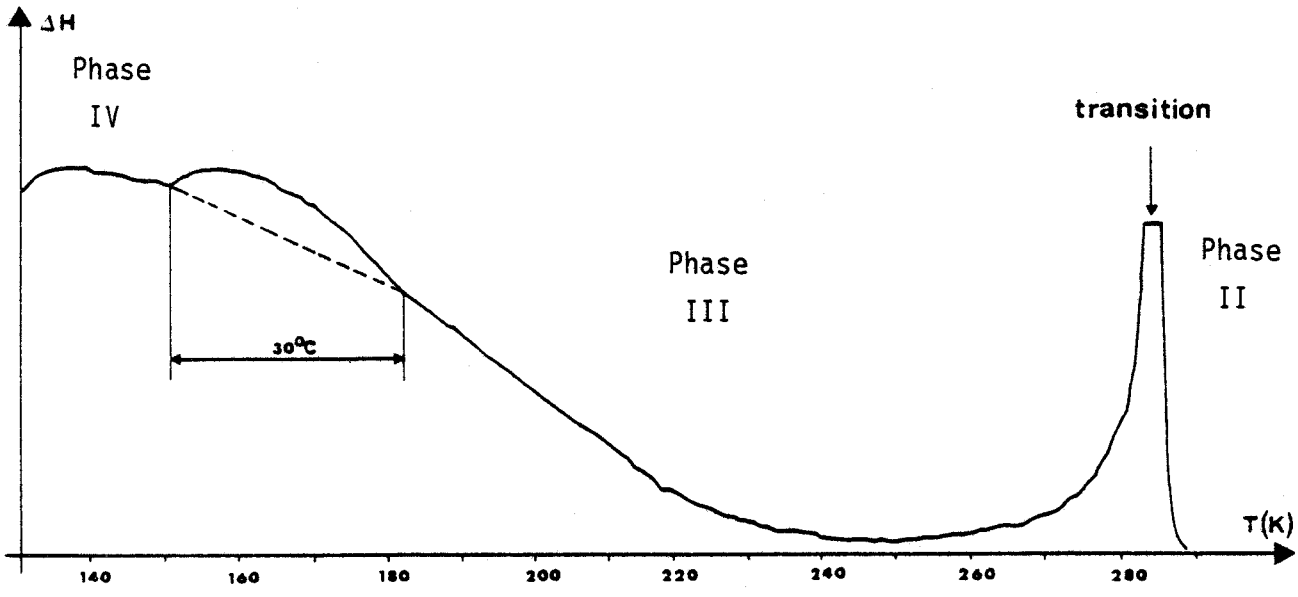

FIGURE X-1

1-Bromoadamantane : Thermogramme mettant en évidence la transition IV → III

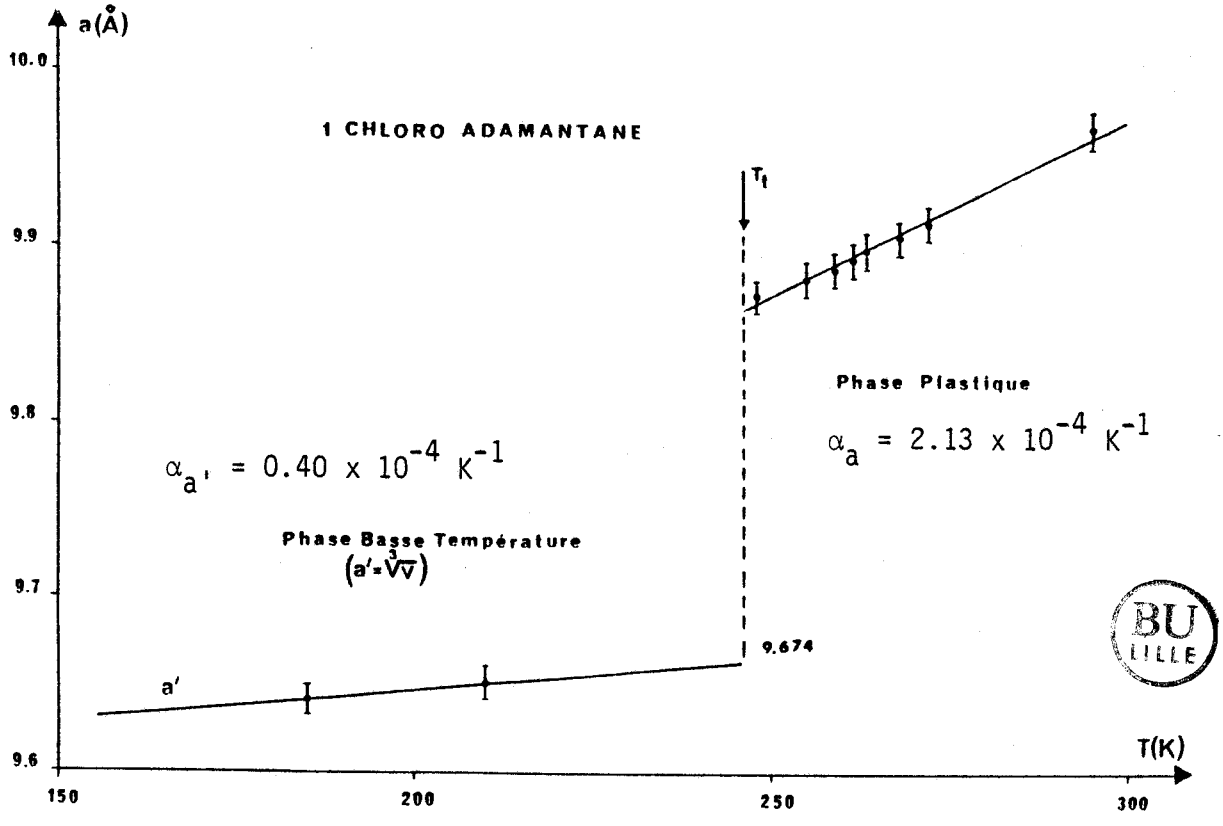

FIGURE X-2

1-Chloroadamantane : Variations des paramètres a (phase cubique) et a' = $\sqrt[3]{V_{III}}$ (phase III) en fonction de la température

T (K)	U_3 (Å)	$\sqrt{T_{11}}$ (Å) $= \sqrt{u^2_\perp}$	$\sqrt{T_{33}}$ (Å) $= \sqrt{u^2_{//}}$	$\sqrt{L_{11}}$ (°) $= \sqrt{\Theta^2_\perp}$	Sans les raies (200) et (111)			Avec les raies (200) et (111)			Avec toutes les raies		
					R %	R_w %	N	R %	R_w %	N	R %	R_w %	N
257 K	-0.046 (9)	0.271 (11)	$= \sqrt{T_{11}}$	4.65 (0.26)	9.4	9.0	31	7.7	8.9	33	10.1	11.8	45
295 K	-0.028 (17)	0.326 (15)	$= \sqrt{T_{11}}$	5.20 (0.42)	13.8	11.0	26	11.7	11.1	28	13.1	11.5	34
257 K	-0.036 (10)	0.236 (19)	0.287 (12)	5.20 (0.30)	9.8	8.1	31	7.8	8.0	33	10.4	10.9	45
295 K	-0.024 (17)	0.300 (28)	0.339 (17)	5.61 (0.50)	13.8	10.6	26	12.2	10,9	28	13,6	11.3	34

U_3 = excentrement : distance G_{ADA} à l'origine du réseau

N = nombre de raies pour le calcul de R et R_w

Affinement par le modèle D.E.C.

CHLOROADAMANTANE

Résultats d'affinements

TABLEAU X-4

groupe spatial	R_w %	R %	$\sqrt{u^2_{//}}$ Å	$\sqrt{u^2_\perp}$ Å	$\sqrt{\Theta^2_{//}}$ °	$\sqrt{\Theta^2_\perp}$ °	Excentrement Å	nombre de positions d'équilibre	Raccourcissement	modèle	NT $F_o/\sigma \geq 3$	Références	nombre paramètres affin
m 3 m	11.5	11.7	0.383 (0.044)	0.340 (0.024)	18.7 (5.0)	4.9 (0.5)	0.016 (0.048)	6 <001> 4 (C_3)	Isotrope	Frenkel	39	Notre étude	6
$\bar{4}$ 3 m	11.5	11.8	0.383 (0.061)	0.342 (0.024)	18.0 (13.0)	4.9 (0.7)	0.013 (0.087)	6 <001> 2 (C_3)	Isotrope	Frenkel	39	"	6
m 3 m D.E.C	11.9	12.3	0.377 (0.048)	0.352 (0.024)	Fixé 0	4.6 (0.5)	- 0.03 (0.04)	6 <001>		D.E.C.	39	"	5
m 3 m	12.0	12.3	0.374 (0.012)	$=\sqrt{u^2_{//}}$	13.1 (8.9)	4.2 (0.3)	fixé 0	6 <001> 4 (C_3)	Isotrope	Frenkel	39	"	4
m 3 m D.E.C	12.2	12.6	0.374 (0.012)	$=\sqrt{u^2_{//}}$	Fixé 0	4.1 (0.3)	Fixé 0	6 <001>	0	D.E.C.	39	"	3

TABLEAU X-5

Bromo-adamantane : Phase Plastique $T \simeq 323$ K

Résultats d'affinements

FIGURE X-4

BROMOADAMANTANE

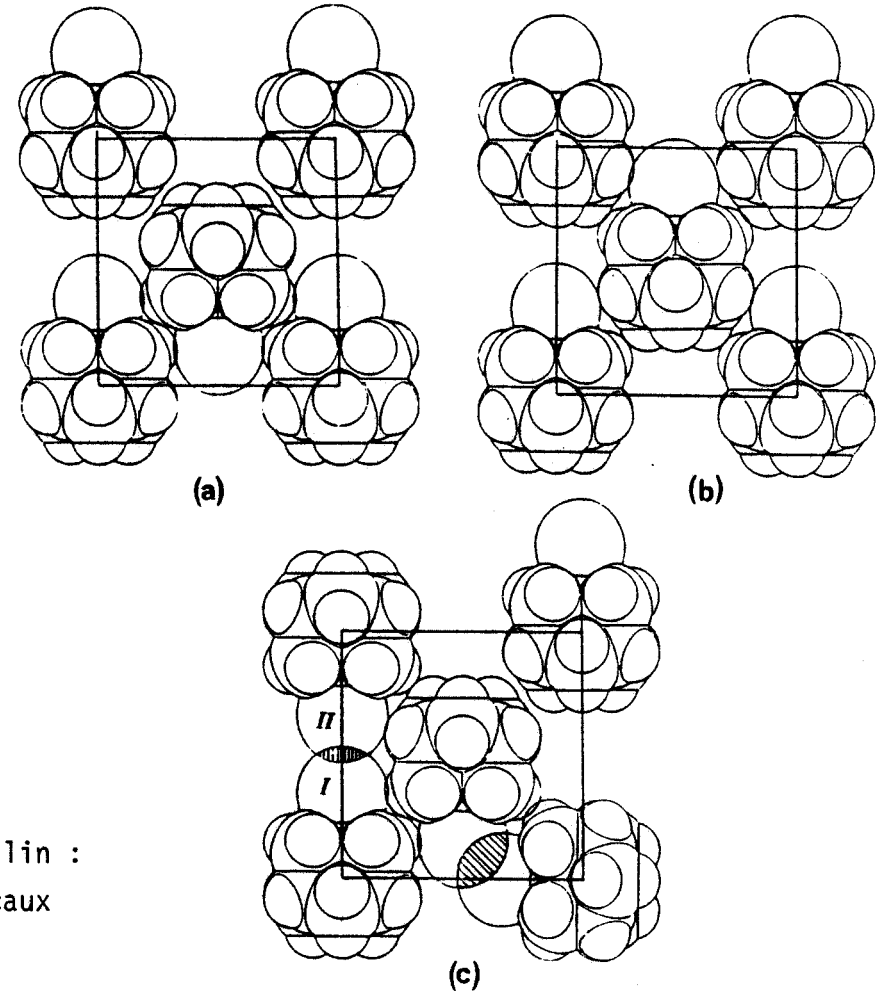

Projections des structures
le long d'un axe 4 cristallin :

Exemple d'arrangements locaux

a) antiferroélectrique

b) ferroélectrique

c) orientations
impossibles

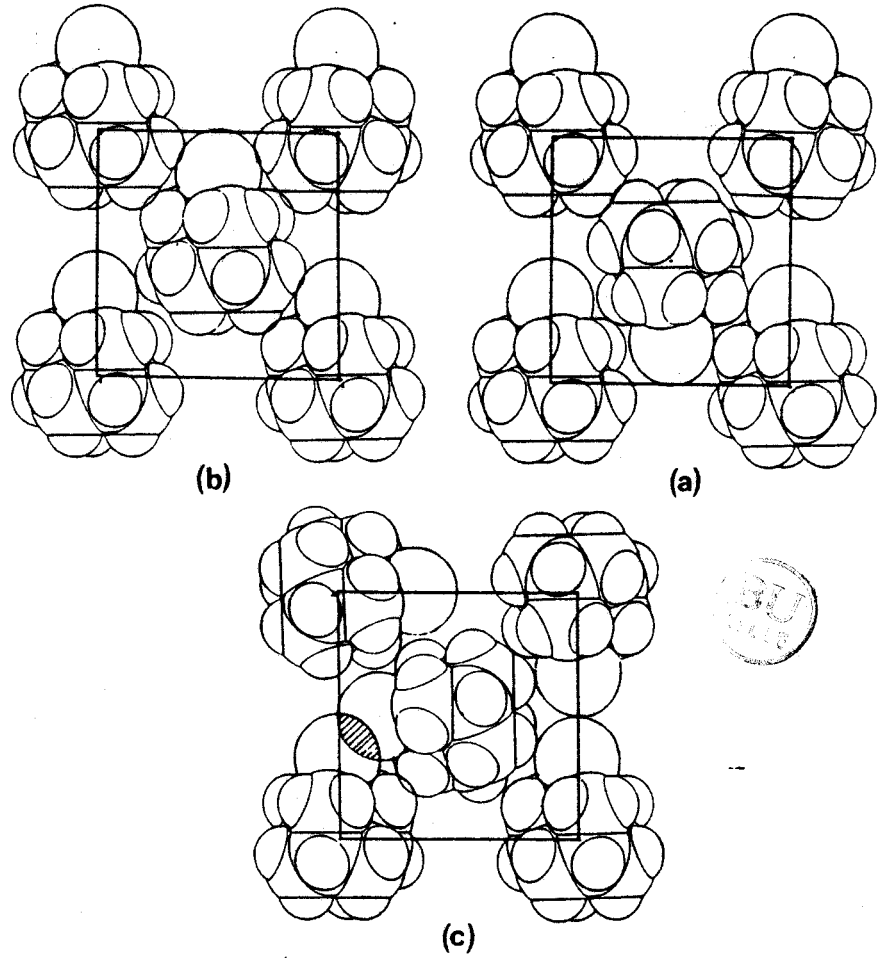

FIGURE X-5

CHLOROADAMANTANE

CHLOROADAMANTANE PHASE III T=210K R = 3.38 % R_w = 3.81 %

CL	- C0	1.827 (3)	C4	- C8	1.521 (4)
C0	- C1	1.522 (3)	C4	- H4	0.999 (30)
C0	- C2	1.527 (4)	C5	- C7	1.525 (4)
C0	- C3	1.522 (4)	C5	- C9	1.522 (4)
C1	- C4	1.525 (4)	C5	- H5	0.991 (22)
C1	- H11	0.994 (27)	C6	- C8	1.526 (4)
C1	- H12	0.987 (28)	C6	- C9	1.522 (4)
C2	- C5	1.527 (4)	C6	- H6	0.870 (27)
C2	- H21	0.991 (30)	C7	- H71	0.917 (27)
C2	- H22	0.867 (29)	C7	- H72	0.982 (27)
C3	- C6	1.525 (4)	C8	- H81	0.947 (29)
C3	- H31	0.987 (27)	C8	- H82	0.960 (30)
C3	- H32	0.968 (28)	C9	- H91	0.908 (29)
C4	- C7	1.534 (4)	C9	- H92	0.893 (33)

CL	- C0	- C1	108.4 (2)	C2	- C5	- C7	109.2 (2)
CL	- C0	- C2	108.5 (2)	C2	- C5	- C9	109.6 (2)
CL	- C0	- C3	109.7 (2)	C2	- C5	- H5	108.4 (13)
C1	- C0	- C2	110.5 (2)	C7	- C5	- C9	109.7 (2)
C1	- C0	- C3	110.2 (2)	C7	- C5	- H5	110.2 (13)
C2	- C0	- C3	109.5 (2)	C9	- C5	- H5	109.8 (13)
C0	- C1	- C4	108.5 (2)	C3	- C6	- C8	109.3 (2)
C0	- C1	- H11	110.0 (15)	C3	- C6	- C9	110.1 (2)
C0	- C1	- H12	108.2 (16)	C3	- C6	- H6	108.8 (17)
C4	- C1	- H11	111.0 (15)	C8	- C6	- C9	109.9 (2)
C4	- C1	- H12	109.6 (16)	C8	- C6	- H6	108.7 (17)
H11	- C1	- H12	109.4 (22)	C9	- C6	- H6	110.0 (17)
C0	- C2	- C5	108.9 (2)	C4	- C7	- C5	109.7 (2)
C0	- C2	- H21	106.1 (16)	C4	- C7	- H71	110.1 (16)
C0	- C2	- H22	109.3 (19)	C4	- C7	- H72	111.7 (15)
C5	- C2	- H21	110.6 (16)	C5	- C7	- H71	109.4 (16)
C5	- C2	- H22	109.8 (19)	C5	- C7	- H72	108.2 (15)
H21	- C2	- H22	112.0 (25)	H71	- C7	- H72	107.7 (22)
C0	- C3	- C6	108.7 (2)	C4	- C8	- C6	109.4 (2)
C0	- C3	- H31	110.5 (15)	C4	- C8	- H81	107.5 (17)
C0	- C3	- H32	110.1 (16)	C4	- C8	- H82	110.1 (18)
C6	- C3	- H31	110.9 (15)	C6	- C8	- H81	109.5 (17)
C6	- C3	- H32	109.1 (16)	C6	- C8	- H82	109.8 (18)
H31	- C3	- H32	107.6 (22)	H81	- C8	- H82	110.5 (25)
C1	- C4	- C7	109.4 (2)	C5	- C9	- C6	109.0 (2)
C1	- C4	- C8	110.0 (2)	C5	- C9	- H91	112.1 (17)
C1	- C4	- H4	108.9 (16)	C5	- C9	- H92	107.3 (21)
C7	- C4	- C8	109.0 (2)	C6	- C9	- H91	110.1 (17)
C7	- C4	- H4	108.7 (16)	C6	- C9	- H92	110.7 (21)
C8	- C4	- H4	110.8 (16)	H91	- C9	- H92	107.5 (27)

TABLEAU X-8

Distances et angles intramoléculaires

Chloroadamantane Phase III : T = 210 K

CHLOROADAMANTANE PHASE III T=210K

	X	Y	Z	U
CL	2718 (1)	6266 (1)	3050 (1)	52 (1)
C0	2610 (2)	4515 (4)	2001 (2)	35 (2)
C1	1145 (2)	4036 (4)	1814 (2)	44 (3)
C2	3224 (3)	5449 (4)	1057 (2)	39 (2)
C3	3378 (3)	2663 (4)	2274 (2)	48 (3)
C4	1051 (2)	2589 (4)	933 (2)	40 (3)
C5	3123 (2)	4003 (4)	173 (2)	42 (2)
C6	3279 (3)	1231 (4)	1386 (2)	50 (3)
C7	1658 (3)	3516 (4)	-22 (2)	43 (3)
C8	1816 (3)	728 (4)	1192 (3)	48 (3)
C9	3884 (3)	2138 (4)	436 (2)	41 (3)
H91	4768 (29)	2366 (37)	535 (20)	47 (6)
H92	3805 (31)	1327 (43)	-94 (27)	64 (7)
H11	640 (24)	5255 (42)	1661 (18)	43 (6)
H12	784 (26)	3428 (37)	2436 (22)	44 (6)
H21	4171 (30)	5713 (37)	1230 (21)	48 (6)
H22	2793 (24)	6514 (42)	909 (21)	48 (7)
H31	4319 (27)	2976 (36)	2430 (19)	40 (6)
H32	2998 (27)	2061 (39)	2873 (22)	45 (6)
H4	90 (30)	2292 (36)	796 (21)	50 (7)
H5	3519 (20)	4622 (32)	-437 (17)	24 (5)
H6	3705 (25)	162 (41)	1545 (19)	41 (6)
H71	1206 (25)	4641 (41)	-189 (19)	44 (6)
H72	1608 (25)	2628 (37)	-609 (21)	44 (6)
H81	1749 (25)	-121 (44)	624 (21)	49 (6)
H82	1442 (24)	122 (46)	1785 (23)	59 (7)

	U11	U22	U33	U23	U13	U12
CL	627 (5)	607 (5)	417 (4)	-145 (3)	8 (3)	47 (4)
C0	389 (13)	336 (15)	302 (12)	-18 (10)	20 (10)	44 (10)
C1	309 (13)	443 (16)	441 (14)	67 (13)	56 (11)	74 (12)
C2	385 (14)	298 (13)	411 (13)	28 (11)	40 (11)	14 (11)
C3	386 (14)	473 (16)	401 (14)	126 (13)	2 (12)	79 (13)
C4	270 (13)	419 (15)	587 (16)	-16 (13)	-20 (12)	-14 (11)
C5	378 (13)	367 (13)	342 (12)	61 (11)	62 (10)	58 (11)
C6	398 (14)	300 (14)	588 (16)	111 (13)	-12 (12)	130 (11)
C7	417 (14)	427 (16)	396 (14)	-11 (13)	-53 (11)	121 (12)
C8	461 (15)	346 (15)	644 (19)	38 (14)	38 (14)	-60 (12)
C9	333 (14)	386 (15)	489 (16)	-50 (13)	20 (12)	67 (11)
H91	478 (68)					
H92	646 (79)					
H11	430 (64)					
H12	449 (65)					
H21	489 (67)					
H22	487 (71)					
H31	405 (61)					
H32	458 (64)					
H4	546 (71)					
H5	249 (51)					
H6	410 (63)					
H71	448 (65)					
H72	442 (64)					
H81	492 (67)					
H82	590 (73)					

TABLEAU X-7

Coordonnées atomiques, tenseurs d'agitation thermique

Chloroadamantane Phase III : T = 210 K

	11	22	33	12	13	23	21	31	32
Tenseur L ^{o2} à partir des U_{ij}	16.28 (0.96)	14.27 (1.45)	18.40 (1.54)	-3.74 (0.92)	-1.96 (0.94)	4.60 (1.03)	$= L_{12}$	$= L_{13}$	$= L_{23}$
Tenseur L ^{o2} groupe rigide (ORION)	16.61 (0.82)	15.46 (1.21)	21.50 (1.31)	-3.58 (0.66)	-1.25 (0.79)	4.27 (0.72)	$= L_{12}$	$= L_{13}$	$= L_{23}$
Tenseur T en A^{o2} à partir des U_{ij} origine au CDG de Cℓ ADM	0.0302 (10)	0.0304 (9)	0.0349 (9)	0.0041 (8)	0.0010 (8)	0.0049 (7)	$= T_{12}$	$= T_{13}$	$= T_{23}$
Tenseur T en A^{o2} en groupe rigide (ORION) origine au CDG de Cℓ ADM	0.0270 (11)	0.0307 (5)	0.0374 (9)	0.0030 (5)	0.0009 (5)	0.0045 (5)	$= T_{12}$	$= T_{13}$	$= T_{23}$
Tenseur S (A°.rads) à partir des U_{ij} origine CDG Cℓ ADM	0.0003 (5)	0.0003 (3)	-0.0006 (22)	-0.0033 (3)	-0.0016 (3)	0.0010 (3)	0.0018 (3)	-0.0014 (4)	-0.0001 (4)
Tenseur S (A°.rads) groupe rigide origine CDG Cℓ ADM	$S_{11}-S_{22}$ 0.0001 (4)	$S_{22}-S_{33}$ 0.0004 (6)	$S_{33}-S_{11}$ -0.0005 (10)	-0.0029 (3)	-0.0016 (3)	0.0009 (3)	0.0015 (3)	-0.0012 (4)	0.0000 (4)
Tenseur L^{o2} exprimé dans le repère d'inertie	16.74	20.35	11.82	-3.94	0.33	3.28	$= L_{12}$	$= L_{13}$	$= L_{23}$
Tenseur T A^{o2} exprimé dans le repère d'inertie	0.0292	0.0373	0.0284	0.0037	-0.0022	0.0028	$= T_{12}$	$= T_{13}$	$= T_{23}$

TABLEAU X-9

CHLOROADAMANTANE : Phase III, T = 210 K

Analyse de l'agitation thermique par les tenseurs $\approx T$, $\approx L$ et $\approx S$

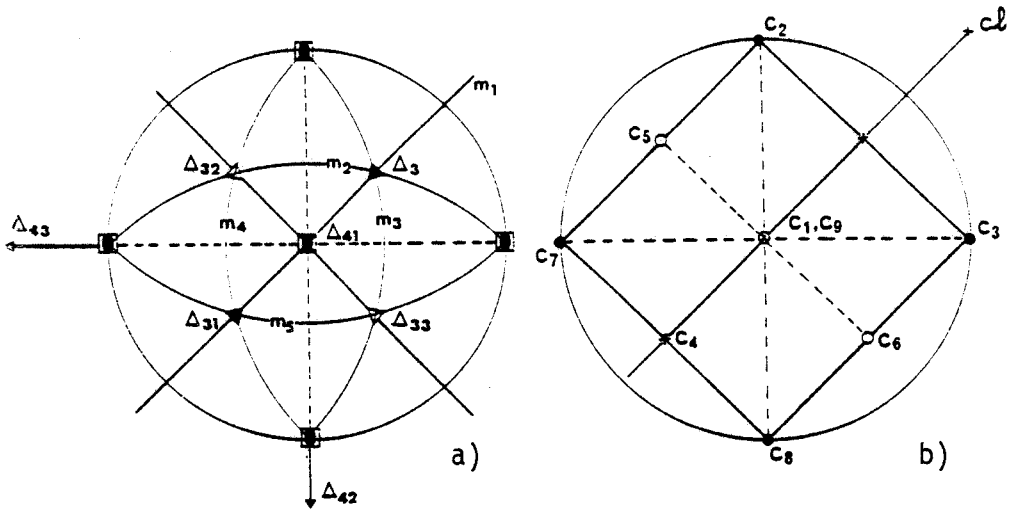

FIGURE X-7

Projections stéréographiques
a) Eléments de symétrie
b) Atomes

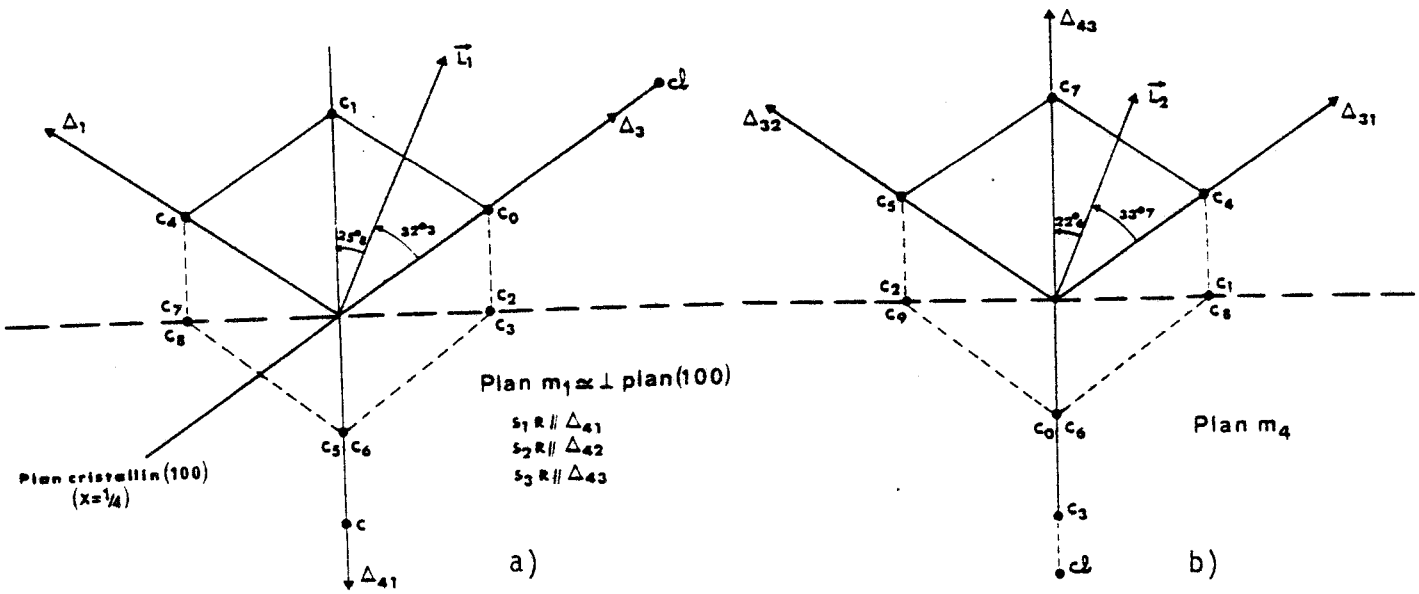

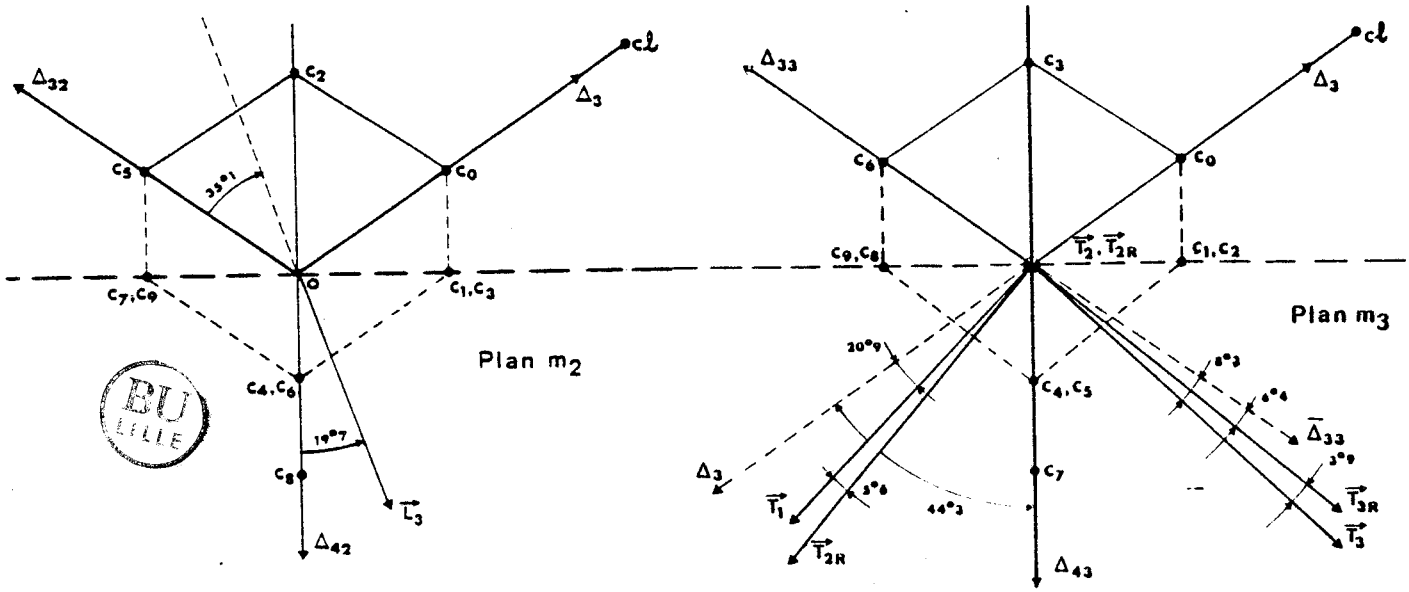

≈ ≈ ≈ FIGURE X-8

Les vecteurs propres des tenseurs L, T, T_R par rapport aux éléments de symétrie moléculai

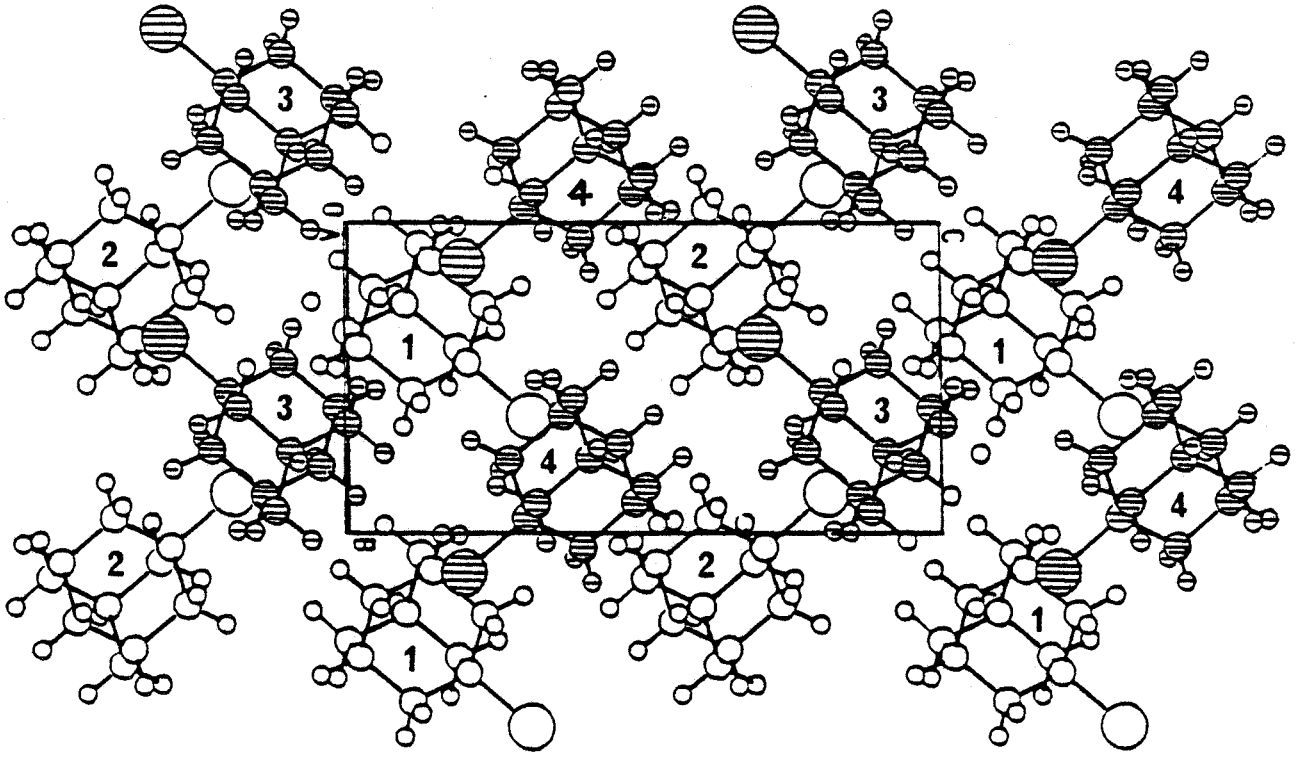

CHLOROADAMANTANE : Phase III FIGURE X-9a

Projection de la structure parallèlement à $\vec{a}$: Molécules 1 et 2 $\in$ plan x = 1/4 (O) ; Molécules 3 et 4 $\in$ plan x = 3/4 (⊜)

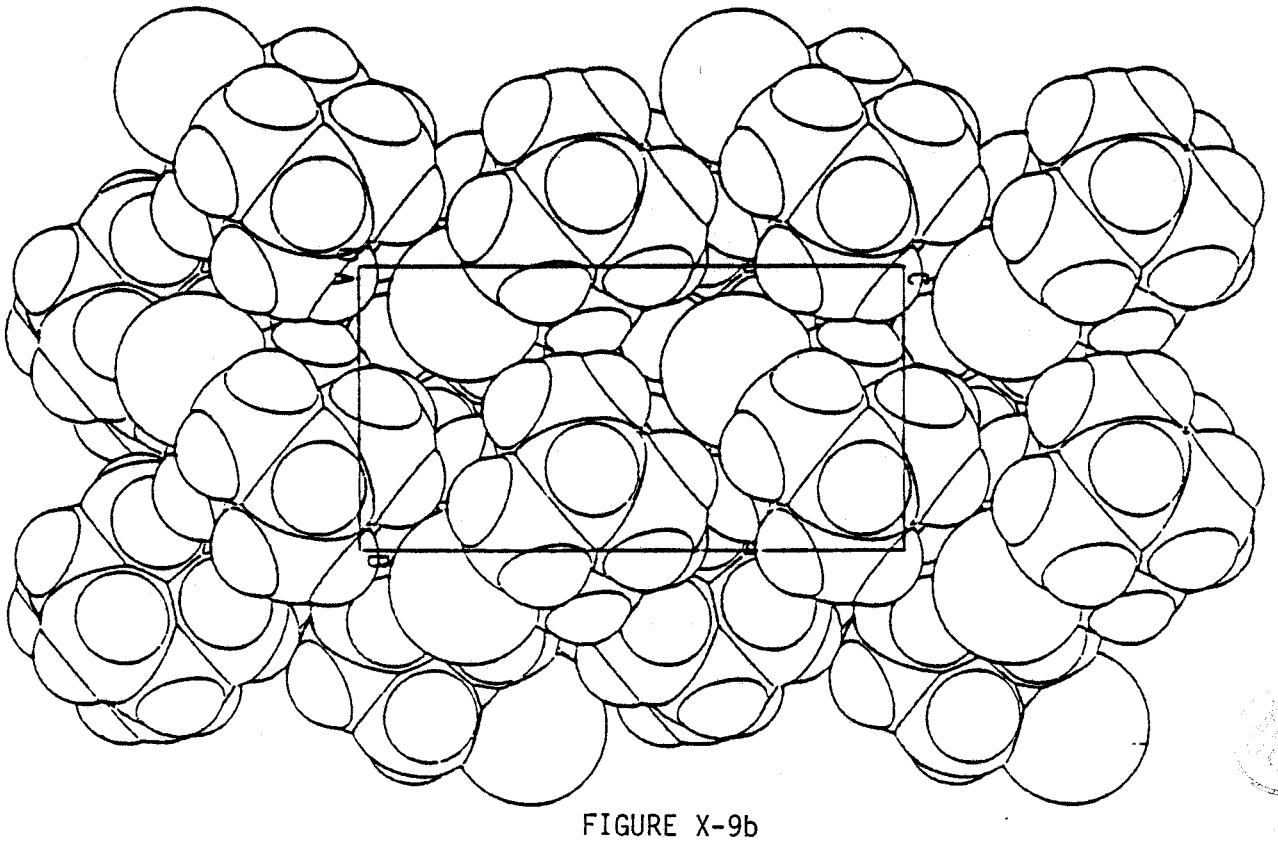

FIGURE X-9b

Projection de la structure parallèlement à $\vec{a}$: Molécules schématisées par leur enveloppe de VAN DER WAALS

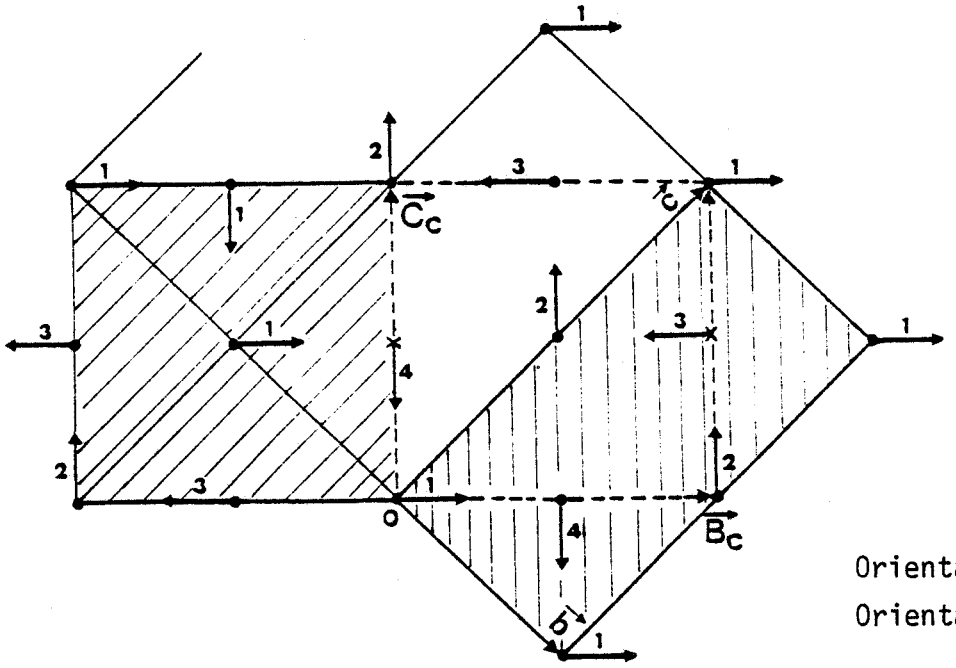

FIGURE X-10

Orientations des axes dipolaires dans les mailles monoclinique et pseudo-cubique.

Projection dans le plan $(\vec{b},\vec{c})$

Orientations 1 et 2 $\in$ x = 1/4

Orientations 3 et 4 $\in$ x = 3/4

Maille Pseudo-cubique

Maille Monoclinique

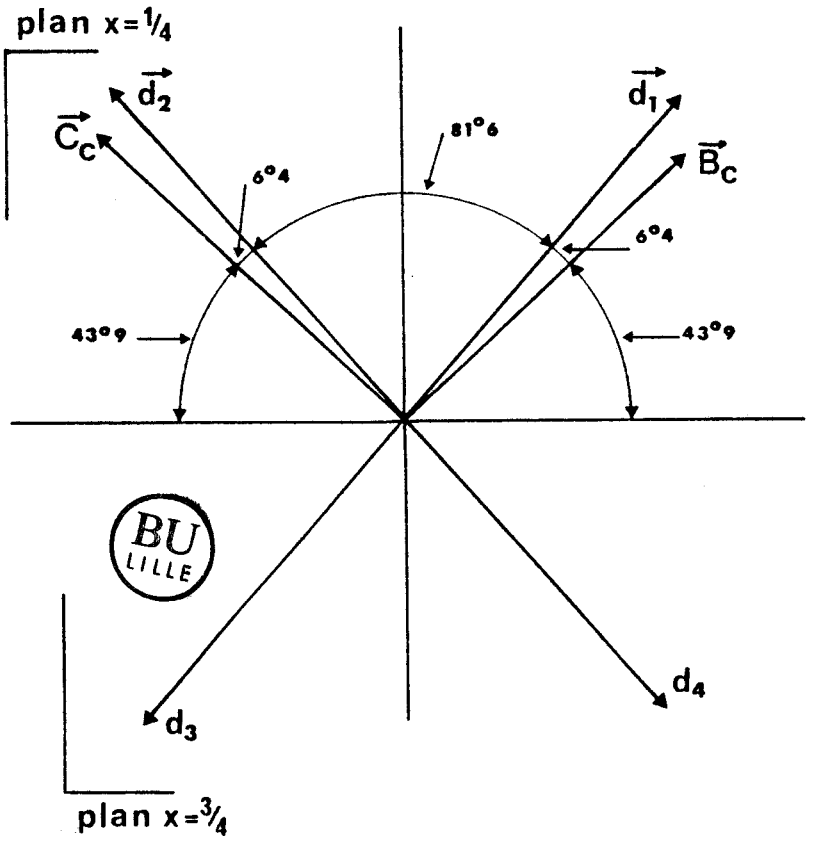

FIGURE X-11

Orientations $\vec{d}_i$ des axes C_3 moléculaires par rapport aux axes $\vec{B}_C$ et $\vec{C}_C$ du réseau pseudo-cubique

BROMOADAMANTANE Phase III T = 253 K R = 5.5 %

BR	- C0	1.994 (7)		C4	- C8	1.539 (11)	
C0	- C1	1.500 (10)		C4	- C9	1.531 (12)	
C0	- C2	1.532 (11)		C5	- H5	0.981	
C0	- C3	1.527 (10)		C5	- C7	1.518 (11)	
C1	- H11	0.979		C5	- C9	1.508 (11)	
C1	- H12	0.979		C6	- H6	0.978	
C1	- C4	1.546 (11)		C6	- C7	1.531 (11)	
C2	- H21	0.967		C6	- C8	1.515 (10)	
C2	- H22	0.980		C7	- H71	0.967	
C2	- C5	1.540 (11)		C7	- H72	1.001	
C3	- H31	0.981		C8	- H81	0.997	
C3	- H32	0.967		C8	- H82	0.965	
C3	- C6	1.540 (11)		C9	- H91	0.989	
C4	- H4	0.981		C9	- H92	0.975	

BR	- C0	- C1	108.1 (5)		C2	- C5	- H5	108.6	
BR	- C0	- C2	109.2 (5)		C2	- C5	- C7	108.4	
BR	- C0	- C3	108.1 (5)		C2	- C5	- C9	109.7	
C1	- C0	- C2	111.3 (6)		H5	- C5	- C7	109.7	
C1	- C0	- C3	110.4 (6)		H5	- C5	- C9	109.5	
C2	- C0	- C3	109.8 (6)		C7	- C5	- C9	110.0	
C0	- C1	- H11	110.5		C3	- C6	- H6	110.0	
C0	- C1	- H12	110.1		C3	- C6	- C7	108.9	
C0	- C1	- C4	108.8 (6)		C3	- C6	- C8	108.9	
H11	- C1	- H12	109.7		H6	- C6	- C7	109.5	
H11	- C1	- C4	108.9		H6	- C6	- C8	109.1	
H12	- C1	- C4	108.8		C7	- C6	- C8	110.4	
C0	- C2	- H21	110.6		C5	- C7	- C6	109.9	
C0	- C2	- H22	108.8		C5	- C7	- H71	111.1	
C0	- C2	- C5	108.0 (6)		C5	- C7	- H72	108.5	
H21	- C2	- H22	110.6		C6	- C7	- H71	110.2	
H21	- C2	- C5	109.8		C6	- C7	- H72	108.4	
H22	- C2	- C5	109.0		H71	- C7	- H72	108.8	
C0	- C3	- H31	110.6		C4	- C8	- C6	109.6	
C0	- C3	- H32	110.7		C4	- C8	- H81	107.2	
C0	- C3	- C6	108.3		C4	- C8	- H82	109.7	
H31	- C3	- H32	110.4		C6	- C8	- H81	109.7	
H31	- C3	- C6	108.0		C6	- C8	- H82	111.3	
H32	- C3	- C6	108.7		H81	- C8	- H82	109.3	
C1	- C4	- H4	108.9		C4	- C9	- C5	109.8	
C1	- C4	- C8	108.2 (6)		C4	- C9	- H91	107.9	
C1	- C4	- C9	108.8 (6)		C4	- C9	- H92	109.1	
H4	- C4	- C8	110.0		C5	- C9	- H91	109.9	
H4	- C4	- C9	110.4		C5	- C9	- H92	111.1	
C8	- C4	- C9	110.4		H91	- C9	- H92	109.0	

TABLEAU X-12

Distances et angles intramoléculaires

	x	y	z	U
BR	2327 (1)	6438 (1)	3091 (1)	51 (1)
C0	2422 (7)	4540 (11)	1954 (5)	13 (4)
C1	3850 (7)	4085 (11)	1767 (6)	25 (9)
H11	4333	5272	1589	59
H12	4247	3493	2368	59
C2	1648 (7)	2698 (12)	2233 (6)	25 (9)
H21	730	3008	2355	59
H22	2052	2113	2834	59
C3	1802 (7)	5491 (11)	1024 (6)	21 (9)
H31	866	5781	1142	59
H32	2274	6666	843	59
C4	3943 (7)	2621 (12)	883 (6)	26 (9)
H4	4876	2321	760	59
C5	1755 (7)	1250 (11)	1349 (6)	31 (10)
H5	1273	57	1525	59
C6	1886 (7)	4037 (11)	141 (6)	22 (9)
H6	1495	4610	-466	59
C7	1133 (7)	2178 (12)	422 (6)	22 (10)
H71	211	2474	535	59
H72	1200	1237	-153	59
C8	3324 (7)	3576 (13)	-58 (6)	26 (10)
H81	3394	2615	-620	59
H82	3414	4737	-231	59
C9	3187 (8)	766 (13)	1164 (7)	41 (11)
H91	3260	-158	594	59
H92	3593	185	1761	59

Coordonnées atomiques

	U11	U22	U33	U23	U13	U12
BR	483 (6)	300 (6)	306 (6)	-102 (4)	-12 (4)	-31 (4)
C0	303 (37)	116 (44)	205 (40)	-79 (33)	-13 (31)	-141 (31)
C1	271 (37)	128 (48)	394 (48)	29 (36)	-66 (33)	4 (32)
H11	599					
H12	599					
C2	348 (39)	157 (46)	282 (44)	75 (37)	-5 (33)	-86 (34)
H21	599					
H22	599					
C3	319 (39)	112 (45)	298 (46)	-9 (35)	-58 (33)	-32 (33)
H31	599					
H32	599					
C4	219 (34)	263 (49)	386 (46)	-55 (40)	5 (32)	-17 (33)
H4	599					
C5	305 (38)	106 (46)	539 (54)	136 (40)	-47 (36)	-81 (32)
H5	599					
C6	325 (38)	72 (46)	329 (46)	71 (35)	-88 (33)	-24 (31)
H6	599					
C7	309 (39)	218 (51)	343 (47)	19 (38)	-87 (34)	-115 (34)
H71	599					
H72	599					
C8	321 (38)	265 (51)	330 (47)	-21 (40)	13 (34)	-106 (35)
H81	599					
H82	599					
C9	427 (46)	259 (53)	504 (55)	18 (43)	-41 (40)	86 (39)
H91	599					
H92	599					

TABLEAU X-11

Tenseurs d'agitation thermique

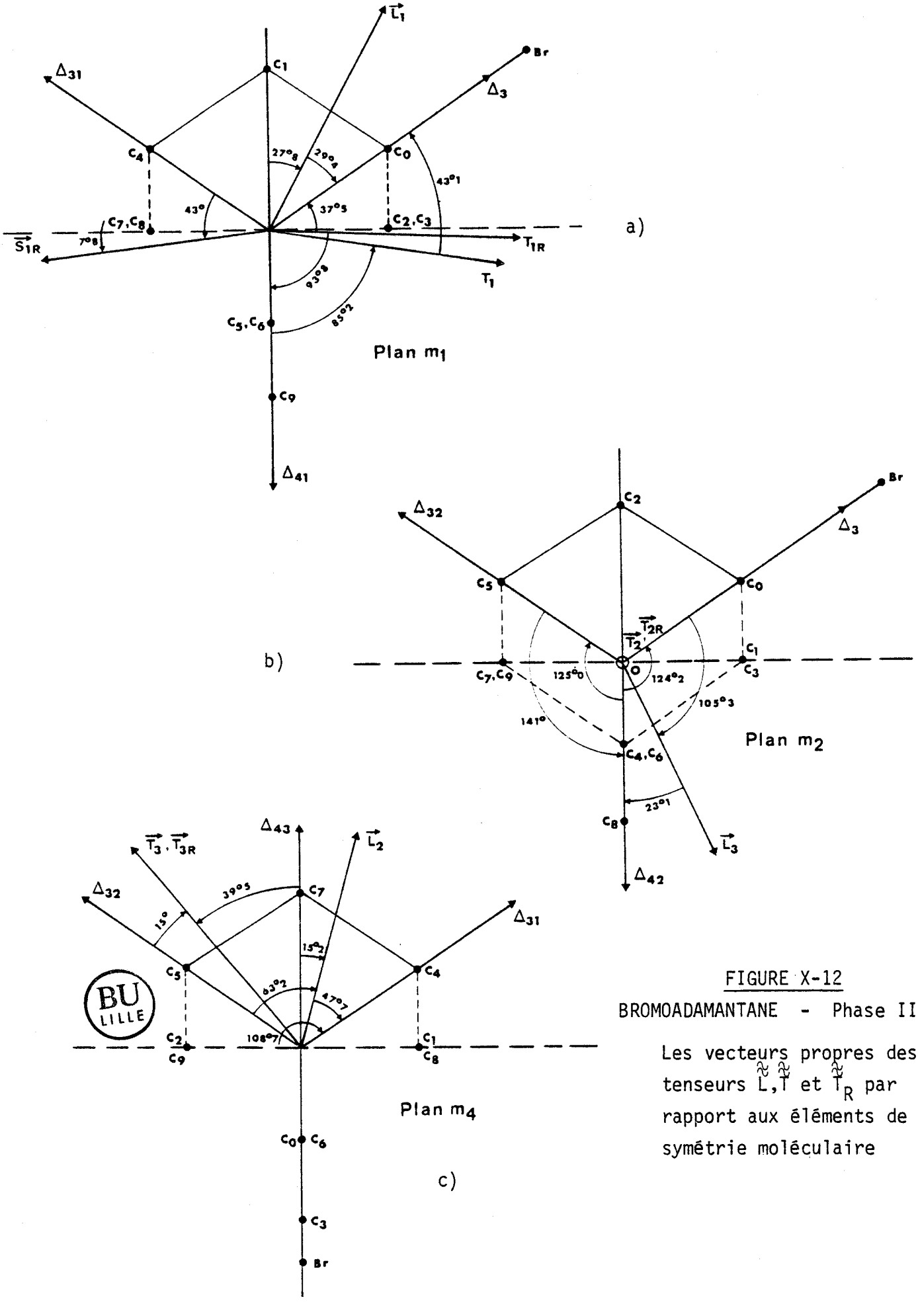

FIGURE X-12

BROMOADAMANTANE - Phase III

Les vecteurs propres des tenseurs $\underset{\approx}{L}$, $\underset{\approx}{T}$ et $\underset{\approx}{T}_R$ par rapport aux éléments de symétrie moléculaire

BROMOADAMANTANE Phase II ; T = 295 K R = 3 %

BR	- C0	1.988 (4)	C4	- C7	1.526 (5)		
C0	- C1	1.526 (6)	C4	- C9	1.527 (6)		
C0	- C2	1.523 (5)	C5	- H5	0.990 (5)		
C0	- C3	1.524 (6)	C5	- C7	1.529 (8)		
C1	- H11	0.989 (5)	C5	- C8	1.527 (6)		
C1	- H12	0.991 (6)	C6	- H6	0.990 (6)		
C1	- C4	1.528 (4)	C6	- C8	1.527 (5)		
C2	- H21	0.990 (6)	C6	- C9	1.528 (8)		
C2	- H22	0.991 (8)	C7	- H71	0.991 (4)		
C2	- C5	1.527 (4)	C7	- H72	0.990 (6)		
C3	- H31	0.990 (8)	C8	- H81	0.990 (8)		
C3	- H32	0.991 (5)	C8	- H82	0.989 (4)		
C3	- C6	1.526 (4)	C9	- H91	0.990 (5)		
C4	- H4	0.989 (8)	C9	- H92	0.989 (4)		

BR	- C0	- C1	109.0 (3)	C2	- C5	- H5	109.5 (5)		
BR	- C0	- C2	109.1 (3)	C2	- C5	- C7	109.4 (4)		
BR	- C0	- C3	109.2 (3)	C2	- C5	- C8	109.6 (4)		
C1	- C0	- C2	109.8 (4)	H5	- C5	- C7	109.5 (5)		
C1	- C0	- C3	109.8 (4)	H5	- C5	- C8	109.5 (5)		
C2	- C0	- C3	110.0 (4)	C7	- C5	- C8	109.4 (4)		
C0	- C1	- H11	109.6 (5)	C3	- C6	- H6	109.5 (5)		
C0	- C1	- H12	109.5 (5)	C3	- C6	- C8	109.5 (4)		
C0	- C1	- C4	109.0 (4)	C3	- C6	- C9	109.4 (4)		
H11	- C1	- H12	109.5 (5)	H6	- C6	- C8	109.4 (5)		
H11	- C1	- C4	109.6 (5)	H6	- C6	- C9	109.6 (5)		
H12	- C1	- C4	109.5 (5)	C8	- C6	- C9	109.4 (4)		
C0	- C2	- H21	109.6 (5)	C4	- C7	- C5	109.5 (4)		
C0	- C2	- H22	109.6 (5)	C4	- C7	- H71	109.5 (5)		
C0	- C2	- C5	109.1 (4)	C4	- C7	- H72	109.5 (5)		
H21	- C2	- H22	109.5 (5)	C5	- C7	- H71	109.4 (5)		
H21	- C2	- C5	109.6 (5)	C5	- C7	- H72	109.4 (5)		
H22	- C2	- C5	109.5 (5)	H71	- C7	- H72	109.5 (5)		
C0	- C3	- H31	109.6 (5)	C5	- C8	- C6	109.5 (4)		
C0	- C3	- H32	109.5 (5)	C5	- C8	- H81	109.4 (5)		
C0	- C3	- C6	109.1 (4)	C5	- C8	- H82	109.5 (5)		
H31	- C3	- H32	109.4 (5)	C6	- C8	- H81	109.5 (5)		
H31	- C3	- C6	109.6 (5)	C6	- C8	- H82	109.5 (5)		
H32	- C3	- C6	109.6 (5)	H81	- C8	- H82	109.4 (5)		
C1	- C4	- H4	109.4 (5)	C4	- C9	- C6	109.4 (4)		
C1	- C4	- C7	109.5 (4)	C4	- C9	- H91	109.5 (5)		
C1	- C4	- C9	109.5 (4)	C4	- C9	- H92	109.5 (5)		
H4	- C4	- C7	109.5 (5)	C6	- C9	- H91	109.4 (5)		
H4	- C4	- C9	109.4 (5)	C6	- C9	- H92	109.5 (5)		
C7	- C4	- C9	109.5 (4)	H91	- C9	- H92	109.5 (5)		

TABLEAU X-14

Distances et angles intramoléculaires

	x	y	z	u
BR	2613 (6)	6312 (5)	3052 (2)	77 (5)
C0	2533 (6)	4466 (5)	1931 (2)	47 (26)
C1	1089 (6)	4020 (5)	1701 (2)	67 (18)
H11	663 (6)	3432 (5)	2283 (2)	AA (7)
H12	628 (6)	5236 (5)	1524 (2)	AA (7)
C2	3191 (6)	5387 (5)	1039 (2)	72 (16)
H21	2723 (6)	6600 (5)	863 (2)	AA (7)
H22	4126 (6)	5685 (5)	1193 (2)	AA (7)
C3	3251 (6)	2602 (5)	2210 (2)	69 (17)
H31	4185 (6)	2898 (5)	2366 (2)	AA (7)
H32	2821 (6)	2014 (5)	2792 (2)	AA (7)
C4	1027 (6)	2603 (5)	839 (2)	57 (21)
H4	93 (6)	2308 (5)	686 (2)	AA (7)
C5	3130 (6)	3969 (5)	178 (2)	63 (17)
H5	3558 (6)	4558 (5)	-404 (2)	AA (7)
C6	3189 (6)	1186 (5)	1349 (2)	74 (20)
H6	3657 (6)	-27 (5)	1525 (2)	AA (7)
C7	1636 (6)	3513 (5)	-58 (2)	77 (22)
H71	1645 (6)	2594 (5)	-617 (2)	AA (7)
H72	1220 (6)	4727 (5)	-235 (2)	AA (7)
C8	3488 (6)	2096 (5)	451 (2)	74 (23)
H81	4783 (6)	2391 (5)	604 (2)	AA (7)
H82	3807 (6)	1178 (5)	-107 (2)	AA (7)
C9	1746 (6)	730 (5)	1112 (2)	74 (22)
H91	1319 (6)	141 (5)	1694 (2)	AA (7)
H92	1705 (6)	-188 (5)	554 (2)	AA (7)

	u11	u22	u33	u23	u13	u12
BR	909 (22)	910 (9)	697 (8)	-179 (8)	56 (31)	-82 (31)
C0	583 (54)	493 (47)	483 (55)	-72 (52)	-7 (**)	-64 (**)
C1	355 (66)	920 (92)	782 (86)	-73 (79)	10 (61)	40 (73)
H11	881 (79)					
H12	881 (79)					
C2	531 (63)	594 (61)	723 (79)	191 (69)	106 (64)	34 (59)
H21	881 (79)					
H22	881 (79)					
C3	699 (71)	707 (76)	703 (78)	55 (70)	-99 (65)	8 (76)
H31	881 (79)					
H32	881 (79)					
C4	471 (78)	791 (95)	834 (97)	-203 (96)	-13 (74)	-140 (79)
H4	881 (79)					
C5	712 (89)	581 (83)	459 (63)	-105 (70)	258 (64)	11 (68)
H5	881 (79)					
C6	902 (99)	369 (62)	882 (89)	92 (80)	-170 (82)	211 (80)
H6	881 (79)					
C7	677 (90)	850 (**)	783 (91)	-40 (90)	-15 (83)	78 (94)
H71	881 (79)					
H72	881 (79)					
C8	367 (81)	815 (**)	1033 (**)	-194 (99)	66 (87)	144 (80)
H81	881 (79)					
H82	881 (79)					
C9	703 (92)	629 (83)	1092 (**)	-171 (93)	58 (93)	-76 (80)
H91	881 (79)					
H92	881 (79)					

TABLEAU X-13

Coordonnées atomiques et tenseurs d'agitation thermique

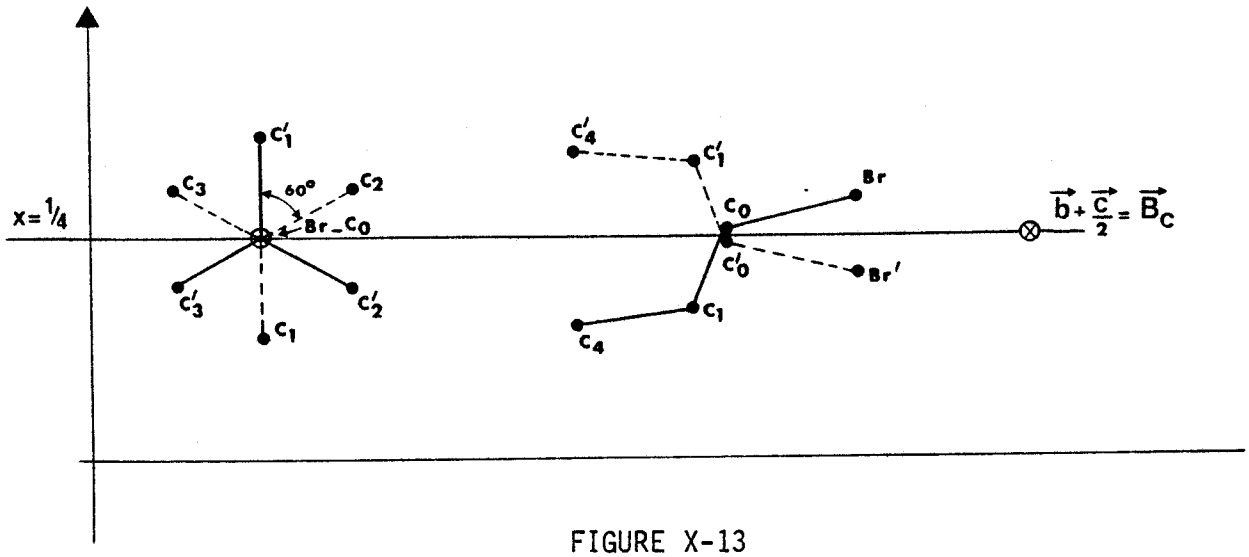

FIGURE X-13

BROMOADAMANTANE : Phase II, T = 295 K

Vue schématisée du désordre

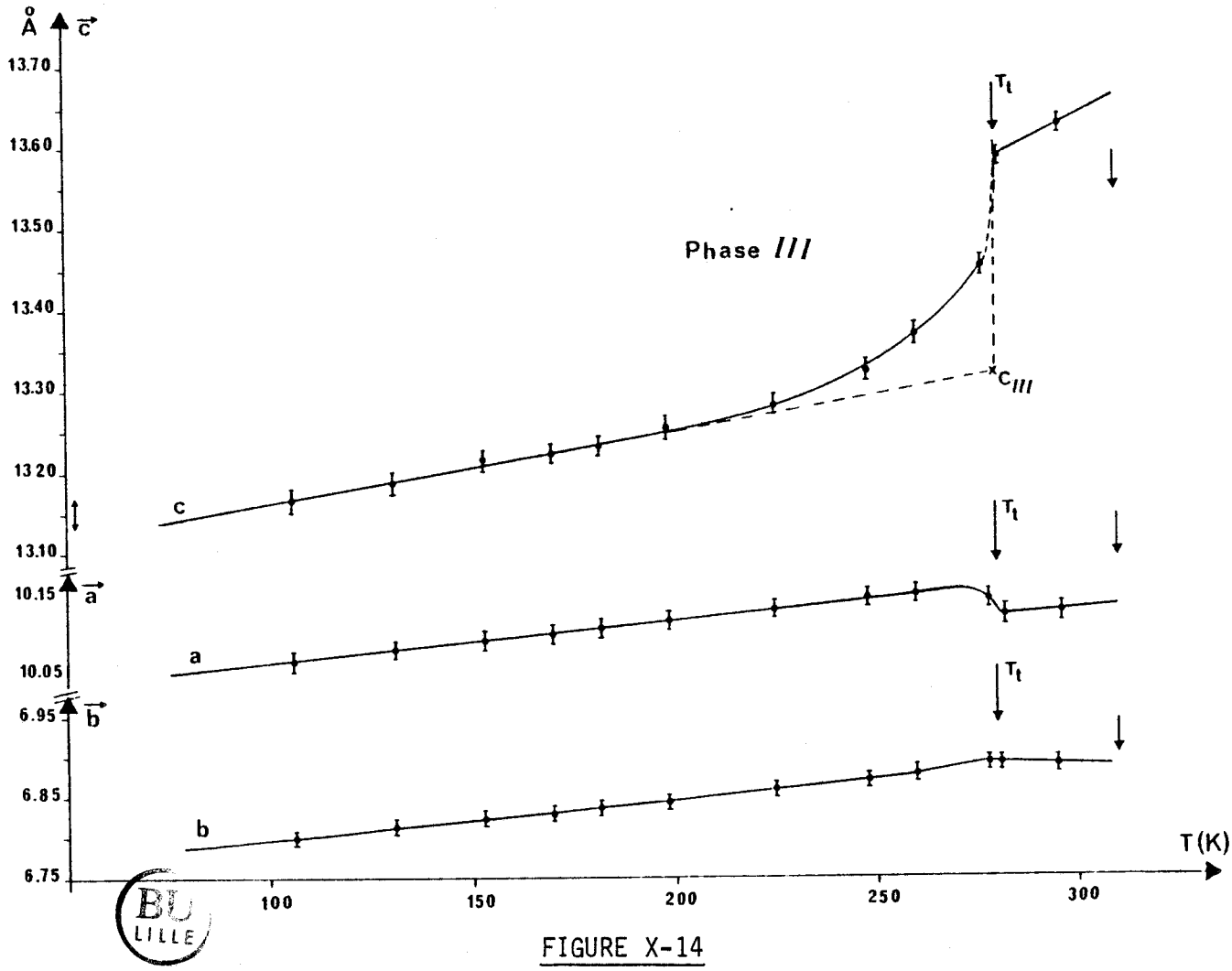

FIGURE X-14

BROMOADAMANTANE : Variations des paramètres cristallins en fonction de la température

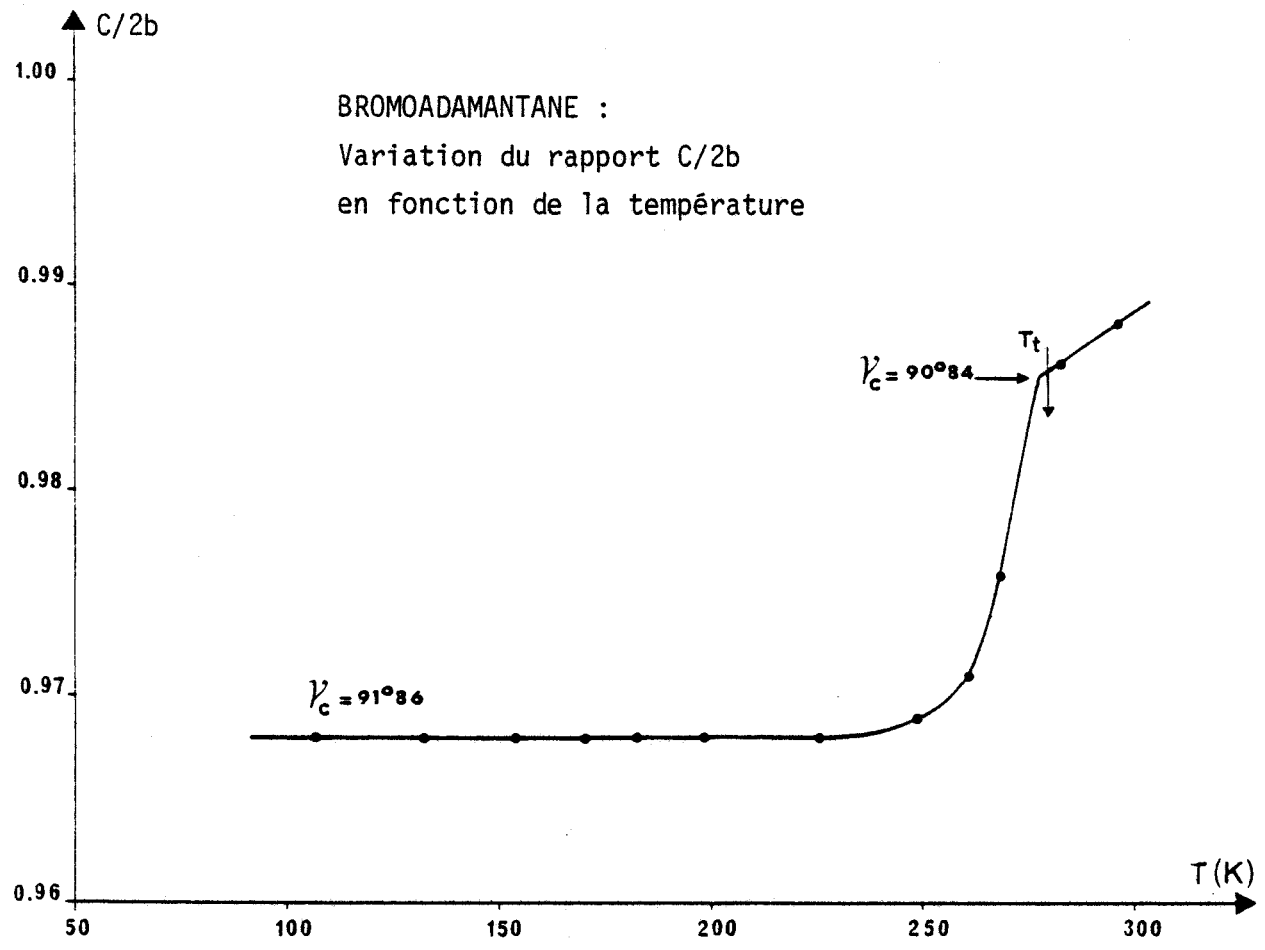

FIGURE X-15

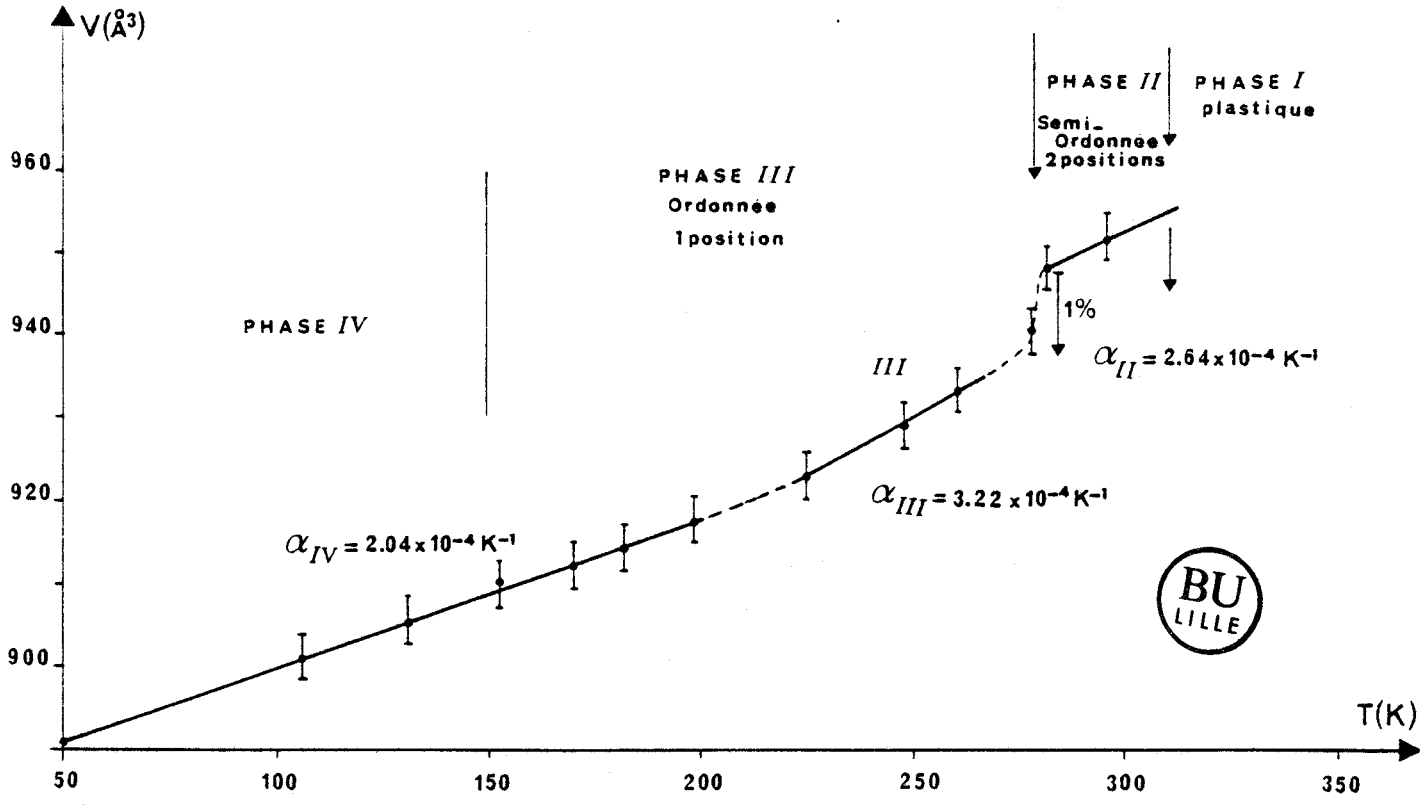

FIGURE X-16

BROMOADAMANTANE : Variation du volume
de la maille en fonction de la température

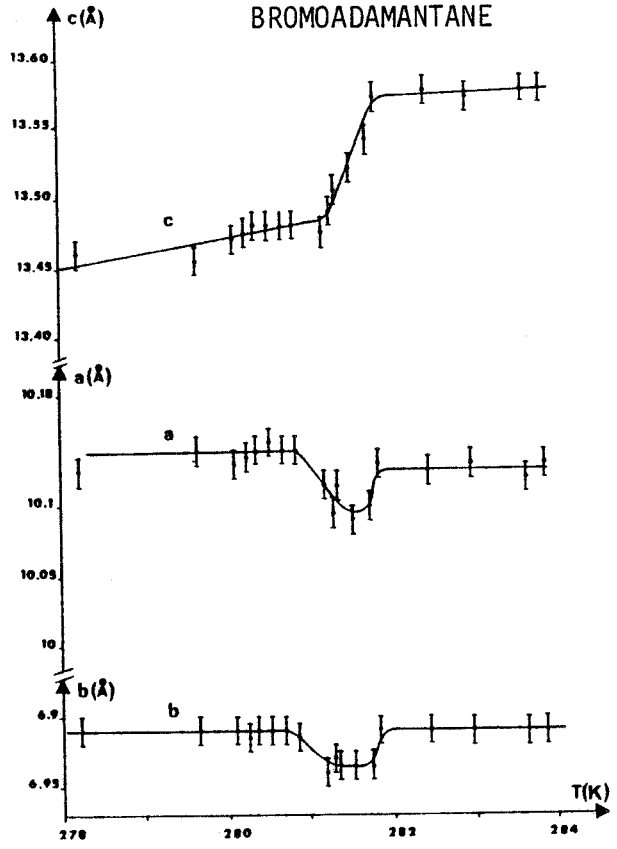

FIGURE X-17
extraite de [I2]

Variations de a,b,c au voisinage de la transition de phase II → III

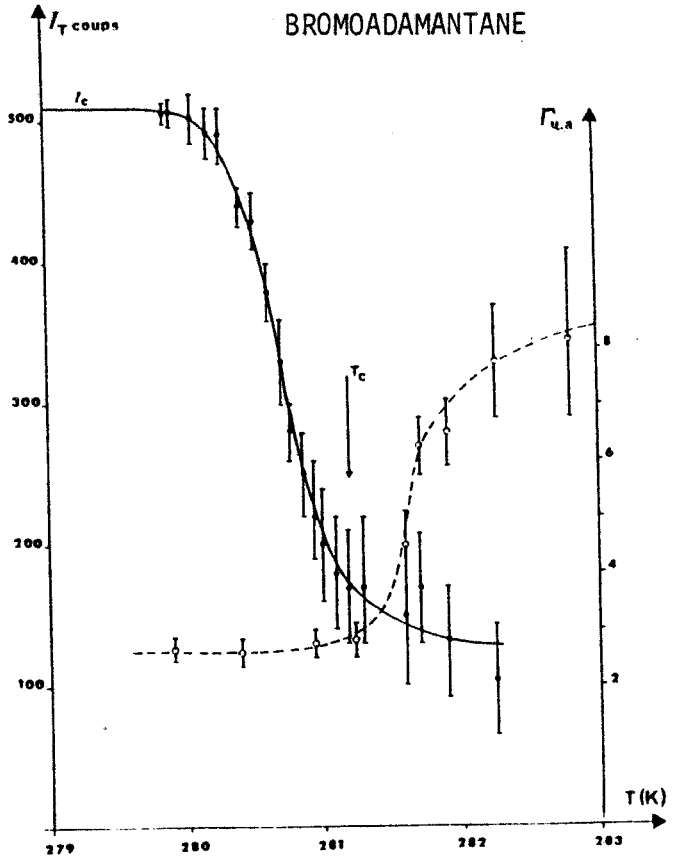

FIGURE X-18
extraite de [I2]

Variations de l'intensité (I_T) et de la largeur (Γ) de la raie (700) au voisinage de la transition de phase II → III

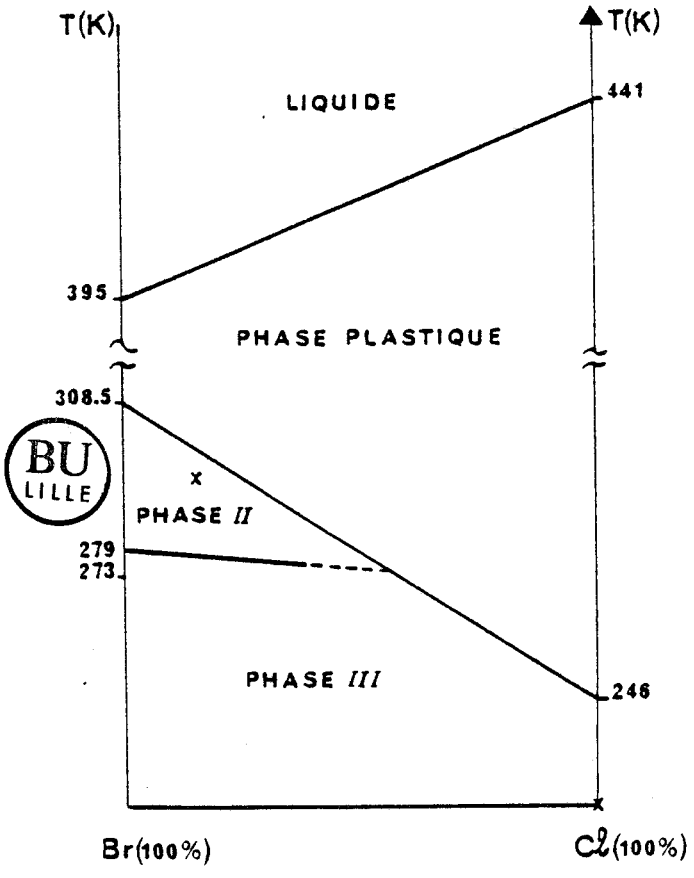

FIGURE X-19

Diagramme de phase des mélanges 1 Br ADM - 1 Cℓ ADM

FIGURES ET TABLEAUX

CHAPITRE XI

FIGURES ET TABLEAUX

CHAPITRE XI

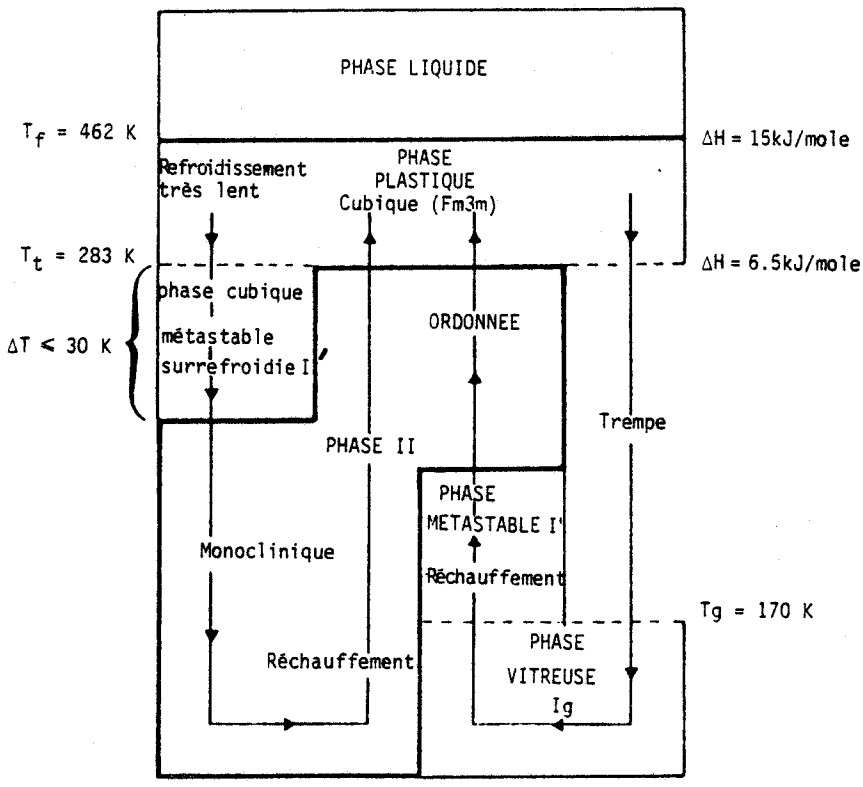

FIGURE XI-1

CYANOADAMANTANE :
Séquences des transitions de phases en fonction du traitement thermique

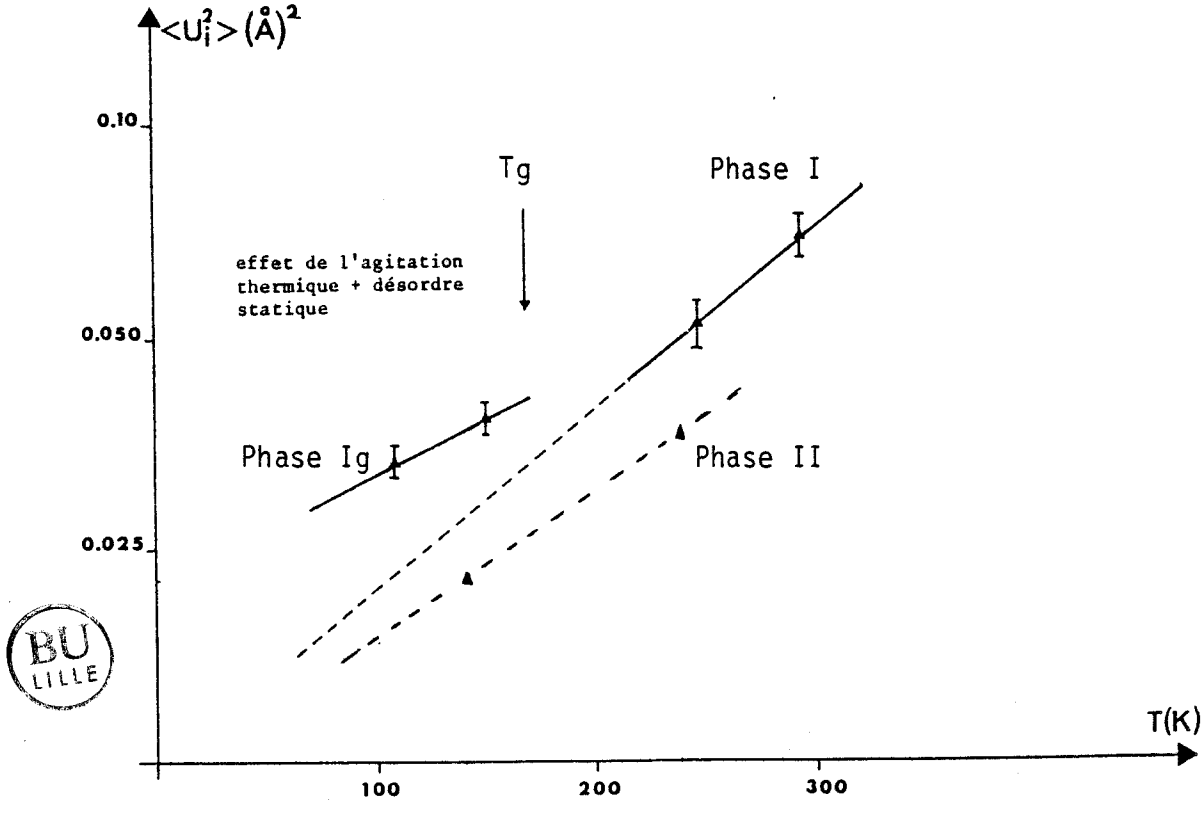

FIGURE XI-2

Variation de $\langle u_i^2 \rangle$ en fonction de la température dans les phases: plastique I, vitreuse Ig et ordonnée II

	T (K)	Z_{GADA}	T_{11} Å^2	T_{33} Å^2	L_{11} (°^{2})	R %	R_w %	a Å	Référence
PHASE	110 K	-0.11 Å	0.0357(25)	0.0342(26)	4.7(1.2)	7.5	10.2	9.638	[30]
VITREUSE	154 K	-0.09 Å	0.0406(10)	0.0389(10)	4.0(1.4)	6.2	6.5	9.671	*
PHASE	250 K	-0.07 Å	0.0500(56)	0.0522(63)	10.0(3.1)	4.5	7.5	9.769	*
PLASTIQUE	295 K	-0.06 Å	0.0621(47)	0.0591(50)	10.3(3.7)	4.6	8.7	9.813	[30]

* Mesures récentes

TABLEAU XI-1

CYANOADAMANTANE : Résultats des affinements des structures des phases I et Ig

	τ_o	E (K)	Tg ??	Source expérimentale
ADM	9.4×10^{-14}	1548	49 K	RMN(1)
	18.9×10^{-14}	1395	45 K	RMN(2)
	17.9×10^{-14}	1397	45 K	IQNS
	18.0×10^{-14}	1587	51 K	Simulation
FADM	9.3×10^{-15}	2960	87 K	IQNS
	3.8×10^{-14}	2282	70 K	R.D.
CNADM	5.06×10^{-16}	6267	170 K	R.D.
	2.34×10^{-16}	5304	141 K	RMN
Cℓ ADM	1.09×10^{-14}	1236.4	37 K	
Br ADM	2.2×10^{-16}	3849	102 K	

TABLEAU XI-2

Temps de résidence dans les phases plastiques

τ_{c4}(ADM) ou $\tau_{c3} = \tau_o \exp(E/T)$

Estimation de la température, Tg, d'une éventuelle transition vitreuse

ANNEXES

CHAPITRE XI

ANNEXE A-XI-1

J. Phys. C: Solid State Phys., 16 (1983) L265–L269 Printed in Great Britain

LETTER TO THE EDITOR

Evidence of a 'glassy crystal' phase obtained by the quenching of the plastic phase of the cyanoadamantane

M Foulon, J P Amoureux, J L Sauvajol, J Lefebvre and M Descamps
Laboratoire de Dynamique des Cristaux Moléculaires, ERA CNRS 465, Université de Lille I, 59655 Villeneuve d'Ascq Cédex, France

Received 6 January 1983

Abstract. In this Letter we present experimental results which show the existence of a 'glassy crystal' phase obtained by the quenching of the 1-cyanoadamantane plastic phase. From the DSC data, the glass transition temperature has been obtained and the glassy crystalline 1-cyanoadamantane has been shown to relax during annealing at 160 K. The 'glassy crystal' is cubic (FCC) and is characterised by the vanishing of some low-frequency Raman contributions of the plastic phase.

Adachi *et al* (1968) have demonstrated the possible existence of glasses of a new kind obtained from the quenching of some molecular crystals initially in their disordered rotator phase (plastic crystals). If the crystal is cooled rapidly enough to prevent the transition towards the low-temperature ordered phase, the disordered system is supercooled and ultimately goes into a glassy state. On gradual reheating it passes through a 'glass transition' at which the glassy form transforms irreversibly into the low-temperature metastable form of the plastic phase. In the glassy phase, the average translational order of the plastic phase is preserved but the orientational disorder would be frozen. These features have led Seki to propose the apparently paradoxical term 'glassy crystal' for this new condensed state of matter (Adachi *et al* 1968), which is particularly attractive because the transition to the glassy state could be selectively observed on the molecular orientations. Up to now these phenomena have been mainly studied on the particular cyclohexanol (Adachi *et al* 1968, James *et al* 1976, Ceccaldi *et al* 1980). In the present Letter, we report the results of preliminary experiments on cyanoadamantane (CN-ADM) whose plastic phase can be easily supercooled even when operating with single crystals. These experiments are DSC, x-ray diffraction and Raman scattering. The molecule exhibits only one conformation and the crystal structure in both the plastic and ordered low temperature phase has been solved (Amoureux *et al* 1981a). The plastic phase has an FCC structure with four molecules in the cubic cell and no long-range order of the molecular orientations. The dipolar axis can randomly take six orientations very closely located along the (001) directions. The corresponding reorientations are slow with correlation times of about $\tau_c \simeq 3 \times 10^{-7}$ s at room temperature. On the other hand, reorientation processes have been detected (Amoureux *et al* 1981b and references therein) in higher frequencies which correspond to fast uniaxial rotations around the dipolar axis. An elementary analysis of figure 1 shows that the sterical repulsions between molecules are a predominant feature of the interactions (Descamps 1982).

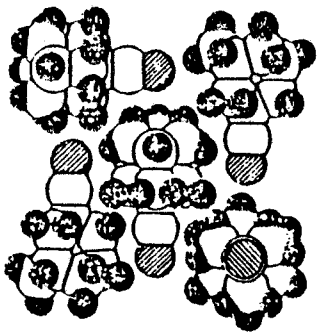

Figure 1. Example of suitable packing in the (001) plane.

DSC curves under various cooling and heating conditions were obtained using a Perkin–Elmer differential scanning calorimeter, the sample being sealed into aluminium calorimetric cells. CN-ADM is in the plastic phase (I) at room temperature and it is easily quenched when cooling more rapidly than -1.5 K min^{-1}. After the crystal is supercooled, the reheating behaviour is of the type shown in figure 2. In this case, the crystal I was supercooled to about 100 K with a cooling rate of -1.5 K min^{-1} and the heating rate was 40 K min^{-1}. The successive events of the curve can be interpreted as follows:

(i) The endothermic anomaly at about 170 K is due to a glass transition from the glassy crystalline phase (I_g) to the metastable phase (I').

(ii) The exothermic irreversible transition at about $T = 205$ K corresponds to the transition from the metastable form (I') to the low-temperature monoclinic phase (II).

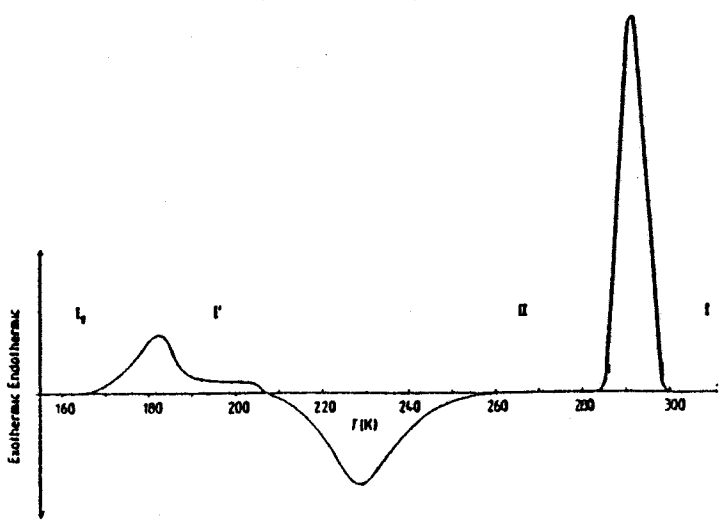

Figure 2. Typical DSC heating curve of CN-ADM : sample quenched with a cooling rate of -1.5 K min^{-1}.

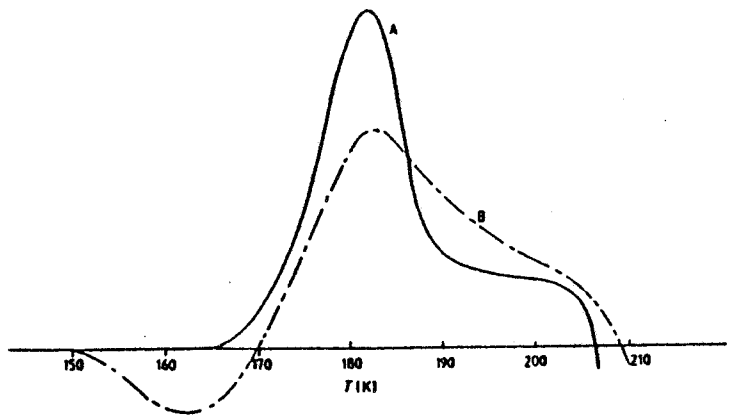

Figure 3. DSC measurements near T_g after different thermal treatments.

(iii) The endothermic peak at $T = 283$ K is the usual non-plastic–plastic transition.

The melting occurs at higher temperature ($T_m = 458$ K). Figure 3 gives more detailed results of calorimetric measurements in the T_g zone after two different thermal treatments.

Curve A: sample quenched from 295 K to 100 K with a cooling rate of -1.5 K min^{-1}, annealed at 160 K and heated with a rate of 40 K min^{-1}: the heat capacity starts to increase rapidly at about 165 K which may define the glass transition temperature T_g; then it passes through a high maximum at approximately 180 K. The narrow cusp is followed by the plateau of the metastable phase which extends on 20°. The height of the peak measured above the plateau is larger than the final heat capacity jump.

Curve B: sample quenched from 295 K to 77 K in a few seconds and immediately heated with a rate of 40 K min^{-1}: the heat capacity curve shows a minimum at about 160 K before increasing and the cusp is much less sharp than in curve A.

The difference between these two curves obtained after different thermal treatments can probably be looked upon as a relaxation phenomenon associated with the glass transition, as has been observed in the cyclohexanol case (Adachi *et al* 1968).

Since crystals of the plastic phase with dimensions suitable for x-ray diffraction and Raman scattering were grown by evaporation and sublimation respectively. CN-ADM is not hygroscopic and sublimes slowly so it can be worked without any protection. Both crystals could be quenched and ultimately gave rise to a single-crystal of the glassy phase.

X-ray data collections have been recorded from the same single crystal: (*a*) in the plastic phase, $T = 295$ K; (*b*) in the glassy phase, $T = 110$ K. In the second case, the monocrystalline sample has been rapidly quenched from 295 K to 110 K in a few seconds. All the diffraction intensities increase in the glassy phase and the number of significant independent Bragg peaks ($F_0/\sigma \geqslant 3$) goes from 42 in the plastic phase to 84 in the glassy phase. In both cases, the lattice is FCC ($Z = 4$) with cubic parameters: $a = 9.813$ Å at 295 K and $a = 9.638$ Å at 110 K.

The Raman measurements were performed using a 'Coderg T 800' spectrometer with incident radiation ($\lambda = 4880$ Å) of 100 mW at the sample and constant energy slit

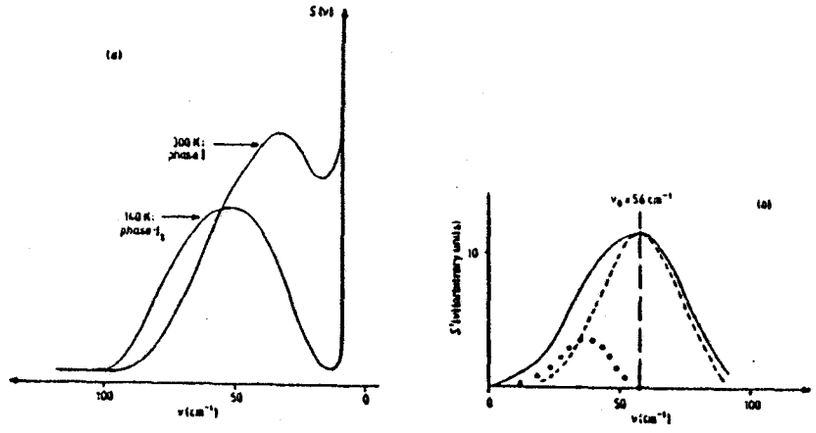

Figure 4. (*a*) Low-frequency Raman spectra $S(\nu)$, in the plastic phase (I) and in the 'glassy crystal phase' (I_g); (*b*) Renormalised low-frequency Raman spectra: —— in the phase I, $Si(\nu)$; – – – – in the phase I_g, $Si_g(\nu)$; . . . $Si(\nu) - Si_g(\nu)$.

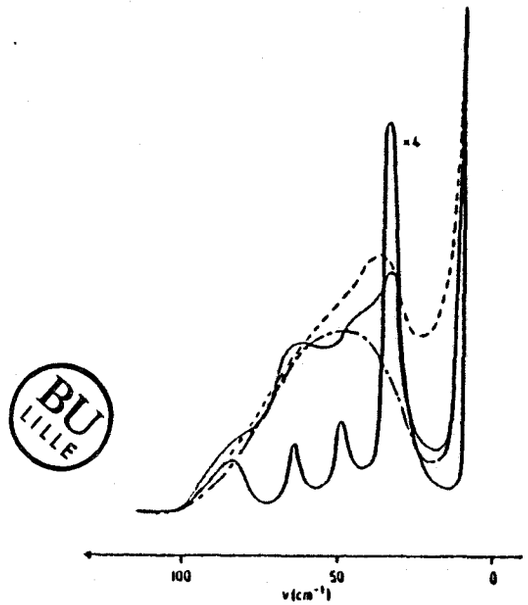

Figure 5. Spontaneous evolution of the Raman spectra. —— $t = 0$; – – – $t = 10$ min; —— $t = 20$ and 40 min.

width of 2 cm^{-1}. The glassy phase was obtained by quenching the crystal to 140 K in few seconds.

The profiles of the Raman spectra in the plastic and glassy phases are shown in figure 4. An important change in the shape of the low-frequency Raman spectrum is observed. This change appears more strongly in the profile of the renormalised spectra obtained from the experimental Stokes spectrum $S(\nu)$ by the usual transformation

$$S'(\nu) = \nu S(\nu)/(n(\nu) + 1)$$

where $n(\nu) + 1$ is the thermal population of the initial states.

The maximum of the $S'(\nu)$ spectrum occurs at $\nu_m = 56\ cm^{-1}$ ($\pm 2\ cm^{-1}$) in the two phases. However, $S'(\nu)$ is a symmetric function in the glassy phase (line width $\Gamma_G = 35\ cm^{-1}$ ($\pm 3\ cm^{-1}$), FWHM). This band is asymmetric in the plastic phase because additional contributions are Raman active in a low-frequency range ($\nu < 40\ cm^{-1}$). In a disordered phase, the shape of the low-frequency Raman spectrum is connected to the envelope of the whole libron frequencies allowed by the different local neighbourings of molecules and the breakdown of the q selection rule (Sauvajol *et al* 1982). The vanishing of the low-frequency contributions in a Raman spectrum of a glassy phase suggests that some order sets in the system and several modes become inactive in the glassy phase.

On the other hand, at a temperature T just above T_g, a spontaneous evolution of the Raman spectrum, from the one of the glassy state to one of low temperature, is observed (figure 5).

All the results presented in this Letter can be coherently interpreted through the possible occurrence of a glassy crystal phase for the CN-AdM with $T_g \approx 170$ K. Operating with powder, this phase can be easily obtained by quenching the plastic phase with a cooling rate as slow as 1.5 K min^{-1} and the thermal comportment under reheating appeared extremely sensitive to an annealing. The monocrystalline sample of the glassy phase obtained by quenching it in a few seconds is cubic FCC and the vanishing of the low-frequency contribution ($\nu < 40\ cm^{-1}$) is the Raman 'signature' of the glassy state. Experiments are actually done to study the local order in this phase; on the other hand, dielectric experiments are performed in order to observe how the slowing down of the dipolar reorientation is implicated in the glassy transition and if it follows a Vogel–Fülcher law.

The authors would like to acknowledge M Muller and C Carpentier for growing the crystals; Dr J P Cavrot for his help during DSC experiments and Dr H Szwarc and R Vacher for kind discussions. We wish to thank A Hüller and W Press for their reading of the manuscript.

References

Adachi K, Suga H and Seki S 1968 *Bull. Chem. Soc. Japan* 41 1073–87
Amoureux J P, Castelain M, Bee M, Arnaud B and Shouteeten M L 1981b *Molec. Phys.* 42 119–27
Amoureux J P, Sauvajol J L and Bee M 1981a *Acta Crystallogr.* A 37 97–104
Ceccaldi D, Denoyer F, Lambert M and Szwarc H 1980 *J. Phys. Lett.* 41 L365–8
Descamps M 1982 *J. Phys. C: Solid State Phys.* 15 7265–82
James D W, Shurvell H F and Parry R 1976 *J. Raman. Spectrosc.* 5 201–9
Sauvajol J L, Bee M and Amoureux J P 1982 *Molec. Phys.* 46 811–26

ANNEXE A - XI - 2

J. Phys. C: Solid State Phys., 17 (1984) 4213–4229. Printed in Great Britain

Different aspects of an interesting glassy crystal: 1-cyanoadamantane

M Foulon†, J P Amoureux†, J L Sauvajol†, J P Cavrot‡ and M Muller†

† Laboratoire de Dynamique des Cristaux Moléculaires (ERA 465), Université des Sciences et Techniques de Lille I, 59655 Villeneuve d'Ascq Cedex, France

‡ Laboratoire de Structure et Propriétés de l'Etat Solide—LA 234, Université des Sciences et Techniques de Lille I, 59655 Villeneuve d'Ascq Cedex, France

Received 9 January 1984

Abstract. All the different crystalline (brittle (II), glassy (I_g), plastic stable (I) and metastable (I')) phases of 1-cyanoadamantane: $C_{10}H_{15}CN$ are characterised by differential scanning calorimetry studies. The transition temperatures and their respective enthalpies are determined: I_g–I' (170 K), II → I (280 K, 5.5 kJ mol^{-1}), I-liquid (458 K, 15 kJ mol^{-1}). A difference of heat capacity between the I_g and I' phases is observed: $\Delta C_p = (16.0 \pm 1.3)$ J mol^{-1} K^{-1}. The structure of the ordered phase is analysed at two temperatures: 138 and 240 K. The space group is Cy/m with $Z = 4$ and $A_M = 11.278$ Å, $B_M = 6.874$ Å, $C_M = 12.092$ Å and $\beta = 101° 37'$ (at 240 K).

In this ordered phase the antiparallel order of the dipole moments is pointed out. From the positions of the molecular mass centres, a pseudo-cubic lattice is built which tends to the cubic plastic lattice at the transition II → I. The orientations of the dipolar axes are compared with those found in the plastic phase. The longitudinal relaxation time T_{1z} in ^{1}H-NMR gives us a very good description with temperature of the molecular motions in all the different crystalline phases. The residence times deduced from this NMR study agree very well with the corresponding ones obtained with dielectric relaxation and incoherent neutron diffusion. In the glassy state a change in the uniaxial rotation occurs which may be attributed to a large distribution of residence times.

1. Introduction

The usual glasses (obtained from the quenching of a liquid) have been currently used for several thousands of years (SiO_2) and nowadays their macroscopic properties are very well characterised but in an empirical way. Indeed the microscopic description of this glassy state is still unknown in spite of the numerous studies pursued in laboratories all over the world. The main reason for this lack of knowledge of the microscopic phenomena arises from the fact that usual glasses are composed of deformable components situated in an embedding without long-range order. Therefore most experiments can only bring averaged information corresponding to the macroscopic properties. Fortunately the existence of glasses (from the thermodynamic point of view) of a new kind, obtained from the quenching of some molecular plastic crystals, has recently been shown (Adachi *et al* 1968). When the crystal in its rotator phase is cooled rapidly enough to prevent the transition towards the low-temperature ordered phase, the disordered system is supercooled and ultimately goes into a glassy state. In this glassy phase the

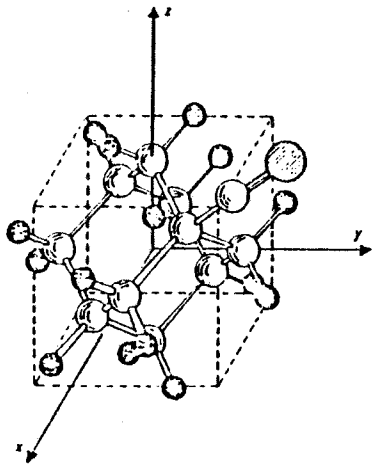

Figure 1. The molecule of cyanoadamantane, carbon atoms are in white, hydrogen in black and nitrogen is dashed. A cube has been drawn to indicate the directions of atoms with respect to each other; it does not correspond to the directions of the unit cell.

average translational order of the plastic phase is preserved but the orientational disorder is partially frozen. These features have led to the apparently paradoxical term 'glassy crystal' for this new condensed state of matter which is particularly attractive because the transition to the glassy state can only influence the molecular orientations. In the present paper, we report the results of some experiments on 1-cyanoadamantane whose plastic phase can easily be supercooled even when operating with single crystals. These experimental results (DSC, X-ray diffraction and NMR) can be coherently interpreted through the occurrence of a glassy state which enables us to put forward some hypothesis on the microscopic description of the glassy state. 1-cyanoadamantane (CN-ADM): $C_{10}H_{15}CN$, formally known as 1-cyano tricyclo[3,3,1,1] decane is composed of *rigid* globular molecules. It can be obtained from adamantane $C_{10}H_{16}$ by substituting a cyano group onto a methine carbon (figure 1). This long cigar-shaped substituent gives a large permanent dipole moment (μ_v = 3.83 D) to the molecule which is in a plastic phase at room temperature (melting point: T_m = 458 K). Microwave spectra (Chadwick *et al* 1972) and ^{13}C chemical shift (Krishnamurthy *et al* 1983) have shown that this substitution does not change the rest of the molecule whose symmetry is then C_{3v}.

2. Differential scanning calorimetry (DSC) studies

2.1. Experimental conditions

DSC curves under various cooling and heating conditions were obtained using a Perkin–Elmer differential scanning calorimeter DSC II. The powder samples sealed into aluminium calorimetric cells weighed between 20 and 27 mg. According to the experiments the cooling rate varied from 1.5 to 320 K min^{-1}. The displayed cooling rates and the real ones were always identical at least above 160 K. The DSC II calorimeter was

calibrated with indium (T_m = 429.55 K, ΔH_m = 28.42 J g^{-1}) and with succinonitril, $(CH_2—C\equiv N)_2$ (T_t = 233 K, ΔH_t = 26.54 J g^{-1}). The transition temperatures at the peaks were always deduced from the extrapolated onset from the base line.

2.2. Description of the various solid phases

All the studies carried out with different techniques have shown that cyanoadamantane exists in four different solid states: a stable plastic phase (I), a supercooled metastable plastic phase (I'), a glassy state (I_g) and an ordered phase (II).

It is certainly possible to obtain another glassy state from the quenching of the liquid phase. However up to now this 'usual' glassy state has not been really seen yet.

If the sample of CN-ADM is cooled rapidly enough, the thermodynamic behaviour, when the temperature is increased, is of the type shown in figure 2. In this case, the sample was warmed at +40 K min^{-1} from 100 K to 300 K after a very long annealing just below the glass transition.

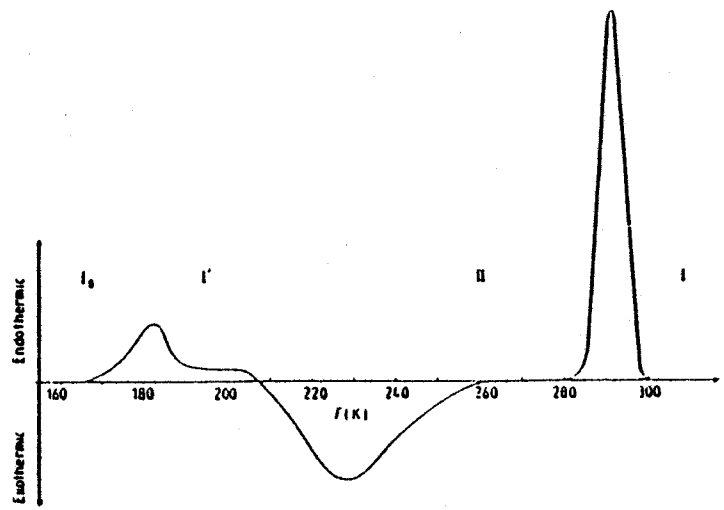

Figure 2. DSC curve obtained during the reheating process (+40 K min^{-1}), corresponding to a quenching followed by a long annealing.

The successive features of this curve can be interpreted as follows:

(i) The endothermic anomaly at $T_g \approx 170$ K is due to the glass transition from the glassy state I_g to the metastable plastic phase I'. Whatever the cooling or heating rates are, this glassy transition is always observed at approximately the same temperature: T_g = (170 ± 3) K. In 'usual' glasses the important internal molecular deformations and the numerous translational diffusion (large vacancy concentration) are perhaps related to the fact that in these compounds, T_g is strongly dependent on the thermal treatments. In CN-ADM, internal deformations and translational diffusion in the solid state (§ 5) do not exist and in the glassy state there still remains only one degree of freedom. In figure

2, one can see that there exists a difference of heat capacity (ΔC_p) between the glassy (I_g) and the supercooled (I') phases. From this DSC curve we have obtained a value of ΔC_p which has recently been confirmed by other calorimetric experiments (Bonjour and Calemczuk 1983, Fuchs 1983):

$$\Delta C_p = (16.0 \pm 1.3)\ \mathrm{J\ mol^{-1}\ K^{-1}}.$$

(ii) The exothermic irreversible transition at about 205 K corresponds to the transition from the metastable form to the low-temperature ordered phase ($I' \rightarrow II$) known as 'recrystallisation'. As usually observed in many plastic crystals, there can occur a noticeable delay in the transformation from the disordered phase to the ordered one ($I' \rightarrow II$). This delay is more or less important according to the crystals and therefore this transition runs over 50 K in this powder sample.

(iii) The endothermic peak at $T_t = 280$ K is the usual brittle-plastic transition ($II \rightarrow I$). The ratio T_g/T_t which is equal to 0.6 for CN-ADM is included between 0.5 and 0.7 as in all glasses. When the temperature is slowly decreased from 300 K, there always exists a very important delay in this transition (>30 K).

(iv) The endothermic peak corresponding to the melting point ($T_m = 458$ K) is not shown in figure 2.

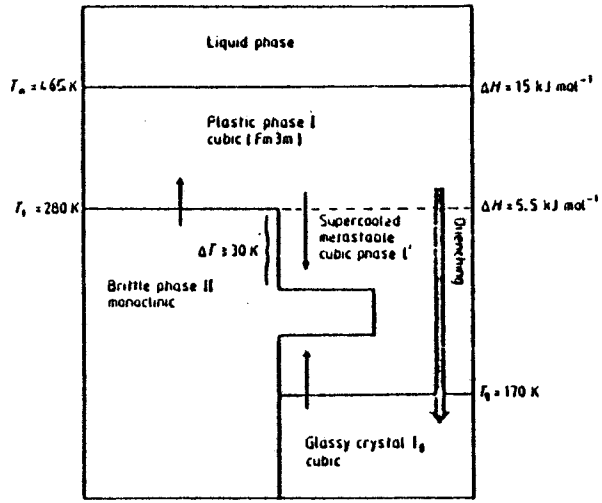

Figure 3. Polymorphic forms and thermal properties of CN-ADM.

We have measured in an accurate way the transition enthalpy change at 280 K: $\Delta H_t = (5.5 \pm 0.2)$ kJ mol^{-1}. The fusion enthalpy change was not measured with a good precision because CN-ADM sublimates at high temperatures and the calorimeter cells were not perfectly sealed. However by measuring the weight of the cells before and after each experiment, we have obtained an estimation of this fusion enthalpy change: $\Delta H_m = (15 \pm 3)$ kJ mol^{-1}. Contrary to most plastic crystals, ΔH_t is considerably lower than ΔH_m. This small value of ΔH_t is perhaps related to the fact that in all the plastic

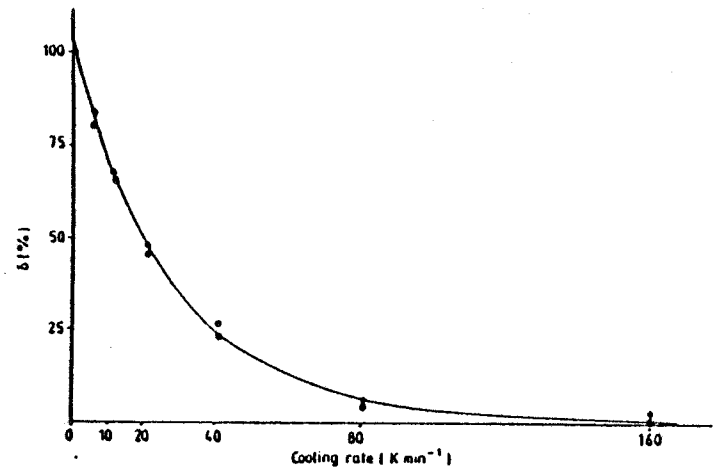

Figure 4. Proportion, δ, of powder CN-ADM that has recrystallised during the quenching plotted against the cooling rate.

phase the disorder of the cyano group can be considered as quasi-static (Amoureux *et al* 1984) which is not the case for other plastic crystals.

2.3. *The recrystallisation ($I' \rightarrow II$)*

When the sample is rapidly quenched (-320 K min^{-1}) from 300 K to 100 K, all the CN-ADM passes into the glassy state and then the enthalpy change of the recrystallisation is identical to that of the transition at 280 K. With different cooling rates, measuring the recrystallisation enthalpy change during the reheating process allows a determination of the proportion, δ, of CN-ADM that has recrystallised during the quenching. One can see in figure 4 that there exists nearly no recrystallisation when a powder sample is cooled faster than 120 K min^{-1}. However it is very important to specify that this behaviour is strongly related to the purity of the product. In our experiments we have always used cyanoadamantane which had been purified by means of repeated sublimations.

We have observed the swiftness of this recrystallisation in another way. The sample was cooled very rapidly (-320 K min^{-1}) from 300 K down to a temperature T higher than T_g, where it was maintained for a time t. The temperature was then increased very quickly. The area of the transition peak at 280 K indicates the proportion, δ, of CN-ADM that has recrystallised (table 1).

Table 1. Proportion δ of CN-ADM which has recrystallised after waiting t minutes at temperature T.

T(K)	t(min)	δ(%)
250	20	2
240	10	3
230	5	60
220	5	80

When a single crystal is quenched, its behaviour is quite different from that observed with powder: this single crystal passes nearly completely either into the glassy phase or into the ordered phase.

2.4. The glassy transition

In order to study specifically the glassy transition it is necessary to use very fast cooling rates ($-320\ K\ min^{-1}$) to prevent recrystallisation, and fast heating rates (40 or $80\ K\ min^{-1}$) to enhance the output signal. To carry out an annealing the sample is first quenched very quickly from 300 K down to a temperature T just below T_g. The sample is maintained for a time t at T. The temperature is then decreased to 90 K and finally the curve obtained when reheating from 90 K to 300 K is analogous to that of figure 2.

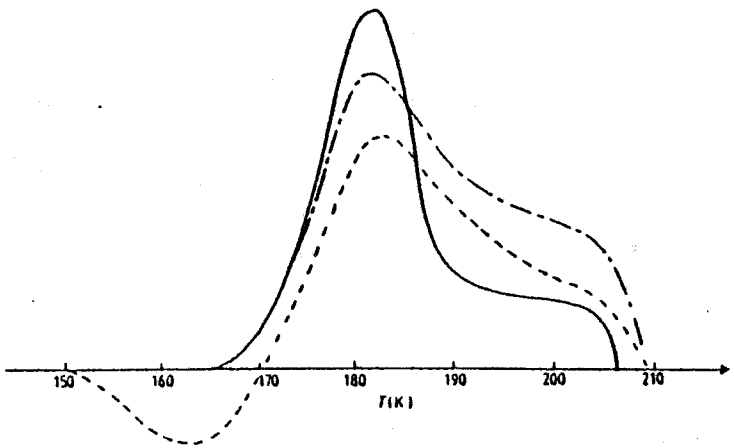

Figure 5. DSC curves obtained during the reheating process ($+40\ K\ min^{-1}$) around the glassy transition for different thermal treatments: ---- the sample was put directly into liquid nitrogen; —— annealing for 10 min at 160 K; —— annealing for 2 h at 160 K. These three curves correspond to three different samples and are in arbitrary units.

If the quenching has not been followed by an annealing, the DSC curve shows a small exothermic surface (figure 5) at about 160 K and it does not exhibit a plateau in the metastable (I′) phase. When the quenching has been followed by an annealing, the DSC curve is composed of a more or less pronounced plateau preceded by a maximum: 'the cusp'. When the annealing time t increases, the plateau extends and the 'cusp' grows up. Moreover the small exothermic area at about 160 K is no longer observed, which indicates that a relaxation phenomenon occurs during this annealing.

Very recently (Descamps *et al* 1983), Raman, x-ray and coherent neutron diffusion experiments have shown that the glassy state is characterised by an important local order, described by a correlation length. Therefore one can think that, during the annealing, this local order is setting in with the correlation length increasing progressively. Obviously, the possible relationship between the local orders in the glassy state and in the ordered phase (II) is of first importance.

Knowledge of the structures of cyanoadamantane in all its phases, whether ordered or not, is therefore necessary.

3. Structure of the ordered phase

The analysis of the structure by x-ray diffraction gives the equilibrium positions of the molecules, their arrangement in the crystal and their thermal motions which permits a comparison of the long-range order in the different phases.

3.1. Crystallisation and diffraction study

As described above, using a single crystal grown at room temperature, phase II is accessible either by slow cooling or by quenching in the glassy state followed by a reheating. In both cases, the crystal becomes polycrystalline, because of an important first-order transition, and cannot be used for further x-ray diffraction studies.

The crystal was therefore grown directly in phase II under T_t at 253 K, by evaporation of a saturated solution in methanol. The crystallisation, the choice of the crystal and its setting up on the goniometer head were carried out in an adapted freezer. The crystal protected from thermal accident was transferred on a PW1100 four-circle diffractometer at 253 K. The 'peak hunting' of 25 reflections revealed that the crystal was constituted of two single crystals widely disorientated.

The measurement of some integrated intensities indicated that one part represents 80% of the whole volume. The two direct lattices correspond to each other by rotation of about 120° along an axis which is perpendicular to their (a, b) planes. This leads to the superposition of some reciprocal lattice points $[(hkl)_1$ with $(\bar{h}\bar{k}l)_2$ and $(hk\bar{l})_1$ with $(hkl)_2]$. After correction of this effect and selection of the biggest crystal in the data collection, it becomes obvious that the crystal belongs to the monoclinic system with C_2/m space group. The diffracted intensities are corrected by the Lorentz polarisation factor but

Table 2. Parameters for C_2/m and $Z = 4$.

	$T = 138$ K	$T = 240$ K
A_M (Å)	11.041 (22)	11.278 (22)
B_M (Å)	6.923 (13)	6.874 (13)
C_M (Å)	11.851 (24)	12.092 (24)
β	98°44 (20)	101°37 (20)
V (Å^3)	896	919
d_{calc}	1.20	1.17
n_C†	856	542
n_R‡	532	408
SHELX (weight = 1.0), R =	4.3%	3.3%
ORION, R =	4.2%	3.7%
ORION, WR =	3.2%	3.1%

† n_C = number of measured intensities in C Bravais lattice.
‡ n_R = number of structure factors ($F/\sigma > 6$) included in the refinement.

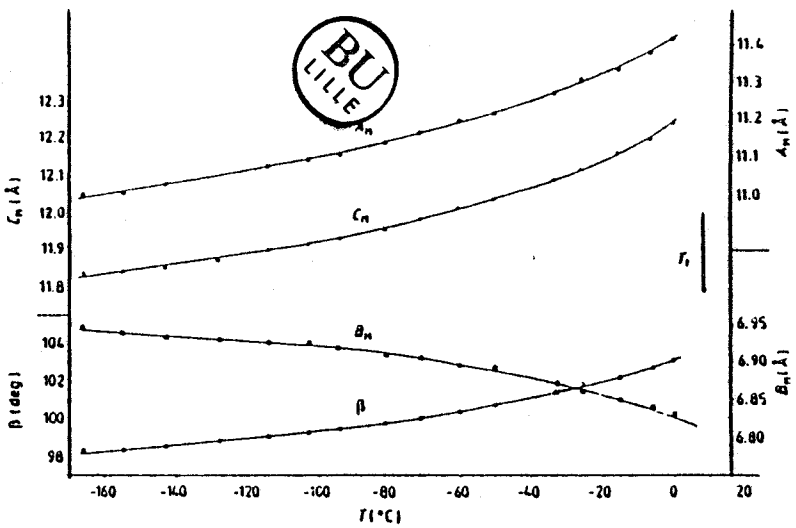

Figure 6. Lattice parameters of phase II plotted against temperature.

not for the absorption (μ_l = 0.733 cm^{-1}). Two sets of intensities were collected at 138 K and 240 K. The crystallographic parameters are represented in table 2. The temperature was then increased up from 108 K to T_t (280 K ± 3 K). The lattice parameters were determined at various temperatures during the reheating (figure 6). They do not vary linearly with temperature and only $|b|$ decreases when the temperature increases.

3.2. *Resolution and refinement of the structure*

All the 'heavy' atoms were located using the MULTAN Program (Germain *et al* 1971). The hydrogen atoms were found later by successive difference Fourier maps. There are four molecules in the unit cell and eight symmetry operations. A molecular symmetry plane coincides with the space group plane *m*. The structure was refined according to two different models of atom coordinates and thermal motions:

(i) independent atoms and anisotropic temperature factors using the SHELX program (Sheldrick 1976);

(ii) a rigid molecular group and its TLS (Shomaker and Trueblood 1968) adapted description of thermal motion using the ORION program (André *et al* 1971).

The TLS tensors are also deduced from (i) by least-squares refinement using the TLS program (Shomaker and Trueblood 1968). The comparison between these tensors in procedures (i) and (ii) enables the validity of the rigid group assumption to be evaluated.

These different refinement processes converge quickly and the conventional *R* factors (about 0.04) (table 2) measures the good agreement between the models and the real structure†. A last refinement, suppressing the space group plane *m*, (space group

† The atomic parameters and the observed and calculated structure factors are available on request from Dr M Foulon.

C2) leads to the same results. The position and orientation of the molecule do not change significantly. A last difference Fourier map exhibits no abnormal residual electronic density.

3.3. *Molecular geometry and packing*

The intramolecular bond distances and angles agree well with those found in the literature (Chadwick *et al* 1972). The fractional coordinates of the molecular centre of mass are X/a = 0.2462, Y/b = 0.0, Z/c = 0.2310, near (¼, 0, ¼). The threefold molecular axes always lie in planes parallel to the crystallographic ones (*a*, *c*) at Y/b = 0 and ½. The angle between these axes and the *a* base vector is 98° 8′ (Mod 180°) at 240 K.

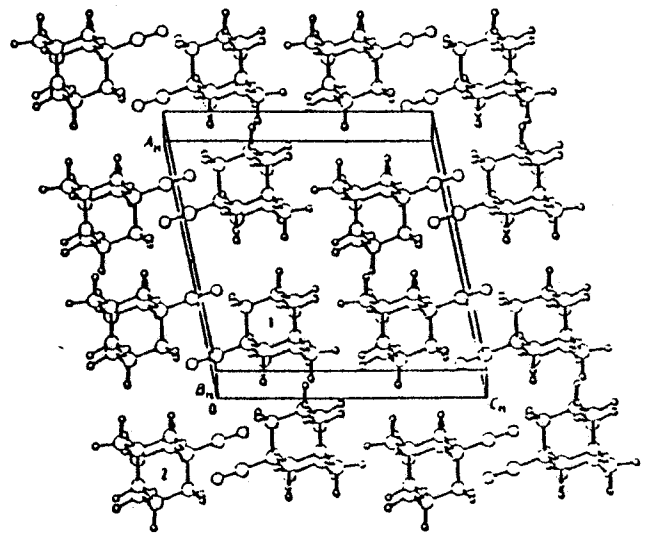

Figure 7. Perspective view of the molecular packing in a direction nearly parallel to the B_n axis.

The structure may be described by a succession of parallel planes of molecules. In such a planar lattice, the pattern is constituted by two molecules related by a symmetry centre (molecules 1 and 2 in figure 7). The antiparallel directions of the dipolar moments lead to an antiferroelectric order. The distances between the atoms of a molecule and those of the neighbouring ones are always greater than the sum of the corresponding Van der Waals radii. Two next-neighbour molecules do not form a dimer in this low-temperature phase. Thus, the steric hindrance is weak when the molecules stay at their equilibrium positions.

The NMR experiments and their interpretation reported below point out that a molecular motion subsists in phase II. According to the single discernible equilibrium position of the molecule in its site, this motion can only be described as a threefold uniaxial rotation along the C—C≡N group.

The calculation of the interatomic distances between a uniaxially rotating molecule and its neighbourhood shows a large steric hindrance during this rotation. Its mechanism

is certainly complicated and may involve a correlated motion of the molecules and (or) a deformation of the C—C≡N group.

3.4. Analysis of the thermal motion

The TLS tensors deduced from the two refinement models are identical (table 3). It proves that the whole molecule may be considered as a rigid group. The analysis of these TLS tensors shows that the librations are of low magnitude and their eigenvectors L_i nearly parallel to the molecular inertial axis (L_3 quasi-parallel to the dipolar axis) (table 3).

Table 3. (a) Thermal motion results: TLS.

	T = 240 K	T = 138 K
T_{11} (Å²)	0.0310 (15)	0.0178 (12) × kt = 0.0310
T_{22} (Å²)	0.0361 (15)	0.0205 (12) × k = 0.0356
T_{33} Å²)	0.0490 (10)	0.0245 (8) × k = 0.0433
T_{12} (Å²)	−0.0060 (10)	−0.0018 (8)
L_{11} (rad²)	0.0035 (3)	0.0005 (3)
L_{22} (rad²)	0.0032 (3)	0.0010 (3)
L_{33} (rad²)	0.0052 (8)	0.0030 (7) × k = 0.0052
L_{12} (rad²)	0.0001 (5)	−0.0001 (4)
S_{11} (Å rad)	−0.0026 (4)	−0.0010 (3)
S_{12} (Å rad)	0.0012 (4)	0.0002 (3)
S_{23} (Å rad)	0.0023 (4)	−0.0010 (3)
S_{31} (Å rad)	0.0007 (6)	−0.0009 (5)

† k = 240 K/138 K.

Table 3. (b) Eigenvalues and eigenvectors of T and L tensors.

T_1 = 0.0293 Å²	$\sqrt{T_1}$ = 0.172 Å	T_1 = 0.0174	$\sqrt{T_1}$ = 0.132 Å
T_2 = 0.0361 Å²	$\sqrt{T_2}$ = 0.190 Å	T_2 = 0.0205	$\sqrt{T_2}$ = 0.143 Å
T_3 = 0.0508 Å²	$\sqrt{T_3}$ = 0.225 Å	T_3 = 0.0249	$\sqrt{T_3}$ = 0.158 Å
L_1 = 0.0035 rad²	$\sqrt{L_1}$ = 3°39	L_1 = 0.0006	$\sqrt{L_1}$ = 1°44
L_2 = 0.0032 rad²	$\sqrt{L_2}$ = 3°25	L_2 = 0.0011	$\sqrt{L_2}$ = 1°87
L_3 = 0.0052 rad²	$\sqrt{L_3}$ = 4°15	L_3 = 0.0028	$\sqrt{L_3}$ = 3°02

At 138 K the L_1 and L_2 terms perpendicular to the dipolar axis decrease significantly, when L_3 does not and takes into account the uniaxial rotation effect. The T translational tensor is quasi-isotropic. The deviations, between the anisotropic temperature factors refined by an independent-atom model and those calculated from the TLS tensors, are greater for the C—C≡N atoms group but not significantly. One cannot conclude on a possible deformation of the C—C≡N group, perhaps because of the spherical atomic scattering approximation.

3.5. Lattice relations between the monoclinic and cubic phases

Taking the centre of mass of a molecule as the origin, the vectors defining the centres of mass of the first neighbouring molecules describe a pseudo-rhombohedral lattice corresponding to a pseudo-face-centred cubic lattice. One obtains the following relations between the monoclinic (M) and pseudo-cubic (C) base vectors:

$$A_C = \tfrac{1}{2}(C_M - A_M) \qquad A_M = -A_C + \tfrac{1}{2}(B_C - C_C)$$

$$B_C = B_M + \tfrac{1}{2}(A_M + C_M) \qquad B_M = \tfrac{1}{2}(B_C + C_C)$$

$$C_C = B_M - \tfrac{1}{2}(A_M + C_M) \qquad C_M = A_C + \tfrac{1}{2}(B_C - C_C).$$

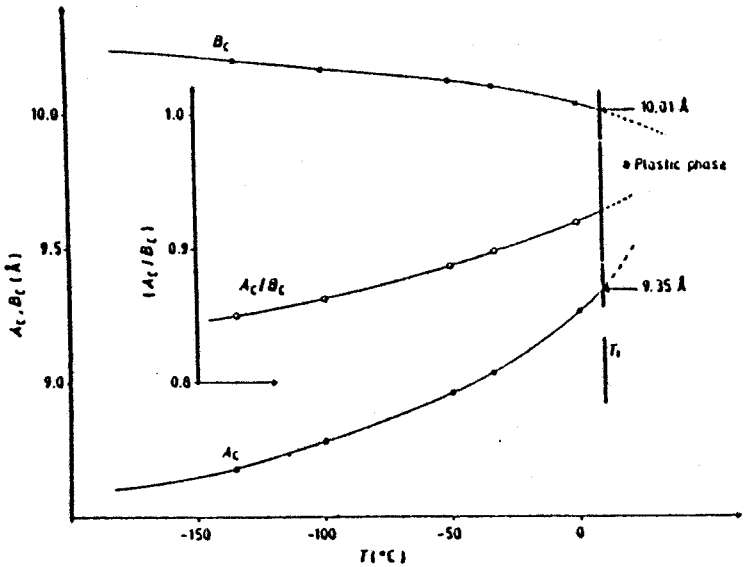

Figure 8. The pseudo-cubic parameters A_C, B_C and their ratio plotted against temperature.

The angles between the A_C, B_C and C_C vectors do not vary significantly with temperature and their values are always in the range 87° to 94°. The variations with temperature of the pseudo-cubic parameters A_C and $B_C = C_C$ calculated from the corresponding ones of the monoclinic phase as well as the A_C/B_C ratio are reported in figure 8. This ratio increases and tends to 1.0 with temperature, which shows the evolution to the cubic phase I at $T > T_t$. The most puzzling result is that the dipolar axes are nearly parallel to the pseudo-cubic $(1\bar{1}\bar{1})$ and $(\bar{1}11)$ directions.

3.6. Discussions and conclusions

A single crystal was grown at 253 K and its structure well resolved at T = 138 K and 240 K. Some particular results will now be analysed in detail.

(i) At first, it was possible to confirm the threefold uniaxial rotation of the molecule in phase II. Its detailed mechanism is not yet known.

(ii) At a given temperature lower than T_t, the difference between the unit cell volume of the cubic phases and that of phase II is low ($\Delta V/V = 5 \times 10^{-3}$) (figure 10). This suggests that the molecular centre of mass arrangement is not very much altered. From their positions, a pseudo-cubic lattice was built which tends to the cubic plastic lattice near T_t.

(iii) At the temperature T_t, this low variation of the volume, compared with other compounds (Cl-ADM or adamantane $\Delta V/V = (6\text{–}8) \times 10^{-2}$), is certainly related to the quasi-static dipolar disorder (100 kHz) in phase I.

Nevertheless, at T_t the dipolar axes must rotate from a direction $(11\bar{1})$ or $(\bar{1}11)$ of the pseudo-cubic lattice ($T < T_t$) to the six directions (001) of the cubic one ($T > T_t$). This reorientation involves rotations of about 50° along the twofold axes of the pseudo-cubic lattice (parallel to B_M, $B_M + C_M$, $B_M - A_M$), which implies an important steric hindrance. This leads to the breaking of the crystal. In spite of this difference concerning the dipolar axis directions, the antiferroelectric order found in the monoclinic phase subsists locally in the cubic plastic phases (as deduced from the Kirkwood g correlation factor (Amoureux *et al* 1983)). The recent neutron and x-ray diffusion experiments (Descamps *et al* 1983) suggest that this local order may be retained in the glassy phase.

In the pseudo-cubic lattice description of phase II, the parameter A_C is always lower than $B_C = C_C$. Accordingly, a relation between the real monoclinic lattice and a pseudo-quadratic one can be considered. The comparison of the low-temperature ordered phase of CN-ADM with that of adamantane is of interest. In adamantane (Donohue and Goodman 1967), the lattice is quadratic and the threefold molecular axes have nearly the same orientations as in CN-ADM. Furthermore, the ratio A_C/B_C

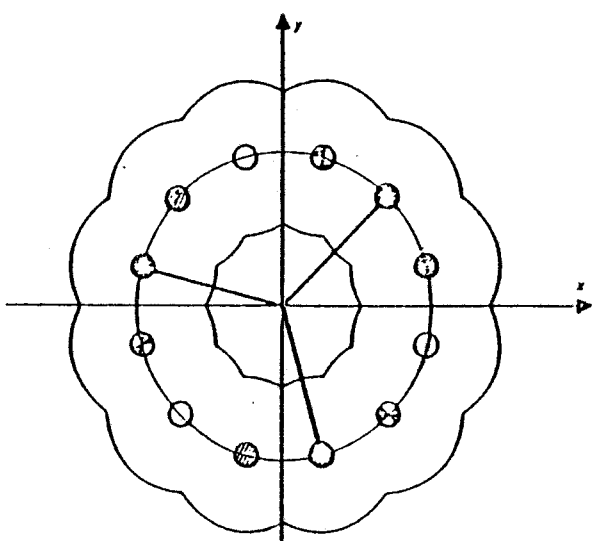

Figure 9. Projection on the XOY plane of the three methine carbons not bounded to the —C≡N group fixed along the [001] axis.

(deduced from the quadratic parameters) is 0.953 for adamantane at 4 K below T_t, which is comparable with that of CN-ADM under the same conditions: 0.93.

4. Structures of the cubic phases and relationship with the molecular motions

The plastic phase has a Fm3m structure (Amoureux and Bée 1979) with four molecules in the cubic cell (lattice parameter $a = 9.81$ Å at 293 K). The molecular dipolar C—C≡N axis can randomly take six orientations very closely located along the (001) directions. For each of the six dipolar orientations, the molecule can occupy four distinct equilibrium positions deduced from each other by 30° rotations around its threefold symmetry axis (figure 9). In the glassy phase, x-ray diffraction data on several single crystals have been collected at 113 K with and without annealing. The detailed analysis of these structures is now being processed, but is not straightforward and must be improved. Moreover the evolution at the glassy transition of the Bragg peak intensities has not been investigated so far. However the first analyses of the experimental data have shown that the molecular equilibrium positions are the same as in the plastic phase. The volume of the cubic lattice (Foulon *et al* 1983) in the disordered phases (I, I', I_g) is very close (figure 10) to that of the monoclinic cell in the ordered phase, which is very different from other plastic crystals. The curve represented on this figure shows a slight change of slope at the glassy transition.

According to this structural description, two very different reorientations may exist in the cubic phases (figure 11):

(i) Uniaxial rotations which are certainly fast as a result of a weak steric hindrance. These uniaxial rotations may be of order 3 or 12 around the molecular C—C≡N axis with corresponding residence times τ_{m3} and τ_{m12}.

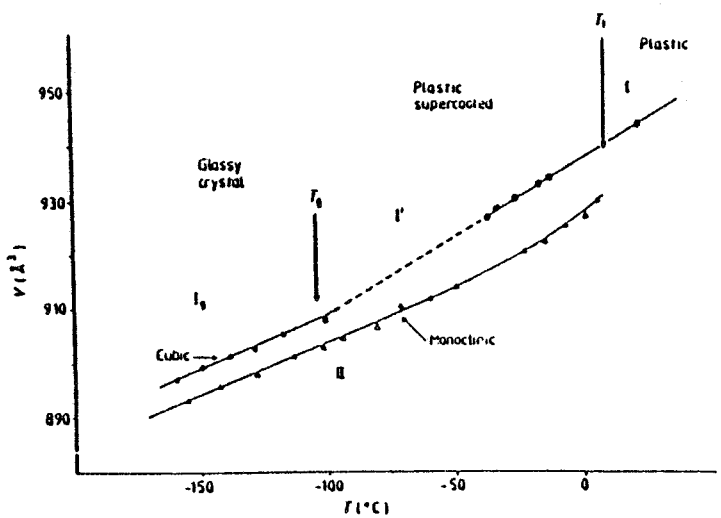

Figure 10. Volume of the cubic lattice (points) and of the monoclinic cell (triangles) plotted against temperature.

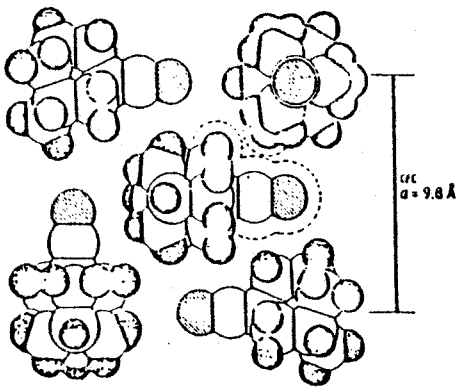

Figure 11. An example of packing in the (001) plane.

(ii) A tumbling reorientation of the dipole moment between the (001) axes. This tumbling motion, related to a large moment of inertia, is certainly very slow as it corresponds to steric hindrance between first and secind neighbouring molecules and then involves a huge local distortion of the cubic lattice. The jumps of the dipolar C—C≡N axis between next neighbouring equilibrium positions are the most probable and they correspond to reorientations with respect to the (111) cubic lattice axes characterised by a residence time τ_{C1}.

The microscopic description of the glassy state requires a knowledge of the temperature evolution of all these residence times. The best technique to provide such different residence times is certainly nuclear magnetic resonance (NMR).

5. Spin–lattice relaxation time T_{1Z} in ^{1}H NMR

The longitudinal relaxation time T_{1Z} has been measured from 113 K to 454 K in ^{1}H NMR at $f_0 = 200$ MHz. We have not obtained experimental results in the metastable phase (I') between 172 K and 238 K as a result of the recrystallisation of cyanoadamantane. It is well known in NMR that the minimum values of T_{1Z} are observed when the residence times τ corresponding to the molecular motions are about $\tau \approx (2\pi f_0)^{-1} = 8 \times 10^{-10}$ s. In cyanoadamantane the curve of T_{1Z} versus temperature exhibits two minima (figure 12): the first at high temperatures corresponds to the slow dipolar tumbling (τ_{C1}) and the second at low temperatures to the uniaxial rotations (τ_{m1}, τ_{m12}). One can see from figure 12 that below 330 K only the uniaxial rotation is observed.

The analysis of the experimental results shows that the values of τ_{C1} deduced from T_{1Z} between 330 K and 454 K are exactly the same as those deduced from dielectric relaxation (Amoureux *et al* 1983, 1984). These last studies had also shown that the dipolar reorientations are completely frozen at T_g with a Vogel–Fulcher law. The glassy state of cyanoadamantane is characterised by a static disorder for the dipole moments. An incoherent quasielastic neutron scattering (IQNS) experiment (Bée *et al* 1980) has demonstrated that in the plastic phases the uniaxial rotations are of order 12. The values of τ_{m12} deduced from the T_{1Z} measurements between 238 K and 350 K are identical to those obtained from IQNS.

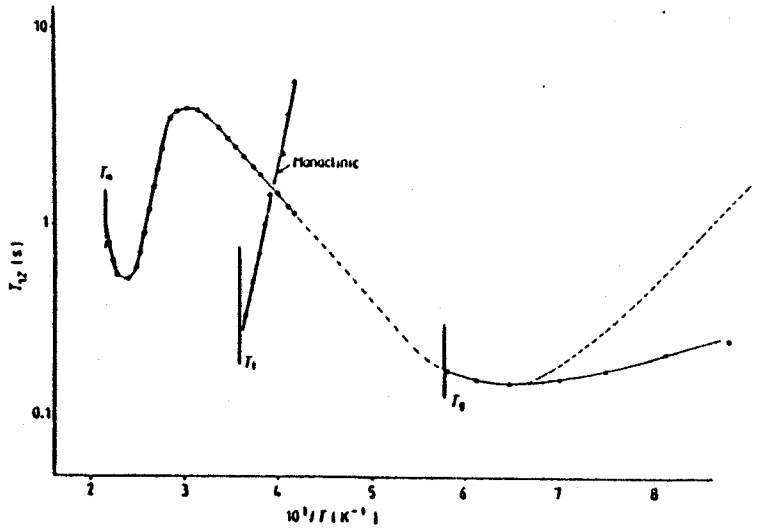

Figure 12. Longitudinal relaxation time T_{1Z} at $f_0 = 200$ MHz versus $10^3/T$. The triangles corresponding to the monoclinic phase were obtained at $f_0 = 30$ MHz. The values of T_{1Z} calculated with a single residence time following an Arrhenius law and corresponding to the experimental points between 150 and 330 K and in the glassy state below 150 K are represented by the broken curve.

In the glassy state, the value of T_{1Z} at T_g is in good agreement with the experimental spin–lattice relaxation times observed between 238 K and 330 K. Moreover the experimental and calculated minimum T_{1Z} values at 150 K are in very good agreement (155 ms). However when the temperature is lower than 150 K the experimental values of T_{1Z} are always much smaller than the corresponding ones calculated with a single residence time τ_{m12} following an Arrhenius law between 113 K and 350 K.

Two hypotheses can be put forward to explain this difference:

(i) The uniaxial rotation, which is of order 12 above T_g, would become of order 3 below T_g. However it seems difficult to believe that the activation energy corresponding to this rotation of 120° observed at low temperatures (2.2 kJ mol^{-1}), can be smaller than that corresponding to the rotations of 30° observed at high temperatures (10.5 kJ mol^{-1}).

(ii) In the glassy state, the uniaxial rotations would correspond to a distribution of residence times as observed in the 'β relaxation' in usual glasses.

With these experimental data we cannot specify more accurately the molecular motions in the glassy state. Therefore we intend to carry out similar studies of T_{1Z} and $T_{1\rho}$ in this glassy state with a very low experimental frequency f_0 of 10 or 20 MHz. At the same time we shall measure the IQNS diffusion in the same temperature scale between 100 K and 170 K. Taking these experiments all together we hope to obtain a very detailed picture of the molecular motions in the glassy state. In the ordered monoclinic phase there exists only one equilibrium position for the molecules which can then only carry out threefold uniaxial rotations between indistinguishable positions. The corresponding

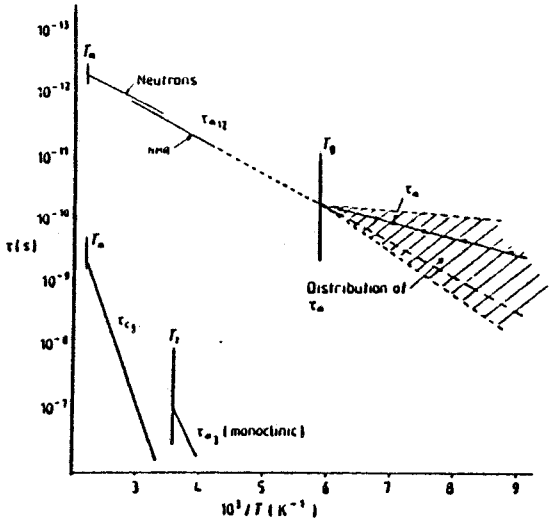

Figure 13. Reorientational residence times in all the crystalline phases of CN-ADM. τ_{m3} (monoclinic): threefold uniaxial rotation in the ordered phase. τ_{C3}: dipolar tumbling between the (001) axes in the plastic phase. τ_{m12}: 12-fold uniaxial rotation in the plastic phase. In the glassy state, the two different hypotheses concerning the uniaxial rotation are represented by a residence time τ_a distributed or not.

time follows an Arrhenius law:

$$\tau_{m3} = 1.6 \times 10^{-15} \exp(4962/T)\ \text{s}.$$

These very long values of τ_{m3} are related to the very important steric hindrance occurring during this threefold rotation (§ 3).

The spin–spin relaxation time T_2 and the second moment of the absorption line M2 are constant in the plastic phase and equal respectively to 32 μs and 0.9 G². These two constant values allow us to claim that the residence time τ_D corresponding to the molecular self-diffusion is always longer than 10^{-4} s in all the plastic phase, even near the melting point. These very important τ_D values are the proof that the vacancy concentration is always negligible even at high temperatures and *a fortiori* near T_t. Therefore we are sure that the glassy state is not connected to the vacancy concentration.

6. Conclusions

The four different crystalline phases of CN-ADM have been characterised by DSC experiments. The transition temperatures and their respective enthalpy changes have been determined. The structure of the ordered phase (space group C_2/m) has been analysed at two temperatures 135 and 240 K.

The molecular arrangements in the ordered and disordered phases are very similar in view of the centres of mass, but with very different dipolar orientations with respect to the lattices. The volumes per molecule in the cubic and monoclinic lattices are very close.

The glassy state is characterised by a complete freezing of the dipolar tumbling, by a slight transformation of the uniaxial rotation, and by an important local order.

The vacancy concentration is always negligible in this compound and therefore cannot be implicated in the glassy transition.

X-ray, Raman and coherent neutron diffusion experiments are currently being performed in our laboratory and we hope to provide a still more detailed microscopic description of the glassy transition.

Acknowledgments

We would like to thank Professors Fouret and B Najy and Doctors Virlet, Descamps and Lefebvre for interesting discussions. We are indebted to M Castelain, El Sahour and D Magnier for their help during the experiments. The authors acknowledge the support of the 'Direction des Recherches Etudes et Techniques'.

References

Adachi K, Suga H and Seki S 1968 *Bull. Chem. Soc. Japan* 41 1073–87
Amoureux J P and Bée M 1979 *Acta Crystallogr.* B 35 2957–62
Amoureux J P, Castelain M, Benadda M D, Bée M and Sauvajol J L 1983 *J. Physique* 44 513–20
Amoureux J P, Noyel G, Foulon M, Bée M and Jorat L 1984 *Mol. Phys.* 52 161–71
André D, Fourme R and Renaud K 1971 *Acta Crystallogr.* B 27 2371–80
Bée M, Amoureux J P and Dianoux J 1980 *Mol. Phys.* 41 325–39
Bonjour E and Calemczuk R 1983 private communication
Chadwick D, Legon A C and Millen 1972 *J. Chem. Soc. Faraday Trans II* 68 2064–9
Descamps M, Lefebvre J and Sauvajol J L 1983 private communications
Donohue J and Goodman S H 1967 *Acta Crystallogr.* 22 352–4
Foulon M, Amoureux J P, Sauvajol J L, Caucheteux C, Lefebvre J and Descamps M 1983 *Réunion de l'AFC (Lille) 1983.*
Fuchs A 1983 *These d'etat* University of Paris-sud, Orsay
Germain G, Main P and Woolfson M M 1971 *Acta Crystallogr.* A 27 368–76
Krishnamurthy V V, Iyer P S and Olah G A 1983 *J. Org. Chem.* 48–20 3373–8
Sheldrick G M 1976 *SHELX—A Programme for Crystal Structure Determination*
Shomaker V and Trueblood K N 1968 *Acta Crystallogr.* B 24 63–76

ANNEXE A - XI - 3

J. Physique 46 (1985) 919-926 JUIN 1985, PAGE 919

Classification
Physics Abstracts
61.10 — 61.40D — 61.50K

Structural aspects of the glassy phase of cyanoadamantane

M. Foulon, J. Lefebvre, J. P. Amoureux, M. Muller and D. Magnier

Laboratoire de Dynamique des Cristaux Moléculaires, UA 801, Bât. P5,
Université des Sciences et Techniques de Lille I, 59655 Villeneuve d'Ascq Cedex, France

(*Reçu le 16 octobre 1984, accepté le 21 février 1985*)

Résumé. — Le cyanoadamantane cristallise dans une phase cubique plastique à température ambiante et présente une phase vitreuse en dessous de 170 K en cas de trempe rapide. Pour ces deux phases, la maille est cubique à faces centrées avec un groupe d'espace moyen Fm3m ($Z = 4$). Les structures à 295 K et 110 K ont été résolues dans l'hypothèse des molécules rigides. Deux méthodes ont été utilisées pour décrire le désordre : le modèle de Frenkel et une densité électronique de symétrie cylindrique. Les facteurs de Debye Waller ont été pris en compte par les tenseurs T.L.S. Pour les deux phases, les deux modèles montrent que l'axe dipolaire de la molécule prend l'une des six orientations équivalentes [001] du cube. La densité électronique du groupe adamantyl autour de cet axe est quasiment constante. Lorsque les molécules présentent un arrangement (anti) ferroélectrique, l'encombrement stérique entre les groupes adamantyl est plus important dans la phase vitreuse ; il exclut, par rapport à la phase plastique, quelques orientations relatives des molécules autour de leur axe dipolaire. Le paramètre de la maille cubique ainsi que l'intensité de deux réflexions de Bragg ont été mesurés en fonction de la température. Il y a un changement significatif dans la pente de la courbe du paramètre de maille près de la température de transition de la phase vitreuse.

Abstract. — The cyanoadamantane molecule crystallizes in a plastic cubic phase at room temperature and displays a crystalline « glassy phase » by rapid cooling below the glassy phase transition temperature $T_g \simeq 170$ K. In both cases the cell is f.c.c. with average space group Fm3m ($Z = 4$). Their structures are solved at 295 and 110 K in the framework of rigid body molecules. Two descriptions are used to describe the disorder : a Frenkel model and a cylindrical electronic density. The Debye Waller factors are described by the classical T.L.S. tensors. For the two phases, the two models show that the molecular dipolar axis can randomly take six orientations along the [001] directions and that the average electronic density for the adamantyl group around this axis is quasi-constant. When two first neighbouring molecules have (anti-) parallel orientations, the steric hindrance between the adamantyl groups is more important in the glassy phase and prevents some relative orientations around the dipolar axis. The lattice parameter and the intensities of two selected Bragg reflections have been measured *versus* temperature. The slope of the lattice parameter curve exhibits a significant change near the glassy phase transition.

1. Introduction.

The existence of glassy phases obtained from the quenching of molecular crystals in their plastic phase has been demonstrated by Adachi *et al.* [1]. In the glassy phase, the average translational order of the plastic phase is preserved, but the orientational disorder would be frozen. Cyclohexanol is a well-known case in which the glassy phase can be easily obtained and is, for the moment, the only example of « glassy crystal » intensively studied [1-4].

In a preliminary paper [5], differential scanning calorimetry, X-ray and Raman experiments show the existence of a glassy phase in cyanoadamantane when the sample is quenched rapidly. The phase transition sequence, when reheating, is summarized in figure 1 in case of fast quenching, slow cooling and slow heating [6].

In its plastic phase, cyanoadamantane crystallizes in the cubic system with space group Fm3m. The —C≡N dipolar axis can randomly take six orientations along the four-fold axes of the cube [7]. The relaxation time for this tumbling motion, measured by dielectric relaxation at room temperature, which is $\tau_e = 3 \times 10^{-7}$ s shows that this motion is slow [8]. On the other hand, uniaxial rotation of the molecule around its dipolar axis at room temperature occurs at higher frequencies : $\tau_{uu} \simeq 10^{-11}$ s [9]. When the sample is slowly cooled, there is only a plastic to ordered phase transition at $T_t = 280$ K. In this

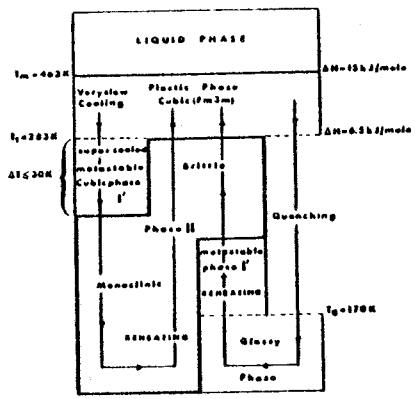

Fig. 1. — Phase transition sequence of 1-cyanoadamantane.

ordered phase, which is monoclinic with space group C2/m, the dipolar axes of the molecules exhibit an antiferroelectric arrangement [6].

The purpose of this paper is the determination of the structure of the glassy phase of cyanoadamantane by X-ray diffraction. Then in section 2, the experimental arrangement is briefly explained. Comments on the variation of the lattice parameter and the intensities of two selected reflections *versus* temperature are given in section 3. In section 4, the groundwork for the Frenkel model and the cylindrical electronic density description are developed in the case of cyanoadamantane. Results and discussion of these two methods for the structure resolution are given in section 5. A comparison of the structures of the plastic phase and the glassy state is drawn.

2. Experimental conditions.

Measurements were performed on an automatic X-ray diffractometer (PW 1100) with the MoK$_\alpha$ radiation (λ = 0.7101 Å). The incident beam was monochromated with a pyrolytic graphite crystal. The low temperature was obtained with a cold gaseous nitrogen flow. With this apparatus, it is easy to get an important fall of the temperature in a few seconds. Thus, the quenching of the single crystal of cyanoadamantane was obtained, from the plastic phase at room temperature, by a cooling rate of about 7 K per minute down to 160 K. For one experiment, the temperature was lowered immediately to 110 K; for another, the crystal was annealed for 16 hours at 160 K before the temperature decrease. In both cases, the data collection of the intensities of Bragg reflections was performed at 110 K. No significant differences are observed on the diffracted intensities showing no influence of the annealing at 160 K on the long range order. Then, the crystal was reheated by steps in order to measure the lattice constant and intensities of selected Bragg reflections at different temperatures. Further on, we shall discuss only the structure of the annealed glassy phase.

To collect intensities, θ-2θ scans were used, with an unvarying scan width of 1.4° and a scan speed of 0.42° per minute in θ. The maximum value of θ was $31.5°\left(\frac{\sin\theta}{\lambda} < 0.74\right)$ 311 reflections in an octant of the reciprocal lattice were measured corresponding to 106 non equivalent reflections. The crystal size was 0.3 × 0.3 × 0.3 mm^3. Data were corrected for Lorentz and polarization effects, but no absorption correction was applied.

The lattice parameters and the observed Bragg intensities lead to a f.c.c. lattice with 4 molecules per unit cell. Among the five possible cubic space groups, F23 and Fm3 are rejected according to the systematic condition $|F(hkl)| = |F(\bar{h}, k, l)|$ verified on all the independent measured reflections.

3. The glassy phase of cyanoadamantane.

After the quenching of the crystal, the Bragg reflections have the same experimental width as in the plastic phase (F.W.H.M. ≃ 0.18°) and no small peaks appear in the vicinity of the Bragg peaks : the sample in the glassy phase is still a single crystal.

During the annealing, the lattice constant is measured from 20 selected Bragg reflections. At the beginning of the annealing, the lattice parameter decreases slightly during the first half-hour, but the determination of this variation is inaccurate ($\Delta a \leqslant$ 0.01 Å).

From the lowest temperature obtained during this experiment (110 K) up to T_g, the lattice parameter is measured and its value is plotted *versus* temperature on figure 2. The T_g temperature is determined by the crystal breakage. This damage occurs in the metastable phase and is easily observed on the width and intensity of the Bragg reflections. To compare with the plastic phase, the lattice parameter is also measured from 235 K (in the supercooled plastic phase) to 300 K.

In the temperature range of the glassy phase, there appears a small change in the slope of the lattice constant at 150 K : for lower temperatures the linear thermal expansion coefficient is $\alpha_a = 0.82 \times 10^{-4}$ K^{-1} and between 150 K and T_g, its value is $\alpha_a = 1.08 \times 10^{-4}$ K^{-1}. In the plastic phase α_a equals 1.10×10^{-4} K^{-1}. Similar values for linear thermal expansion coefficient in the glassy state and in the plastic phase of cyanoadamantane are to be noted. By comparison with other molecular crystals, $\alpha_a = 0.65 \times 10^{-4}$ K^{-1} for hexamethylenetetramine [10], which is an ordered crystal; while $\alpha_a = 1.64 \times 10^{-4}$ K^{-1} for adamantane [11] and 1.85×10^{-4} K^{-1} for succinonitrile [12] in their plastic phase. α_a values for cyanoadamantane seem to be intermediate between ordered and orientationally disordered molecular crystals. The extrapolation of the lattice parameter at T_g from the a_p value of the plastic phase leads to a = 9.690 Å, which is close to the experimental value 9.689 Å (Fig. 2). This proves that the variation of the lattice parameter shows no discontinuity over the scanned range of temperature.

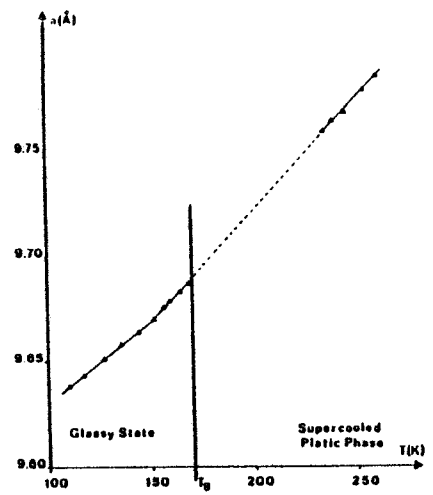

Fig. 2. — Lattice parameter of the cyanoadamantane cubic cell *versus* temperature.

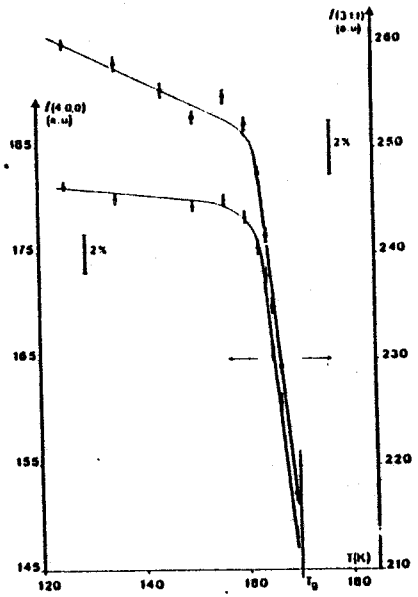

Fig. 3. — Intensities of (3, 1, 1) and (4, 0, 0) Bragg reflections *versus* temperature.

The intensities of two selected Bragg reflections have been measured *versus* temperature in the glassy phase (Fig. 3). Experimental conditions are exactly the same as for the data collection. For the two reflections (3, 1, 1) and (4, 0, 0), there is a normal temperature dependence of the intensity up to 160 K (10 K below T_g), the small decrease of the intensity corresponds to the normal increase of the Debye Waller factor with temperature. Between 160 K and 170 K, there is an important decrease of the intensity : 13 % for (3, 1, 1) and 17 % for (4, 0, 0).

4. The fitting procedure.

The atomic coordinates are deduced from the intramolecular distances and from the angles found in the low temperature monoclinic phase (Table I), [6]. The free molecule has C_{3v} symmetry. In its plastic phase, the disordered structure of cyanoadamantane has been solved using three different models :

(i) by means of a Frenkel model. In this case, the molecule of cyanoadamantane is assumed to be in one of its equilibrium positions. Best fits have been obtained when the C≡N group is along one of the six fourfold axes of the cubic cell. The disorder along the axial —C≡N group is taken into account by discrete positions of the molecule. One of the three symmetry planes of the molecule lies on one of the (1, 1, 0) planes of the cube [7].

(ii) by use of symmetry adapted functions. With this method, the positions of the atoms are known by means of an orientational probability function.

Table I. — *Parameters defining the molecule of cyanoadamantane. R_j is the distance between atom j and the centre of the adamantyl shell. The positions of the atoms are given in the T_d symmetry (symmetry of the adamantane molecule, —C≡N group along a threefold axis). θ is the angle between a secondary carbon and its two bonded hydrogen atoms.*

Parameter	Atoms	Distance (Å)	Position
—	—	—	—
R_{CT}	4 tertiary C	1.54	(x, x, x)
R_{CS}	6 secondary C	1.78	$(0, 0, z)$
R_{HT}	3 tertiary H	2.62	(x, x, x)
R_{HS}	12 secondary H	2.56	$(x, \bar{x}, z)$
R_{CNT}	C bonded to N	3.02	(x, x, x)
R_{NT}	N	4.16	(x, x, x)
θ	—	109.47°	—
R_{CM}	mass centre	0.57	(x, x, x)

As in the first method, the orientational probability displays a maximum when the —C≡N group is along the fourfold axes of the cube [13].

(iii) by a model intermediate between the previous ones, where the molecule can take many orientations around the dipolar axis. This can be described through a cylindrical electronic density for the atoms of the adamantyl group. As for model (i), dipolar axes occupy randomly the six fourfold axes of the cubic cell [7].

If we take into account the relaxation times of the two reorientational motions of the molecule (tumbling and uniaxial rotation), and the good location of the C≡N groups in the cell, the first and third methods yield the best fits. In the following, the structure of cyanoadamantane in its glassy phase will be solved with a Frenkel and a cylindrical description.

In both cases, the whole molecule is regarded as a rigid body and the ORION program [14] is used for the Frenkel model. For the cylindrical description, refinements are performed with an ORION version, modified by the authors.

The weighting scheme $W(F) = \frac{1}{\sigma(F)}$ used in the fitting procedure is taken as $\sigma(F) = K\sigma_0(F)$, with $\sigma_0(F) = \sqrt{\sigma_c^2 + E^2 F^2}$. The factor K is the multiplicity of the independent Bragg reflections. It is introduced in the least squares procedure to restore *the very different multiplicity of the reflections in the cubic system*. σ_c is the usual counting standard deviation, while the factor E is an adapted coefficient which reduces the high contribution of some very strong reflections (200, 111, 311, 400) compared with the others. The same structure fitting procedures were *performed for the plastic phase and the glassy state in* order to make a comparison. A reflection is considered as observed when $F \geqslant 3\,\sigma_0(F)$, there are 42 independent such reflections for the plastic phase and 84 for the glassy state.

4.1 THE FRENKEL MODEL. — As for the plastic phase, the prototypic molecule of symmetry C_{3v} is chosen with its C—C≡N group lying along the [0, 0, 1] cubic direction. For symmetry reasons the dipolar axis can then take six orientations. The dielectric relaxation measurements [15] show that this disorder is static in the glassy state. Taking into account the fourfold cubic axis, the axial disorder around the C—C≡N group can be described by 2, 4 or 8 discrete equilibrium positions. The three space groups which remain possible, are F432, F$\bar{4}$3m and Fm3m. In order to simplify the refinement procedure, we assume that a molecular mirror coincides with a [100] or [1$\bar{1}$0] lattice plane. In this case the Fm3m and F432 space groups lead to the same equilibrium positions. For F$\bar{4}$3m, there are only 2 equivalent positions around the dipolar axis when a molecular symmetry plane coincides with a [1, $\bar{1}$, 0] plane. The Fm3m space group introduces 4 or 8 (distinct) equilibrium positions. Finally, the mass centre of the molecule, located by symmetry arguments at (0, 0, Z_M) is able to shift along the fourfold axis of the cube.

Assuming a rigid group for the molecule, the thermal vibrations may be described by the T.L.S. tensors [16]. The symmetry of one molecule and its neighbourhood induces constraints on the components of the T.L.S. tensors. According to the local order we shall consider only the C_{3v} and σ_v cases. For the former, the local order is assumed to be uniaxial of order n (n multiple of 3) around the —C≡N axis, while for the latter, it displays a mirror coinciding with one of the molecules. When we add the scale factor and the value Z_M of the mass centre, there are 7 independent parameters in the C_{3v} description and 14 in the σ_v one.

4.2 CYLINDRICAL ELECTRONIC DENSITY DESCRIPTION. — The r_j vector joining the jth atom to the molecular mass centre is expressed in a cylindrical system $r_j = (\rho_j, \phi_j, z_j)$ in which the dipolar axis is along Oz. Atoms with the same ρ_j and z_j set up a shell, containing n_j atoms. Because of the uniaxial symmetry required for this model, the coordinates of the mass centre are (0, 0, Z_M). Thus, for a continuous cylindrical electronic density, the structure factor is given by :

$$F(Q) = F(h, k, l) = \sum_{i,j} p_i n_j f_j(Q)\, e^{-W_{ij}(Q)} \times \exp\{ iQ_{//}(Z_M + z_j) \}\, J_0(Q_{\perp i}\, \rho_j) \quad (1)$$

The j sum runs over the shells of the molecule and the i sum over all the possible orientations of the rotation axis. p_i is the probability of finding the molecule with its rotation axis along the orientation i. For cyanoadamantane, the rotation axes are along the fourfold axes of the cubic cell and $p_i = 1/6$. $Q_{//}$ and $Q_{\perp i}$ are, respectively, the parallel and perpendicular parts of the scattering vector for the ith orientation of the rotation axis. $f_j(Q)$ is the scattering factor of atoms of the jth shell and J_0 is the zero-order cylindrical Bessel function. $W_{ij}(Q)$ is the Debye Waller factor. It takes into account translational thermal vibrations of the whole molecule, as well as rotational ones around directions perpendicular to the rotation axis. The Debye Waller factor $W_{ij}(Q)$ is, in fact, expressed from the parameters T_{11}, T_{33} and L_{11} *introduced in the Frenkel model*.

When the electronic density distribution is not constant, the probability to find an atom of the jth shell with the polar angle ϕ becomes [17] :

$$P^j(\phi) = \frac{n_j}{2\pi}\left\{ 1 + \sum_{s=1}^{\infty} a_s^j \cos sn(\phi - \phi_0^j) \right\} \quad (2)$$

in which ϕ_0^j corresponds to an equilibrium position for the shell, n is the number of such equilibrium positions and a_s^j are coefficients ; the factor $1/2\pi$ ensures normalization. In this case, cylindrical Bessel functions of order sn are to be introduced in the structure factor relation. For cyanoadamantane, the minimum value of n is 12 and the Q range of the X-ray measurements is not pertinent to give significant values of $J_{12}(Q_{\perp i}\, \rho_j)$ for carbon shells. For this reason, our investigation has been limited to the constant cylindrical description.

5. Structure resolutions - results and discussion.

5.1 DIFFICULTIES IN THE REFINEMENT. — Some difficulties limit the possibilities in this structure refinement :

(i) The small number of significant independent structure factors limits the set of varying parameters. The scale factor and the T and L tensors are strongly correlated.

(ii) The high ratio of diffracted intensities leads to a critical study of the weighting scheme.

(iii) The high molecular orientational disorder appears to be taken into account by the Debye Waller factors, and leads to abnormal values of the librational thermal parameters.

5.2 RESULTS WITH THE FRENKEL MODEL. — To take into account the axial disorder with the Frenkel model, we have analysed models with 2, 4 or 8 equilibrium positions around the C≡N axis using T.L.S. tensors with a C_{3v} symmetry.

5.2.1 *Two positions.* — The description with two positions corresponds to the F$\bar{4}$3m space group and is dismissed because of the poor quality of the refinements (R = 13.2 % and R_w = 19.7 % for the glassy phase) and the negative value of the L_{11} parameter.

5.2.2 *Four positions.* — The refinements of the structures, with four uniaxial equilibrium positions, give the same results for the two possible distinct orientations (a molecular plane coincides with the [100] or [1$\bar{1}$0] planes), and this proves their coexistence in the crystal. This leads to a Frenkel model with eight equilibrium positions.

5.2.3 *Eight positions.* — The results obtained with eight uniaxial orientations confirm the previous one and give no significant decrease of the R and R_w factors. Furthermore, this disorder description leads to an electronic density distribution quite similar to a cylindrical one.

5.2.4 *Discussion of the Frenkel model.* — This discussion concerns only the case with four positions and a T.L.S. adapted to a C_{3v} symmetry. The difficulties to refine the structure with a Frenkel model come from the fact that the L_{33} coefficient has no physical meaning.

This parameter is very sensitive to the disorder around the dipolar axis and does not really measure the librational amplitude of the molecule. To take into account this rotational effect on the bond lengths we introduce a shortening of the atomic distances to the dipolar axis [18]. The R and R_w factors present a minimum for too high a relative shortening (3×10^{-2}) and for $\sqrt{L_{33}} = 14.4°$. With the twelve equivalent positions for a carbon atom of the adamantyl group and for a given direction of the —C≡N group, the rotational probability function for such an atom can be calculated using a Gaussian distribution :

$$P(\phi) = \frac{3}{12(2\pi L_{33})^{1/2}} \sum_{i=1}^{12} \exp\{ -(\phi - \phi_0^i)^2 / 2 L_{33} \} \quad (3)$$

in which ϕ_0^i is the ith equilibrium angle value. The factor 3 is the number of the atoms on the shell. This rotational probability function drawn on figure 4 nearly accounts for a cylindrical description. Using relation (2) for the $P(\phi)$ probability function limited up to $s = 1$, one gets a very small value for the first term. $a_{12} = 0.0034$ for $\sqrt{L_{33}} = 14.4°$. This fact explains the equivalent success of the model with 4 and 8 uniaxial equilibrium positions and the favourable result of the refinements with the cylindrical model as will be discussed later.

5.2.5 *Four positions with T.L.S. adapted to σ_v symmetry.* — Last attempts were made with T.L.S. tensors taking into account the σ_v symmetry with four equilibrium positions. 14 parameters are to be refined and the improvement of the results is not significant. This model has not been retained either.

5.3 RESULTS WITH THE CYLINDRICAL MODEL. — For both phases, the cylindrical description and the Frenkel model with four positions lead to about the

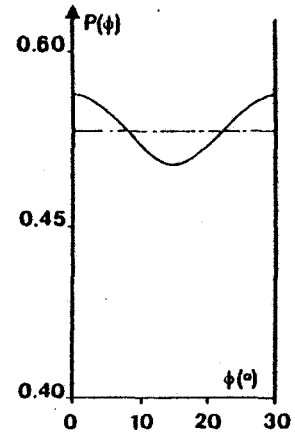

Fig. 4. — Rotational probability function around the dipolar axis for a carbon atom of the adamantyl shell. Full line : calculated from relation (3) with the Frenkel model. Mixed line ; uniaxial free rotation model $f(\phi) = 3/2\pi$.

Table II. — *Results of the best fit of the glassy state and the plastic phase of cyanoadamantane with the cylindrical Model.*

	Z_M mass centre Å	T_{11} (Å²)	T_{33} (Å²)	L_{11} (°²)	R %	R_W	E^2
Glassy state	0.46	0.0357 (25)	0.0342 (26)	4.7 (1.2)	7.5	10.2	1×10^{-4}
Plastic phase	0.51	0.0621 (47)	0.0591 (50)	10.3 (3.7)	4.6	8.7	5×10^{-5}

$$R = \frac{\sum |F_{obs} - F_{calc}|}{\sum F_{obs}} \qquad R_W = \frac{\sum w^2 (F_{obs} - |F_{calc}|)^2}{\sum w^2 F_{obs}^2}$$

same reliability indices R and R_W including, respectively, 5 and 7 parameters. The T_{11}, T_{33}, L_{11} parameters have about the same values for the two models. The cylindrical one is retained and the results of the best fits are reported in table II for the glassy state (110 K) and for the plastic phase (295 K). (The table of observed and calculated structure factors for the two phases in the framework of the cylindrical method can be provided by the authors upon request.)

In the glassy and plastic phases, the two translational thermal terms T_{11} and T_{33} are almost equal. The translational thermal motions can be regarded as isotropic. The unusual high value $\langle T \rangle = \sum_{i=1}^{3} T_{ii}/3$ equal to 0.035 Å² in the glassy state should be noted.

The mean values $\langle T \rangle$ for the glassy and the plastic phases are reported in figure 5. It also shows $\langle T \rangle$ for the ordered monoclinic phase at two different temperatures [6]. This $\langle T \rangle$ value is quasi-proportional to the temperature in the monoclinic phase. If a linear law is assumed for the cubic phases, the extrapolated value at 0 K is about 0.020 Å² and is too large to have a physical interpretation in terms of thermal motions. This large value has also been observed at low temperature for the glassy phase of cyclohexanol [4].

Indeed, it has been shown that this average cubic structure may be described by domains with lower symmetry than f.c.c. [19, 20]. Consequently, the positions of the molecular mass centres vary, according to the orientations and sizes (domain walls) of the domains.

Therefore, in this glassy phase, one can suppose that the translational term $\langle T \rangle$ takes into account two different effects :

i) the usual thermal translation nearly proportional to the temperature.

ii) the positional static disorder which has certainly a large contribution at low temperature.

An X-ray diffraction experiment at very low temperature should be very useful to show up the latter effect.

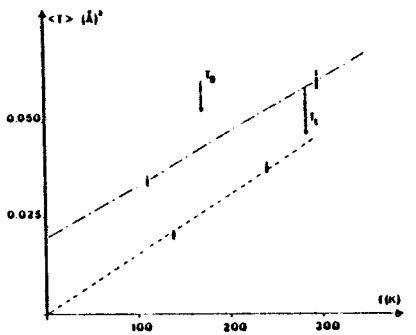

Fig. 5. — $\langle T \rangle$ *versus* temperature. Circles : monoclinic ordered phase [6], triangles : cubic (glassy and plastic) phases.

The L_{11} term, corresponding to librations perpendicular to the —C≡N group, has « normal » low values : $\sqrt{L_{11}} = 2°2$ in the glassy phase and 3°2 in the plastic phase. These values give a true measurement of the libration according to the static reorientational disorder in the glassy phase and the very slow tumbling of the molecule in the plastic phase.

The shifts of the adamantyl mass centres from the lattice origin are nearly equal for the two cubic phases (0.11 Å for the glassy phase and 0.06 Å for the plastic phase). There is, then, no obvious change in the relative positions of the molecular mass centres.

5.4 STERIC HINDRANCE BETWEEN NEIGHBOURING MOLECULES. — In cyanoadamantane, there must be correlations of a steric hindrance origin between neighbouring molecules. We discuss here this steric effect in terms of impossible configurations including the C≡N groups or the hydrogen atoms. These impossible configurations are determined by the comparison of the distances between atoms of neighbouring molecules and the sum of atomic Van der Waals radii.

Figures 6 and 7 (a, b) show projections of some molecular arrangements in the glassy phase. An individual molecule is drawn as a solid shape in which the atoms are represented by spheres with their Van der Waals radii.

Figure 6 shows, projected along **a**, the cases of impossible configurations between the C≡N groups of first (I and IV) and second (II and III) neighbouring molecules. No steric hindrance occurs when the dipolar axes are parallel or antiparallel (ferro or antiferroelectric domains). The low Kirkwood dielectric correlation factor [8, 15] suggests a local antiferroelectric arrangement. X-ray and coherent neutron scattering experiments confirm the existence of domains which are most probably antiferroelectric and tetragonal [19, 20]. If, for example, the dipolar axes correspond to the (001) direction, all the molecules on planes such as (00l), l being integer, have their dipole in the same direction ; dipoles of molecules in planes $(0, 0, l + \frac{1}{2})$ are in the opposite sense. In this case, the contact is made only between first neighbouring molecules *via* hydrogen atoms. The study of steric hindrance may be simplified by the knowledge of the molecular mutual orientations in planes (**a**, **b**) and (**b**, **c**) or (**a**, **c**). Figure 7a shows a projection along **c** on plane (**a**, **b**) of a molecule A$(\frac{1}{2}, \frac{1}{2}, 0)$ and its four first neighbours. In this case, the calculation of intermolecular distances between first neighbour molecules rotating around their dipolar axis in 15° steps, shows that no steric hindrance appears for a set of particular configurations. Figure 7b shows a projection along **a** on plane (**b**, **c**) of one molecule B at $(0, \frac{1}{2}, \frac{1}{2})$ and its four first neighbours, in a configuration with steric hindrance for some particular orientations also deduced by rotations of $n \times 15°$. The existence of 8 uniaxial equilibrium positions is then possible from steric hindrance.

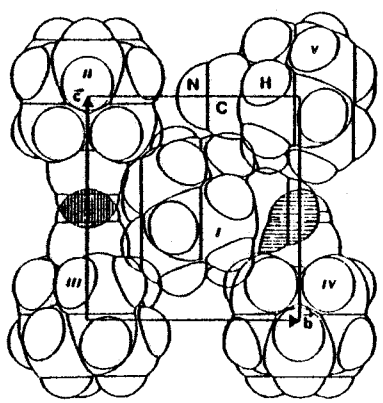

Fig. 6. — A projection in the (**b**, **c**) plane : C≡N groups with impossible orientations.

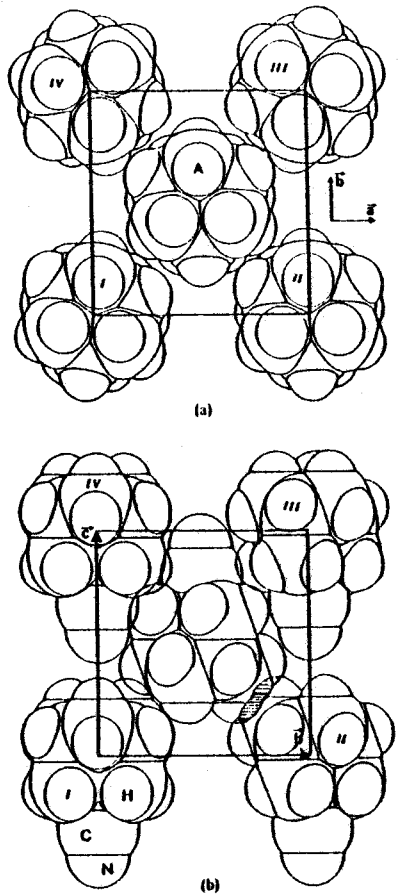

Fig. 7. — Projections in the (**a**, **b**) plane (a), and (**b**, **c**) plane (b), of possible configurations in the glassy phase of cyanoadamantane with an antiferroelectric arrangement (Dipolar axes are along **c**).

This is a second argument which corroborates the success of the cylindrical description, and points out that, in the glassy phase, geared motion may be favoured. Recent experiments of NMR [6] and IQNS [21] show a distribution of the relaxation time, which can explain the hypothesis of a collective phenomenon related to the molecular axial rotations. This motion corresponds to the usual distributed « β » relaxation observed in the glassy state.

In the plastic phase, the thermal lattice expansion is sufficient to reduce the steric hindrance effects

between hydrogen atoms. This enables a molecule to rotate around its dipolar axis quasi-independently of its first neighbours. In this case a single relaxation time is effectively observed [9].

The average structure (long-range order) of the glassy and plastic phases of cyanoadamantane are very similar.

Acknowledgments.

The authors would like to express their thanks to M. Descamps, R. Fouret and J. L. Sauvajol for helpful discussions. This research was supported by the « Direction des Recherches, Etudes et Techniques » (D.R.E.T.).

References

[1] Adachi, K., Suga, H. and Seki, S., *Bull. Chem. Soc. Japan* **41** (1968) 1073-1087.

[2] James, D. W., Shurwell, H. F. and Parry, R., *J. Raman Spectrosc.* **5** (1976) 201-9.

[3] Ceccaldi, D., Denoyer, F., Lambert, M. and Szwarc, H., *J. Physique Lett.* **41** (1980) L365-8.

[4] André, D., Ceccaldi, D. and Szwarc, H., *J. Physique* **45** (1984) 731-37.

[5] Foulon, M., Amoureux, J. P., Sauvajol, J. L., Lefebvre, J. and Descamps, M., *J. Phys. C : Solid State Phys.* **15** (1983) L 265-9.

[6] Foulon, M., Amoureux, J. P., Sauvajol, J. L., Cavrot, J. P. and Muller, M., *J. Phys. C : Solid State Phys.* **17** (1984) 4213-4229.

[7] Amoureux, J. P. and Ble, M., *Acta Cryst.* **B 35** (1979) 2957-62.

[8] Amoureux, J. P., Castelain, M., Benada, M., Bee, M. and Sauvajol, J. L., *J. Physique* **44** (1983) 513.

[9] Bee, M., Amoureux, J. P., Dianoux, *Molec. Phys.* **41** (1980) 325.

[10] Dolling, G. and Powell, B. M., *Proc. Roy. Soc. London* **A 319** (1970) 209-35.

[11] Damien, J. C., Thesis (1978), Université de Lille I.

[12] Fontaine, H., Thesis (1973), Université de Lille I.

[13] Amoureux, J. P., Sauvajol, J. L., Ble, M., *Acta Cryst.* **A 37** (1981) 97-104.

[14] André, D., Fourme, R. and Renaud, M., *Acta Cryst.* **B 27** (1971) 2371.

[15] Amoureux, J. P., Noyel, G., Foulon, M., Bee, M. and Jorrat, L., *Mol. Phys.* **52** (1984) 161-171.

[16] Schomaker, V. and Trueblood, K. N., *Acta Cryst.* **B 24** (1968) 63-76.

[17] Lefebvre, J., Fouret, R. and Zeyen, C. M. E., *J. Physique* **45** (1984) 1317-1327.

[18] Cruickshank, D. W. J., *Acta Cryst.* **14** (1961) 896.

[19] Descamps, M., Cauchetteux, C., Oddou, G. and Sauvajol, J. L., *J. Physique Lett.* **45** (1984) L719-727.

[20] Lefebvre, J., Ricland, J. P., Sauvajol, J. L. and Hennion, B., *J. Phys. C* **18** (1985) 241-255.

[21] Bee, M., (1984), Private communication.

ANNEXE A - XI - 4

MOLECULAR PHYSICS, 1984, VOL. 52, No. 1, 161-171

Low frequency dielectric properties of 1-cyanoadamantane $C_{10}H_{15}CN$

by J. P. AMOUREUX†, G. NOYEL‡, M. FOULON†, M. BÉE† and L. JORAT‡

† Laboratoire de Physique des Solides.
Equipe de Dynamique des Cristaux moléculaires associée au C.N.R.S., N. 465,
Université de Lille I, 59655 Villeneuve d'Ascq Cedex, France.

‡ Laboratoire de Physique des matériaux, U.E.R. Sciences,
23. Rue du Dr. Paul Michelon, 42023 St. Etienne Cedex.

(*Received* 10 *October* 1983; *accepted* 16 *December* 1983)

Dielectric properties of 1-cyanoadamantane $C_{10}H_{15}CN$ are analysed with very low frequencies between 80 K and 320 K. The critical frequency in the (stable and supercooled) plastic phases does not follow an Arrhenius law. This behaviour corresponds to the glassy state of cyanoadamantane. However, β relaxation in the glassy phase certainly does not exist in this compound.

1. Introduction

For some years we have undertaken an extensive and comparative study of substituted adamantanes. This series of compounds are particularly interesting owing to their high symmetry and to the fact that most of them are in a cubic plastic phase at room temperature. One of the most interesting substituted adamantanes is 1-cyanoadamantane (CN-ADM): $C_{10}H_{15}CN$. Its interest arises from its long cylindrical substituent, from its very large permanent dipole moment ($\mu_v = 3{\cdot}83$ D) and from its being in a plastic phase at room temperature (melting point $T_m = 458$ K). This compound, formally known as 1-cyano tricyclo [3, 3, 1, 1] decane, is composed of globular molecules and is obtained from adamantane, $C_{10}H_{16}$, by substituting a cyano group onto a methine carbon (figure 1). Microwave spectra [1] and ^{13}C NMR chemical shifts [2] have shown that this substitution does not change the rest of the molecule whose symmetry is then C_{3v}. The molecular motions of this compound have been studied by Incoherent Quasi-elastic Neutron Scattering (IQNS [3]), ^1H-NMR [4] and high-frequency dielectric relaxation [5]. In these three experiments we have never really observed the transition between the plastic and the brittle phases. In order to explain this lack of transition we have then carried out some DSC experiments.

2. Cyanoadamantane is a glassy crystal

The possible existence of a glassy crystal phase obtained by quenching of some molecular plastic crystals has been discussed [6]. If the crystal in the

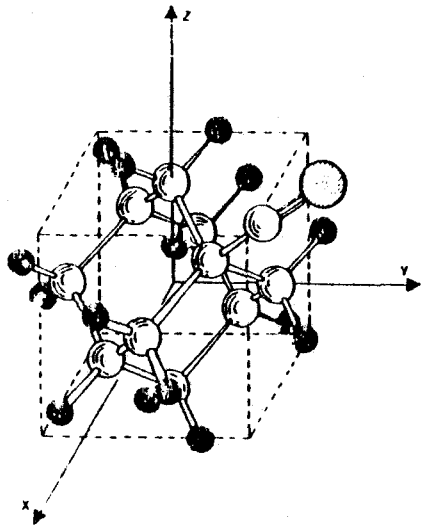

Figure 1. The molecule of cyanoadamantane, carbons are in white, hydrogens in black and nitrogen is cross-hatched. A cube has been drawn to indicate the directions of atoms with respect to each other, it does not correspond to the directions of the unit cell.

plastic phase (phase I) is cooled rapidly enough to prevent the transition towards the low temperature ordered phase (phase II), the disordered system is supercooled and ultimately goes into a glassy state (phase I_g). That is the case for cyanoadamantane. The successive peaks in the DSC curve (figure 2), obtained after quenching from 300 K to 90 K, can be interpreted as follows (figure 3):

(i) The endothermic anomaly at $T_g = 170$ K is due to a glass transition from the glassy crystalline phase I_g to a metastable phase I', which we shall see is the supercooled plastic phase.

(ii) The exothermic irreversible transition at about 205 K corresponds to the transition from the metastable form (I') to the low temperature brittle phase (II). As usually observed in many plastic crystals there can exist a noticeable delay in the transformation from the disordered state to the ordered one (I'→II). This delay is more or less important according to the crystals and therefore this transition runs over 50 K in this powdered sample.

(iii) The endothermic peak at about $T_t = 280$ K is the usual non plastic–plastic transition. As in all the other known glassy crystals [7] the ratio $T_g/T_t = 0{\cdot}6$ lies between 0·5 and 0·7.

When the temperature is lowered slowly from 300 K, the plastic phase is supercooled and the transition to the brittle phase occurs below 250 K at a temperature which depends on the cooling rate. X-ray diffraction data have been recorded on single crystals in both the brittle and glassy phases. The

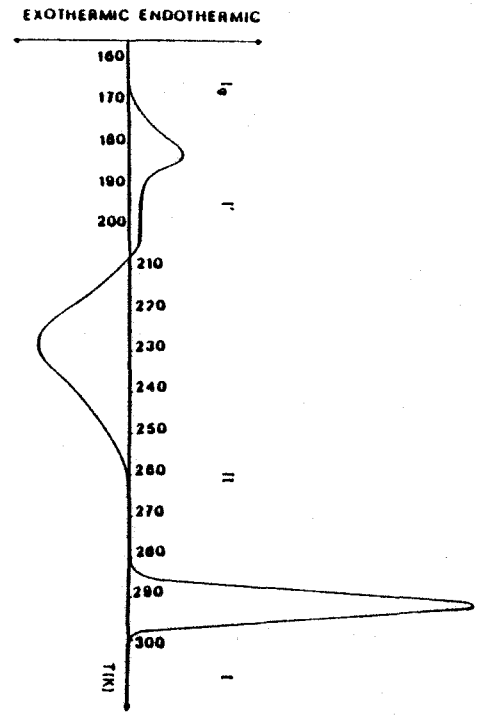

Figure 2. A DSC curve of CN-ADM corresponding to quenching followed by warming (40 K/min).

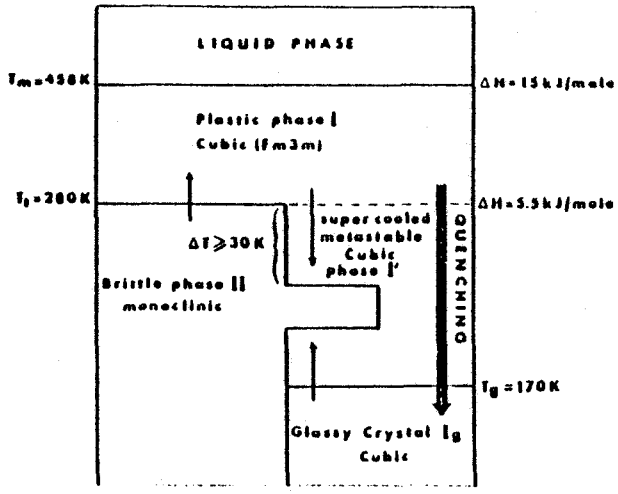

Figure 3. Polymorphic forms and thermal properties of cyanoadamantane.

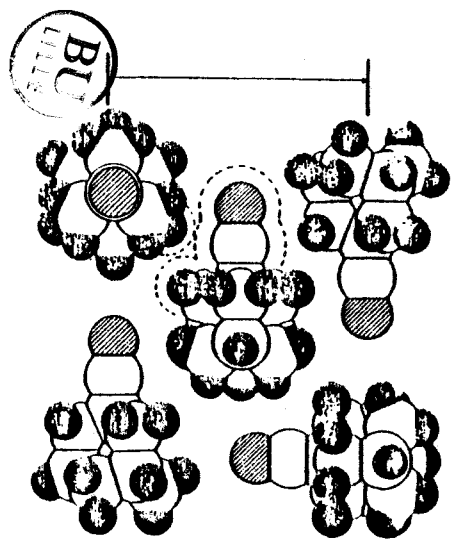

Figure 4. An example of packing of cyanoadamantane in the (001) plane.

brittle phase (II) is monoclinic (space group $C2/m$) and an anti parallel local order has been pointed out [8].

The glassy (I_g) and the plastic (I, I') phases have exactly the same f.c.c. structure [9, 10] with four molecules in the cubic cell. The dipolar C–C≡N axis can take randomly six orientations very closely located along the ⟨001⟩ directions. The analysis of the Bragg peak intensities have shown that for each of the six dipolar orientations, the molecule can occupy four distinct equilibrium positions derived from each other by 30° rotations around its three-fold symmetry axis. In figure 4 we have shown an example of packing and one can see that for each particular molecule some positions are impossible consequent on the steric hindrance between first and even second next-neighbour molecules : there thus exists a local order. However when a macroscopic sample is observed, all the equilibrium positions for the averaged molecule have the same probability.

According to this structural description, two very different motions may exist in the cubic phases : a fast quasi-free uniaxial rotation [3, 4] around the C–C≡N group and a slow tumbling reorientation of the dipole moment between the ⟨001⟩ axes of the cubic lattice [5]. At room temperature, in the plastic phase, the corresponding frequencies are very different : 10^{11} Hz and 10^{5} Hz. Raman spectra recorded in the glassy phase [11] have shown the vanishing (with respect to the plastic phase) of the low frequency contributions, which suggests that a local order takes place in the glassy phase of CN-ADM. Dielectric relaxation experiments had then to be carried out at low temperatures to see if the slowing down of the dipolar reorientations is implicated in the transition to the glassy state.

3. Experimental conditions for the dielectric relaxation of CN-ADM

The complex permittivity of CN-ADM has been obtained directly with a spectrometer using a data sampling process and a digital calculator at low frequencies [12] and with an automatic impedance bridge (HP 4275 A) monitored by a microcomputer (HP 85 F) at higher frequencies.

Generally, the experiments were carried out at fixed frequency, the experimentally varied parameter being the temperature. Eight high (above 10 kHz) and three low (under 100 mHz) frequencies were used. When the samples were quenched the temperature was decreased from 300 K to 80 K in about 600 s. The uncertainty in the position of each relaxation peak is about 0·25 K. The temperature gradient in the sample (0·5 K) was always identical with our experimental conditions and thus does not affect the relative temperature accuracy. After quenching, when the sample was warmed (heating rate 0·5 K/min), the complex permittivity was measured every 0·25 K in the relaxation zones.

Since the material under investigation has cubic symmetry, the complex permittivity is isotropic and can be measured directly on a powder sample. Therefore, the experiments were performed on homogeneous mixtures of powdered CN-ADM (concentration θ) with air. In a recent paper [13] it was shown that the dynamical dielectric properties of a concentrated mixture are well described by Böttcher's formula :

$$\frac{\epsilon_{exp}^{*}-1}{3\epsilon_{exp}^{*}}=\theta\,\frac{\epsilon^{*}-1}{2\epsilon_{exp}^{*}+\epsilon^{*}},$$

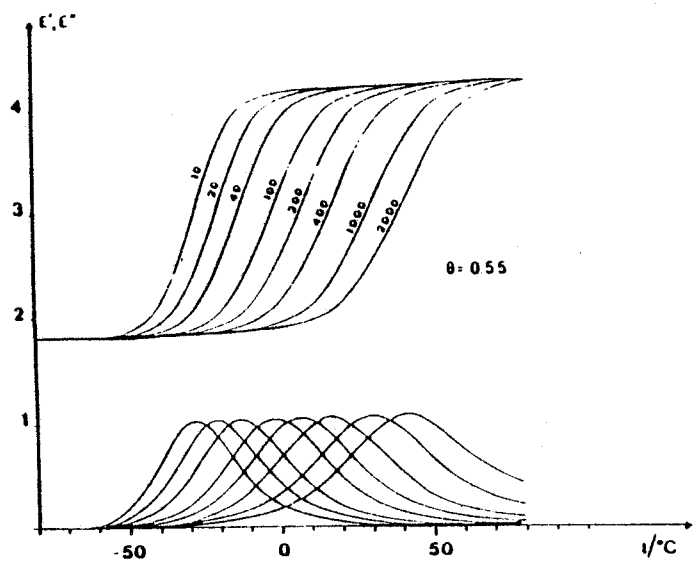

Figure 5. Experimental complex permittivity (θ = 0·55) corresponding to a slow (−0·5 K/min) cooling from the plastic phase. The frequency is indicated in kHz.

where ϵ^* and $\epsilon_{exp}{}^*$ are respectively the complex permittivity of the single crystal and of the homogeneous mixture.

The powder sample was put in a cylindrical capacitor 5 cm long with inner and outer conductor diameters respectively of 25·1 and 31·0 mm. For each different filling of the dielectric cell, a spectrum measured at room temperature allowed us to recalibrate, in a more precise way, these results ($\theta \simeq 0{\cdot}58$) with those obtained previously [5] with a larger concentration ($\theta = 0{\cdot}95$).

4. High frequency results

Eight different frequencies were used : 10, 20, 40, 100, 200, 400, 1000, 2000 kHz. In a first series of experiments, the temperature was decreased slowly (−0·5 K/min) from 353 K to 120 K. The corresponding complex permittivities (figure 5) agree with those previously published [5]. According to the temperature, the sample was in the stable I ($T > 280$ K) or in the supercooled I′ plastic phase. The transition from plastic to brittle phases was not observed with these experimental conditions. Hence the frequencies must be too high.

In a second series of experiments, the temperature was then increased slowly (0·5 K/min) from 120 K and the transition was then clearly visible at 280 K. However the results obtained in this case are identical to those of figure 5 only if the temperature is shifted by about 6 or 7 degrees.

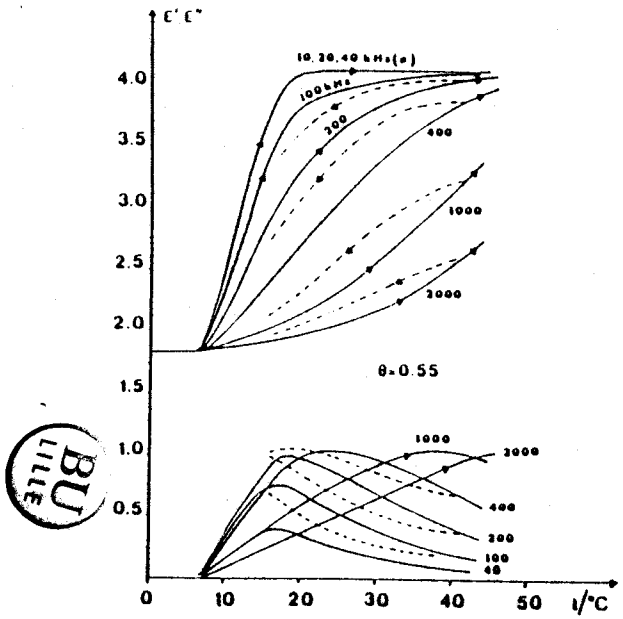

Figure 6. Experimental complex permittivity ($\theta = 0{\cdot}55$) corresponding to a slow warming from the brittle phase (continuous curves) followed by a slow cooling from 315 K (dashed curves).

This hysteresis effect was pointed out more obviously in a third series of experiments in which the temperature was first increased from 120 K to 315 K and then decreased to 288 K. Indeed one can see in figure 6 that the complex permittivities are different depending on whether the temperature is increased from the brittle phase or lowered from the plastic phase.

5. Low frequency results

Two different fillings of the cell were successively used, but corrected to the pure bulk material they gave the same results.

The samples were successively quenched quickly and warmed slowly. For the three experimental low frequencies (33, 50·4, 82·6 mHz) the complex dielectric permittivity showed the same aspect (figure 7) which can be interpreted as follows :

(i) Between 90 K and 170 K, in the glassy phase (I_g), the critical frequency F_c (corresponding to the maximum value ϵ''_M of the loss factor) is lower than 50 mHz : $\epsilon'' = 0$. Another relaxation zone, below 90 K and with these three experimental frequencies, is improbable as the ϵ' value (2·7) corresponds to a quite possible refractive index [14] : $n = \sqrt{(2{\cdot}7/1{\cdot}05)} = 1{\cdot}6$. Relaxation phenomena (if any) in the glassy phase (classically called β relaxations [7]) may perhaps occur, but with very low experimental frequencies ($< 10^{-3}$ Hz), which would be in contrast with other known glassy crystals [7].

(ii) The relaxation phenomena (called relaxation α [7]) occurs in the metastable phase I′, between 170 K and 200 K. ϵ' increases with temperature

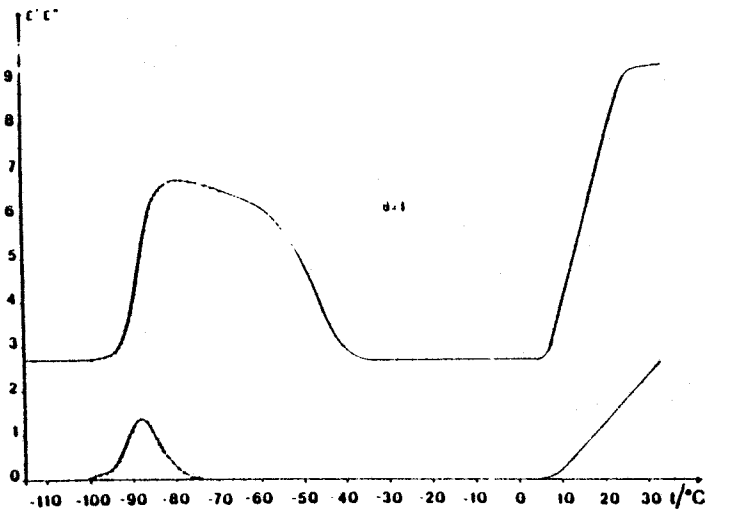

Figure 7. Isofrequency plot ϵ'', ϵ' versus T (50·4 mHz ; 0·5 K/min) corrected to single crystal, after a quenching (300 K − 80 K). We have represented the experimental points only in the relaxation zone.

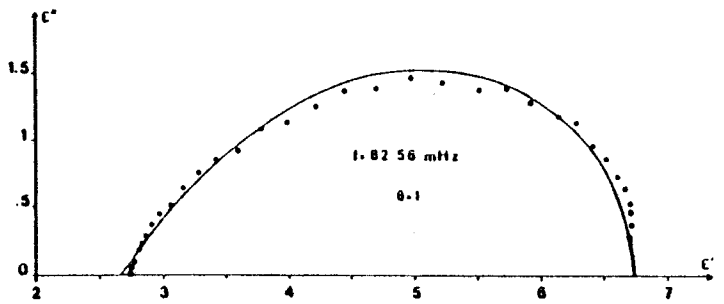

Figure 8. Isofrequency Cole–Cole plot ϵ'' versus ϵ' (82·6 mHz ; 0·5°C/min) with $\beta = 0{\cdot}57$. The experimental points are corrected for single crystal.

from $\epsilon_\infty(\mathrm{I}')$ to the static dielectric $\epsilon_s(\mathrm{I}')$, and the loss factor ϵ'' shows a relaxation aspect. The Kirkwood–Frohlich theory [15] (generalized to solids by Bordewijk [16]) allows the calculation of the static dielectric Kirkwood g factor which takes into account the short-range correlations between molecules :

$$g = \frac{1}{\mu^2}\left\langle \mu_1 \sum_i \mu_i \right\rangle.$$

If locally the dipole moments μ are (anti) parallel, then $g > 1$ ($g < 1$). If there are no correlations or if the correlations arrange the permanent dipoles in a perpendicular way, then $g = 1$. If we assume that this theory is applicable in this metastable phase, one obtains an anti-parallel local order for this I′ phase : $g = 0{\cdot}15$ at 190 K. We have represented on figure 8 the Cole–Cole plot (ϵ'' versus ϵ') measured at 82·56 mHz. Obviously this curve corresponds to a Cole–Davidson macroscopic distribution

$$\epsilon^*(\omega) = \epsilon_\infty + \frac{\epsilon_s - \epsilon_\infty}{(1 + i\omega\tau)^\beta}.$$

If one assumes that the distribution does not change in the temperature range corresponding to the relaxation, the parameter β is equal to 0·57.

(iii) At about 200 K, the CN-ADM changes from the metastable (I′) to the brittle (II) phases. X-ray studies have shown [8] that in the monoclinic phase the dipole moments are ordered, which corresponds to the lack of relaxation phenomena : $\epsilon'' = 0$ and $\epsilon' = 2{\cdot}7$. This value of 2·7 for ϵ', identical in the glassy and brittle phases, is a new demonstration for the refractive index $n = 1{\cdot}6$.

(iv) At 280 K, CN-ADM transforms into the cubic plastic phase. The critical frequency F_c being equal to 120 kHz in this phase, the ϵ' value is equal to $\epsilon_s(\mathrm{I})$. When the temperature increases from 280 K, cyanoadamantane presents some superficial conductivity visible at these low experimental frequencies (and not above 10^4 Hz : figure 5). Therefore ϵ' and ϵ'' are not constant, but these variations do not correspond to the molecular reorientations.

A very important question arises from the previous studies : is the metastable phase (I′), the continuation of the supercooled plastic phase ? In order to elucidate this question, we carried out another experiment in which the temperature was decreased (−1 K/min) from 300 K to 120 K. At about 220 K a large proportion (≃85 per cent) of the sample transformed into the brittle phase, but the remainder relaxed at the same temperature as previously. This relaxation was visible only on ϵ' (figure 9), because the experimental variations of ϵ'' were certainly too small (ϵ''_M (calculated) = 0·07). The experimental critical frequency is identical when the temperature is increased from the glassy phase or lowered from the plastic phase. Therefore the three critical low frequencies have to be related to those already measured [5] in high frequency range.

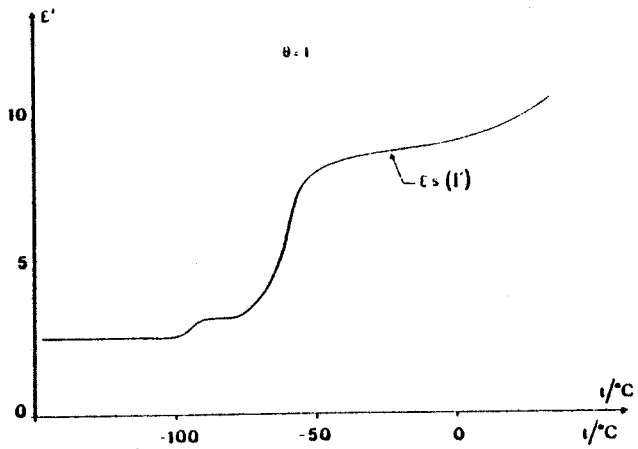

Figure 9. Experimental complex permittivity (corrected for single crystal) corresponding to a slow cooling from the plastic phase with $f = 50{\cdot}4$ mHz.

6. Conclusions

Obviously the critical frequency in the (stable and supercooled) plastic phases does not follow an Arrhenius law in all the temperature range above T_g (figure 10). An Arrhenius law can only describe the critical frequencies above 100 Hz : $F_c = 2{\cdot}03 \times 10^{14} \exp(-5940/T)$ Hz.

If one uses the phenomenological law of Vogel-Fulcher-Tamman : $F_c = F_c^\infty \exp(-T_1/(T - T_0))$, a good description of the critical frequencies between 0·03 and 10^7 Hz is then obtained with :

$$F_c^\infty = 60{\cdot}2 \text{ GHz}, \quad T_1 = 2176 \text{ K}, \quad T_0 = 107{\cdot}1 \text{ K}.$$

This description with respect to the temperature of the critical frequency is characteristic of compounds having a glassy state [7]. However, contrary

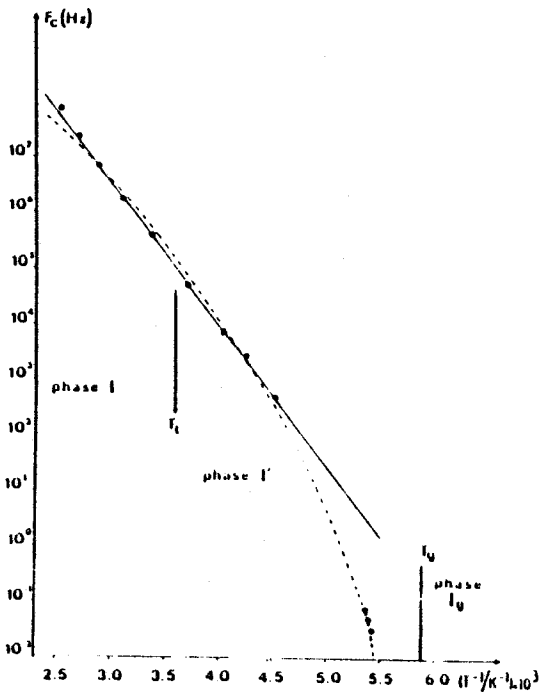

Figure 10. Critical frequency F_c versus $10^3/T$(K). The continuous line corresponds to the Arrhenius law and the dashed curve to Vogel–Fulchel–Tamman : $F_c = 6{\cdot}02 \times 10^{10} \exp(-2176/(T-107{\cdot}1))$ Hz.

to most of these compounds, CN-ADM certainly does not present a β dielectric relaxation in the glassy phase.

The correlation time corresponding to the tumbling motion of the cyano group is much more distributed in the supercooled plastic phase between 170 K and 200 K. In all the plastic phase the Kirkwood correlation g factor shows an anti parallel local order.

The authors acknowledge the support of the ' Direction des Recherches Etudes et Techniques '.

References

[1] Chadwick, D., Legon, A. C., and Millen, A., 1972, *J. chem. Soc. Faraday Trans. II*, 68, 2064.
[2] Maciel, G. E., Dorn, H. C., Greene, R. L., Kleschick, W. A., Peterson, M. R., and Wahl, G. H., 1974, *Org. magn. Res.*, 6, 178.
[3] Bée, M., Amoureux, J. P., and Dianoux, J., 1980, *Molec. Phys.*, 41, 325.
[4] Amoureux, J. P., Castelain, M., Bée, M., Arnaud, B., and Shoutteten, M. L., 1981, *Molec. Phys.*, 42, 119.
[5] Amoureux, J. P., Castelain, M., Benadda, M. D., Bée, M., and Sauvajol, J. L., 1983, *J. Phys.*, 44, 513.

[6] Adachi, K., Suga, H., and Seki, S., 1968, *Bull. chem. Soc. Japan*, 41, 1073.
[7] Johari, G. P., 1976, *Ann. N.Y. Acad. Sci.*, 279, 117.
[8] Foulon, M., Amoureux, J. P., Sauvajol, J. L., Cavrot, J. P., and Muller, M., 1984, *J. Phys.* C (in the press).
[9] Amoureux, J. P., and Bée, M., 1979, *Acta crystallogr.* B, 35, 2957.
[10] Foulon, M., Lefebvre, J., and Amoureux, J. P., 1983 (private communication).
[11] Sauvajol, J. L., 1983, Thesis, University of Lille, France.
[12] Noyel, G., Huck, J., and Bondeau, A., 1979, *Rev. Phys. Appl.*, 14, 653.
[13] Benadda, M. D., Carru, J. C., Amoureux, J. P., Castelain, M., and Chapoton, A., 1982, *J. Phys.* D, 15, 1477.
[14] Böttcher, C. J. F., 1973, *Theory of Electric Polarization*, second edition, Vol. 1 (Elsevier), p. 180.
[15] Kirkwood, J., 1969, *J. chem. Phys.*, 7, 911. Froehlich, H., 1949, *Theory of Dielectrics* (Clarendon Press).
[16] Bordewijk, P., 1978, *Chem. Phys.*, 33, 451.

ANNEXE A-XI-5

J. Phys. C: Solid State Phys. 20 (1987) 337–349. Printed in the UK

The glassy phase of 1-cyanoadamantane; a study of the molecular reorientations by high-resolution quasi-elastic neutron scattering

M Bée†‡, M Foulon†, J P Amoureux†, C Caucheteux† and C Poinsignon‡

† Laboratoire de Dynamique des Cristaux Moléculaires (UA 801), Université des Sciences et des Techniques de Lille I, 59655 Villeneuve d'Ascq Cédex, France

‡ Institut Laue–Langevin, 156 X, 38042 Grenoble Cédex, France

Received 25 March 1986

Abstract. Using the incoherent quasi-elastic neutron scattering (IQNS) technique, the motions of 1-cyanoadamantane $C_{10}H_{15}CN$ are investigated below 170 K in the glassy phase obtained by rapid quenching of the room-temperature orientationally disordered phase. The broadening of the experimental spectra is evidence for the existence of rotations of the molecules about their symmetry axes on the timescale 10^{-11}–10^{-9} s. However, from a direct Fourier transform analysis, it is demonstrated that the experimental data cannot be described in terms of any simple jump model involving a single correlation time. In accordance with the conclusions of the studies by NMR and x-ray techniques, an interpretation based upon a distribution of the correlation times is proposed. Finally, we discuss whether this time distribution is a characteristic feature of this glassy state.

1. Introduction

The existence of a new type of glasses was demonstrated by Adachi *et al* (1968): by rapidly cooling some molecular crystals, initially in their orientationally disordered phase (plastic phase), the normal transition into an ordered low-temperature phase can be avoided and the specimen passes into a 'glassy state'. A common description of such a phase is that the average translational order is preserved, but the orientational disorder is frozen. Because of the crystalline nature of these glassy phases, the study of them should provide a better understanding of the usual amorphous glasses.

This type of glassy transition has been observed for 1-cyanoadamantane $C_{10}H_{15}CN$ (hereafter referred to as ADM-CN), shown schematically in figure 1. The molecule has the general shape of a globular adamantyl cage, onto which is bonded a rather elongated radical C ≡ N. The resulting molecular symmetry is C_{3v}. The whole molecule bears a large dipole moment (3.9D).

The crystal structure of the FCC plastic phase (space group F_{m3m}, $Z = 4$) has already been described in some detail (Amoureux and Bée 1979, Amoureux *et al* 1981b), as also has the nature of the dynamical disorder. Several experimental techniques, i.e. NMR (Amoureux *et al* 1981a, 1986), dielectric relaxation (Amoureux *et al* 1983), and incoherent quasi-elastic neutron scattering (IQNS) (Bée *et al* 1980) show that two types of molecular motions exist simultaneously. The first motion corresponds to the reorientation of the molecule's threefold axis (dipole axis) from one ⟨001⟩ lattice direction to

0022-3719/87/030337 + 13 $02.50

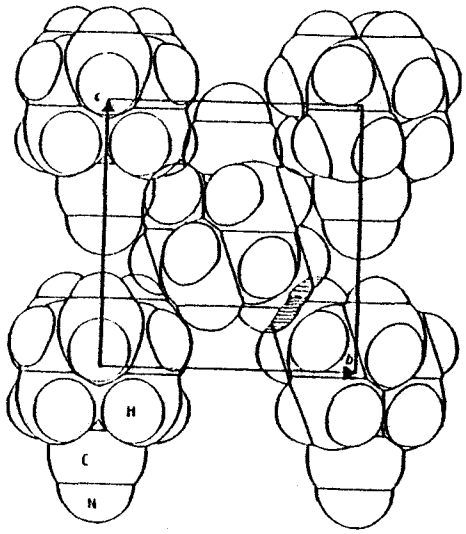

Figure 1. A possible configuration of 1-cyanoadamantane molecules in the glassy state with an antiferroelectric arrangement (Foulon *et al* 1985).

another, while the second is the rotation of the molecule about this axis. The former motion is strongly hindered by the first- and second-neighbouring molecules. Hence the mean residence time of the molecule dipolar axis along the (001) directions is rather large. Conversely, the latter motion appears to be more free. It has been described as 30° jumps among twelve equilibrium positions. The related correlation time $\tau_{m_{12}}$ is about 1.6×10^{-12} s at $T = 300$ K. The ordered phase below $T = 280$ K is monoclinic, C2/m. The crystal structure can be described as a succession of parallel planes composed of molecules with their dipoles in antiparallel order, along one (111) pseudo-cubic direction (Foulon *et al* 1984). NMR measurements prove that the motion around the molecular threefold axis still exists, in spite of a strong steric hindrance (Foulon *et al* 1984, Amoureux *et al* 1986).

Below the glassy transition temperature ($T_g \simeq 170$ K), the glassy state exhibits the same average space group as the plastic phase, in which the molecules occupy the same equilibrium positions (Foulon *et al* 1985). X-ray and coherent neutron scattering measurements (Descamps *et al* 1985, Lefebvre *et al* 1985) have demonstrated the progressive increase in the numbers of interlocked antiferroelectric domains. The glass transition preserves the translational order and affects the molecular orientations.

Therefore, the knowledge of the evolution, as a function of temperature, of the dipole residence time among the equilibrium positions is an essential factor in obtaining an understanding of the exact mechanism of the glass transition.

Low-frequency dielectric relaxation measurements (Amoureux *et al* 1984, Pathmanathan and Johari 1985) have clearly shown that the dipole tumbling is frozen at T_g according to a Vogel–Fülcher law. Conversely, the uniaxial reorientation still continues to be observable using NMR below T_g (Foulon *et al* 1984, Amoureux *et al* 1986).

The IQNS technique permits observation of each individual scatterer inside a molecule

and consequently constitutes a way of investigating the motions of the molecule itself. Because the number of hydrogen atoms in the ADM-CN molecule is rather large, and due to the large incoherent cross section of this element, this compound is particularly suitable for investigation using this technique. In this paper, we report on IQNS measurements recently performed with ADM-CN, using the high-resolution back-scattering method.

2. Experimental conditions

The experiments were carried out at the Institut Laue–Langevin, in Grenoble. The back-scattering spectrometer IN10 was chosen because of its high resolution in energy for the range expected to be relevant. Use of a powder sample enabled us to avoid a lot of technical difficulties linked with the growing and the cutting of single crystals with large enough area and small enough thickness to obtain a sufficient scattered intensity without significant contamination from multiple scattering. In theory, using a polycrystalline specimen rather than a single crystal leads to a loss of information because of the averaging over all the directions of the scattering vector Q. However, on the timescale of the experiment the dipolar orientational disorder can be considered static (Bée *et al* 1980). The scattering law related to uniaxial rotation has to be averaged over the six possible (100) directions, and the use of a single crystal would not actually provide much more information.

The following temperatures were chosen for the measurements: $T = 138$, 149 and 159 K ($T_g = 170$ K). Si [111] analysers were set up about the average scattering vector values, $Q = 1.2$, 1.55, 1.72 and 1.93 Å^{-1}, in order to avoid Debye circles corresponding to Bragg reflections ($\lambda = 6.28$ Å). The instrument resolution was of the order of 1 μeV (FWHM) for an energy range of the analysis of ± 13 μeV. The multiple scattering did not need to be taken into account because of the very small thickness of the specimen, about 0.3 mm, corresponding to a transmission of 0.9 when the sample was perpendicular to the neutron beam. The flat sample, 38×35 mm^2 in dimension, was oriented at 45° to the incoming neutrons. A rapid quenching was achieved by directly dipping the sample into liquid nitrogen and this was followed by a slow heating up to the required temperature. Thus, commencement of crystallisation into the monoclinic phase may be considered improbable.

Another series of measurements was performed at $T = 159$ K, where, for improving the instrument resolution, polished analyser plates were employed. The FWHM of the resolution function was decreased to about 0.42 μeV. An even better value could have been obtained by using a polished monochromator, but we did not use one because we wanted to keep sufficient incident neutron flux. In this experiment, data were collected for only three values of Q, 1.31, 1.72 and 1.93 Å^{-1}.

The usual corrections for absorption, self-shielding and sample holder scattering were applied to the data, and then they were analysed on the basis of dynamical models.

3. Analysis of the experimental results

Basic hypotheses and fundamental expressions arising in IQNS have already been discussed at some length in reference textbooks (Leadbetter and Lechner 1979, Springer 1972) and will not be reported here. The relevant equation in the study of molecular

reorientations is the rotational scattering law

$$S_{inc}(Q, \omega) = a_0(Q)\delta(\omega) + \sum_{i=1}^{n} a_i(Q)\frac{1}{\pi}\frac{\tau_i}{1 + \omega^2\tau_i^2}. \quad (1)$$

which appears to be composed of two contributions. The first term on the RHS of (1) corresponds to a purely elastic scattering. The coefficient of the δ-function, $a_0(Q)$, is called the elastic incoherent structure factor (EISF). It provides information about the geometry of the motion. The second term on the RHS is known to be quasi-elastic from the presence of the lorentzian functions. Their number, n, and their respective weights, $a_i(Q)$, depend on the precise model considered. Their half-widths at half-maximum τ_i^{-1}, involve the different jump-rate probabilities per unit time for the molecule. The EISF and the quasi-elastic structure factors ($a_i(Q)$) are linked together through the relation

$$a_0(Q) + \sum_{i=1} a_i(Q) = 1. \quad (2)$$

From the integration over the energy values of the spectra recorded at constant Q, it is clear from (1) that the EISF can be determined experimentally:

$$a_0(Q) = I_{el}(Q)/(I_{el}(Q) + I_q(Q)) \quad (3)$$

where $I_{el}(Q)$ and $I_q(Q)$ are the elastic and quasi-elastic scattered intensities, respectively.

3.1. *Analysis of the elastic scattering*

Experimental values of the EISF were obtained for ADM-CN in its glassy phase at each temperature by refining a purely phenomenological model to the spectra collected at each Q-value. Spectra predicted by this model were composed of a purely elastic contribution and of a quasi-elastic part, itself formed of two lorentzian functions, convoluted with the instrument resolution. The magnitudes of each of these three components and the widths of the lorentzian functions were introduced as parameters in the refinement procedure. Good fits were obtained (see figure 2). The quasi-elastic part of the spectra could be particularly well described by the combination of the two lorentzian functions. From the relative magnitudes of the elastic intensities, experimental values of the EISF were deduced and compared with those predicted by theoretical models.

The conclusions of the dielectric relaxation study are that the tumbling of the dipolar axis is frozen and the only relevant motions are the uniaxial rotations. This is the fundamental result from all our analysis. The molecule with symmetry C_{3v} is aligned along the (001) fourfold axes.

According to these symmetries, the time- and space-averaged structure, analysed by x-ray diffraction, indicates 12 equilibrium positions for one hydrogen atom (corresponding to four discernible molecular ones). This static description does not presume the dynamical one. In fact, in a jump-model framework, it can be assumed that one individual hydrogen atom can carry out uniaxial rotation over $N = 3, 4, 6$ or 12 sites.

The relevant correlation times, τ_i, for these models are listed in table 1. They are easily evaluated from the general relation

$$\tau_i^{-1} = 2\tau_{m_x}^{-1}\sin^2(\pi i/N) \quad (4)$$

where N is the number of sites and τ_{m_x} the residence time at each site.

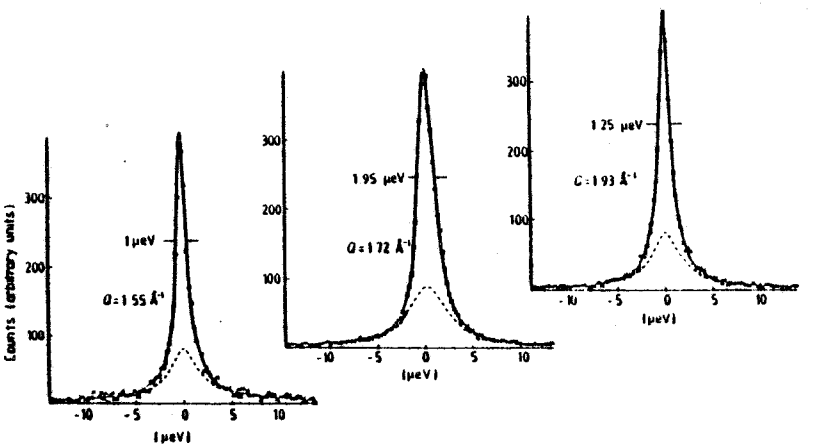

Figure 2. An example of the separation of the experimental spectra into a purely elastic component and a quasi-elastic part.

The EISF $a_0(Q)$ is an average over the p relevant incoherent scatterers within the molecule, rotating over individual circles of radii r_j. Expression (5) gives the EISF in the case of a rotation of order three:

$$a_0(Q) = \frac{1}{3p}\sum_{j=1}^{p}\left(1 + 2\frac{\sin(3^{1/2}Qr_j)}{3^{1/2}Qr_j}\right). \quad (5)$$

The two models corresponding to $N = 6$ and $N = 12$ have EISF values that are nearly the same, so the six-jump model will no longer be considered.

The structure factors, $a_i(Q)$, for $N = 12$ are illustrated in figure 3. It also shows the comparison of the experimental EISF values with the theoretical values predicted by the models for $N = 3$, 4 or 12. Clearly, experimental values lie above the curve related to the twelve-site model, which was successfully used to interpret the IQNS data for the plastic phase, but appears completely inadequate for the glassy state. However, the most striking feature is the failure of the two other models (for $N = 3$ or 4) and especially that of the three-site model, in spite of the larger amount of elastic scattering that it predicts.

The analysis of the elastic scattering part in terms of a uniaxial rotation associated with a unique residence time shows that this simple model disagrees with the experimental EISF.

Table 1. Characteristic times for reorientational jump models for jumps between three, four and twelve sites.

Three-site model	Four-site model	Twelve-site model
$1/\tau_0 = 0$	$1/\tau_0 = 0$	$1/\tau_0 = 0$
$1/\tau_1 = 1.5/\tau$	$1/\tau_1 = 1/\tau$	$1/\tau_1 = 0.134/\tau$
	$1/\tau_2 = 2/\tau$	$1/\tau_2 = 0.5/\tau$
		$1/\tau_3 = 1/\tau$
		$1/\tau_4 = 1.5/\tau$
		$1/\tau_5 = 1.866/\tau$
		$1/\tau_6 = 2/\tau$

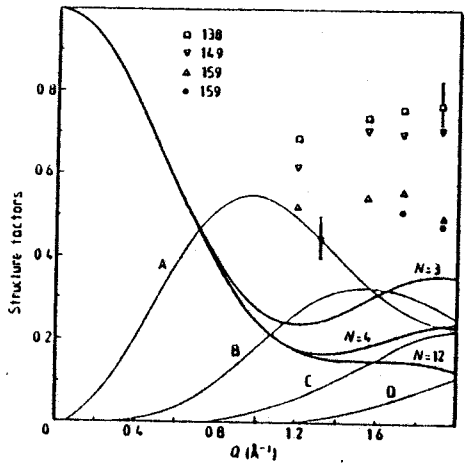

Figure 3. A comparison of the experimental EISF values with the theoretical variations predicted by jump models among 3, 4 or 12 equilibrium sites. Typical error bars are shown. The quasi-elastic structure factors for the twelve-site model have also been reported. The widths of the corresponding lorentzian functions are listed in table 1: (A) $1/\tau_1 = 0.134/\tau$; (B) $1/\tau_2 = 0.5/\tau$; (C) $1/\tau_3 = 1/\tau$; (D) $1/\tau_4 = 1.5/\tau$. The key gives the values of temperature (in K).

3.2. *Analysis of the quasi-elastic scattering*

It is possible to go one step further in the analysis of the quasi-elastic part of the spectra. Using a fast-Fourier-transform procedure, the direct deconvolution of the scattering functions $S(Q, \omega)$ from the instrument resolution was performed, yielding the well known intermediate-scattering function

$$I(Q, t) = \frac{1}{2\pi} \int S(Q, \omega) \exp(\mathrm{i}\,\omega t)\, \mathrm{d}\omega. \tag{6}$$

It is worth pointing out that the three-site jump model involves a single correlation time and therefore a single lorentzian function in the quasi-elastic part of the energy spectra at any Q-value. The explicit expression for the intermediate-scattering function is

$$I(Q, t) = a_0(Q) + (1 - a_0(Q)) \exp(-t/\tau_{m_3}). \tag{7}$$

The function

$$\log(I(Q, t) - I(Q, \infty) = -t/\tau_{m_3} + \log(1 - a_0(Q)) \tag{8}$$

should exhibit the same linear variation as a function of the time, t, for all Q-values. It is shown in figure 4 that at least two straight lines with distinct slopes can be observed, which proves that the molecular uniaxial motion cannot be described by a simple model with a single exponential term.

Now it must be pointed out that the intermediate-scattering functions corresponding to four and twelve sites involve n characteristic times ($n = 2$ or 6), but these times are linked together through relation (4) and depend on a single parameter, τ_{m_4} or $\tau_{m_{12}}$, the

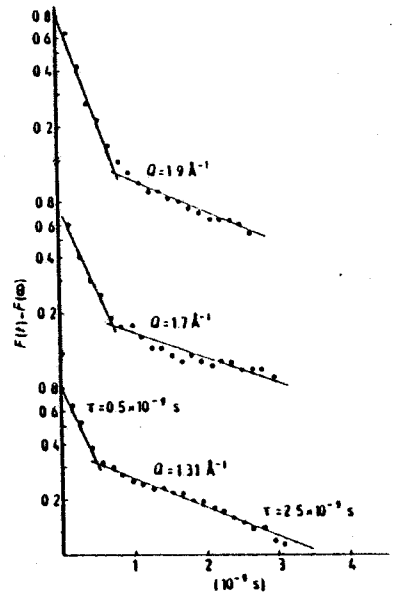

Figure 4. A direct determination of the characteristic times from the experimental data (T = 159 K.)

residence time between two jumps from one site to the neighbouring one. In figure 4 it is shown that the extremal values of the two slopes are in the ratio one to five. By referring to the expressions for the characteristic times listed in table 1 we can see clearly that the four-site model is not in accordance with this result, predicting a ratio of one to two. Such a difference is much larger than the error in the determination of the values of the two slopes in figure 4. We see by referring again to table 1 that the twelve-site model could provide values of characteristic times with a ratio in the range obtained experimentally: $\tau_2/\tau_1 = 0.268$, $\tau_4/\tau_2 = 0.33$ etc; but the experimental values of the slopes do not vary as a function of Q, as shown in figure 4. Conversely, the relative weights of the lorentzian functions associated with the different characteristic times follow the Q-dependence of the structure factors (see figure 3). Therefore, the exponential terms related to short times should be predominant at large Q. That is not observed experimentally and it seems that the twelve-jump model must be discarded too.

3.3. *Recrystallisation*

A possible explanation of the anomaly in the elastic part of the scattering is the partial recrystallisation of ADM-CN from its glassy phase into its monoclinic low-temperature phase. As already mentioned, the method used for quenching the sample allows us to discard this hypothesis. The phenomenon of nucleation by irradiation is improbable, as the experimental scattering spectra exhibit no variation with time. DSC experiments showed that the tendency towards recrystallisation is greater at temperatures near T_g. The EISF should then increase with temperature. In contrast, however, the experimental

EISF increases when the temperature is lowered. A partial recrystallisation of the product cannot explain why the value of the EISF is too high. Furthermore, it has no influence on the quasi-elastic part, because the 120° jumps between indistinguishable positions that are known to occur in the monoclinic phase (Foulon *et al* 1984) are far too slow to produce any appreciable broadening.

4. Discussion

The jump probability for a given molecule strongly depends on its local neighbourhood. In connection with the progressive increase in the numbers of antiferroelectric domains, shown to occur in the glassy phase from x-ray and coherent neutron scattering results, it is reasonable to assume that the immediate surroundings will not be the same for all molecules. Therefore, reorientations can be more or less favoured. A series of relaxation times is possible and the shape of the quasi-elastic spectra should be analysed under the assumption of a distribution of the relaxation times. This hypothesis is strengthened by the results of other experimental techniques. The study of the longitudinal relaxation time T_{1z} in proton NMR clearly shows that the uniaxial motion still exists in the glassy phase.

The value of T_{1z} at the glassy transition T_g coincides with the theoretical value predicted by simple extrapolation of the values in the plastic phase. This agreement shows that the glassy transition does not significantly change the frequency of the uniaxial rotation. Below T_g, in the glassy state, the experimental values of T_{1z} are always smaller than the corresponding ones calculated with the residence time $\tau_{m_{12}}$ deduced from the values of T_{1z} between T_g and 370 K. However, the experimental activation energy becomes much smaller (2.2 kJ mol^{-1}) below T_g than above this temperature (9 kJ mol^{-1}).

All these features of the glassy state can only be explained if a distribution of residence times is assumed (Amoureux *et al* 1986). When the temperature is lowered, the thermal translational motions of the molecules are progressively frozen, as shown by the linear evolution of the average translation tensor (Foulon *et al* 1985). In the glassy phase of ADM-CN, a positive deviation with respect to the normal variation is observed, which can be interpreted as a static distribution of the centres of mass of the molecules about the mean sites of the cubic lattice. The origin would be the local appearance of quadratic domains, with a local antiferroelectric arrangement, as suggested by the low Kirkwood dielectric correlation factor (Amoureux *et al* 1984). An analysis of the steric hindrance in such domains reveals that among the configurations *a priori* possible, the local environment of a given molecule can vary considerably and that the dynamics of each molecule is strongly correlated with that of its neighbours. All these arguments support the hypothesis of a distribution of correlation times. To describe the broadening of the IQNS spectra, all the correlation times have to be included in the scattering function, weighting the related lorentzian function with a distribution function $G(\tau, \tau_i)$ according to

$$S^{D}_{inc}(Q, \omega) = a_0(Q)\delta(\omega) + \sum_{i=1}^{6} a_i(Q) \int_0^{\infty} \frac{1}{\pi} \frac{\tau}{1+\omega^2\tau^2} G(\tau, \tau_i)\, d\tau. \qquad (9)$$

In fact, this expression provides a theoretical and experimental EISF identical to that given by (1), as long as the instrument resolution has not been taken into account, i.e. while it is much narrower than the experimental broadening and can be considered as a

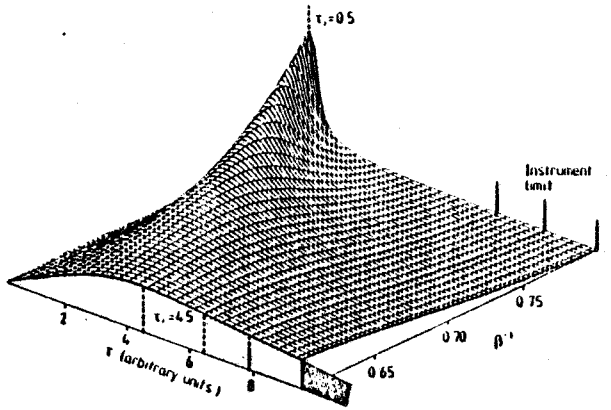

Figure 5. A sketch of the evolution of the distribution of the correlation times as a function of the temperature. Several instrument limits are indicated. Characteristic times longer than these limits contribute to the elastic intensity.

Dirac δ-function. Actually, the instrument resolution is finite. When the temperature is lowered, the motions are slowed down. The widths of the lorentzian functions related to longer correlation times progressively go outside the measurable energy range and the corresponding scattered intensity appears to be elastic (figure 5). This explains the increase of the apparent experimental EISF when the temperature decreases.

Without taking into account this probable correlation time distribution, an average relaxation time can be deduced from the spectra, by refinement of the twelve-jump model, providing that the purely elastic intensity is allowed to vary from the value predicted by the model. The resulting value, $\tau_{m_{12}} \simeq 6 \times 10^{-10}$ s is of the order of magnitude of the value extrapolated from the Arrhenius law for the plastic phase (Bée *et al* 1980). This confirms that the plastic–glassy phase transition is of only little influence on the uniaxial rotation.

In order to demonstrate the effect of a distribution of relaxation times on the shape of the scattering spectrum, a simulation of the experimental spectra was performed. The distribution function $G(\tau, \tau_i)$ was arbitrarily chosen as that introduced by Fuoss–Kirkwood (Connor 1964):

$$G(\tau, \tau_i) = F(z) = (\beta/\pi)\cos(\beta\pi/2)\cosh(\beta z)/[\cos^2(\beta\pi/2) + \sinh^2(\beta z)] \qquad (10)$$

with $z = \log(\tau/\tau_i)$ where τ_i is the correlation time corresponding to the maximum value of $F(z)$. The β-parameter ($0 < \beta \leq 1$) is equal to one for non-distributed relaxation times. Using equation (9), an analytical expression can be obtained for the scattering law:

$$S^{D}(Q, \omega) = a_0(Q)\delta(\omega) + \sum_{i=1}^{6} a_i(Q) \frac{\beta}{\omega} \frac{(\omega\tau_i)^{\beta}}{1+(\omega\tau_i)^{2\beta}}. \qquad (11)$$

The simulated experimental spectrum S^{D}_{exp} is calculated from the convolution of $S^{D}(Q, \omega)$ with the instrument resolution function, which was introduced as a normalised

gaussian function:

$$S^{D}_{exp} = \frac{1}{\alpha(2\pi)^{1/2}}\left[a_0(Q)\exp\frac{-\omega^2}{2\alpha^2} + \frac{1}{\pi}\sum_{i=1}^{6} a_i(Q)\beta \times \int_{-\infty}^{+\infty}\frac{1}{\omega'}\frac{(\omega'\tau_i)^{\beta}}{1+(\omega'\tau_i)^{2\beta}}\exp\left(\frac{-(\omega-\omega')^2}{2\alpha^2}\right)d\omega'\right] \quad (12)$$

with $\alpha = 0.425\ \Delta\omega_g$. Because of the divergence at $\omega' = 0$, in the domain $[-\varepsilon, +\varepsilon]$ $(\varepsilon \to 0)$, this integral was approximated to be

$$2\exp(-\omega^2/2\alpha^2)\tau_1^{\beta}(\varepsilon^{\beta}/\beta - \varepsilon^{3\beta}\tau_1^{\beta}/3\beta).$$

The width of the gaussian resolution function (denoted $\Delta\omega_g$) was set to 1 μeV, close to the experimental value. All calculations were performed on the basis of the twelve-jump model. The spectra with and without distribution (denoted S^{D}_{exp}, S^{ND}_{exp}) were calculated for $Q = 1.5\ \text{Å}^{-1}$ and $2/\tau_1 = \Delta\omega_1 = 3.2\ \mu$eV. $\Delta\omega_1$ is the width of the narrower lorentzian function contributing to the quasi-elastic scattering for the non-distributed spectrum. The β-parameter of the Fuoss–Kirkwood function was set to 0.6. In all cases (distributed or not), the total scattered intensity and the EISF values are constant. The resulting spectra are shown in figure 6. The quasi-elastic contributions are shown as broken curves.

Clearly, from figure 6, there are noticeable differences between the spectra $S^{D}_{exp}(Q, \omega)$ and $S^{ND}_{exp}(Q, \omega)$.

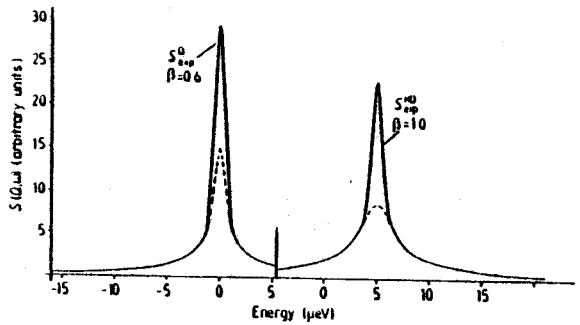

Figure 6. Distributed S^{D}_{exp}, and non-distributed, S^{ND}_{exp}, spectra (broken curves show the quasi-elastic contributions).

The amplitude at $\hbar\omega = 0$ is much more important in the case of the distributed spectrum (i.e. $S^{D}_{exp}(Q, 0)/S^{ND}_{exp}(Q, 0) = 1.26$). Furthermore, the broadening at half-maximum of the quasi-elastic part for the distributed spectrum is about half that for the non-distributed one. Thus, assuming a single residence time, a *graphical* evaluation of the broadening leads to an overestimation of τ_1. To go one step further, the distributed spectrum $S^{D}_{exp}(Q, \omega)$ was classically *refined*, according to a single residence time $\tau_{m_{12}}$ (a pure lorentzian function). $\Delta\omega_1$ and a scale factor could be varied during the refinement. (The latter parameter has to be refined when considering real experimental data.) The refinement is of bad quality and leads to the final value $\Delta\omega_1 = 3.35\ \mu$eV. Simultaneously

the scale factor was found to be much smaller (0.69) than for a non-distributed spectrum (1.0).

The simulated (distributed) spectrum and the corresponding refined one, S^{ND}_{ref}, are illustrated in figure 7. This refinement procedure enables us to take into account the excess of the elastic amplitude, at $\hbar\omega = 0$, introduced by the distribution: $S^{D}_{exp}(Q, 0)/S^{ND}_{ref}(Q, 0) = 2$, which corroborates the experimental results. Nevertheless, the refined value of $2/\tau_1$ (3.35 eV) is in good agreement with that introduced in the calculation of the distributed spectrum (3.2 μeV).

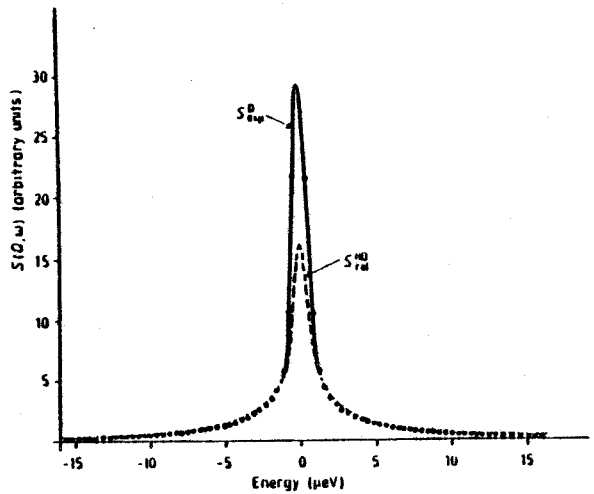

Figure 7. Simulated S^{D}_{exp} and corresponding S^{ND}_{ref} refined spectra (S^{ND}_{ref} is shown as the broken curve).

The refinement seems to favour the quasi-elastic contribution rather than the elastic one. This may be related to the low EISF value (for $Q = 1.5\ \text{Å}^{-1}$, $a_0(Q) = 0.149$) and to the relatively large quasi-elastic broadening compared with the instrument resolution ($\Delta\omega_1/\Delta\omega_g = 3.2$).

Keeping a constant instrumental resolution width of 1 μeV, distributed spectra were calculated with decreasing values of $\Delta\omega_1$. The refinements lead to an increasing deviation, the final and expected values being only in good agreement for sufficiently fast motions, as $\Delta\omega_1 = 2/\tau_1 > 3\Delta\omega_g$. Moreover refinements with pure lorentzian functions always yield an overestimated EISF value, and the choice of the appropriate model describing the molecular dynamics becomes difficult. When dealing with the interpretation of experimental data, it is clear that the more the temperature is lowered, the more the distribution widens (the β-parameter decreases) the longer the mean residence time becomes. Physical considerations, detailed above, suggest a description of the molecular motion on the basis of the twelve-jump model, but the mean residence time, deduced from the refinement of the real data using a non-distributed law, is too small.

To determine τ_1, more accurately, one might envisage performing experiments with better instrument resolution, at least three times smaller than the phenomena being analysed. Unfortunately, this was not possible with the IN10 instrument as regards the investigation of the 'glassy' phase of ADM-CN.

The question arises of whether this distribution of molecular relaxation times also exists for the plastic phase. IQNS experiments have been carried out using the four-chopper time-of-flight spectrometer IN5 at the Institut Laue–Langevin (Bée *et al* 1980). For the lowest temperatures investigated, the broadening of the quasi-elastic contribution was about two times larger than the instrument resolution. The eventual distribution, in this plastic phase, will be much narrower ($\beta \rightarrow 1.0$) than that in the glassy phase, the molecular motions being more free. From the above discussion, it is conceivable that the existence of this distribution might not be revealed. New experiments using IN5, where the resolution can be easily varied, at the same incoherent energy, should provide precise information on this point.

5. Conclusion

The molecular reorientations of ADM-CN in its glassy phase cannot be correctly described by a model involving a unique relaxation time. As suggested by conclusions of other experimental techniques, an interpretation in terms of a distribution of the relaxation times seems more appropriate. It is also demonstrated that no drastic change occurs at T_g as regards the uniaxial rotation of the molecule.

Acknowledgments

The authors would like to thank M Muller for preparing a purified product. They are obliged to Professor R Fouret for his constant interest in this work and to Professor J P Beaufils for critically reading the manuscript. This research was supported by the 'Direction des Recherches Etudes et Techniques' (DRET).

References

Adachi K, Suga H and Seki S 1968 *Bull. Chem. Soc. Japan* **41** 1073–87
Amoureux J P and Bée M 1979 *Acta Crystallogr.* B **35** 2957–62
Amoureux J P, Castelain M, Bée M, Arnaud B and Shoutecnten M L 1981a *Mol. Phys.* **42** 119–27
Amoureux J P, Castelain M, Benadda M D, Bée M and Sauvajol J L 1983 *J. Physique* **44** 513–20
Amoureux J P, Noyel G, Foulon M, Bée M and Jorat L 1984 *Mol. Phys.* **52** 161–71
Amoureux J P, Sahour M, Castelain M, Decressain R and Nagy Y 1986 to be published
Amoureux J P, Sauvajol J L and Bée M 1981b *Acta Crystallogr.* A **37** 97–104
Bée M, Amoureux J P and Dianoux A J 1980 *Mol. Phys.* **41** 325–39
Connor T M 1964 *Trans. Faraday Soc.* **60** 1574–91
Descamps M, Odou G and Caucheteux J C 1985 *J. Physique Lett.* **46** L261–5
Foulon M, Amoureux J P, Sauvajol J L, Cavrot J P and Muller M 1984 *J. Phys. C: Solid State Phys.* **17** 4213–29
Foulon M, Lefebvre J, Amoureux J P, Muller M and Magnier D 1985 *J. Physique* **46** 919–26
Leadbetter A J and Lechner R E 1979 *The Plastically Crystalline State* ed. J N Sherwood (New York: Wiley)

Lefebvre J, Rolland J P, Sauvajol J L and Hennion B 1985 *J. Phys. C: Solid State Phys.* **18** 241–55
Pathmanathan K and Johari G P 1985 *J. Phys. C: Solid State Phys.* **18** 6535–45
Springer T 1972 *Quasielastic Neutron Scattering for the Investigation of Diffusive Motions in Solids and Liquids; Springer Tracts in Modern Physics* vol 64 (Berlin: Springer)

ANNEXE A - XI - 6

J. Lascombe (Editor), *Dynamics of Molecular Crystals*

REORIENTATIONS AND LOCAL ORDER IN THE GLASSY AND PLASTIC PHASES OF 1-CYANO-ADAMANTANE $C_{10}H_{15}CN$

M. BÉE, M. FOULON and J.P. AMOUREUX
Lab. Dynam. Crist. Molec. (U.A. 801) 59655 Villeneuve d'Ascq Cedex (France)

ABSTRACT

In the glassy-state of 1-cyanoadamantane obtained by rapid quenching from the plastic phase, the rate of the reorientations is not unique but widely distributed because the local order which varies from one molecule to another has been frozen. This distribution still exists in the plastic phase, even if the local order is partly averaged by the slow tumbling motion. Similar effects were recently observed with mixed crystals $(C_{10}H_{15}CN)_x(C_{10}H_{15}Cl)_{1-x}$.

INTRODUCTION

The existence of a new type of glasses, obtained by quenching of some molecular crystals initially in their orientationally disordered phase was evidenced by Adachi et al (Ref. 1). The normal transition into an ordered low-temperature phase is avoided and the specimen passes into a "glassy state", in which the average translational order of the plastic phase is preserved, but where the orientational disorder is frozen (at least partially). This type of glass-transition has been observed with the 1-cyanoadamantane $C_{10}H_{15}CN$. The molecule has the general shape of a spherical adamantyl cage, on which is bonded the elongated radical C ≡ N (see Fig. 1). By rapid quenching, the normal transition (T_t = 280 K) to the ordered monoclinic phase is avoided and the sample passes at T_g = 170 K into a glassy-crystal phase with the same averaged f.c.c. structure as the plastic phase (Fm3m, Z = 4). This latter has been largely described (Refs.2,3) and also the nature of the dynamical disorder.

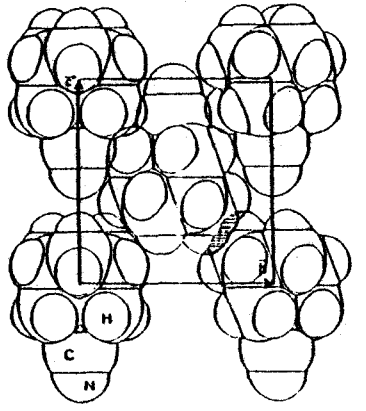

Fig. 1 A possible configuration of 1-cyanoadamantane molecules with an antiferroelectric arrangement.

NMR, dielectric relaxation and Incoherent Quasielastic Neutron Scattering (IQNS) experiments have evidenced the simultaneous occurrence of two types of motions (Refs. 4-7) : i) reorientations of the molecule threefold-axis (dipole-axis) amongst <100> lattice directions, strongly hindered by the first and second neighbouring molecules and ii) a rotation of the molecule about this axis, much less hindered and described as 30° jumps over a circle.

Below T = 280 K, the crystal structure is monoclinic $C_{2/m}$, formed by a succession of parallel planes composed of molecules with their dipoles in antiparallel order (Ref. 8). In spite of a strong steric hindrance, the uniaxial rotation is still existing in that phase (Ref. 5). In the glassy phase (T_g = 170 K), the molecules occupy the same equilibrium positions as in the plastic phase (Ref. 9). X-ray and coherent neutron scattering evidenced the progressive apparition of interlocked antiferroelectric domains (Refs. 10,11). Whilst the dipole tumbling is frozen at T_g (Ref. 12), the uniaxial rotation still continues to be observed by NMR (Refs. 5,8).

HIGH-RESOLUTION IQNS IN THE GLASSY-PHASE

The experiments have been carried out at the Institut Laue-Langevin, in Grenoble. The backscattering spectrometer IN10 was chosen because of its high-resolution in energy, (c.a. 1 μeV) on the expected relevant range (typically ± 13 μeV). The flat specimen, 38 x 35 x 0.3 mm in size (transmission 0.9) was oriented at 45° of the incoming neutrons. Quenching was realised by directly dipping the sample into liquid nitrogen and then slowly heating up to the required temperature.

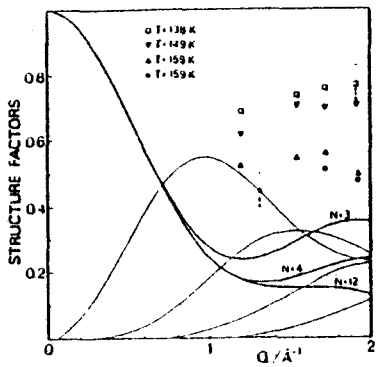

Fig. 2. Experimental EISF values compared to jump-models over 3, 4 or 12 sites.

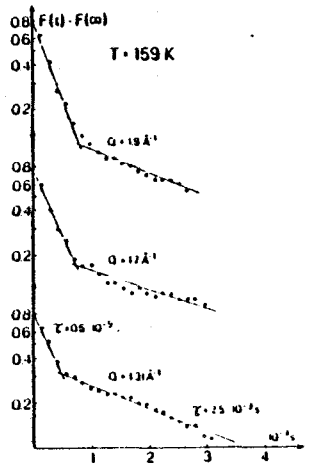

Fig. 3. Direct determination of the characteristic times from the experimental data.

Experimental values of the Elastic Incoherent Structure Factor (EISF) were obtained from the ratio of the purely elastic scattered intensity over the whole-spectrum intensity. They were compared with the values predicted by the models based upon reorientations over 3, 4 or 12 sites on a circle. It turns out that experimental values definitely lie above the predicted one, even for the 3-site model, in spite of its large amount of elastic scattering (see Fig. 2).

By Fourier-transformation, the scattering function was deconvoluted from the instrument resolution and the intermediate scattering function was obtained. A logarithmic plot as a function of time does not exhibit a simple linear decrease and thus proves that the motion cannot be described by any model involving a single exponential term (i.e. N = 2 or 3) (see Fig. 3). Moreover, at least two straight lines with distinct slopes in the ratio 1:5 can be observed, thus ruling out the N = 4 model predicting a ratio 1:2. Finally, the N = 12 model can also be eliminated, the ratio 1:5 being constant with Q.

An interpretation was proposed, strengthened by the results of other experimental techniques. X-ray and coherent neutron scattering evidenced the progressive occurrence of antiferroelectric domains. Thus, the immediate surrounding can differ from one molecule to another, with a net influence on their dynamics. The shape of the spectra should rather be analysed in terms of a distribution of the relaxation times and taking into account the instrument resolution. When the temperature decreases, the motions become slower. The widths of the Lorentzian functions related to longer correlation times go progressively outside the measurable energy range. The corresponding scattered intensity appears as elastic, producing an increase of the apparent EISF (see Fig. 4).

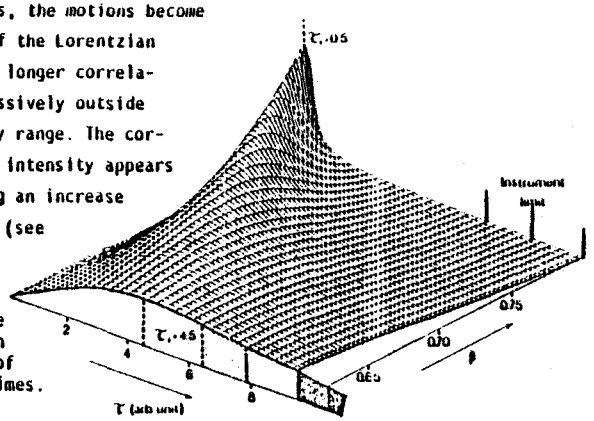

Fig. 4 Sketch of the temperature evolution of the distribution of the characteristic times.

TIME-OF-FLIGHT IQNS IN THE PLASTIC PHASE

Cyanoadamantane

The question arises if this distribution of molecular relaxation times also exists in the plastic phase. Earlier time-of-flight experiments (Ref. 7) exhibited at T = 300 K a small deviation of the EISF, in the range 1.1 $Å^{-1}$ < Q < 1.4 $Å^{-1}$ with respect to the 12-site model, the experimental values being above the theoretical curve. Recent experiments carried out over a large Q-range, with

several instrument-resolutions, definitely confirm this discrepancy. The EISF is found dependent on both the temperature and the resolution (see Fig. 5). This behaviour can be interpreted by a distribution of the relaxation times related to the progressive occurrence, when the temperature decreases, of clusters with local arrangement of the molecules. However, because of the slow tumbling reorientation of the molecule dipole moments, it is reasonable to consider that the distribution is more sharply peaked than in the glassy state. As soon as the temperature increases above room-temperature, most of the reorientations occur on the instrument time-scale. Near the melting point (T_m = 460 K), nearly all of them occur with a unique correlation time.

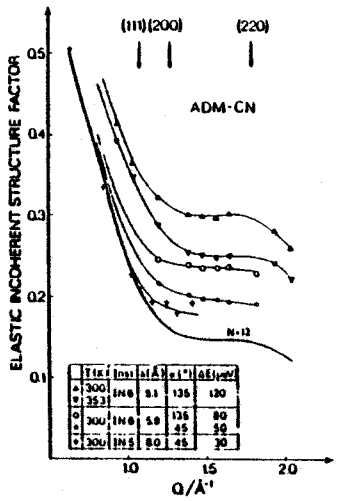

Fig. 5 Experimental EISF values for $C_{10}H_{15}CN$ obtained with different instrument resolutions.

Cyanoadamantane/chloroadamantane alloys

Owing to their similarities, $C_{10}H_{15}CN$ and $C_{10}H_{15}Cl$ can crystallise together to form mixed crystals $(C_{10}H_{15}CN)_x(C_{10}H_{15}Cl)_{1-x}$. Both molecules have the same equilibrium orientations along 001 directions of f.c.c. lattice with similar parameters. They undergo the same type of reorientations but, while the frequency of the uniaxial rotation is nearly the same, the tumbling for $C_{10}H_{15}Cl$ occurs at a much faster rate (10^9 Hz) than for $C_{10}H_{15}CN$ (10^4 Hz at T = 250 K). Calorimetric measurements (DSC), NMR or dielectric relaxation, X-ray structure determinations clearly indicate that dynamics of these mixed crystals tend to that of cyanoadamantane, i.e. a quasi-static disorder of the orientations of the molecule dipole-axes, for x → 1. Conversely, for x → 0, the behaviour is similar to that of chloroadamantane, i.e. we are concerned with a dynamical disorder of the dipoles. IQNS experiments were carried out with a series of mixed crystals with intermediate concentrations, x = 0.20, 0.33 and 0.67. In order to analyse more precisely the dynamical behaviour of each species, measurements were also performed with partially deuterated samples $(C_{10}H_{15}CN)_x(C_{10}D_{15}Cl)_{1-x}$.

Experimental EISF values were found strongly temperature-dependent, as illustrated in Fig. 6 for the fully hydrogenated species x = 0.33. At each temperature, the curve is intermediate between the curves for pure species x = 0 and x = 1, but, it never corresponds to their simple weighted average. That proves

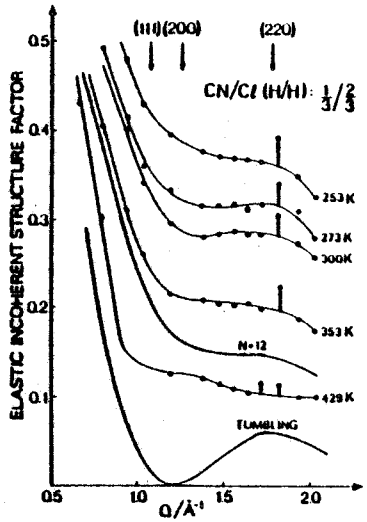

Fig. 6. Experimental EISF values for the fully hydrogenated mixed crystal x = 0.33 at different temperatures.

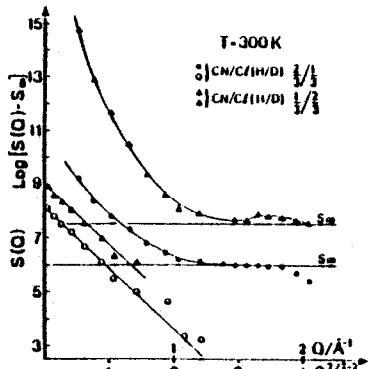

Fig. 7. Scattered intensity versus Q and Guinier plot for the two partially deuterated mixed crystals at T = 300 K.

that we are actually concerned with a molecular mixture of the two species.

The partially-deuterated specimen gives rise to a strong coherent scattering (see Fig. 7), especially at smaller Q-values. After subtracting the incoherent part, the amount of coherent scattering is found proportional to the concentration of $C_{10}D_{15}Cl$. A Guinier plot yields a radius of about 2.6 Å which corresponds to the radius of one individual molecule.

The coherent scattering was proved to be elastic in nature. After correction for its contribution to the scattered intensity, the experimental values of the EISF are found similar for hydrogenated and partially deuterated specimen. Clearly, there is no difference in the dynamics of $C_{10}D_{15}Cl$ and $C_{10}H_{15}Cl$, for the same concentration (Fig. 8).

The mixed crystal corresponding to x = 0.20 is found to have a behaviour very similar to pure chloroadamantane, and the variation with temperature of the EISF for x = 0.66 tends to be close to that for pure cyanoadamantane. The specimen for x = 0.33 exhibits a stronger temperature dependence, which is likely related to the thermal activation of the tumbling of the chloroadamantane molecules in it.

CONCLUSION

The exact nature of the local ordering has yet to be elucidated. New experiments are planned in order to get some insight on the molecular arrangement on

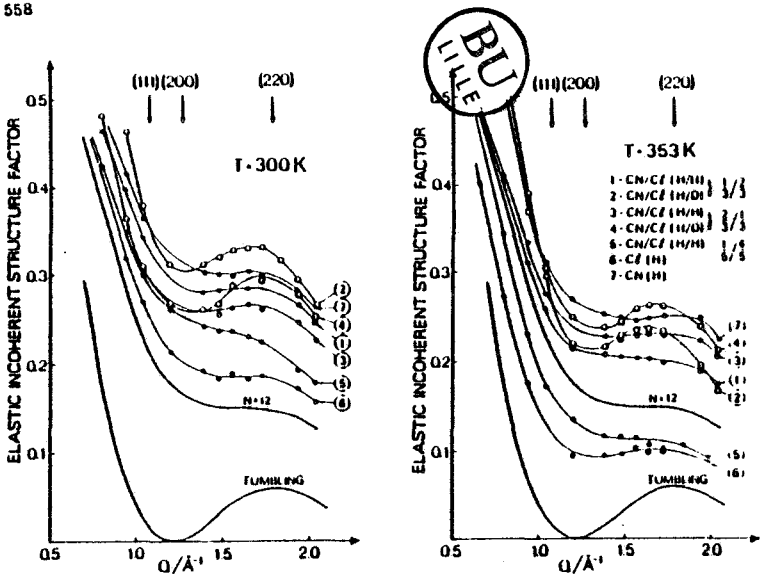

Fig. 8. Experimental EISF value for the various specimens at T = 300 K and T = 353 K.

both sides of the transition temperature, in the plastic and glassy phases.

REFERENCES

1 K. Adachi, H. Suga and S. Seki, Bull. Chem. Soc. Japan 41 (1968) 1073.
2 J.P. Amoureux and M. Bée, Acta Cryst. B 35 (1979) 2957.
3 J.P. Amoureux, J.L. Sauvajol and M. Bée, Acta Cryst. A 37 (1981) 97.
4 J.P. Amoureux, M. Castelain, M. Bée, B. Arnaud and M.L. Shouteenten, Mol. Phys. 42, 1 (1981) 119.
5 J.P. Amoureux, M. Sahour, M. Castelain, R. Decressain and Y. Nagy, to be published.
6 J.P. Amoureux, M. Castelain, M.D. Benadda, M. Bée and J.L. Sauvajol, J. de Physique 44 (1983) 513.
7 M. Bée, J.P. Amoureux and A.J. Dianoux, Mol. Phys. 41, 2 (1980) 325.
8 M. Foulon, J.P. Amoureux, J.L. Sauvajol, J.P. Cavrot, and M. Muller, J. Phys. C : Solid State Physics 17 (1984) 4213.
9 M. Foulon, J. Lefebvre, J.P. Amoureux, M. Muller and D. Magnier, J. Physique 46 (1985) 919.
10 M. Descamps, G. Odou and C. Caucheteux, J. Physique-Lettres 46 (1985) L-261.
11 J. Lefebvre, J.P. Rolland, J.L. Sauvajol and B. Hennion, J. Phys. C : Solid State Physics 18 (1985) 241.
12 J.P. Amoureux, G. Noyel, M. Foulon, M. Bée and L. Jorat, Mol. Phys. 52, 1 (1984) 161.

ANNEXE A - XI - 7

J. Lascombe (Editor), *Dynamics of Molecular Crystals*

PHENOMENOLOGICAL DESCRIPTION OF PHASE TRANSITIONS IN DERIVATIVES OF ADAMANTANE

P. ZIELINSKI* and M. FOULON

UNIVERSITE DES SCIENCES ET TECHNIQUES DE LILLE FLANDRES-ARTOIS

Laboratoire de Dynamique des Cristaux Moléculaires - U.A. 801

* Permanent address : INSTITUTE OF NUCLEAR PHYSICS

Ul. Radzikowskiego 152, 31-342 KRAKOW - Poland

ABSTRACT

The structures of different phases of chloroadamantane, bromoadamantane iodoadamantane and cyanoadamantane have been measured by X-ray diffraction.

The physical nature of the order parameters implied by the symmetry reduction is established for the observed phase transition. A model is proposed for description of phase transitins in cyanoadamantane on the basis of thermal variation of strains in its low temperature phase.

INTRODUCTION

Except for iodoadamantane (I-ADM) the derivatives of adamantane $C_{10}H_{15}X$ (called below X-ADM) have their highest temperature solid plastic phases caracterized by the space group Fm3m (Z = 4).

The low temperatures phases of these substances exhibit a variety of structures with different degrees of molecular order according as the substituting element X changes. The existence of relationships between the high and low temperature lattices allows to establish formal structural order parameters that gives indications on the transition mechanism.

SOLID PHASES OF SOME DERIVATIVES OF ADAMANTANE

Main results of X-ray diffraction investigations of Cl-ADM, Br-ADM, CN-ADM and I-ADM are presented in Table I along with the phase transition temperatures. The ordering of molecular dipoles in the phases investigated are schematised in Fig. 1.

The phase transitions P - O in all substances and P - SO in Br-ADM are strongly discontinuous and end up with powdering of crystals. The glassy phase G of CN-ADM is got only by a rapid quenching of the plastic phase (ref.1). The dipoles order shown in fig. 1c has a local nature the extent of corresponding domains being of the dimension 40Å (ref. 2).

	T_t(K)	T(K)	Space group	a_A°	b_A°	c_A°	β	Z	V_A° 3	Phase
CHLORO- Adamantane	246	295	Fm3m	9.97	9.97	9.97	90°	4	991.0	P
		210	$P2_1/c$	10.018	6.823	13.147	90°	4	898.6	O
BROMO - Adamantane	310.5	325	Fm3m	10.10	10.10	10.10	90°	4	1030.3	P
	279	295	Pmcn	10.12	6.89	13.613	90°	4	949.2	SO
	150	253	$P2_1/c$	10.12	6.854	13.259	90°24	4	919.7	O
		116	$P2_1/c$?	10.071	6.802	13.167	90°26	4	902	O
IODO- Adamantane	210	256	Pmmn	8.64	6.693	8.854	90°	2	512.0	SO
			?	UNKNOWN STRUCTURE						O
CYANO- Adamantane	280	295	Fm3m	9.813	9.813	9.813	90°	4	944.9	P
		240	C2/m	11.278	6.874	12.092	101°37	4	937.4	O
	170	110	Fm3m	9.63	9.63	9.63	90°	4	893.1	G

Table I : CRYSTALLINE PHASES of some I substituted adamantane

P for plastic phase O for ordered phase
SO for semi ordered phase G for "glassy phase"
T_t phase transition temperature
T temperature X ray diffraction study

The same type of antiferroelectric order is observed in I-ADM but the lattice is rather distorted in the plane (001) with respect to the tetragonal symmetry of domains in phase G of CN-ADM.

A uniaxial disorder of molecules in phase SO of Br-ADM admits six equivalent orientations with two crystallographically discernable positions of which only one subsits in phase O. The number of equivalent orientations reduces to three in phase O on the way of a nondestructive phase transition SO - O (ref. 3)

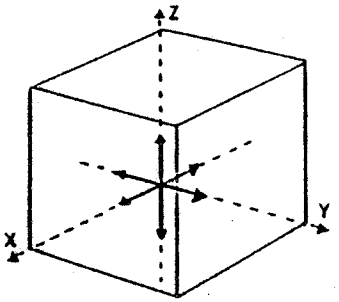

Fig. 1a

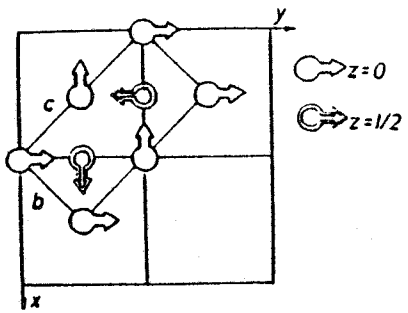

Fig 1b

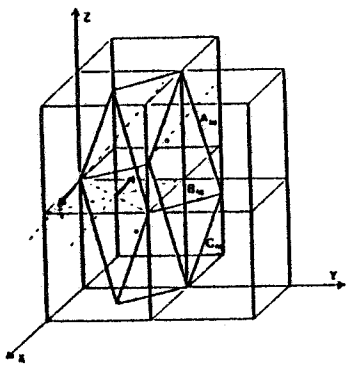

Fig. 1c

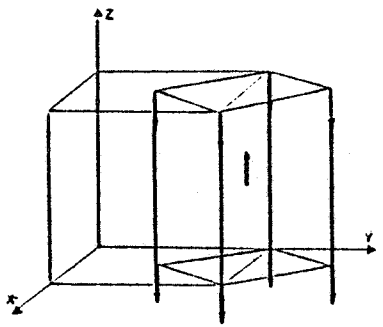

Fig. 1d

Fig. 1a) Six equivalent orientations of dipole in phase I' of CN-ADM, Br-ADM and Cl-ADM

Fig. 1b) Dipoles'orientation in phases SO and O of Br-ADM and Cl-ADM

Fig. 1c) Dipoles'orientation in phase O of CN-ADM

Fig. 1d) Order of dipoles in tetragonal domain of phase G of CN-ADM. A similar order exists in phase SO of I-ADM

GROUP THEORETICAL DESCRIPTION OF DIPOLES ORDERING IN Br-ADM and Cl-ADM

The reduction of symmetry for the phase transitions P → SO in Br-ADM ; P → O in Cl-ADM and SO → O in Br-ADM read respectively

$Fm\bar{3}m \rightarrow (k_4 = (\gamma\pi/a\ ,\ \gamma\pi/a, 0)\ ;\ \gamma = 1,\ \tau^3,\ \eta_1 = \eta_2 = \eta) \rightarrow Pmcn$ (1)

$Fm\bar{3}m \rightarrow (k_4\ ,\ \gamma = 1,\ \tau^3\ ,\ \tau^2;\ \eta_1 = \eta_2,\ \zeta_1 = \zeta_2 = \zeta) \rightarrow P2_1/c$ (2)

$Pmcn \rightarrow (k_9 = 0,\ \tau^2 = B_{2g}) \rightarrow P2_1/c$ (3)

Notation of irreducible representations $(k_i,\ \tau^\eta)$ after ref 4.

η_i and ζ_i are the components of the real physically irreducible representations engendered by the loaded ones τ^3, and τ^2 respectively.

The phase transition SO → O is close to second order in accordance with one dimensional active representation.

The physical quantities fluctuations compatible with the representations involved in (1) and (2) are exhibited in Tig 2. The corresponding order of molecules is not complete.

Thus, one introduces an additional order parameter defined by symmetry reduction scheme

$Fm\bar{3}m \rightarrow (k_{10} = (0,0,2\pi/a)\quad \tau^{10},\ \upsilon_1 = \upsilon_2 = \upsilon) \rightarrow Pmmn \supset Pmcn$ (4)

Such a change of order is always discontinous because of the existence of Lifshitz invariant in the representations $(k_4,\ \tau^1)$. An alternative possibility of the instability in η being triggered by the one in υ also leads to a discontinuity. A strong coupling with strain (volume contraction 5.4°/. in Cl-ADM) makes the transitions destructives.

MODEL FOR PHASE TRANSITIONS IN CN-ADM

The sequence of phases in CN-ADM is shown Fig.3. The symmetry reduction leading to the tetragonal structure of annealled phase G reads

$Fm\bar{3}m \rightarrow (k_{10},\ \tau^5, \upsilon \neq 0) \rightarrow P4/nmm$ (5)

The one domain crystal of the tetragonal symmetry is never observed because of limited molecular mobility. Than the glassy phase G is represented as a composition of different tetragonal domaines of symmetry P4/nmm.

The possible symmetry reduction in phase transition P → O are following

$Fm\bar{3}m \rightarrow (k_9 = (\pi/a\ ,\ \pi/a,\ \pi/a),\ \tau^6, \eta \neq 0) \rightarrow C2/m$ (6)

$Fm\bar{3}m \rightarrow (k_9 = \tau,^2\ \rho = 0) \rightarrow R\bar{3}m \rightarrow (k = 0\ ,\ Eg)\ \ C2/m$ (7)

The order parameter ρ governs the molecules' orientations whereas the one η the displacements of their mass centres. With the strain components defined as $\alpha = (\varepsilon_1 + \varepsilon_2 - 2\varepsilon_3)/6$

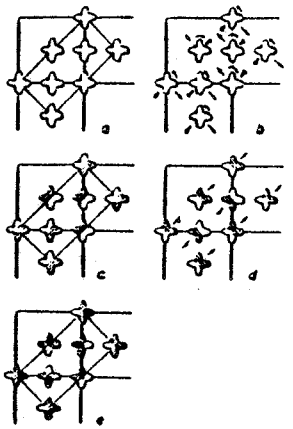

Fig. 2

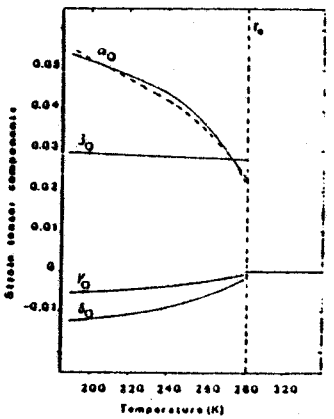

Fig. 4

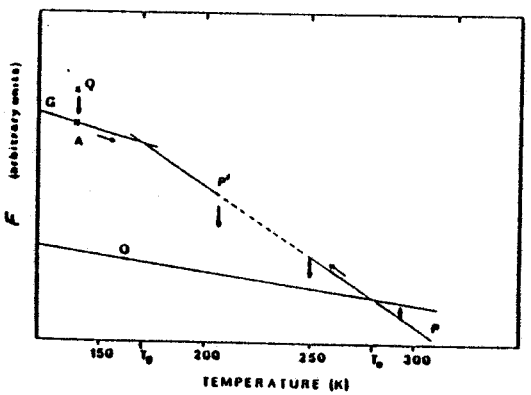

Fig. 3

Fig. 2 Projection of orientational distribution in phase P (a) translationed (↑) and orientational (↑↑) displacements of symmetry (k_4, τ^3) (b) orientational probability fluctuations of symmetry (k_4, τ^3) (c) and (k_{10}, τ^{10}) (d). Effective orientational order parameter (e)

Fig.3 Scheme of free energies of CN-ADM in its different phases. Q-Quenched A-annealed glassy state.

Fig. 4 Temperature dependence of spontaneous strain component in phase O of CN-ADM. Dazhed line theoretical curve implied by $K = K_0 + K_1(T-To)$ in (9)

$\delta = (\varepsilon_1 + \varepsilon_2 + \varepsilon_3)/3$, $\beta = (\varepsilon_4 + \varepsilon_5 + \varepsilon_6)/3$ $\gamma = (2\varepsilon_6 - \varepsilon_5 - \varepsilon_4)/6$

The simplest free energy expansion in phase O reads

$$F = (a_\rho/2)\rho^2 + (b_\rho/4)\rho^4 + (a_\eta/2)\eta^2 + (b_\eta/4)\eta^4 + (d_\eta/6)\eta^6 + (C_1/2)\alpha^2 + (C_2/2)\beta^2 - (K/2)\eta^2\rho^2 - L\alpha\eta^2 - M\beta\rho^2 - N\beta\eta^2$$

The lack of pretransitional effects in phase P implies that a_η, a_η , C_1 and C_2 are constants with temperature Assuming almost perfect order of the dipoles in phase O different possibilites of linear thermal dependence of the expansion (9) coefficients have been examined to get the best fit with experimental variation of the α component of spontaneous strain. This procedure indicated the coefficient $K = K_0 + K_1T$ as the most temperature dependent in the vicinity of phase transition (Fig. 4). Thus the phase transition P → O is attributed to the thermal dependence of orientation-translation coupling coefficient (réf. 5)

REFERENCES

1) M. Foulon et al. J. Phys. C Solid State Physic 17 (1984) 4213

2) M. Descamps, C. Caucheteux, G. Odou, J. de Physique 46 C8 - 329

3) M. Foulon et al. Poster session : *Réunion de l'Association Francaise de Cristallographie* 6/83 - Lille

4) A.K.Kovalev, Irreducible representations of the space Groups : Gordon & Breach 1965

5) P. Zielinski; to appear in J. Phys. C Solid State Physics.

FIGURES ET TABLEAUX

CHAPITRE XII

FIGURES ET TABLEAUX

CHAPITRE XII

	Masse moléculaire uma	Volume moléculaire	Moment d'inertie // C3	Moment d'inertie ⊥ C3 (G)	Moment dipolaire (D)
CNADM	161.3	162	298.6	583	3.9
Cℓ ADM	170.7	161	298.6	593.3	2.4

TABLEAU XII-1

Caractéristiques moléculaires

	T fusion ΔH_f (KJ/mole)	T_t(II→I) $\Delta H_{II→I}$ (KJ/mole)	Tg	Groupe spatial phase I	Groupe spatial phase II	Groupe spatial phase Ig	Paramètre à phase I près de T_t	ε compacité Phase I à T_t	Directions axes dipolaires phase I	Directions axes dipolaires phase II
CNADM	425 K 15	280 K 5.5	170 K	Fm3m	C_2/m	Fm3m	9.805	0.687	6 < 001 >	$2<111>_{pseudo}$
Cℓ ADM	442 K 4.9	246 K 6.0	Non observée	Fm3m	P_{2_1}/c		9.864	0.671	6 < 001 >	$4<001>_{pseudo}$

TABLEAU XII-2

Température et enthalpies des transitions
caractéristiques structurales des ≠ phases

	Type d'expérience	τ_{C_3} phase I		$\tau_{m_{12}}$ phase I		$\tau_{m_{12}}$ phase Ig		τ_{m_3} phase II ou III	
		τ_o	E (K)	τ_o	E (K)	τ_o	E (K)	τ_o	E (K)
CNADM	RMN	3.4×10^{-14}	5470	3.9×10^{-15}	1206	Pas de discontinuité avec la phase I		1.6×10^{-15}	4960
	R.D.	5.06×10^{-16}	6267						
	IQNS			5.62×10^{-14}	1000				
Cℓ ADM	R.D.	1.09×10^{-14}	1237	1.23×10^{-14}	2576				

TABLEAU XII-3

Les temps de résidence dans les différentes phases du CNADM et du Cℓ ADM

$\tau = \tau_o \exp(E/T)$ (T en K)

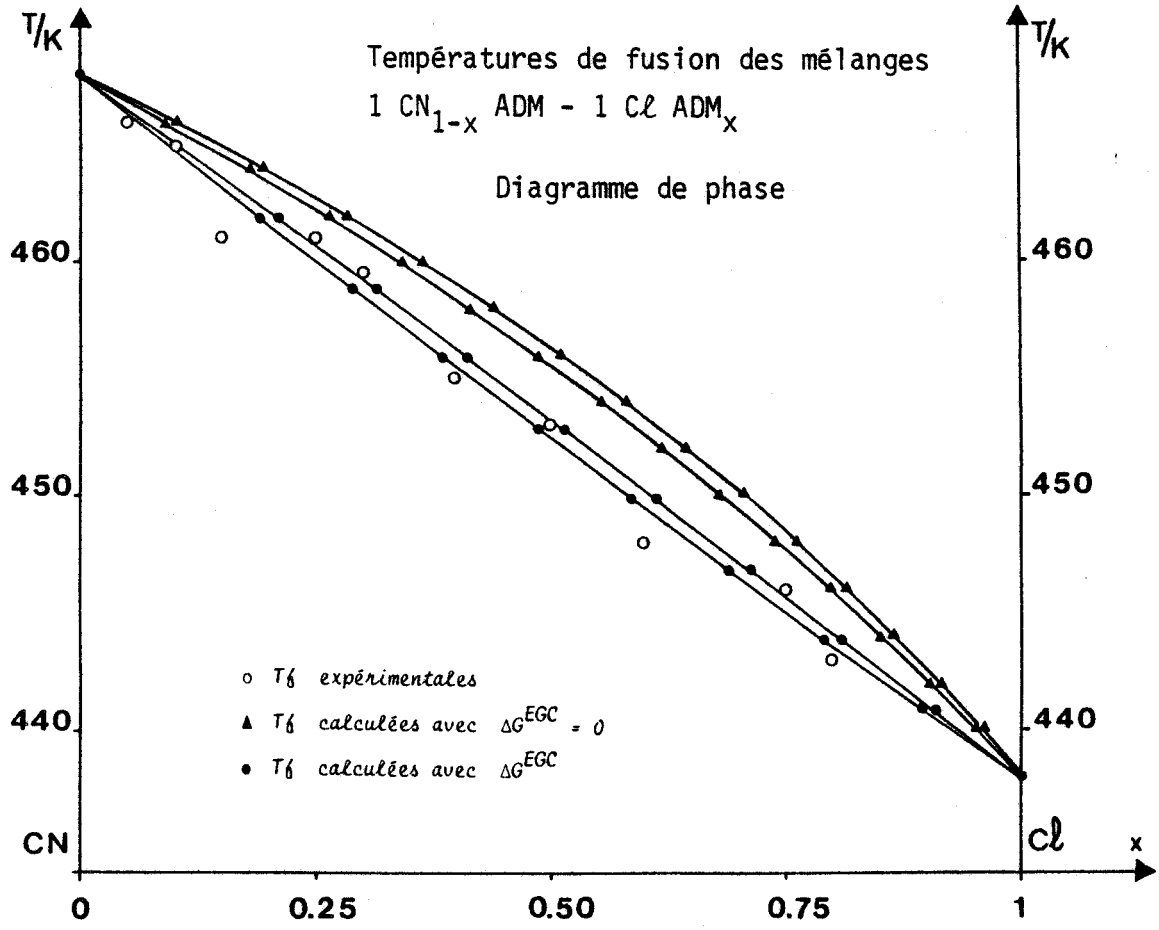

FIGURE XII-1 extraite de [1]

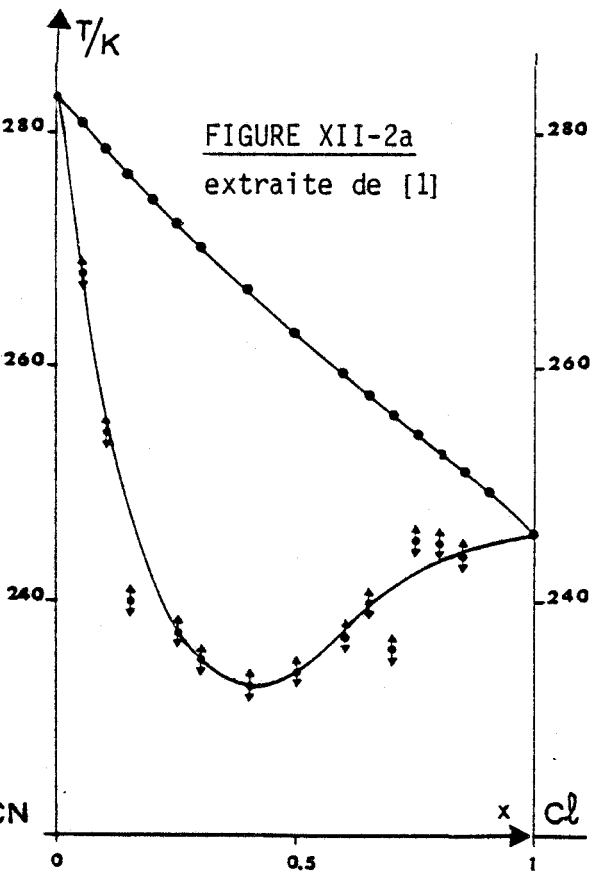

FIGURE XII-2a
extraite de [1]

Variation des températures de transition expérimentale (‡) ligne zéro (•)

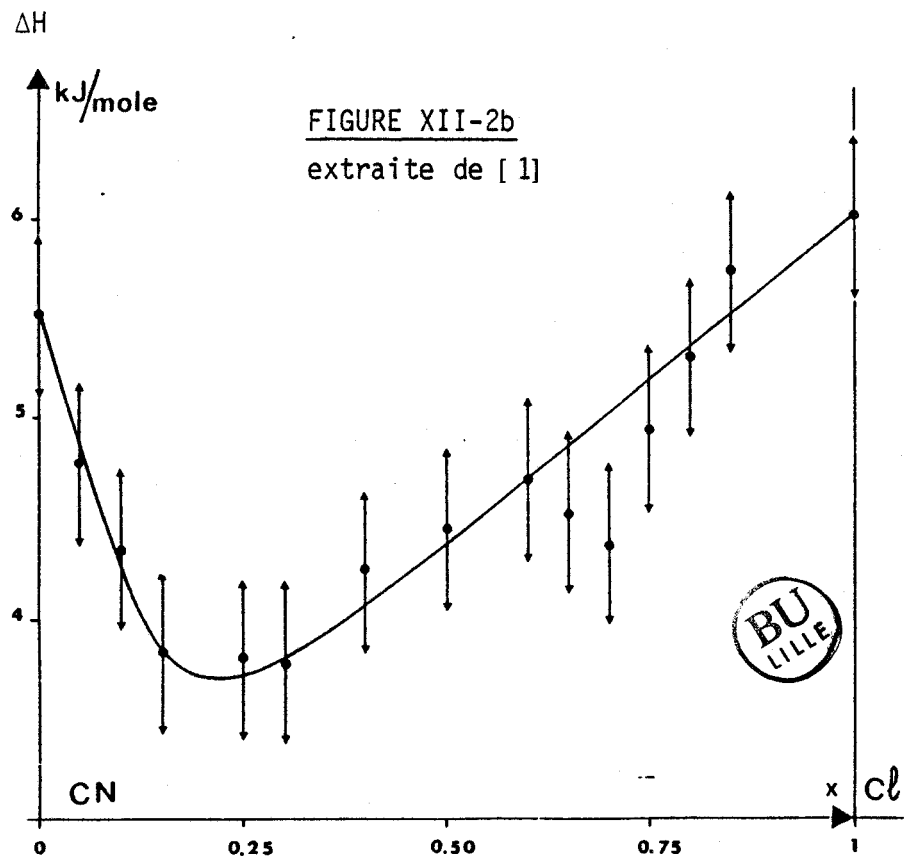

FIGURE XII-2b
extraite de [1]

Variation de l'enthalpie de transition vers la phase plastique en fonction de la concentration

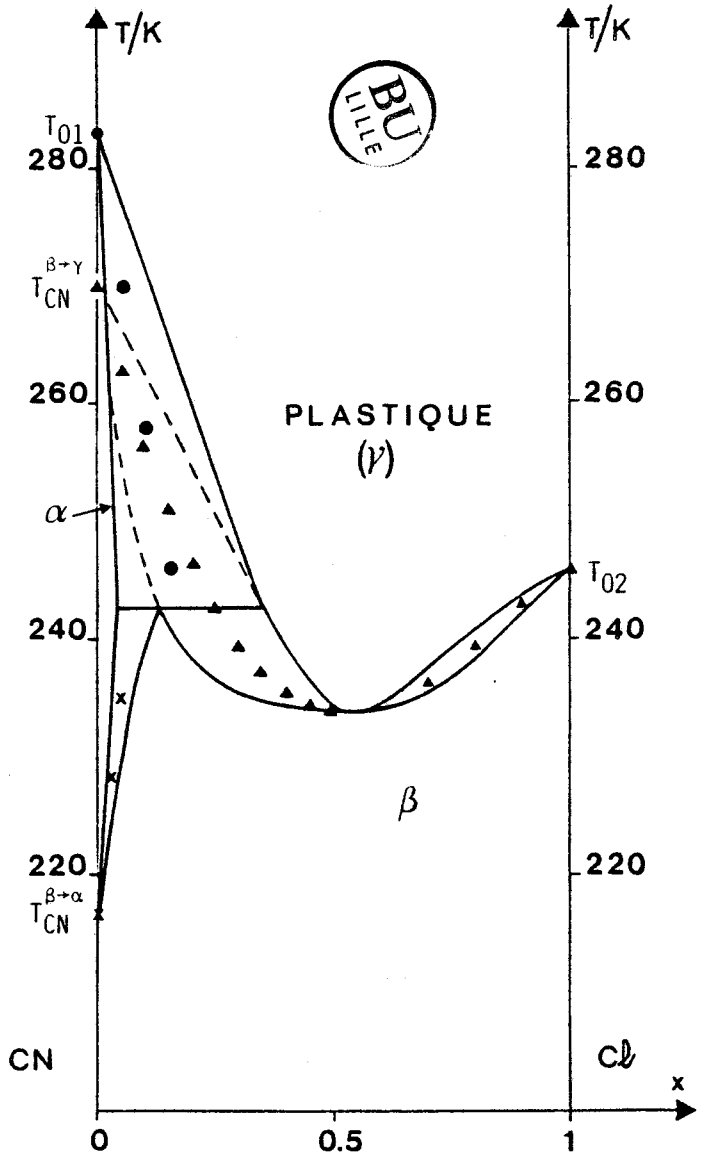

Diagramme de phase n° 2

FIGURE XII-4

extraite de [1]

• T_{EGC} ($\alpha\to\gamma$) ▲ T_{EGC} ($\beta\to\gamma$) x T_{EGC} ($\alpha\to\beta$)

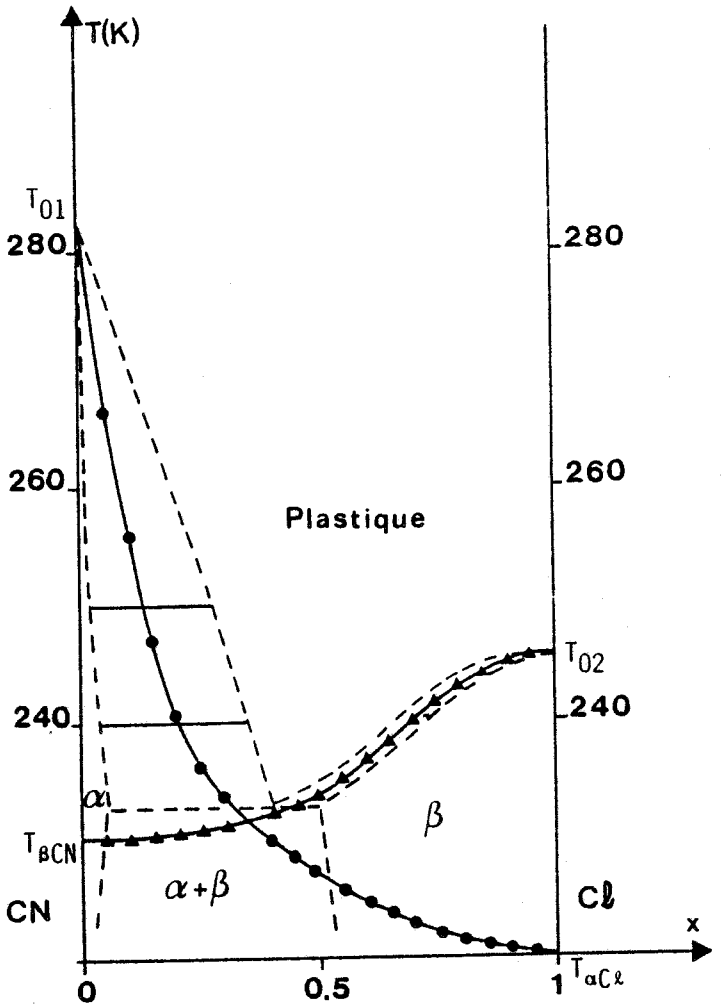

FIGURE XII-3

extraite de [1]

Diagramme de phase n° 1

T_{EGC} ($\alpha\to$ plastique) T_{EGC} ($\beta\to$ plastique)

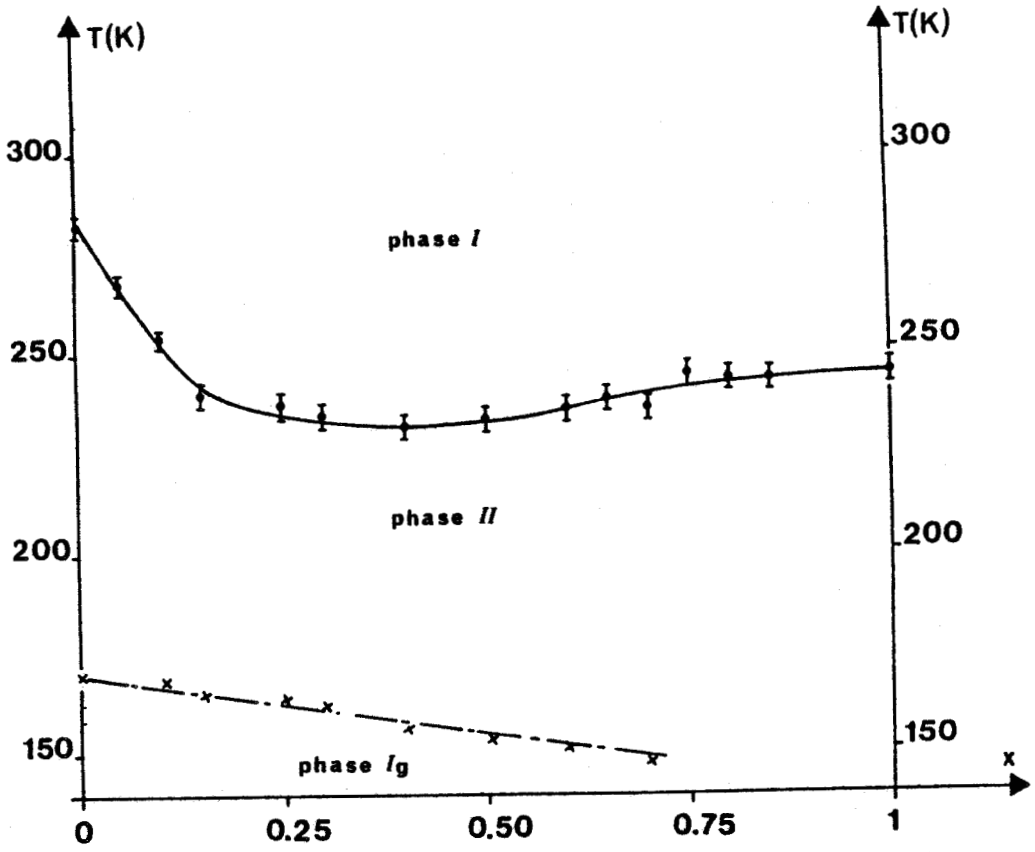

FIGURE XII-5
extraite de [1]

Variations des températures de transitions en fonction de la concentration x→Tg ●→T_t

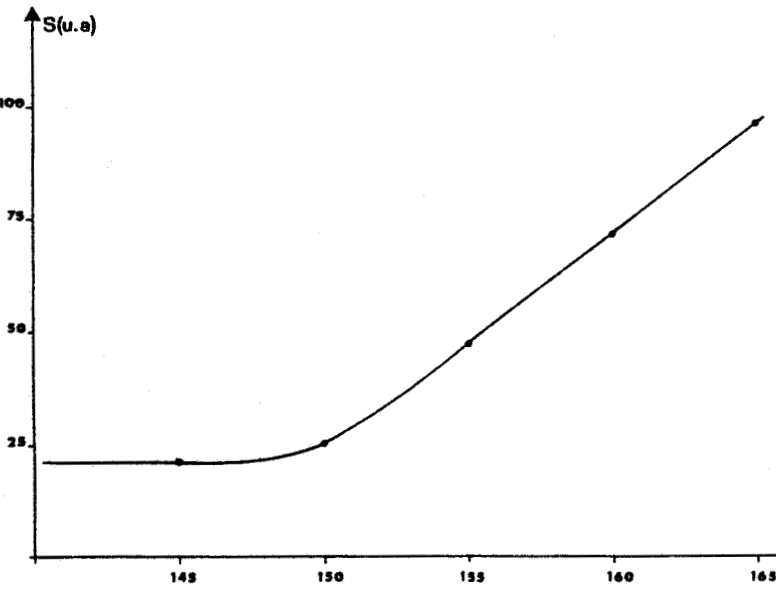

FIGURE XII-7 extraite de [1]

Influence de la température de recuit (T) sur la surface du "Cusp"

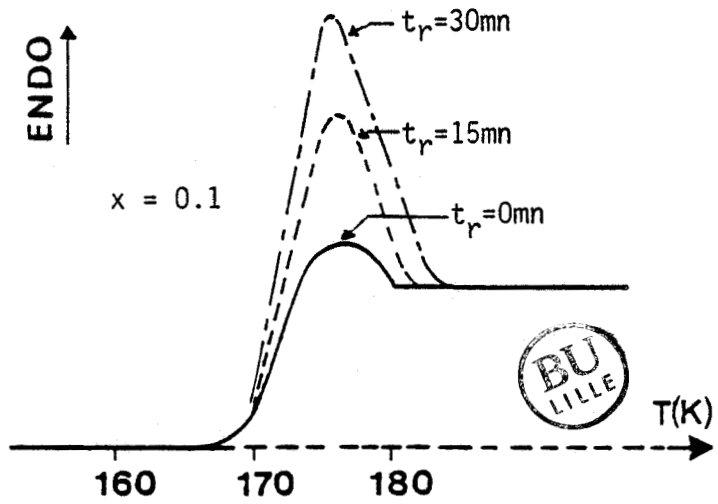

FIGURE XII-6

extraite de [1]

Surface du "Cusp" en fonction du temps de recuit à T = 165 K

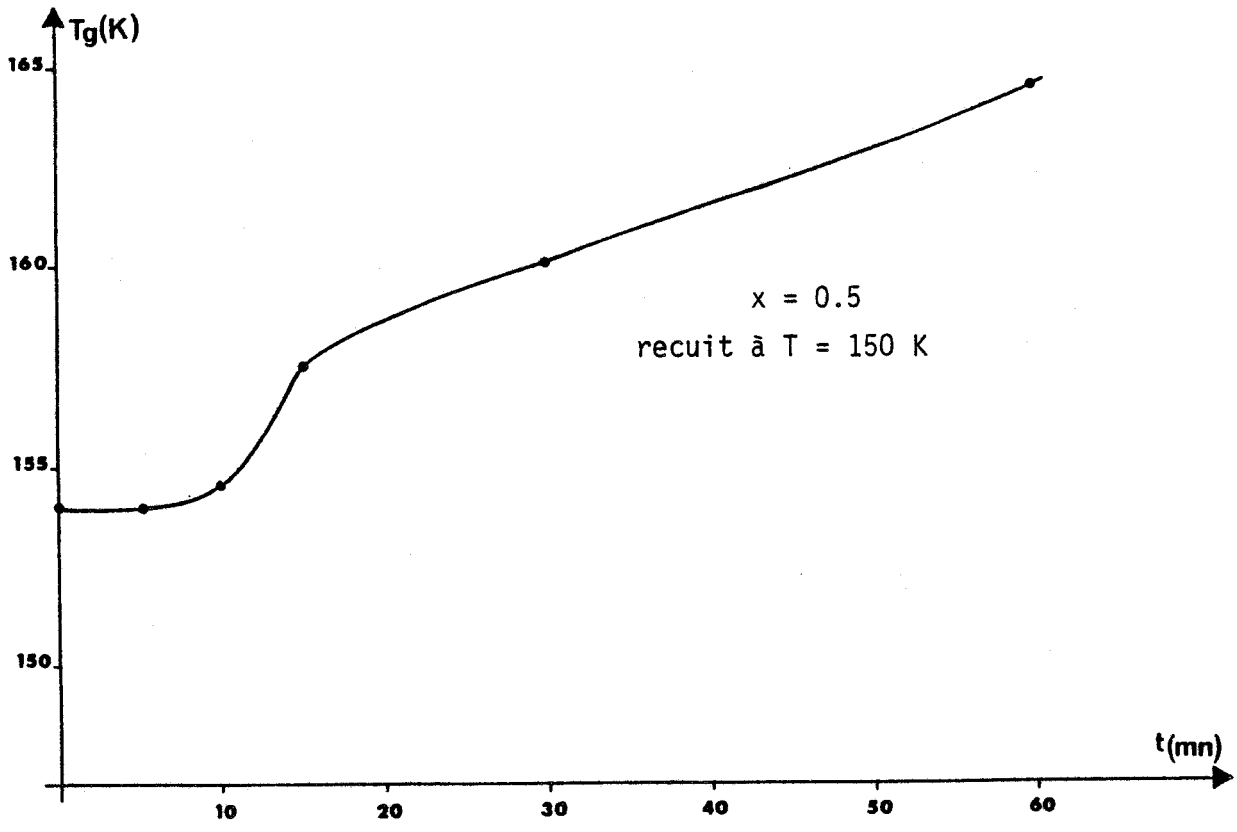

FIGURE XII-8 extraite de [1]

Variation de Tg en fonction du temps, t, de recuit

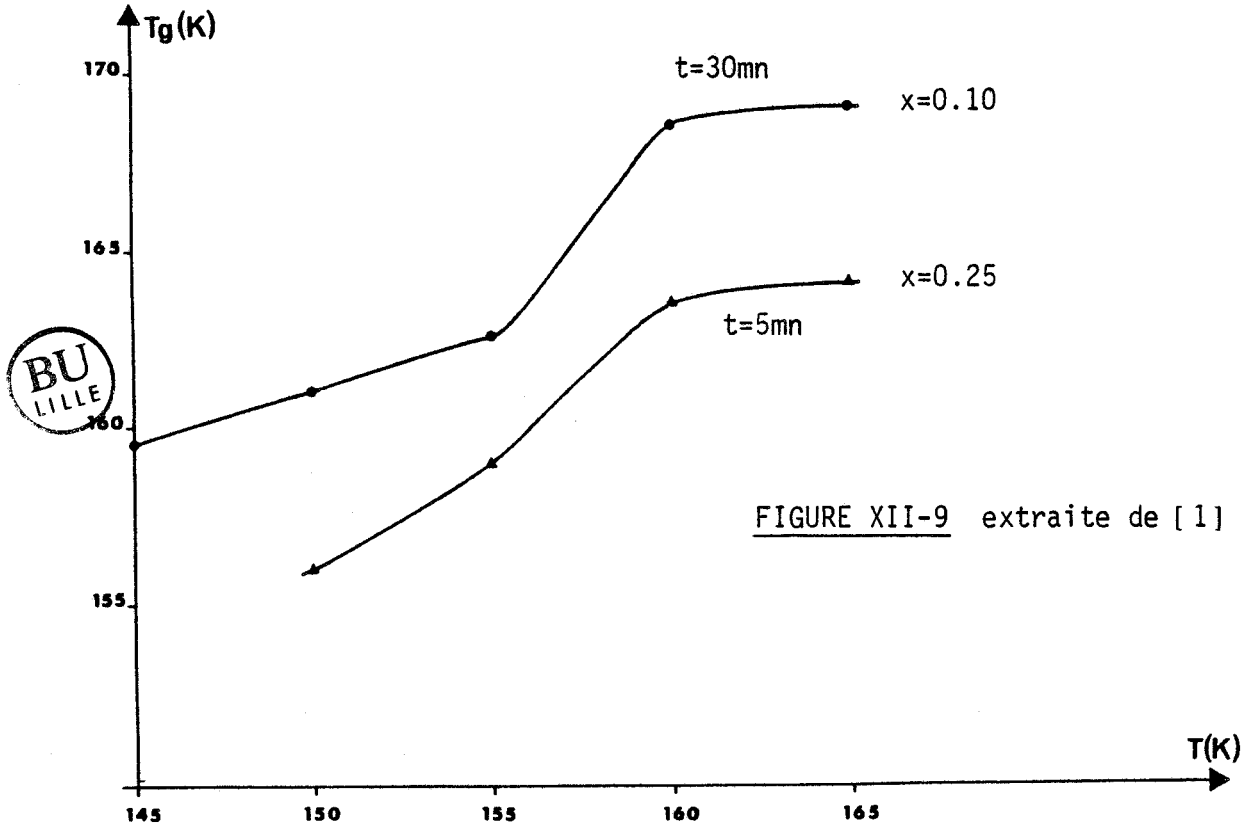

FIGURE XII-9 extraite de [1]

Variation de Tg en fonction de la température de recuit, T

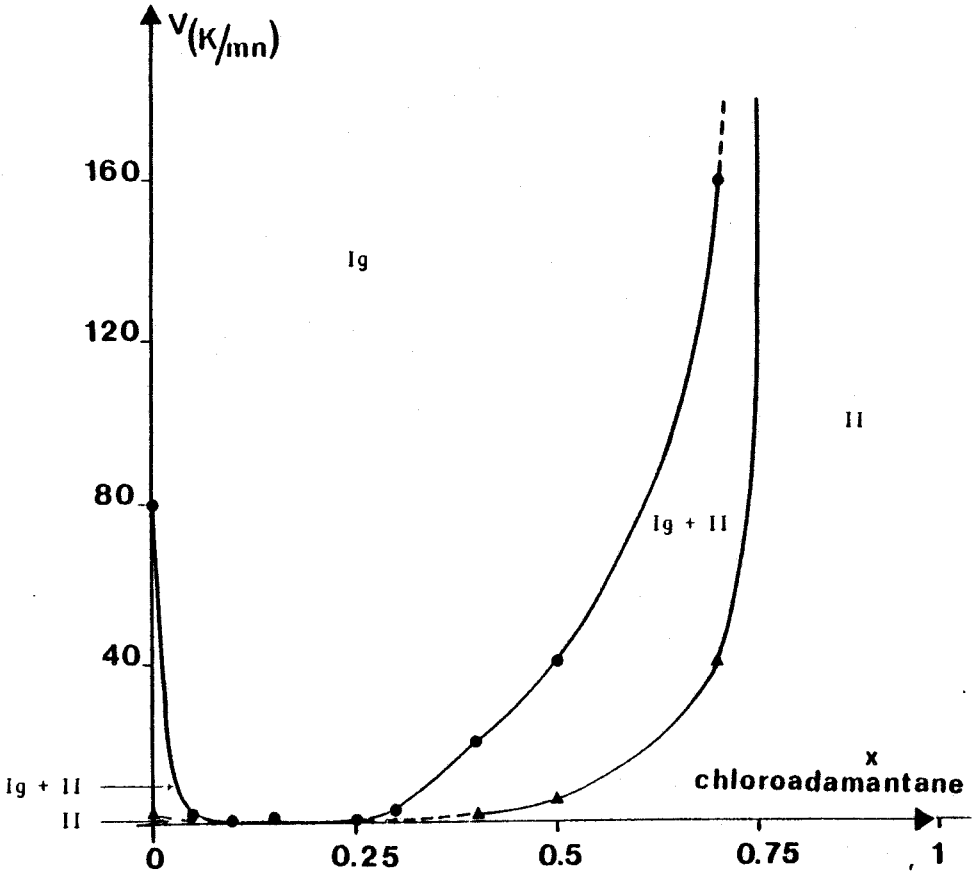

FIGURE XII-11 extraite de [1]

- Vitesse de trempe minimale pour "vitrifier" la totalité du mélange
- ▲ Vitesse de trempe maximale pour que tout le mélange transite dans la phase II

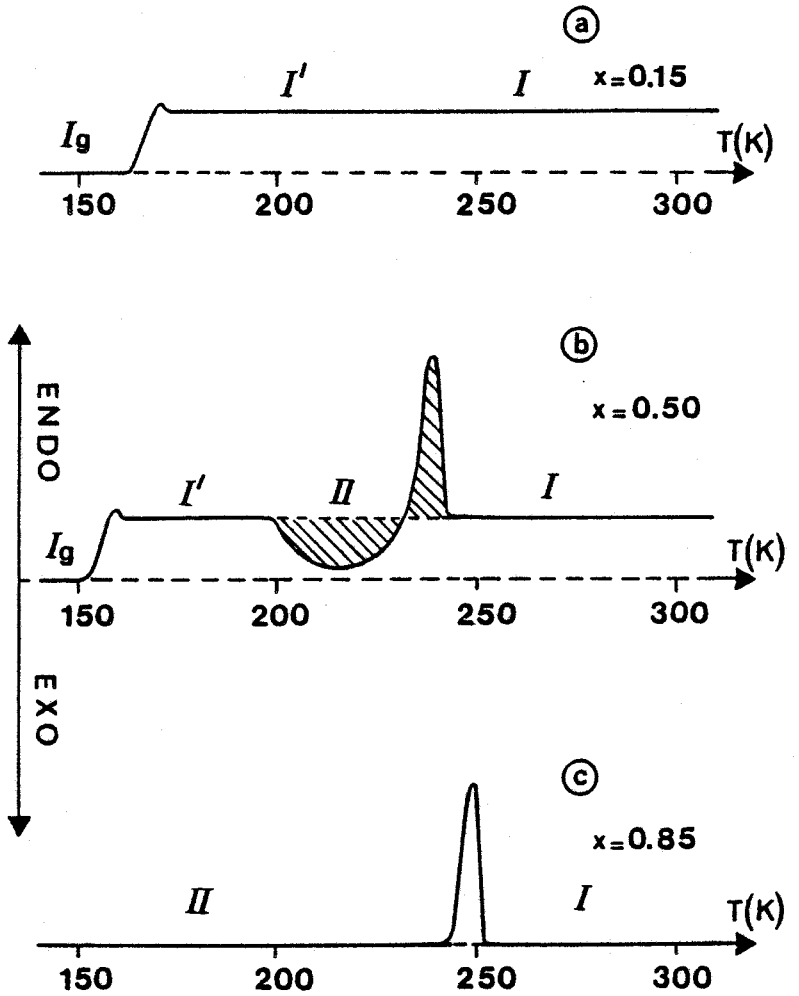

FIGURE XII-10 extraite de [1]

Thermogrammes schématiques montrant les transitions de phases observées au réchauffement immédiat après trempe des mélanges à 100 K

x	$T_{(K)}$	SPE degré/s	SWD degré	REFLEXIONS MESUREES	REFLEXIONS NON EQUIVALENTES	REFLEXIONS AVEC $F > 3\sigma$ (F)	Θ MAXIMUM
0.15	295	0.020	1.40	417	72	42	26.20
0.25	295	0.008	1.50	1265	103	43	31.00
0.25	110	0.016	1.50	1201	148	77	36.50
0.40	295	0.016	1.30	670	141	31	36.50
0.40	110	0.016	1.20	674	149	69	36.50
0.50	295	0.020	1.20	568	80	40	29.00
0.50	251	0.024	1.20	279	93	46	29.00
0.50	110	0.024	1.40	345	115	68	32.50
0.60	295	0.010	1.40	277	209	69	42.00
0.60	110	0.010	1.40	404	200	95	42.00

TABLEAU XII-4 extraite de [1]

Paramètres des collections de données de la diffraction X

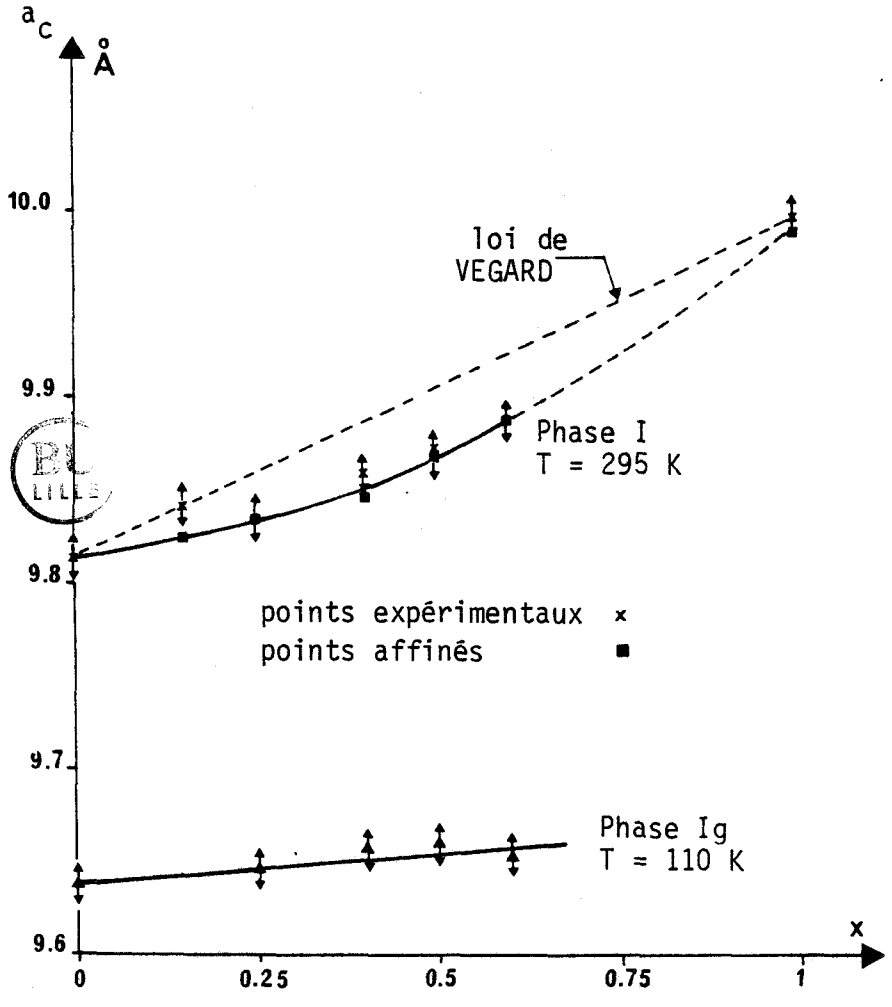

FIGURE XII-12

Variations des paramètres, a_c, dans les phases plastique et vitreuse, en fonction de la concentration

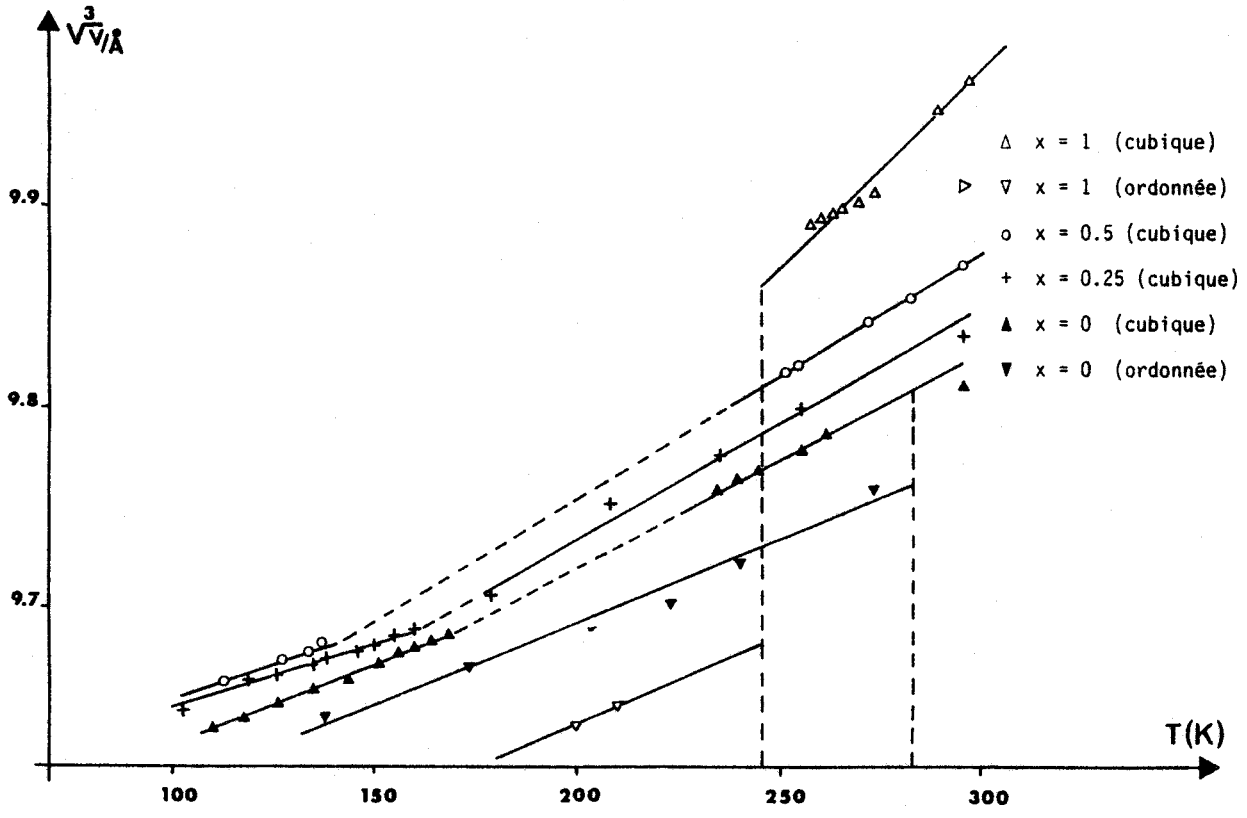

FIGURE XII-13 extraite de [1]

Variation de $\sqrt[3]{V}$ en fonction de la température pour différentes concentrations, x

	x →	0	0.25	0.50	1.0
PHASES I et I'	α_v	3.19	3.50	3.56	7.2
PHASES Ig	α_v	2.60	2.00	2.00	—
PHASES II	α_v	2.60	—	—	3.3

TABLEAU XII-5

Coefficient de dilatation volumique ($\alpha_v \times 10^4\ K^{-1}$)

← F(h,k,ℓ) avec $h^2 + k^2 + \ell^2 < 100$ (ou 170), sans 200 et 111 →										← avec 200 et 111 →			
x	T(K)	PHASE	U_3 (Å)	$\sqrt{T_{11}}$ (Å)	$\sqrt{L_{11}}$ (°)	R (%)	R_w (%)	G	Nb	R (%)	R_w (%)	G	Nb
0.00	295	I	-0.089 (11)	0.264 (8)	3.30 (0.28)	8.16	8.78	2.7	32	7.58	8.76	2.4	34
0.00	110	Ig	-0.111 (11)	0.198 (5)	1.90 (0.22)	9.9	10.53	9.3	68	8.32	10.46	9.2	70
0.15	295	I	-0.066 (11)	0.266 (7)	3.36 (0.26)	8.05	6.92	3.1	33	7.86	6.92	2.7	35
0.25	110	Ig	-0.080 (7)	0.200 (6)	2.43 (0.22)	10.12	10.18	6.1	63	8.87	10.12	5.7	65
0.40	295	I	-0.057 (14)	0.274 (10)	3.98 (0.32)	8.92	7.13	2.6	29	5.89	7.01	2.2	31
0.40	110	Ig	-0.064 (6)	0.208 (6)	2.57 (0.20)	8.25	9.03	4.3	61	7.50	8.97	4.0	63
0.50	295	I	-0.054 (18)	0.287 (15)	4.70 (0.53)	10.60	8.42	14.8	32	12.28	8.95	15.2	34
0.50	251	I	-0.059 (10)	0.253 (9)	3.85 (0.25)	8.46	8.94	4.7	37	8.63	8.94	4.1	39
0.50	110	Ig	-0.061 (6)	0.209 (6)	2.84 (0.19)	9.04	8.65	3.4	62	7.29	8.58	3.1	64
0.60	295	I	-0.055 (14)	0.285 (13)	4.78 (0.38)	11.58	9.32	27.1	33	7.89	9.14	24.9	35
0.60	110	Ig	-0.064 (6)	0.207 (6)	2.80 (0.13)	8.25	9.03	4.3	61	7.50	8.97	4.0	63
1.00	295	I	-0.028 (17)	0.326 (15)	5.20 (0.12)	13.8	11.0	7.7	26	11.7	11.1	6.8	28
1.00	257	I	-0.046 (9)	0.271 (11)	4.65 (0.26)	9.4	9.0	5.7	31	7.7	8.9	4.8	33
0.25	295	I	-0.066 (13)	0.268 (9)	3.80 (0.27)	8.98	8.68	6.1	35	7.78	8.55	5.2	37

TABLEAU XII-6a [1]

Résultats des affinements avec un tenseur de translation isotrope
(Nb : nombre de raies introduites dans l'affinement ; G : facteur "Goodness of fit

← F(h,k,ℓ) avec $h^2 + k^2 + \ell^2 < 100$ (ou 170), sans 200 et 111 →										← avec 200 et 111 →			
x	T(K)	PHASE	U_3 (Å)	$\sqrt{T_{11}}$ (Å)	$\sqrt{T_{33}}$ (Å)	$\sqrt{L_{11}}$ (°)	R(%)	R_w(%)	G	Nb	R(%)	R_w(%)	G	Nb
0.00	295	I	-0.084(11)	0.270(10)	0.257(11)	3.18 (33)	8.17	8.62	2.7	32	7.29	8.59	2.3	34
0.00	110	Ig	-0.108 (5)	0.209 (7)	0.187 (7)	1.67 (27)	9.61	10.13	8.7	68	8.41	10.06	8.5	70
0.15	295	I	-0.067(12)	0.265 (9)	0.268 (13)	3.37 (27)	8.11	6.91	3.2	33	7.75	6.90	2.7	35
0.25	295	I	-0.066(14)	0.268 (11)	0.267(14)	3.80 (27)	8.96	8.68	6.3	35	7.52	8.53	5.2	37
0.25	110	Ig	-0.080 (7)	0.201 (8)	0.199 (10)	2.42 (22)	10.11	10.18	6.2	63	8.96	10.14	5.7	65
0.40	295	I	-0.062(15)	0.266 (12)	0.292 (18)	4.06 (32)	9.55	6.96	2.6	29	6.30	6.84	2.1	31
0.40	110	Ig	-0.064 (6)	0.209 (8)	0.207 (9)	2.53 (23)	8.25	9.01	4.4	61	7.64	8.98	4.0	63
0.50	295	I	-0.054(21)	0.272 (23)	0.301 (22)	4.89 (56)	10.62	8.30	14.4	32	11.82	8.79	14.6	34
0.50	251	I	-0.060(10)	0.244 (11)	0.266 (13)	3.96 (25)	8.60	8.67	4.6	37	8.99	8.70	3.9	39
0.50	110	Ig	-0.062 (6)	0.208 (8)	0.211 (8)	2.86 (21)	9.05	8.64	3.4	62	7.46	8.59	3.1	64
0.60	295	I	-0.054(14)	0.266 (22)	0.278 (20)	4.83 (46)	12.62	8.93	25.0	33	7.09	8.70	22.5	35
0.60	110	Ig	-0.063 (4)	0.199 (7)	0.213 (6)	2.95 (23)	9.08	7.96	4.7	61	8.40	7.97	4.3	63
1.00	295	I	-0.024(17)	0.300 (28)	0.339 (17)	5.61 (50)	13.8	10.6	7.6	26	12.2	10.9	6.5	28
1.00	257	I	-0.036(10)	0.236 (19)	0.287 (12)	5.20 (30)	9.8	8.1	4.8	31	7.8	8.0	3.9	33

TABLEAU XII-6b [1]

Résultats des affinements avec un tenseur de translation anisotrope
(Nb : nombre de raies introduites dans l'affinement ; G : facteur "Goodness of fit

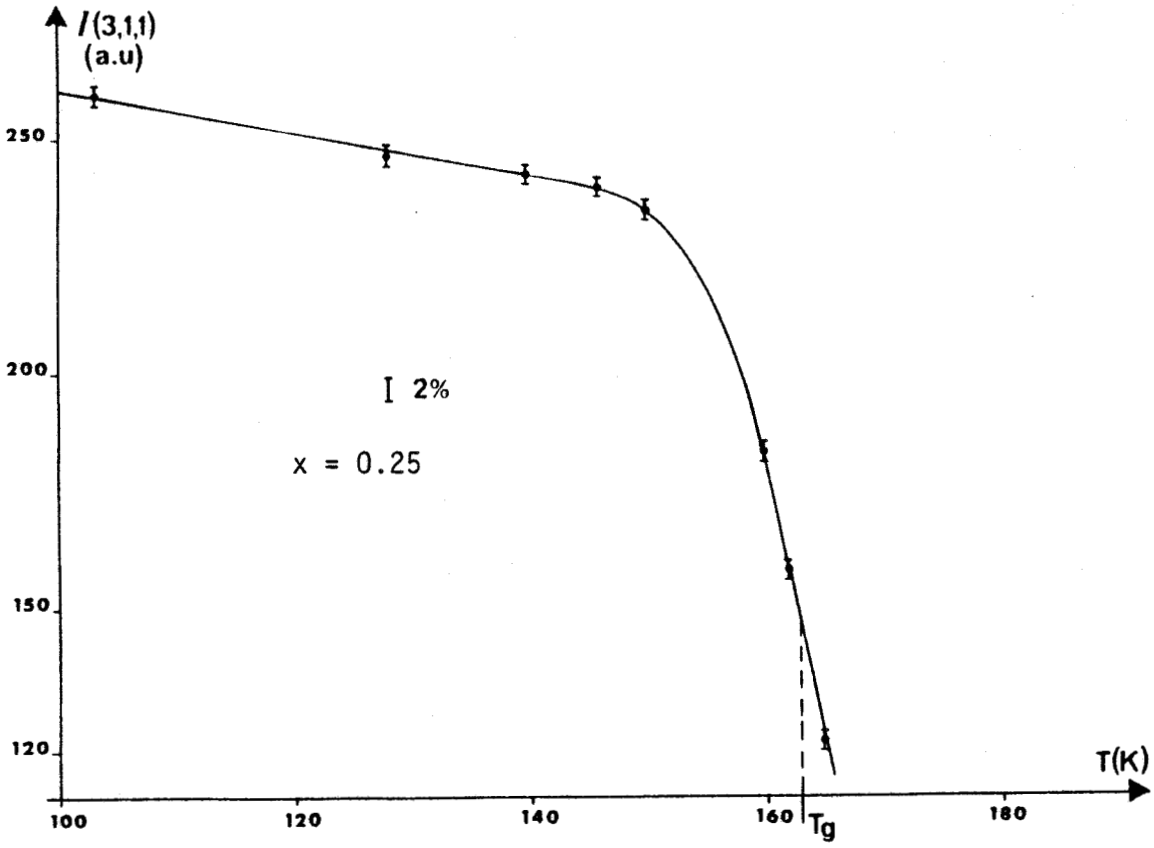

FIGURE XII-14 extraite de [1]

Variation de l'intensité de la raie (311) en fonction de la température

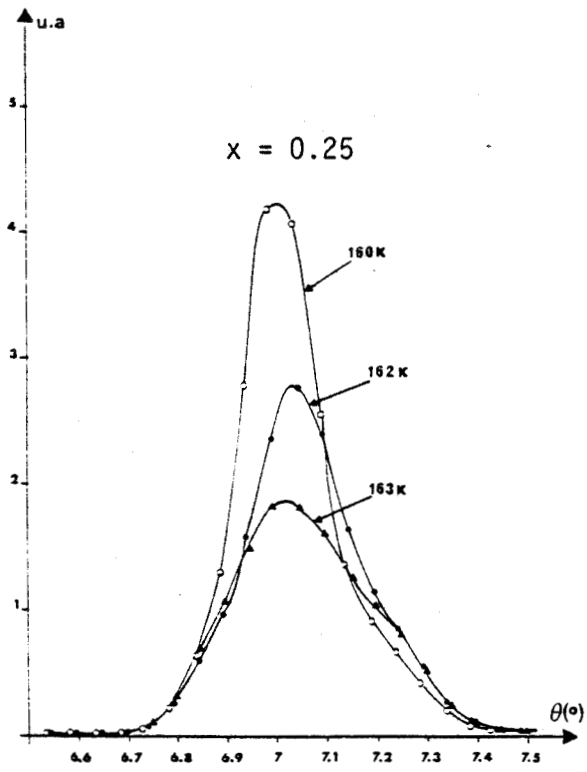

FIGURE XII-15a [1]

Evolution de la raie (311) à la remontée en température près de Tg

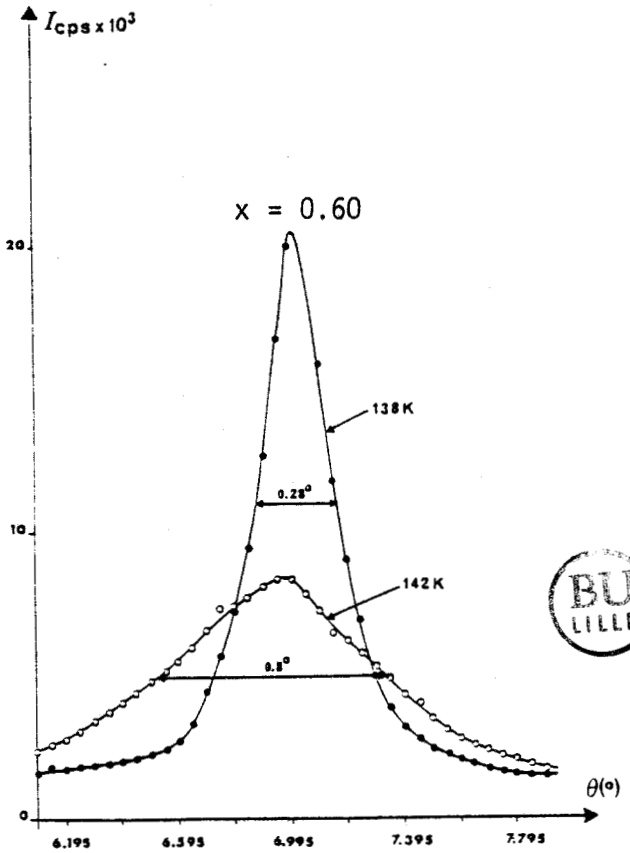

FIGURE XII-15b [1]

Evolution de la raie (311) en fonction de la température

← F(h,k,ℓ) sans 200 et 111 →								← avec 200 et 111 →			
T(K)	U_3 (Å)	$\sqrt{T_{11}}$ (Å)	$\sqrt{L_{11}}$ (°)	R	R_W	G	Nb	R	R_W	G	Nb
178 (I')	-0.065 (11)	0.228 (9)	3.18 (27)	8.85	9.45	8.7	34	8.15	9.41	7.5	36

TABLEAU XII-7a [1]

Résultats de l'affinement de la structure à 178K (phase I')
pour la concentration x = 0.25 : modèle de translation isotrope

← F(h,k,ℓ) sans 200 et 111 →								← avec 200 et 111 →			
T(K)	$\sqrt{U_3}$ (Å)	$\sqrt{T_{11}}$(Å)	$\sqrt{T_{33}}$(Å)	$\sqrt{L_{11}}$(°)	R	R_W	G	Nb	R	R_W	G	Nb
178(I')	-0.066(15)	0.229(15)	0.227(18)	3.11(36)	8.8	10.0	10.5	34	8.1	9.4	7.6	36

TABLEAU XII-7b 1

Résultats de l'affinement de la structure à 178K (phase I')
pour la concentration x = 0.25 : modèle de translation anisotrope

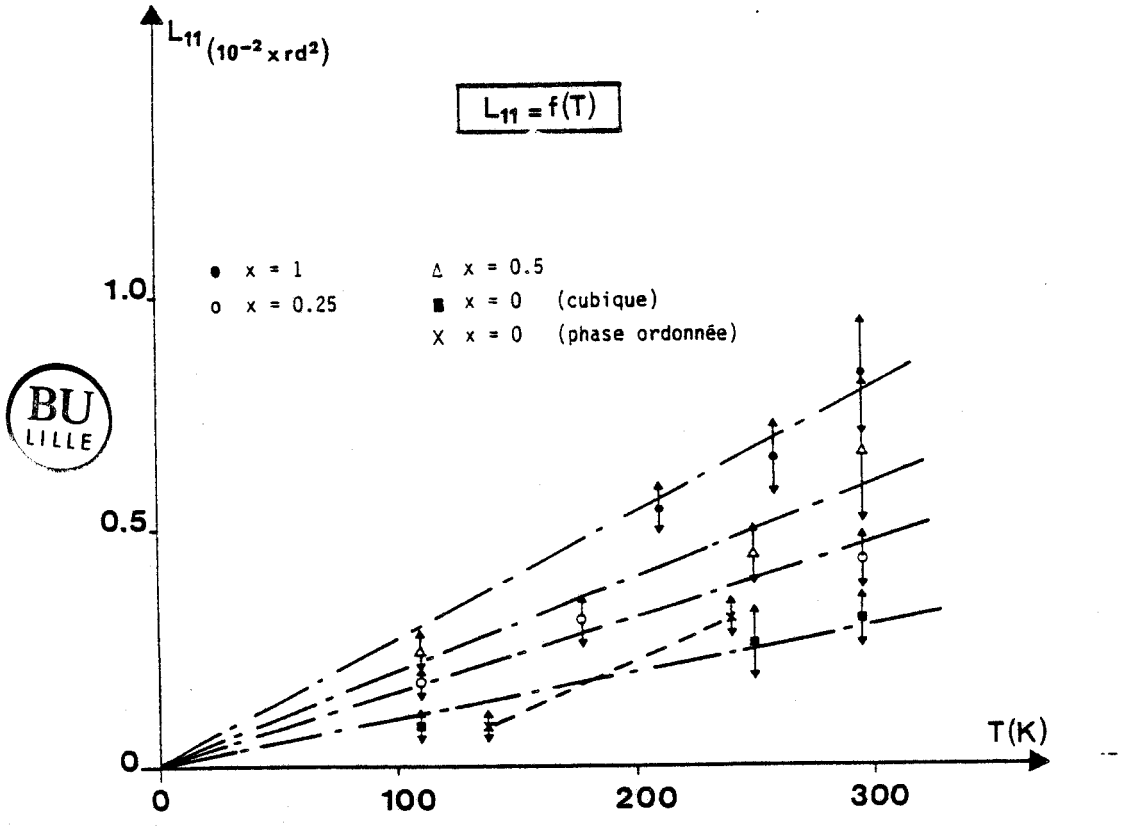

FIGURE XII-16 extraite de [1]

Variation de l'amplitude quadratique moyenne de libration ; L_{11} (⊥ axe dipolaire), en fonction de la température

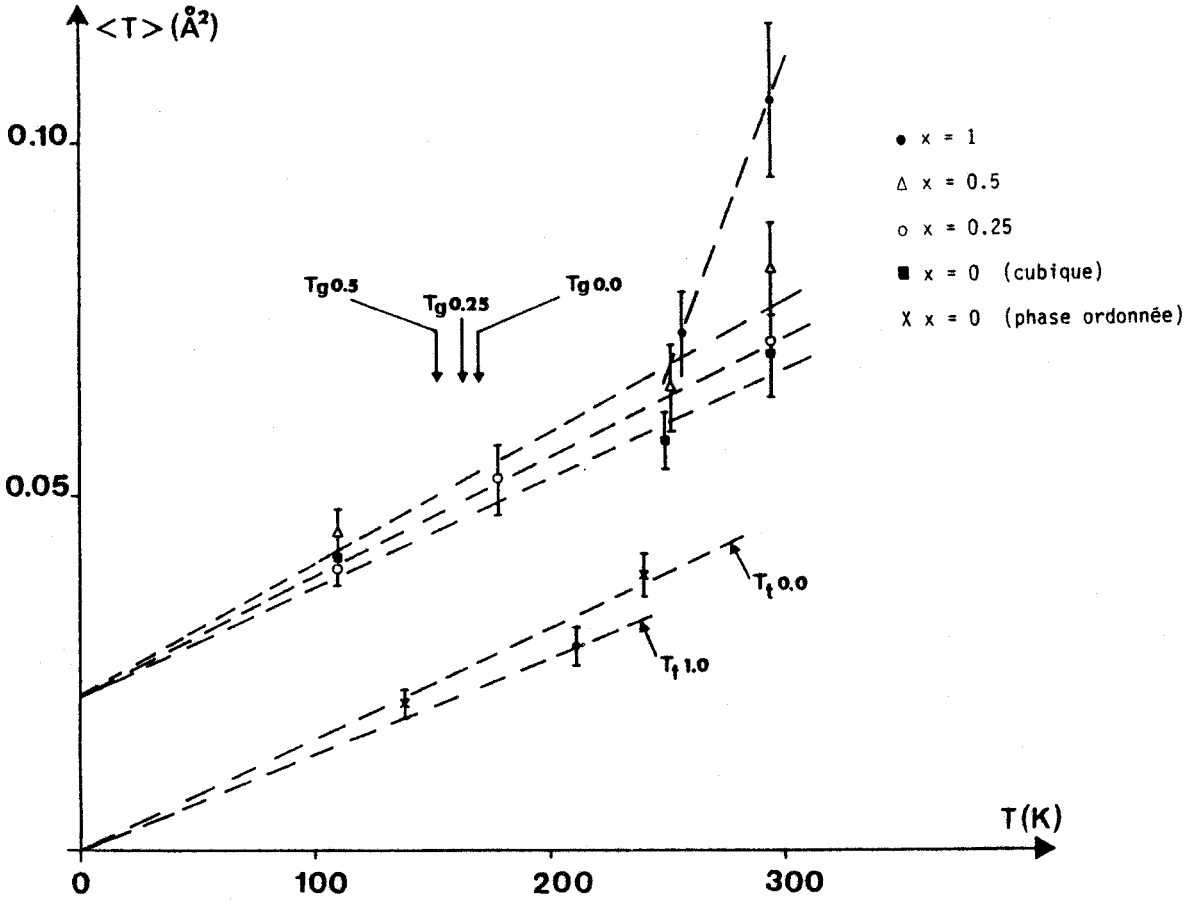

FIGURE XII-17 extraite de [1]

Variation du terme de translation, <T>, en fonction de la température

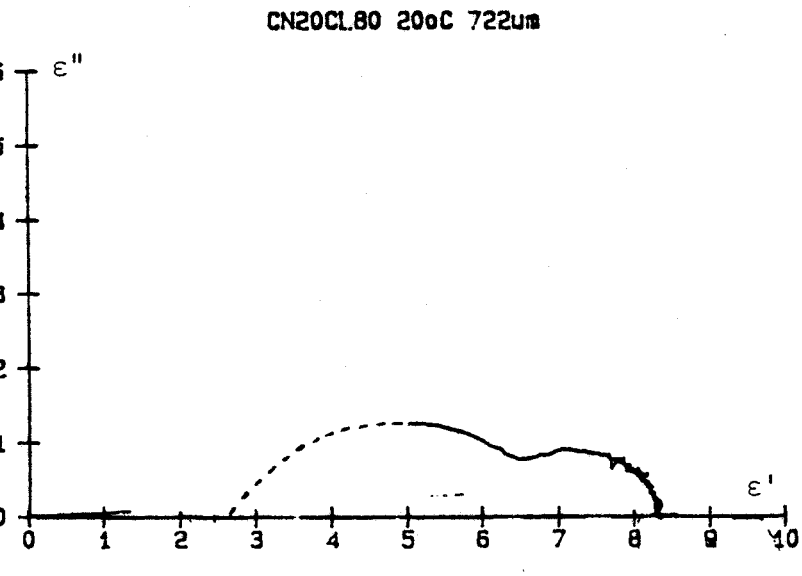

FIGURE XII-18

Relaxation diélectrique d'un mélange $CNADM_{0.2}$ $C\ell\ ADM_{0.8}$. Diagramme $\varepsilon'' = f(\varepsilon')$

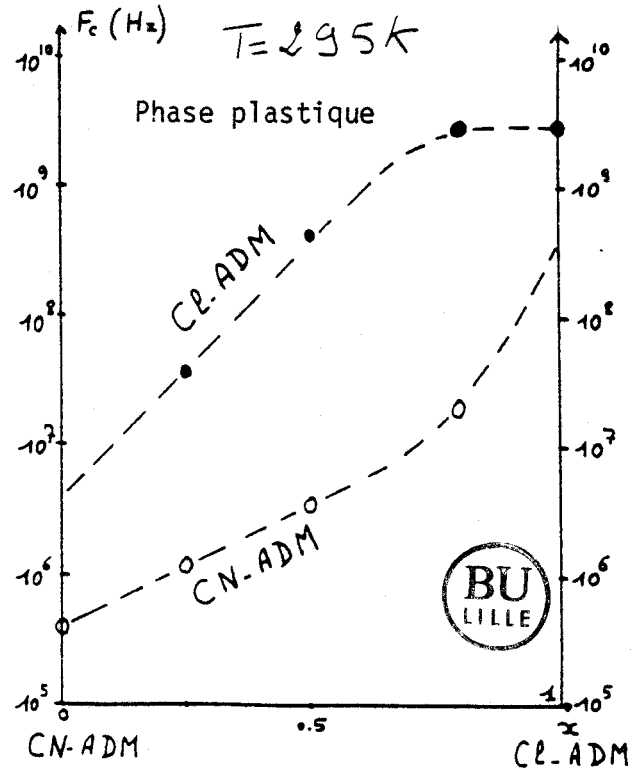

FIGURE XII-19

Fréquence critique de basculement du CNADM et du Cℓ ADM dans les mélanges

	253K	273K	300K	353K	423K	Instrument Longueur d'onde Å Résolution µeV
CNH			1.50	0.96		IN5 30
CNH			1.18			IN6 5.9 50
CNH			1.06			IN6 5.1 80
CNH			0.98	0.74		IN6 5.1 120
CNH/ClH (2/3, 1/3)	1.36		1.13	0.77		IN6 5.1 120
CNH/ClD (2/3, 1/3)	1.52		1.11	0.74		IN6 5.1 120
CNH/ClH (1/3, 2/3)	1.18	1.09	0.91	0.65	0.48	IN6 5.1 120
CNH/ClD (1/3, 2/3)			0.98	0.70		IN6 5.1 120
ClH			0.77			IN6

TABLEAU XII-8

Le temps de résidence affiné, $\tau_{m12} \times 10^{13}$s, pour des concentrations et des températures différentes (modèle d'ordre 12 sans tenir compte des distributions)

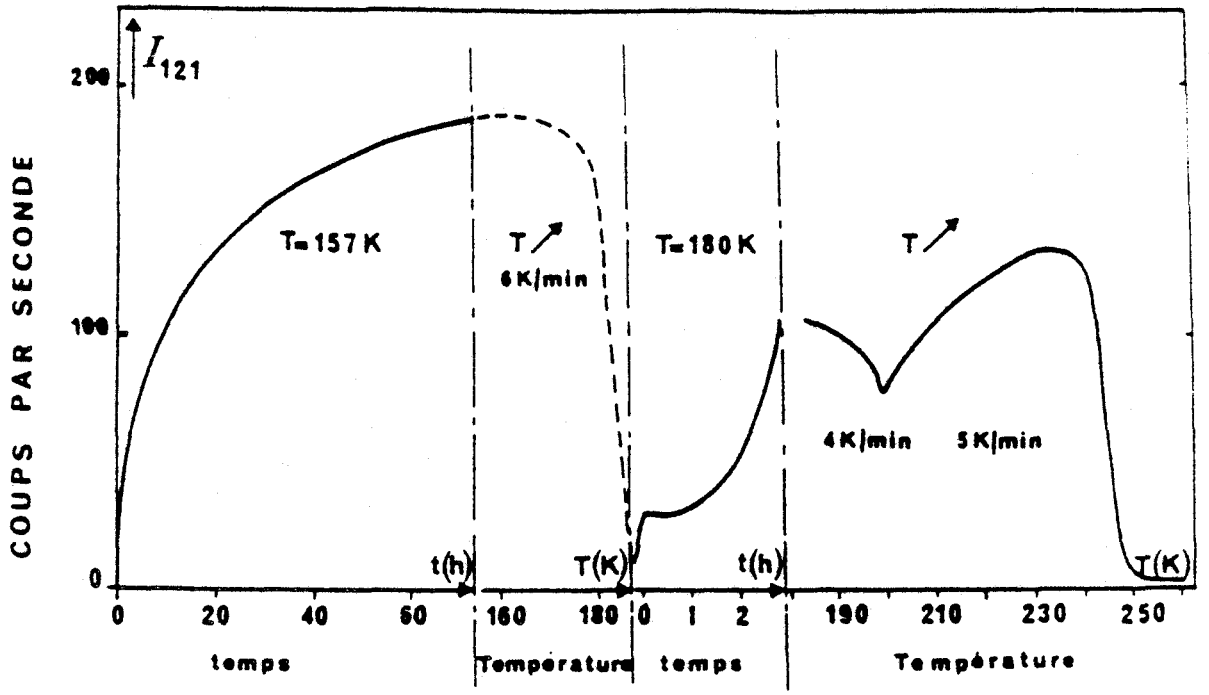

FIGURE XII-20 extraite de [2]

$Cl_{25}CN_{75}$-ADM

Evolutions de l'intensité au pic de surstructure 121 au cours des différents traitements thermiques subis par le cristal :

a) *vieillissement à 157K pendant 70 heures*

b) *réchauffage : réversion vers 180K*

c) *vieillissement à 180K pendant 3 heures*

d) *réchauffage : transition III - I vers 237K.*

Température de recuit	Demi largeur du profil 121 juste avant le réchauffage (u.r.r.)	Taille des domaines (Å)	Température du début de la réversion
157K	0.115	35	179K
168K	0.09	48	186K
170K	* 0.08	54	190K
176K	* 0.07	62	193K
180K	* 0.05	86	pas de réversion mais transition à 237K

TABLEAU XII-9 extrait de [2]

* : cristal pour lequel nous avons noté une saturation

- La vitesse de réchauffage a toujours été de l'ordre de 6K/minute

ANNEXE

LISTES DES FACTEURS DE STRUCTURE OBSERVES ET CALCULES

ANNEXE

LISTES DES FACTEURS DE STRUCTURE OBSERVES ET CALCULES

FACTEURS DE STRUCTURE

OBSERVES ET CALCULES

F_{cFREN} Modèle de FRENKEL

F_c H.Cub Modèle des Fonctions Adaptées à la Symétrie

PHASE PLASTIQUE

F L U O R O A D A M A N T A N E

A D A M A N T A N E

h	k	l	220K F_o	220K σ 220K	220K F_c FREN	220K F_c H.Cub	295K F_o	295K σ	295K F_c FREN	295K F_c H.Cub
0	0	2	601	0.7	610	620	442	8.8	438	434
0	0	4	65	0.8	64	65	16	4.1	27	18
0	0	6	134	0.4	123	132	69	1.4	72	64
0	0	8	23	1.7	15	21	16	4.1	20	15
0	0	10	118	1.1	120	122	44	1.0	42	45
0	0	12	53	1.0	50	58	20	1.3	17	21
0	0	14	17	3.1	12					
0	0	18	18	3.0	3					
0	2	2	51	0.4	52	50	39	3.7	41	38
0	2	6	18	2.4	15	17				
0	2	8	48	1.3	42	55	19	4.3	27	24
0	2	10	56	0.8	58	53	22	1.2	22	20
0	2	14	19	2.4	14					
0	4	4	211	0.5	208	211	105	2.7	104	104
0	4	6	201	0.6	205	205	105	2.1	105	108
0	6	6	245	0.7	253	232	118	2.3	118	115
0	6	12	15	2.8	3					
0	8	8	42	1.0	41	50	17	1.4	16	19
0	8	10	19	2.2	3					
0	10	10	24	1.9	20					
0	10	12	23	2.2	10					
1	1	1	883	0.6	961	971	685	3.7	666	677
1	1	3	206	0.5	187	195	139	2.8	123	138
1	1	5	68	0.5	69	70	31	0.8	34	31
1	1	7	46	0.8	39	44	14	1.2	17	14
1	1	9	18	2.7	22	18				
1	1	11	80	0.7	78	79	31	1.0	31	30
1	1	15	12	3.6	3					
1	3	3	208	0.3	197	198	135	2.7	128	137
1	3	5	44	0.6	47	47	21	0.9	23	22
1	3	7	26	4.4	35	28	10	2.5	10	9
1	3	9	34	1.6	35	38	16	1.4	16	17
1	3	13	24	1.9	21					
1	5	5	297	0.8	306	293	150	3.0	154	154
1	5	7	93	1.2	97	98	47	1.5	47	47
1	5	9	21	1.6	19	14	10	2.6	10	8
1	5	11	17	2.3	11	8				
1	7	9	25	5.2	27	29	10	2.1	11	11
1	7	13	15	3.8	7		10	3.0	2	5
1	9	9	16	2.7	8					
1	9	11	17	3.9	12					
1	11	11	27	1.9	14					
2	2	2	640	0.9	626	636	481	7.6	395	398
2	2	4	278	0.3	268	270	167	3.3	168	161
2	2	6	24	1.3	30	19	8	2.3	7	4
2	2	8	108	0.5	109	102	47	1.6	47	44
2	2	10	13	4.2	6	6				
2	2	14	19	2.5	17					
2	2	18	14	4.1	3					
2	4	4	51	0.7	47	48	31	0.8	31	31
2	4	6	70	1.9	69	68	41	1.0	44	40
2	4	8	77	0.7	83	76	34	0.9	36	34
2	4	10	12	3.6	5	4				
2	4	12	16	2.7	6					
2	4	14	13	3.7	10					
2	6	6	58	2.3	67	67	31	1.7	34	31
2	6	8	30	1.3	29	31	13	2.0	12	13
2	8	8	45	5.7	48	48	20	1.2	16	19
2	10	10	20	2.4	11					
3	3	3	554	0.4	541	531	316	5.9	318	315
3	3	5	15	2.9	25	26	10	1.6	11	10
3	3	7	92	0.5	99	94	36	2.3	37	36
3	3	9	79	0.7	82	75	36	1.0	34	35
3	3	13	22	2.4	20					
3	3	15	13	3.8	2					
3	5	5	29	5.2	39	41	23	1.2	24	24
3	5	7	36	1.0	39	39	16	1.4	19	18
3	5	11	24	1.8	24	27				
3	7	7	42	1.0	36	34	15	1.5	12	14
3	7	9	23	1.8	28	17				
4	4	4	39	3.3	44	33	19	1.0	22	19
4	4	6	20	2.1	17	17				
4	4	8	53	1.4	58	64	28	1.0	29	29
4	4	10	27	4.3	29	31	9	2.9	9	9
4	4	12	15	2.9	11					
4	6	6	16	2.1	4	6				
4	6	10	29	2.6	32	32	9	2.9	9	7
4	6	12	17	2.8	14					
4	8	8	28	1.5	27	25	12	2.0	9	11
5	5	5	28	4.1	22	34				
5	5	9	27	4.6	28	24				
5	5	11	47	1.2	44		16	1.7	12	14
5	7	7	24	1.6	9	12				
5	7	11	22	2.2	22					
5	7	13	15	3.3	5					
5	7	15	15	3.5	3					
5	9	9	20	3.3	4					
6	6	6	22	1.6	21	15				
6	6	10	35	1.5	35		13	2.1	11	9
6	6	12	16	3.0	13					
6	6	16	14	3.9	2					
6	8	8	19	3.1	7					
6	8	12	17	2.8	5					
7	7	7	16	2.5	14	12	9	2.5	5	8
7	7	9	12	3.7	3					
7	7	15	13	4.1	7					
9	9	9	17	4.2	9					
9	9	11	13	4.0	3					

h	k	l	223K F_o	223K σ_c	223K F_c FREN	223K F_c H.Cub	295K F_o	295K σ_c	295K F_c FREN	295K F_c H.Cub
0	0	2	918	0.9	921	922	841	17.8	785	847
0	0	4	108	0.5	112	108	27	1.2	5.2	27
0	0	6	54	1.0	54	52	40	0.9	37	40
0	0	8	13.5	3.1	3.1	7				
0	0	10	155	0.8	150	156	78	1.7	77	78
0	2	2	174	0.4	180	176	135	2.7	142	135
0	2	4	27	7.0	28	32	60	1.3	44	61
0	2	6	34	0.9	44	41	34	0.8	45	33
0	2	8	62	0.8	67	67	44	1.1	52	44
0	2	10	73	0.9	65	67	36	1.0	40	35
0	4	4	282	0.5	270	280	188	3.8	169	186
0	4	6	268	0.8	270	272	187	3.8	187	192
0	4	8	28	1.7	31	25	15	2.2	21	15
0	6	6	249	0.6	254	249	160	3.2	159	160
0	6	8	17.8	2.1	13.2	19	9	3.0	9	9
1	1	1	1150	0.9	1165	1164	1105	23.1	1019	1101
1	1	3	230	0.4	219	224	204	4.2	185	204
1	1	5	47	0.7	65	62	22	0.9	46	24
1	1	7	50	0.7	48	50	25	0.9	32	26
1	1	9	37	1.3	29	24	7	2.0	3	9
1	3	3	330	1.0	328	326	270	5.6	272	273
1	3	5	108	0.6	113	115	79	1.6	81	81
1	3	7	36	1.0	40	34	14	1.5	17	15
1	3	9	44	3.0	49	51	32	1.0	32	34
1	5	5	355	0.5	361	360	243	4.9	241	242
1	5	7	96	0.7	96	97	65	1.5	62	67
1	7	7	24	1.7	19	28	10	1.9	6	9
2	2	2	771	1.2	751	752	604	13.1	572	588
2	2	4	298	0.4	285	287	229	4.8	218	224
2	2	6	42	3.1	40	38	19	1.0	11	22
2	2	8	125	0.8	131	128	84	1.6	83	83
2	4	4	38	1.4	41	38	29	0.8	39	29
2	4	6	74	2.4	75	76	60	1.3	60	60
2	4	8	92	0.7	95	90	54	1.2	56	54
2	6	6	84	0.9	92	84	56	1.3	63	58
2	6	8	53	1.0	48	53	30	1.0	26	29
3	3	3	514	0.4	515	512	377	7.8	385	371
3	3	5	66	0.6	72	71	43	1.1	46	42
3	3	7	117	0.6	122	117	66	1.4	67	66
3	3	9	76	0.8	78	76	45	1.2	46	46
3	5	5	61	0.7	60	58	44	1.1	45	43
3	5	7	42	1.0	39	41	22	1.3	22	22
4	4	4	60	0.7	66	66	39	1.1	46	39
4	4	6	19	2.0	14	13				
4	4	8	64	0.9	72	70	46	1.2	48	46
4	6	6	12	3.9	7	7				
5	5	5	22	1.6	25	33	12	2.8	12	16
5	5	7	16	2.5	12	11	13	1.7	14	13
0	0	12	46	1.1	45	65	28	1.3	24	31
0	0	14	28	1.8	24					
0	2	14	30	1.6	24					
0	4	12	19	2.3	11	23				
0	8	8	56	3.1	59	69	33	1.1	32	34
0	10	10	34	1.6	25					
1	1	13	30	1.6	27	20	13	2.1	13	7
1	3	13	33	1.5	32	37				
1	3	11	23	1.8	28	23	16	1.6	21	16
1	5	13	18	2.7	16					
1	7	9	39	1.2	39	42	21	1.3	21	22
2	2	12	15	2.9	5	5				
2	6	10	12	3.2	9	14				
2	8	8	65	0.9	58	65	32	1.1	28	32
3	3	11	17	2.3	18	21	13	3.0	13	14
3	3	13	26	1.9	25	23				
3	5	11	38	1.3	34	42	19	1.6	16	19
3	7	9	22	1.9	18	18	11	2.3	9	10
3	7	11	17	2.8	17	22				
4	4	10	46	1.0	36	46	20	1.5	13	19
4	4	12	19	2.4	15	22				
4	6	12	18	3.1	14					
4	6	10	54	1.2	45	50	21	1.3	18	22
4	8	8	20	2.1	19	22				
4	8	10	13	3.8	9	11				
5	5	9	44	1.2	36	39	14	1.5	10	13
5	5	11	61	1.0	53	57	28	1.2	22	25
5	7	11	27	1.8	21					
5	7	9	25	1.8	18	17				
6	6	10	49	1.3	41	38	19	1.4	17	19
8	8	8	22	2.1	18					
0	2	12					10	3.0	10	10
1	1	11					53	1.2	55	52
1	5	9					17	1.5	19	18
2	2	10					11	3.2	16	10
3	5	9					14	2.2	17	14
3	7	7					33	1.0	27	33
4	6	8					13	1.9	14	16

OBSERVED AND CALCULATED STRUCTURE FACTORS FOR ADAMANTANE LOW TEMPERATURE PHASE T=188K

H	K	L	10FO	10FC	H	K	L	10FO	10FC	H	K	L	10FO	10FC
0	2	0	58	54	2	7	1	25	26	4	4	2	81	84
1	6	4	25	24	0	1	6	28	31	0	4	0	140	145
2	6	1	58	59	4	5	2	51	53	1	4	4	31	31
0	2	6	53	54	0	6	0	141	146	2	4	1	38	38
5	6	2	29	28	1	3	4	34	32	0	3	6	43	44
0	8	0	22	19	2	3	1	23	27	5	5	2	28	27
1	2	4	74	73	1	7	6	19	14	1	8	0	30	29
3	4	1	35	37	6	6	2	29	29	2	2	4	164	169
1	2	6	44	48	1	6	0	83	86	3	5	1	50	51
0	8	3	36	36	2	3	4	67	68	2	2	6	114	110
1	5	0	152	152	4	7	1	34	34	0	7	3	38	37
2	4	4	58	58	2	3	6	53	55	1	4	0	64	65
4	6	1	64	66	0	4	3	68	66	2	5	4	35	38
2	4	6	51	51	1	2	0	56	55	4	5	1	31	29
0	3	3	244	229	2	6	4	38	41	2	6	6	29	24
1	1	0	402	402	5	6	1	64	65	0	2	3	203	196
2	8	4	40	39	3	7	6	37	35	2	2	0	62	63
5	7	1	28	27	0	1	3	75	70	3	7	4	39	35
3	6	6	25	25	2	4	0	41	38	0	0	2	350	355
1	2	3	145	137	3	5	4	46	47	3	5	6	32	34
2	5	0	70	70	0	1	2	104	106	1	3	3	151	144
3	4	4	42	42	3	4	6	35	36	3	7	0	26	25
0	2	2	358	345	1	4	3	51	50	3	3	4	156	155
3	3	6	137	136	3	6	0	31	32	0	3	2	213	208
1	5	3	59	59	4	4	4	44	44	4	4	6	33	28
3	3	0	30	29	0	4	2	48	43	1	6	3	51	52
4	5	4	27	28	4	6	6	18	16	4	5	0	54	53
0	8	2	39	42	1	7	3	29	29	4	7	4	42	41
0	4	7	31	29	4	6	0	72	74	1	8	2	51	53
1	8	3	27	25	6	6	4	21	24	0	3	7	94	98
4	7	0	29	30	1	7	2	56	55	2	8	3	46	43
0	7	5	20	18	0	2	7	66	72	5	7	0	30	30
1	6	2	59	63	2	7	3	38	40	0	3	5	30	27
1	2	7	57	60	5	6	0	44	45	1	5	2	30	29
2	6	3	50	51	0	2	5	18	17	1	3	7	61	65
5	5	0	96	97	1	4	2	30	28	2	5	3	66	73
0	1	5	23	25	1	4	7	34	32	6	6	0	39	37
1	3	2	161	154	2	4	3	37	38	1	2	5	53	52
1	5	7	36	36	0	8	1	25	22	1	2	2	151	151
2	3	3	59	60	1	3	5	70	73	1	6	7	35	31
0	5	1	161	164	1	1	2	109	105	3	4	3	48	54
1	4	5	50	48	1	7	7	22	19	0	4	1	26	24
2	2	2	36	38	3	5	3	59	64	1	7	5	31	31
2	7	7	27	22	0	3	1	142	141	2	3	2	42	41
3	6	3	46	49	1	8	5	39	39	2	6	7	35	36
0	2	1	161	160	2	4	2	37	34	4	7	3	22	15
2	8	5	39	39	2	5	7	53	52	0	1	1	457	461
2	5	2	74	76	4	6	3	27	27	2	7	5	35	34
2	4	7	27	28	1	2	1	106	106	2	6	2	64	67
4	5	3	63	65	2	4	5	54	55	2	3	7	37	34
1	3	1	62	63	2	8	2	25	24	0	0	4	80	82
2	3	5	206	208	3	4	7	37	36	1	4	1	61	62
3	8	2	21	22	0	2	4	105	103	3	4	5	66	69
3	5	7	42	43	1	5	1	108	113	3	6	2	49	48
0	3	4	108	100	3	7	5	31	28	3	6	7	30	29
1	6	1	59	60	3	5	2	77	81	0	4	4	27	25
4	7	5	53	52	4	5	7	49	48	1	8	1	27	29
3	4	2	42	42	0	7	4	22	18	5	6	5	23	21
0	0	8	52	50	2	8	1	28	27	3	3	2	32	34
1	8	4	59	59	0	0	6	28	25	0	2	8	76	79

OBSERVED AND CALCULATED STRUCTURE FACTORS FOR ADAMANTANE LOW TEMPERATURE PHASE T=188K

H	K	L	10FO	10FC	H	K	L	10FO	10FC	H	K	L	10FO	10FC
0	3	8	64	68	2	5	8	47	46	0	5	9	63	63
1	5	9	41	40	1	4	10	22	18	1	6	8	30	29
2	6	8	38	37	0	3	9	41	42	1	6	9	27	28
1	1	10	63	65	1	5	8	23	16	3	6	8	29	24
0	2	9	36	37	2	4	9	20	15	0	1	11	57	58
1	3	8	63	63	3	5	8	51	52	0	1	9	68	69
0	0	10	140	142	0	0	12	29	26	1	2	8	43	45
3	4	8	21	25	1	3	9	25	26	0	4	10	43	43
0	10	0	26	25	2	2	8	32	33	4	4	8	60	60
1	4	9	23	16	1	5	10	58	58	1	10	0	37	34
2	4	8	28	26										

FACTEURS DE STRUCTURE

OBSERVES ET CALCULES

1 ADAMANTANE

PHASE BASSE TEMPERATURE

T = 188 K

H	K	L	10FO	10FC
2	0	0	3817	4195
4	0	0	1935	1822
6	0	0	1525	1524
8	0	0	661	648
9	1	0	400	388
7	1	0	1113	1103
5	1	0	1894	1853
3	1	0	2162	2136
1	1	0	4379	5405
0	2	0	2624	2619
2	2	0	1815	1843
4	2	0	1929	1939
6	2	0	1573	1582
8	2	0	615	617
7	3	0	803	849
5	3	0	1512	1528
3	3	0	1430	1496
1	3	0	1546	1567
0	4	0	1595	1593
2	4	0	1252	1277
4	4	0	1014	1022
6	4	0	687	700
5	5	0	389	360
3	5	0	690	652
1	5	0	1181	1173
0	6	0	689	714
2	6	0	452	433
4	6	0	194	167
1	7	0	154	172
9	0	1	456	468
8	0	1	437	451
7	0	1	798	784
6	0	1	878	851
5	0	1	1666	1605
4	0	1	1747	1703
3	0	1	2993	2960
2	0	1	2134	2086
1	0	1	532	539
0	0	1	1503	1775
0	1	1	1090	1103
1	1	1	1987	2019
2	1	1	2696	2736
3	1	1	1887	1752
4	1	1	2117	2037
5	1	1	1131	1091
6	1	1	896	885
7	1	1	549	568
8	1	1	558	573
8	2	1	339	354
7	2	1	440	445
6	2	1	605	612
5	2	1	850	850
4	2	1	1182	1087
3	2	1	2220	2115
2	2	1	1837	1811
1	2	1	2805	2775
0	2	1	1939	1845
0	3	1	2033	1965
1	3	1	1406	1361
2	3	1	1886	1809
3	3	1	1128	1124
4	3	1	919	903
5	3	1	586	600
6	3	1	314	322
7	3	1	341	347
8	3	1	330	319
7	4	1	283	283
6	4	1	317	327
5	4	1	395	422
4	4	1	512	527
3	4	1	768	761
2	4	1	767	766
1	4	1	882	876
0	4	1	775	737
0	5	1	187	185
1	5	1	385	401
2	5	1	350	372
3	5	1	352	371
4	5	1	400	439
5	5	1	259	276
6	5	1	277	298
4	6	1	198	198
3	6	1	284	297
2	6	1	223	232
1	6	1	117	119
0	6	1	216	217
0	7	1	152	143
0	0	2	1889	2054
1	0	2	3135	3540
2	0	2	1204	1158
3	0	2	2171	2065
4	0	2	595	607
5	0	2	1373	1332
6	0	2	485	474
7	0	2	851	832
8	0	2	189	191
8	1	2	540	509
7	1	2	335	327
6	1	2	1090	1071
5	1	2	584	578
4	1	2	1673	1668
3	1	2	730	759
2	1	2	2475	2468
1	1	2	1393	1338
0	1	2	3007	3245
0	2	2	851	828
1	2	2	2098	2017
2	2	2	637	638
3	2	2	1628	1643
4	2	2	606	618
5	2	2	1202	1206
6	2	2	470	453
7	2	2	674	657
8	2	2	169	172
8	3	2	296	322
7	3	2	234	229
6	3	2	686	692
5	3	2	454	438
4	3	2	1018	1036
3	3	2	442	456
2	3	2	1215	1163
1	3	2	498	493
0	3	2	1540	1577
0	4	2	481	458
1	4	2	973	985
2	4	2	376	375
3	4	2	760	782
4	4	2	304	303
5	4	2	569	553
6	4	2	179	186
7	4	2	282	302
6	5	2	204	218
5	5	2	93	91
4	5	2	369	375
3	5	2	200	192
2	5	2	555	541
1	5	2	350	327
0	5	2	656	655
0	6	2	171	182
1	6	2	310	306
2	6	2	134	113
3	6	2	208	206
8	0	3	654	642
7	0	3	104	86
6	0	3	1238	1187
5	0	3	228	222
4	0	3	2234	2158
3	0	3	476	472
2	0	3	2893	2852
1	0	3	426	404
0	0	3	2329	2609
0	1	3	206	210
1	1	3	2681	2787
2	1	3	399	385
3	1	3	2424	2326
4	1	3	316	336
5	1	3	1554	1497
6	1	3	123	88
7	1	3	806	823
8	2	3	480	507
6	2	3	897	903
5	2	3	89	85
4	2	3	1572	1514
3	2	3	346	358
2	2	3	2284	2291
1	2	3	423	409
0	2	3	2530	2477
0	3	3	281	286
1	3	3	1799	1765
2	3	3	253	243
3	3	3	1444	1429
4	3	3	89	100
5	3	3	870	873
7	3	3	494	503
6	4	3	449	464
4	4	3	728	732
3	4	3	95	78
2	4	3	1028	1022
0	4	3	1092	1075
1	5	3	569	573
2	5	3	505	507
5	5	3	375	377
2	6	3	307	300
0	6	3	292	286
0	0	4	3186	3648
1	0	4	2342	2312
2	0	4	2087	1988
3	0	4	1592	1543
4	0	4	1160	1075
5	0	4	1095	1100
6	0	4	854	852
7	0	4	626	623
8	0	4	395	381
8	1	4	414	402
7	1	4	613	628
6	1	4	824	819
5	1	4	1030	1005
4	1	4	1316	1296
3	1	4	1282	1219
2	1	4	1766	1714
1	1	4	2378	2325
0	1	4	2191	2159
0	2	4	1492	1429
1	2	4	1544	1504
2	2	4	1135	1098
3	2	4	1322	1296
4	2	4	1030	1012
5	2	4	920	924
6	2	4	831	855
7	2	4	516	505
7	3	4	444	478
6	3	4	533	537
5	3	4	794	815
4	3	4	839	842
3	3	4	797	825
2	3	4	1079	1047
1	3	4	928	922
0	3	4	1192	1151
0	4	4	831	845
1	4	4	794	768
2	4	4	668	704
3	4	4	647	642
4	4	4	551	570
5	4	4	438	439
6	4	4	391	401
5	5	4	236	222
4	5	4	314	308
3	5	4	380	370
2	5	4	459	445
1	5	4	602	616
0	5	4	526	524
0	6	4	372	378
1	6	4	292	280
2	6	4	255	241
7	0	5	728	723
6	0	5	133	122
5	0	5	1377	1356
4	0	5	243	243
3	0	5	2201	2135

H	K	L	10FO	10FC
1	0	5	1546	1535
0	1	5	1646	1650
1	1	5	249	265
2	1	5	2123	2076
3	1	5	288	299
4	1	5	1679	1648
5	1	5	141	133
6	1	5	847	834
7	2	5	463	460
5	2	5	864	847
4	2	5	100	119
3	2	5	1734	1690
2	2	5	263	246
2	3	5	1468	1451
3	3	5	94	97
3	4	5	873	864
6	3	5	386	390
5	4	5	396	425
4	4	5	725	712
3	4	5	99	81
4	5	5	818	812
3	5	5	1545	1530
1	3	5	217	204
1	4	5	463	460
2	4	5	1734	1690
1	5	5	847	834
0	6	5	1549	1535
0	0	6	2270	2244
1	0	6	655	632
2	0	6	1649	1631
3	0	6	630	617
4	0	6	1049	1026
5	0	6	403	385
6	0	6	751	725
6	1	6	276	261
5	1	6	895	886
4	1	6	467	465
3	1	6	1157	1180
2	1	6	651	619
1	1	6	1798	1749
0	1	6	650	605
0	2	6	1305	1275
1	2	6	580	548
2	2	6	1054	1049
3	2	6	438	437
4	2	6	890	906
5	2	6	253	256
6	2	6	690	675
5	3	6	639	640
4	3	6	223	233
3	3	6	701	713
2	3	6	348	357
1	3	6	853	834
0	3	6	448	457
0	4	6	710	697
1	4	6	242	258
2	4	6	584	578
3	4	6	140	203
4	4	6	465	454
5	5	6	102	122
1	5	6	482	467
0	5	6	98	112
6	0	7	550	548
5	0	7	571	570
4	0	7	883	834
3	0	7	868	830
2	0	7	1236	1190
1	0	7	942	969
0	0	7	1372	1376
0	1	7	927	942
1	1	7	1255	1240
2	1	7	898	872
3	1	7	992	940
4	1	7	692	659
5	1	7	675	667
5	2	7	427	436
4	2	7	703	693
3	2	7	691	668
2	2	7	915	907
1	2	7	819	807
0	2	7	1024	1014
0	3	7	632	623
1	3	7	677	696
2	3	7	585	586
3	3	7	601	607
4	3	7	423	421
3	4	7	352	336
2	4	7	428	448
1	4	7	390	392
0	4	7	454	485
0	0	8	157	144
1	0	8	1339	1312
3	0	8	1182	1189
4	1	8	978	973
6	1	8	1221	1222
0	1	8	1312	1276
1	2	8	1147	1120
2	2	8	96	67
3	2	8	961	961
2	3	8	816	811
0	3	8	913	887
2	0	9	788	818
1	0	9	547	514
0	0	9	880	932
0	1	9	544	525
1	1	9	808	829
2	1	9	586	562
10	0	0	319	305
12	0	0	211	196
11	1	0	255	247
10	2	0	217	241
11	3	0	157	144
9	3	0	234	245
8	4	0	215	253
10	4	0	116	115
7	5	0	176	197
6	6	0	147	139
7	7	0	108	124

H	K	L	10FO	10FC	H	K	L	10FO	10FC	H	K	L	10FO	10FC	H	K	L	10FO	10FC	H	K	L	10FO	10FC
5	1	9	465	459	2	1	10	264	267	0	2	12	320	320										
6	1	9	266	266	1	1	10	685	690	1	2	12	310	307										
7	1	9	291	273	0	1	10	305	319	13	1	0	115	103										
8	1	9	173	165	0	2	10	575	561	12	2	0	140	149										
7	2	9	164	161	1	2	10	247	247	12	4	0	109	79										
6	2	9	321	318	2	2	10	499	496	12	2	3	111	85										
5	2	9	285	268	3	2	10	202	200	12	0	4	119	112										
4	2	9	457	465	4	2	10	388	396	12	2	4	104	87										
3	2	9	449	466	5	2	10	143	150	11	2	5	126	110										
2	2	9	601	602	6	2	10	270	275	9	6	5	107	46										
1	2	9	531	539	5	3	10	260	260	11	1	7	108	84										
0	2	9	665	679	4	3	10	145	134	10	1	8	180	164										
0	3	9	393	418	3	3	10	321	333	9	2	8	198	208										
1	3	9	479	484	2	3	10	191	164	11	2	8	113	90										
2	3	9	399	399	1	3	10	401	403	9	4	8	110	119										
3	3	9	405	401	0	3	10	179	173	8	5	8	130	103										
4	3	9	271	265	0	4	10	298	301	10	0	9	120	94										
5	3	9	298	304	1	4	10	119	112	9	1	9	133	133										
6	3	9	148	145	2	4	10	250	262	8	3	9	108	108										
7	3	9	192	181	4	4	10	193	202	8	0	10	168	164										
6	4	9	154	162	3	5	10	146	138	7	2	10	128	93										
5	4	9	125	143	1	5	10	169	182	8	2	10	119	143										
4	4	9	228	240	5	0	11	355	378	7	3	10	154	155										
3	4	9	224	223	3	0	11	523	519	6	4	10	148	132										
2	4	9	322	310	1	0	11	632	645	7	0	11	241	233										
1	4	9	222	246	0	0	11	215	173	6	1	11	276	289										
0	4	9	346	351	0	1	11	596	627	8	1	11	173	158										
0	5	9	123	126	1	1	11	114	111	7	2	11	186	181										
1	5	9	232	206	2	1	11	546	560	6	3	11	164	186										
2	5	9	139	143	4	1	11	432	431	8	3	11	121	97										
3	5	9	190	161	5	2	11	315	314	5	4	11	164	160										
4	5	9	117	128	3	2	11	436	433	3	4	11	237	222										
0	0	10	785	788	1	2	11	496	511	0	5	11	151	161										
1	0	10	298	323	0	3	11	373	389	2	5	11	156	146										
2	0	10	668	684	2	3	11	368	365	4	5	11	132	113										
3	0	10	233	231	4	3	11	287	291	4	0	12	276	294										
4	0	10	496	499	1	4	11	244	258	5	0	12	244	238										
5	0	10	167	168	0	0	12	354	350	6	0	12	193	186										
6	0	10	329	321	1	0	12	287	277	7	0	12	140	132										
7	1	10	225	230	2	0	12	348	361	7	1	12	137	139										
6	1	10	125	140	3	0	12	333	349	6	1	12	147	149										
5	1	10	387	393	2	1	12	332	328	5	1	12	233	216										
4	1	10	180	192	1	1	12	347	350	4	1	12	298	287										
3	1	10	534	549	0	1	12	277	276	3	2	12	265	283										

H	K	L	10FO	10FC	H	K	L	10FO	10FC	H	K	L	10FO	10FC
5	7	0	133	123	9	3	4	130	144	6	1	7	393	412
4	8	0	105	106	8	3	4	261	261	7	1	7	375	393
6	8	0	117	109	7	4	4	236	249	8	1	7	250	248
11	0	1	115	113	8	4	4	132	147	9	1	7	203	178
10	0	1	214	213	9	4	4	134	130	9	2	7	136	145
9	1	1	296	303	8	5	4	135	116	8	2	7	233	229
10	1	1	243	251	6	5	4	190	191	7	2	7	271	265
11	1	1	145	126	3	6	4	229	200	6	2	7	459	471
10	2	1	175	169	4	6	4	106	105	5	3	7	443	454
9	2	1	344	348	5	6	4	143	134	6	3	7	262	260
9	3	1	190	193	6	6	4	96	85	7	3	7	242	255
10	3	1	167	172	7	6	4	109	91	8	3	7	170	151
9	4	1	216	198	4	7	4	122	94	9	3	7	125	105
8	4	1	177	188	2	7	4	136	108	7	4	7	149	148
7	5	1	157	166	1	7	4	107	108	6	4	7	203	220
8	5	1	193	170	0	7	4	114	116	5	4	7	244	239
7	6	1	114	104	9	0	5	418	429	4	4	7	350	343
6	6	1	138	127	8	0	5	94	75	0	5	7	225	217
5	6	1	236	243	8	1	5	513	524	1	5	7	303	308
1	7	1	116	133	10	1	5	239	245	2	5	7	234	211
2	7	1	197	170	9	2	5	327	322	3	5	7	220	225
3	7	1	113	119	8	3	5	310	309	4	5	7	186	184
4	7	1	128	123	10	3	5	162	167	5	5	7	152	142
1	8	1	138	114	9	4	5	195	188	6	5	7	131	133
9	0	2	349	343	7	4	5	281	283	5	6	7	113	97
11	0	2	122	147	6	5	5	257	274	4	6	7	116	81
10	1	2	222	214	8	5	5	169	166	3	6	7	138	118
9	1	2	123	112	7	6	5	118	111	2	6	7	139	138
9	2	2	264	277	5	6	5	203	218	1	6	7	145	128
11	2	2	127	116	3	6	5	265	274	0	6	7	168	171
10	3	2	103	133	1	6	5	190	183	5	0	8	837	835
9	4	2	115	133	0	7	5	157	149	7	0	8	489	483
8	5	2	105	110	2	7	5	175	163	9	0	8	277	258
5	6	2	133	130	4	7	5	115	125	8	1	8	334	336
2	7	2	111	93	1	8	5	128	100	6	1	8	593	592
0	7	2	101	113	7	0	6	239	224	5	2	8	627	629
10	0	3	273	285	8	0	6	334	319	7	2	8	366	366
9	1	3	411	422	9	0	6	115	109	8	3	8	233	218
11	1	3	167	162	10	0	6	143	146	6	3	8	351	357
10	2	3	231	226	9	1	6	198	195	4	3	8	585	590
9	3	3	251	264	8	1	6	152	153	1	4	8	573	561
11	3	3	118	106	7	1	6	534	512	3	4	8	459	477
10	4	3	126	114	7	2	6	161	158	5	4	8	312	324
8	4	3	245	256	8	2	6	274	289	7	4	8	207	202
7	5	3	211	219	10	2	6	110	118	6	5	8	195	174
9	5	3	140	106	9	3	6	108	125	4	5	8	244	263
6	6	3	155	159	8	3	6	106	99	2	5	8	294	315
4	6	3	249	254	7	3	6	335	358	0	5	8	323	323
1	7	3	175	168	6	3	6	134	143	1	6	8	175	182
3	7	3	148	141	5	4	6	131	140	3	6	8	163	176
9	0	4	313	295	6	4	6	285	296	5	6	8	132	133
10	0	4	166	171	8	4	6	125	118	0	7	8	120	102
11	0	4	135	147	5	5	6	193	169	8	0	9	207	201
11	1	4	131	138	3	5	6	293	298	7	0	9	229	232
10	1	4	184	198	0	6	6	244	252	6	0	9	380	381
9	1	4	241	227	2	6	6	173	176	5	0	9	390	389
8	2	4	361	360	10	0	7	126	130	4	0	9	565	587
9	2	4	230	234	9	0	7	198	191	3	0	9	574	556
10	2	4	117	138	8	0	7	275	281	3	1	9	639	651
10	3	4	140	129	7	0	7	359	346	4	1	9	473	455

1 IODOADAMANANTANE PHASE I

H	K	L	10FO	10FC	H	K	L	10FO	10FC	H	K	L	10FO	10FC
-5	3	6	59	47	0	5	7	41	39	4	2	9	158	161
-6	3	6	74	76	1	5	7	204	208	3	2	9	87	89
-5	4	6	191	192	-6	0	8	284	286	2	2	9	188	193
-4	4	6	88	90	-5	0	8	165	169	0	2	9	133	131
-3	4	6	196	199	-4	0	8	199	205	-1	2	9	89	89
-2	4	6	35	11	-3	0	8	86	84	-2	2	9	140	141
-1	4	6	217	212	-2	0	8	33	32	-3	2	9	136	138
0	4	6	317	316	0	0	8	149	148	-4	2	9	173	178
1	4	6	241	239	2	0	8	222	228	-5	2	9	95	97
2	4	6	279	277	4	0	8	216	218	-4	3	9	90	90
3	4	6	95	94	5	0	8	60	61	-3	3	9	35	25
5	4	6	64	64	6	0	8	296	292	-2	3	9	39	43
2	5	6	39	36	5	1	8	87	85	-1	3	9	103	102
1	5	6	81	84	4	1	8	36	34	0	3	9	34	28
-1	5	6	48	45	3	1	8	157	152	1	3	9	117	116
-2	5	6	99	99	1	1	8	158	160	3	3	9	98	98
-3	5	6	135	141	0	1	8	90	89	1	4	9	152	151
-6	1	7	122	122	-1	1	8	323	327	0	4	9	45	45
-5	1	7	81	81	-2	1	8	90	98	-1	4	9	100	98
-4	1	7	86	89	-3	1	8	218	212	-5	0	10	210	213
-3	1	7	181	179	-4	1	8	112	117	-4	0	10	239	240
-2	1	7	46	38	-5	1	8	48	39	-3	0	10	99	97
-1	1	7	263	252	-6	1	8	108	108	-2	0	10	488	490
0	1	7	65	67	-3	2	8	103	98	-1	0	10	242	244
1	1	7	219	212	-2	2	8	108	106	0	0	10	355	353
2	1	7	139	142	-1	2	8	75	78	1	0	10	105	104
3	1	7	154	156	2	2	8	55	52	2	0	10	116	110
5	1	7	141	143	3	2	8	50	54	3	0	10	113	120
6	1	7	86	83	4	2	8	63	59	4	0	10	77	74
7	1	7	131	135	5	2	8	71	76	5	0	10	134	141
6	2	7	173	173	6	2	8	60	57	4	1	10	108	108
5	2	7	112	116	5	3	8	88	87	3	1	10	173	169
4	2	7	255	256	4	3	8	117	85	2	1	10	143	147
3	2	7	91	87	3	3	8	49	41	1	1	10	183	183
2	2	7	174	179	2	3	8	57	52	-1	1	10	35	34
1	2	7	151	142	1	3	8	171	168	-2	1	10	201	201
-1	2	7	264	267	0	3	8	87	86	-4	1	10	37	36
-2	2	7	32	23	-1	3	8	151	149	-1	2	10	59	59
-3	2	7	215	215	-2	3	8	42	42	0	2	10	76	80
-4	2	7	38	28	-3	3	8	205	207	1	2	10	82	84
-5	2	7	106	108	-4	3	8	90	92	2	2	10	83	80
-6	2	7	56	55	-5	3	8	157	155	3	2	10	101	106
-6	3	7	144	140	-3	4	8	92	93	2	3	10	42	42
-4	3	7	189	188	-2	4	8	53	45	0	3	10	60	57
-3	3	7	110	108	-1	4	8	155	163	-1	3	10	64	68
-2	3	7	178	181	0	4	8	52	55	-3	1	11	151	154
-1	3	7	107	101	1	4	8	159	161	-2	1	11	95	92
0	3	7	170	177	2	4	8	108	111	-1	1	11	191	200
1	3	7	87	87	-5	1	9	121	124	0	1	11	58	57
2	3	7	126	123	-4	1	9	64	66	1	1	11	144	142
3	3	7	75	78	-3	1	9	238	240	2	1	11	117	120
5	3	7	47	45	-2	1	9	58	58	3	1	11	101	98
6	3	7	44	37	-1	1	9	339	343	2	2	11	106	105
3	4	7	47	45	0	1	9	92	98	1	2	11	194	195
2	4	7	121	122	1	1	9	208	209	0	2	11	120	116
1	4	7	68	63	2	1	9	89	90	-1	2	11	195	200
0	4	7	213	212	3	1	9	74	70	-2	2	11	77	76
-3	4	7	42	38	4	1	9	83	83	0	0	12	110	108
-4	4	7	137	139	5	1	9	54	52	0	6	0	163	156
-1	5	7	184	186	5	2	9	95	96	1	5	0	192	196

FACTEURS DE STRUCTURE OBSERVES ET CALCULES

1 CHLORO - ADAMANTANE

PHASE III

T = 210 K

H	K	L	10FO	10FC	H	K	L	10FO	10FC	H	K	L	10FO	10FC
-8	0	4	183	185	-3	4	4	351	346	1	4	5	126	126
-6	0	4	120	128	-2	4	4	150	152	0	4	5	96	96
-5	0	4	206	210	-1	4	4	271	273	-1	4	5	202	203
-4	0	4	178	183	0	4	4	56	55	-2	4	5	45	39
-3	0	4	197	198	1	4	4	104	101	-3	4	5	60	57
-2	0	4	377	384	2	4	4	90	89	-4	4	5	33	40
-1	0	4	224	219	3	4	4	217	214	-5	4	5	46	43
0	0	4	129	130	4	4	4	60	63	-1	5	5	59	61
1	0	4	515	525	5	4	4	174	174	2	5	5	104	102
2	0	4	153	153	6	4	4	35	33	3	5	5	43	42
3	0	4	330	334	4	5	4	170	164	-7	0	6	59	58
4	0	4	65	64	3	5	4	44	45	-6	0	6	75	75
5	0	4	148	159	2	5	4	225	226	-5	0	6	145	148
6	0	4	75	78	1	5	4	72	72	-3	0	6	243	249
7	0	4	135	135	0	5	4	89	88	-2	0	6	290	281
8	0	4	99	100	-1	5	4	54	51	-1	0	6	261	265
6	1	4	82	78	-2	5	4	175	172	0	0	6	260	265
5	1	4	80	83	-3	5	4	53	55	1	0	6	316	323
4	1	4	233	230	-4	5	4	115	115	2	0	6	230	229
3	1	4	76	79	-8	1	5	44	45	3	0	6	276	283
2	1	4	223	210	-7	1	5	65	60	4	0	6	179	186
1	1	4	168	164	-6	1	5	113	114	6	0	6	141	141
0	1	4	321	320	-4	1	5	137	143	7	0	6	178	182
-1	1	4	142	135	-3	1	5	274	278	7	1	6	151	153
-2	1	4	658	650	-1	1	5	230	226	6	1	6	81	83
-3	1	4	148	153	0	1	5	72	69	5	1	6	169	174
-4	1	4	208	208	1	1	5	164	161	3	1	6	191	198
-5	1	4	271	275	2	1	5	140	139	2	1	6	178	172
-7	1	4	176	178	3	1	5	181	182	1	1	6	214	215
-8	1	4	44	50	4	1	5	170	177	0	1	6	388	379
-7	2	4	189	188	5	1	5	135	139	-1	1	6	155	147
-6	2	4	93	91	6	1	5	76	73	-2	1	6	223	226
-5	2	4	138	139	7	1	5	131	134	-3	1	6	218	209
-4	2	4	72	71	6	2	5	130	131	-4	1	6	157	158
-3	2	4	208	203	4	2	5	224	226	-6	1	6	119	118
-2	2	4	44	42	3	2	5	208	199	-7	2	6	81	76
-1	2	4	32	23	2	2	5	199	189	-6	2	6	161	163
0	2	4	268	266	1	2	5	695	677	-5	2	6	41	35
1	2	4	314	296	0	2	5	210	193	-4	2	6	32	26
2	2	4	187	180	-1	2	5	854	827	-3	2	6	83	78
3	2	4	31	18	-2	2	5	121	119	-2	2	6	190	189
4	2	4	63	66	-3	2	5	460	452	0	2	6	221	202
6	2	4	154	154	-4	2	5	136	133	1	2	6	112	111
7	2	4	149	148	-5	2	5	125	120	2	2	6	164	158
8	2	4	97	95	-6	2	5	297	299	3	2	6	126	122
7	3	4	122	125	-6	3	5	167	163	4	2	6	72	70
6	3	4	101	101	-5	3	5	34	32	5	2	6	202	199
5	3	4	178	182	-4	3	5	129	131	6	2	6	36	35
2	3	4	228	232	-3	3	5	67	71	7	2	6	66	66
1	3	4	39	44	-2	3	5	120	123	6	3	6	184	190
0	3	4	499	472	-1	3	5	69	61	5	3	6	310	317
-2	3	4	150	143	0	3	5	99	108	4	3	6	246	245
-3	3	4	47	47	2	3	5	176	180	3	3	6	176	178
-4	3	4	140	143	3	3	5	36	43	2	3	6	138	134
-5	3	4	99	101	4	3	5	275	276	1	3	6	208	200
-6	3	4	264	266	5	3	5	85	86	0	3	6	127	127
-7	3	4	71	69	6	3	5	208	203	-1	3	6	100	96
-6	4	4	100	99	7	3	5	125	124	-2	3	6	174	173
-5	4	4	99	96	4	4	5	69	68	-3	3	6	92	87
-4	4	4	126	126	2	4	5	70	74	-4	3	6	76	70

H	K	L	10FO	10FC	H	K	L	10FO	10FC	H	K	L	10FO	10FC
-9	4	1	53	52	9	3	3	57	54	9	3	5	76	74
-8	5	1	56	57	10	3	3	50	41	8	4	5	44	40
-7	5	1	105	115	9	4	3	74	75	6	4	5	31	31
-6	5	1	68	67	7	4	3	43	43	-6	4	5	37	41
6	5	1	59	59	-7	4	3	109	109	-6	5	5	103	107
7	5	1	101	96	-8	4	3	40	45	-5	5	5	50	50
8	5	1	41	34	-9	4	3	60	56	-4	5	5	119	119
6	6	1	56	52	-8	5	3	40	49	4	5	5	103	106
5	6	1	58	57	-6	5	3	74	73	6	5	5	35	34
4	6	1	115	113	6	5	3	32	33	7	5	5	66	65
3	6	1	94	93	8	5	3	50	43	1	6	5	37	31
-3	6	1	58	57	6	6	3	36	36	0	6	5	55	53
-4	6	1	106	108	5	6	3	72	75	-1	6	5	125	124
-5	6	1	81	84	3	6	3	118	117	-2	6	5	39	42
-6	6	1	54	51	2	6	3	139	141	-3	6	5	84	89
-4	7	1	48	52	-2	6	3	70	62	-4	6	5	40	30
-3	7	1	117	114	-4	6	3	62	57	-5	6	5	35	32
-2	7	1	34	33	-5	6	3	55	57	-2	7	5	37	34
-11	0	2	48	36	-6	6	3	53	55	0	7	5	66	68
-10	0	2	183	190	-3	7	3	67	65	2	7	5	104	107
10	0	2	33	22	-2	7	3	54	55	-9	0	6	45	48
11	0	2	95	90	0	7	3	114	123	8	0	6	74	77
11	1	2	86	84	2	7	3	63	69	9	0	6	122	124
10	1	2	60	59	-10	0	4	141	142	10	0	6	66	60
-10	1	2	138	139	-9	0	4	141	141	9	1	6	79	78
-9	2	2	55	54	9	0	4	59	60	8	1	6	92	97
9	2	2	83	88	10	0	4	53	44	-8	1	6	55	53
10	3	2	39	40	10	1	4	66	65	-9	1	6	60	51
9	3	2	78	81	9	1	4	40	30	-10	1	6	32	24
8	3	2	34	24	-10	1	4	57	66	-9	2	6	77	68
-9	3	2	38	38	-10	2	4	52	54	-8	2	6	78	76
-8	4	2	153	152	9	2	4	47	45	9	3	6	48	41
-7	4	2	41	44	8	3	4	126	134	7	3	6	131	138
7	4	2	150	151	-8	3	4	129	131	-7	3	6	71	74
8	4	2	41	48	-9	3	4	52	54	-8	3	6	143	148
9	4	2	52	49	-8	4	4	94	90	-9	3	6	38	36
8	5	2	36	22	-7	4	4	50	54	-8	4	6	82	78
7	5	2	35	32	7	4	4	56	51	-7	4	6	72	71
-6	5	2	105	110	8	4	4	99	99	-6	4	6	47	51
-8	5	2	90	96	9	4	4	73	69	8	4	6	52	51
-6	6	2	51	54	7	5	4	53	45	7	5	6	61	63
-5	6	2	56	54	6	5	4	80	73	6	5	6	33	42
-4	6	2	31	31	5	5	4	35	28	5	5	6	67	70
-3	6	2	71	74	-5	5	4	41	41	4	5	6	42	32
2	7	2	80	82	-3	6	4	102	105	-4	5	6	104	100
1	7	2	66	66	-1	6	4	73	76	-5	5	6	55	60
0	7	2	136	136	0	6	4	55	58	-6	5	6	65	66
-1	7	2	65	65	1	6	4	57	60	-4	6	6	82	89
-3	7	2	120	119	3	6	4	90	79	-2	6	6	63	70
-4	7	2	58	66	1	7	4	42	41	1	6	6	48	51
-10	1	3	73	72	-1	7	4	38	33	-9	1	7	38	29
-9	1	3	117	123	-2	7	4	33	38	-8	1	7	55	56
9	1	3	42	34	9	1	5	57	61	8	1	7	70	69
10	1	3	84	76	10	2	5	66	65	9	1	7	71	69
9	2	3	141	149	8	2	5	39	33	9	2	7	61	59
-9	2	3	47	51	-8	2	5	196	198	8	2	7	63	68
-10	2	3	68	69	-10	2	5	35	33	-7	2	7	111	112
-10	3	3	37	38	-9	3	5	75	68	-8	2	7	48	48
-9	3	3	65	60	-8	3	5	131	129	-9	2	7	137	133
-8	3	3	32	44	8	3	5	43	42	-8	3	7	43	44

FACTEURS DE STRUCTURE OBSERVES ET CALCULES

1 CHLORO-ADAMANTANE

PHASE III

T = 210 K

(Suite)

H	K	L	10FO	10FC	H	K	L	10FO	10FC	H	K	L	10FO	10FC
2	4	0	315	309	-9	0	2	76	79	-4	4	3	80	77
2	6	0	37	41	-8	0	2	265	275	-4	3	3	74	70
3	5	0	93	98	-8	1	2	94	94	-3	5	3	195	194
3	4	0	34	40	-8	2	2	70	70	-2	5	3	257	248
4	4	0	181	184	-7	3	2	49	48	-2	4	3	244	249
4	5	0	39	37	-7	2	2	66	69	-1	4	3	82	88
5	5	0	124	124	-7	1	2	120	116	-1	5	3	150	145
5	4	0	118	121	-6	0	2	251	258	-1	6	3	51	46
5	3	0	107	114	-6	2	2	121	127	0	6	3	148	156
6	1	0	68	71	-6	3	2	43	37	0	5	3	211	207
7	4	0	128	131	-6	4	2	221	223	0	4	3	117	118
7	3	0	118	124	-5	5	2	94	94	1	5	3	42	43
7	2	0	46	44	-5	4	2	50	48	1	6	3	77	74
7	1	0	70	71	-5	3	2	30	34	2	5	3	100	97
7	0	0	194	190	-4	4	2	136	134	3	4	3	56	56
8	1	0	138	141	-3	5	2	300	301	3	5	3	72	66
8	2	0	66	63	-3	4	2	71	72	4	5	3	103	102
9	1	0	36	44	-2	4	2	66	66	4	3	3	279	269
9	0	0	34	33	-2	5	2	39	32	5	2	3	394	396
-9	1	1	119	123	-2	6	2	65	62	5	3	3	140	137
-8	1	1	38	36	-1	6	2	69	66	6	1	3	109	106
-7	1	1	153	158	-1	5	2	290	287	7	2	3	381	387
-7	2	1	73	65	1	6	2	119	119	7	3	3	115	115
-7	3	1	54	51	1	5	2	115	110	8	2	3	33	35
-7	4	1	139	143	2	5	2	99	102	10	0	0	31	37
-6	4	1	105	105	2	6	2	52	45	11	0	0	60	56
-6	2	1	153	148	3	5	2	35	19	10	1	0	75	74
-6	1	1	173	166	3	4	2	75	84	10	1	0	76	74
-5	3	1	136	136	4	4	2	30	23	9	3	0	33	35
-5	4	1	87	88	4	5	2	86	90	9	3	0	33	35
-5	5	1	105	106	5	5	2	46	36	9	4	0	72	73
-4	5	1	40	35	5	4	2	182	181	8	4	0	37	30
-2	6	1	185	184	5	3	2	33	34	8	4	0	31	30
-2	5	1	76	73	6	0	2	233	230	9	4	0	72	73
-2	4	1	88	84	6	1	2	124	134	8	5	0	37	41
-1	5	1	36	40	6	2	2	159	159	7	5	0	133	140
-1	6	1	66	64	6	3	2	46	52	6	5	0	64	64
0	6	1	146	144	6	4	2	114	115	6	5	0	61	64
1	5	1	122	120	7	3	2	198	205	7	5	0	139	140
1	6	1	134	142	7	2	2	148	157	8	5	0	51	41
2	6	1	110	111	7	1	2	31	36	5	6	0	61	61
2	5	1	29	23	7	0	2	157	164	4	6	0	50	49
2	4	1	130	133	8	0	2	60	51	4	6	0	50	49
3	4	1	33	24	8	1	2	230	229	5	6	0	59	61
3	5	1	71	77	8	2	2	154	151	4	7	0	79	78
4	5	1	73	78	9	0	2	72	70	3	7	0	85	84
4	4	1	100	98	-8	2	3	115	117	1	7	0	38	40
5	3	1	46	49	-8	1	3	153	151	1	7	0	39	40
5	5	1	53	53	-7	1	3	153	157	3	7	0	87	84
6	4	1	83	82	-7	2	3	232	233	4	7	0	79	78
6	3	1	139	135	-7	3	3	101	103	-11	1	1	46	45
6	2	1	163	164	-6	4	3	57	63	10	1	1	42	36
6	1	1	286	290	-6	3	3	34	41	11	1	1	56	44
7	1	1	207	208	-6	2	3	231	240	9	2	1	121	118
7	2	1	131	135	-6	1	3	118	118	-9	2	1	95	93
7	3	1	85	88	-5	2	3	224	228	-10	2	1	38	38
7	4	1	48	44	-5	3	3	121	119	-10	3	1	53	50
8	3	1	90	92	-5	4	3	112	117	10	3	1	42	49
8	2	1	110	113	-5	5	3	63	59	8	4	1	87	87
8	1	1	119	114	-4	5	3	63	65	-8	4	1	77	81

H	K	L	10FO	10FC	H	K	L	10FO	10FC	H	K	L	10FO	10FC
-7	3	7	103	102	4	4	9	35	34	3	3	11	37	17
7	3	7	79	76	2	4	9	50	50	4	3	11	98	102
-6	4	7	61	63	-3	4	9	32	41	6	3	11	71	68
-6	5	7	71	70	-5	4	9	34	46	4	4	11	62	61
-5	5	7	53	58	-5	5	9	54	51	-1	4	11	37	35
-4	5	7	102	104	-4	5	9	38	47	-2	4	11	44	54
-2	5	7	85	87	-3	5	9	74	74	-3	4	11	58	66
3	5	7	51	50	-2	5	9	38	41	-1	5	11	74	69
4	6	7	143	142	-1	5	9	93	85	-6	0	12	38	33
2	6	7	152	153	0	5	9	35	41	-5	0	12	66	65
0	6	7	61	57	1	5	9	81	75	-4	0	12	105	104
-2	6	7	58	58	3	5	9	34	40	-2	0	12	193	199
-3	6	7	44	37	4	5	9	88	87	-1	0	12	39	34
-4	6	7	73	70	0	6	9	92	91	1	0	12	144	147
-9	0	8	75	74	-8	0	10	40	39	2	0	12	38	33
-8	0	8	129	125	-7	0	10	233	235	3	0	12	177	182
-7	0	8	142	142	-6	0	10	60	61	4	0	12	71	73
7	0	8	79	82	6	0	10	76	75	5	0	12	53	53
8	0	8	263	271	7	0	10	43	43	6	0	12	61	60
9	0	8	87	83	8	1	10	85	85	6	1	12	151	148
8	1	8	31	29	6	1	10	87	83	5	1	12	41	39
7	1	8	56	56	5	1	10	42	45	4	1	12	90	89
-7	1	8	77	77	-5	1	10	95	97	3	1	12	65	58
-8	1	8	83	85	-6	1	10	74	73	2	1	12	30	6
-8	2	8	115	114	-7	1	10	64	68	1	1	12	101	104
6	3	8	74	76	-5	2	10	54	48	0	1	12	83	82
-6	3	8	90	94	6	3	10	94	97	-2	1	12	132	133
-7	3	8	65	63	4	3	10	83	81	-4	1	12	44	37
-8	3	8	130	132	-3	3	10	83	81	-5	1	12	82	87
-7	4	8	36	28	-4	3	10	103	101	-2	2	12	39	47
-5	4	8	76	70	-5	3	10	54	56	-1	2	12	33	35
-4	4	8	40	37	-4	4	10	107	99	1	2	12	116	115
4	4	8	226	228	-3	4	10	54	53	2	2	12	81	83
5	4	8	99	106	-2	4	10	126	118	3	2	12	56	56
6	4	8	179	190	0	4	10	131	126	4	2	12	54	55
7	4	8	52	56	1	4	10	66	66	5	2	12	51	55
3	5	8	94	93	2	4	10	96	93	4	3	12	55	57
1	5	8	188	188	3	4	10	58	63	3	3	12	44	48
-1	5	8	118	116	4	4	10	36	38	2	3	12	137	137
-2	5	8	61	64	5	4	10	39	30	0	3	12	130	136
-3	5	8	49	54	3	5	10	74	73	-1	3	12	34	28
-4	5	8	96	98	1	5	10	74	75	-2	3	12	67	68
-5	5	8	49	39	-1	5	10	95	94	-3	3	12	33	24
-3	6	8	50	45	-3	5	10	76	75	-4	3	12	57	47
-1	6	8	71	73	-7	1	11	39	38	-2	4	12	34	41
3	6	8	41	30	-5	1	11	51	54	-1	4	12	79	80
-8	1	9	87	80	4	1	11	204	208	1	4	12	69	74
-7	1	9	104	107	5	1	11	67	65	-5	1	13	49	49
-6	1	9	126	127	6	1	11	141	145	-4	1	13	103	95
6	1	9	49	46	6	2	11	40	37	-2	1	13	96	91
7	1	9	58	58	3	2	11	59	57	-1	1	13	41	47
7	2	9	94	96	-3	2	11	53	56	0	1	13	65	66
6	2	9	47	57	-4	2	11	88	90	1	1	13	42	39
-6	2	9	75	68	-6	2	11	99	101	2	1	13	31	38
-7	2	9	71	75	-5	3	11	81	77	3	1	13	38	42
-8	2	9	39	43	-4	3	11	39	50	5	1	13	63	61
-6	3	9	76	75	-3	3	11	103	100	4	2	13	91	95
5	3	9	87	85	-1	3	11	74	70	3	2	13	135	135
7	3	9	43	38	1	3	11	41	37	1	2	13	94	93
5	4	9	73	70	2	3	11	47	47	0	2	13	80	84

FACTEURS DE STRUCTURE OBSERVES ET CALCULES

1 CHLORO ADAMANTANE

PHASE III

T = 210 K

(Suite)

H	K	L	10FO	10FC	H	K	L	10FO	10FC	H	K	L	10FO	10FC
-1	2	13	71	75	-3	1	1	173	172	0	3	2	216	210
-2	2	13	50	62	-3	2	1	92	99	0	4	2	123	123
-3	2	13	61	65	-3	3	1	325	332	1	3	2	245	235
-4	2	13	57	54	-2	3	1	87	86	1	2	2	325	314
-2	3	13	100	99	-2	2	1	273	275	1	1	2	459	455
-1	3	13	32	26	-2	1	1	100	106	1	0	2	679	703
0	3	13	134	139	-1	1	1	586	597	2	0	2	364	354
2	3	13	90	93	-1	3	1	346	348	2	1	2	193	201
-3	0	14	82	81	-1	4	1	41	43	2	2	2	68	65
-2	0	14	94	69	0	3	1	101	106	2	3	2	514	473
-1	0	14	108	107	0	2	1	496	492	3	3	2	288	276
0	0	14	34	29	0	1	1	196	205	3	2	2	395	377
1	0	14	111	107	1	1	1	535	538	3	0	2	697	680
3	0	14	54	55	1	2	1	429	417	4	0	2	524	508
3	1	14	37	35	1	3	1	25	19	4	1	2	134	131
2	1	14	60	55	2	3	1	23	19	5	2	2	59	54
1	1	14	38	40	2	2	1	692	677	5	1	2	109	98
0	1	14	59	60	2	1	1	54	52	5	0	2	632	614
-2	1	14	84	83	3	1	1	381	370	-5	1	3	125	127
-3	1	14	35	40	3	2	1	400	392	-4	2	3	283	295
-1	2	14	51	50	3	3	1	173	154	-4	1	3	182	188
0	2	14	46	44	4	3	1	58	60	-3	1	3	211	217
1	2	14	42	47	4	2	1	194	192	-3	2	3	136	136
0	4	0	238	235	4	1	1	388	386	-3	3	3	101	98
1	3	0	81	83	5	1	1	453	428	-2	3	3	151	148
1	2	0	66	64	5	2	1	139	141	-2	2	3	70	76
1	1	0	609	648	-5	2	2	87	91	-2	1	3	513	525
1	0	0	135	137	-5	1	2	228	232	-1	1	3	410	420
2	0	0	1245	1309	-5	0	2	69	64	-1	2	3	135	138
2	1	0	89	88	-4	0	2	303	310	-1	3	3	172	180
2	2	0	288	280	-4	3	2	41	26	0	3	3	322	326
2	3	0	242	244	-3	3	2	162	159	0	2	3	171	168
3	3	0	33	26	-3	1	2	194	203	0	1	3	402	403
3	2	0	34	34	-3	0	2	181	183	1	1	3	243	249
3	1	0	633	625	-2	0	2	453	455	1	2	3	98	100
3	0	0	486	480	-2	1	2	243	252	1	3	3	173	172
4	0	0	225	213	-2	2	2	85	84	2	3	3	498	473
4	2	0	190	189	-2	3	2	121	120	2	2	3	61	61
4	3	0	132	131	-1	3	2	138	137	2	1	3	272	269
5	2	0	34	33	-1	2	2	72	76	3	1	3	43	48
5	1	0	461	441	-1	1	2	337	341	3	2	3	166	175
5	0	0	496	472	-1	0	2	699	746	3	3	3	62	60
6	0	0	58	53	0	0	2	230	226	4	2	3	85	83
-5	1	1	104	110	0	1	2	822	865	4	1	3	36	42
-4	2	1	313	313	0	2	2	96	93	5	1	3	33	31
-4	1	1	210	202										

H	K	L	10FO	10FC	H	K	L	10FO	10FC	H	K	L	10FO	10FC	H	K	L	10FO	10FC	H	K	L	10FO	10FC
1	0	0	186	172	-1	0	2	233	219	-4	0	4	250	239	-1	0	6	675	672	3	6	0	78	61
2	0	0	1038	1977	0	0	2	541	617	3	0	4	694	696	0	0	6	644	638	4	6	0	301	316
3	0	0	587	625	0	1	2	902	1253	-3	0	4	811	844	0	1	6	712	716	5	6	0	39	29
4	0	0	314	317	1	1	2	673	773	2	0	4	475	472	1	1	6	105	104	6	6	0	154	164
5	0	0	691	703	-1	1	2	735	816	-2	0	4	273	250	-1	1	6	545	534	7	6	0	109	130
6	0	0	311	300	2	1	2	544	558	1	0	4	741	810	2	1	6	553	550	6	1	1	231	197
5	1	0	792	803	-2	1	2	607	623	-1	0	4	932	1134	-2	1	6	462	435	-6	1	1	488	468
4	1	0	193	183	3	1	2	582	607	0	0	4	116	103	3	1	6	84	67	7	1	1	379	363
3	1	0	921	1081	-3	1	2	256	234	0	1	4	769	841	-3	1	6	554	536	-7	1	1	356	339
2	1	0	205	190	4	1	2	191	163	1	1	4	70	47	2	2	6	260	239	8	1	1	90	84
1	1	0	115	96	-4	1	2	254	263	-1	1	4	237	209	-2	2	6	63	48	-8	1	1	269	261
0	2	0	276	253	5	1	2	594	605	2	1	4	973	1145	1	2	6	183	166	9	1	1	258	262
1	2	0	121	113	-5	1	2	93	10	-2	1	4	685	686	-1	2	6	27	20	-9	1	1	57	63
2	2	0	79	56	5	2	2	86	62	3	1	4	327	302	0	2	6	156	127	10	1	1	74	66
3	2	0	133	124	-5	2	2	262	230	-3	1	4	221	201	2	1	7	117	119	-10	1	1	143	146
4	2	0	44	35	4	2	2	185	187	4	1	4	612	599	-2	1	7	220	197	11	1	1	114	123
5	2	0	60	46	-4	2	2	117	101	-4	1	4	632	616	1	1	7	563	549	-11	1	1	43	30
4	3	0	193	185	3	2	2	129	82	5	1	4	471	457	-1	1	7	509	487	10	2	1	174	181
3	3	0	90	95	-3	2	2	583	570	-5	1	4	262	229	0	1	7	194	179	-10	2	1	33	11
2	3	0	316	304	2	2	2	306	283	4	2	4	26	18	0	2	7	414	421	9	2	1	210	200
1	3	0	224	202	-2	2	2	277	242	-4	2	4	119	105	0	0	8	639	644	-9	2	1	337	341
1	4	0	32	18	1	2	2	230	201	3	2	4	74	56	7	0	0	443	425	8	2	1	255	260
5	1	1	402	375	-1	2	2	522	493	-3	2	4	157	154	8	0	0	244	229	-8	2	1	36	28
-5	1	1	655	618	0	2	2	99	98	2	2	4	96	83	9	0	0	225	214	7	2	1	167	151
4	1	1	227	180	0	3	2	377	323	-2	2	4	218	201	10	0	0	54	59	-7	2	1	433	433
-4	1	1	588	573	1	3	2	251	219	1	2	4	226	201	11	0	0	181	177	6	2	1	510	513
3	1	1	493	503	-1	3	2	401	360	-1	2	4	535	500	11	1	0	78	83	-6	2	1	83	53
-3	1	1	610	622	-2	3	2	633	599	0	2	4	345	306	10	1	0	220	214	5	3	1	543	555
2	1	1	49	27	3	3	2	296	263	0	3	4	683	645	9	1	0	181	177	-5	3	1	310	283
-2	1	1	239	215	-3	3	2	428	403	1	3	4	86	50	8	1	0	330	312	6	3	1	125	87
1	1	1	726	948	5	1	3	318	314	-1	3	4	34	31	7	1	0	326	310	-6	3	1	435	419
-1	1	1	720	852	-5	1	3	47	7	2	3	4	318	293	6	1	0	266	253	7	3	1	354	346
0	1	1	105	99	4	1	3	436	421	-2	3	4	358	339	6	2	0	135	126	-7	3	1	232	224
0	2	1	902	1029	-4	1	3	326	320	4	1	5	412	399	7	2	0	39	27	8	3	1	130	120
1	2	1	225	184	3	1	3	433	420	-4	1	5	393	358	8	2	0	131	121	-8	3	1	320	315
-1	2	1	655	685	-3	1	3	107	92	3	1	5	246	226	9	2	0	56	50	9	3	1	174	192
2	2	1	752	821	2	1	3	743	805	-3	1	5	394	368	10	2	0	16	5	-9	3	1	75	81
-2	2	1	949	1169	-2	1	3	597	584	2	1	5	227	230	10	3	0	46	64	10	3	1	144	148
3	2	1	118	44	1	1	3	569	578	-2	1	5	425	394	9	3	0	81	88	-10	3	1	198	201
-3	2	1	666	696	-1	1	3	357	333	1	1	5	92	80	8	3	0	54	51	9	4	1	138	133
4	2	1	735	786	0	1	3	669	713	-1	1	5	371	338	7	3	0	217	213	-9	4	1	99	96
-4	2	1	579	571	0	2	3	32	26	0	1	5	202	199	6	3	0	61	57	8	4	1	231	229
5	2	1	83	56	1	2	3	634	647	0	2	5	396	350	5	3	0	228	220	-8	4	1	155	153
-5	2	1	469	476	-1	2	3	629	628	1	2	5	1160	1370	2	4	0	712	719	7	4	1	239	227
4	3	1	66	23	2	2	3	336	331	-1	2	5	1040	1163	3	4	0	123	114	-7	4	1	108	102
-4	3	1	403	393	-2	2	3	165	135	2	2	5	214	188	4	4	0	515	504	6	4	1	333	331
-3	3	1	231	217	3	2	3	545	536	-2	2	5	473	444	5	4	0	252	249	-6	4	1	218	217
2	3	1	217	193	-3	2	3	635	637	3	2	5	910	949	6	4	0	207	201	5	4	1	158	142
-2	3	1	324	319	4	2	3	596	607	-3	2	5	594	574	7	4	0	262	278	-5	4	1	175	176
1	3	1	848	877	-4	2	3	136	95	1	3	5	45	48	8	4	0	82	90	4	4	1	290	274
-1	3	1	505	482	3	3	3	431	435	-1	3	5	174	178	9	4	0	175	193	-4	4	1	319	294
5	0	2	282	220	-3	3	3	83	41	0	3	5	573	575	8	5	0	174	182	3	4	1	53	50
-5	0	2	933	1037	2	3	3	611	580	0	3	5	578	575	7	5	0	361	393	-3	4	1	198	181
4	0	2	752	796	-2	3	3	961	1008	4	0	6	207	190	6	5	0	225	230	2	4	1	237	230
-4	0	2	740	766	1	3	3	486	465	-4	0	6	592	581	5	5	0	439	451	-2	4	1	429	390
3	0	2	515	468	-1	3	3	425	379	3	0	6	704	702	4	5	0	183	189	1	5	1	25	11
-3	0	2	934	1150	0	3	3	850	849	-3	0	6	556	541	3	5	0	489	481	-1	5	1	142	102
2	0	2	796	959	5	0	4	625	626	2	0	6	610	607	2	5	0	73	71	2	5	1	122	111
-2	0	2	656	684	-5	0	4	533	522	-2	0	6	640	619	1	5	0	666	677	-2	5	1	51	17
1	0	2	337	338	4	0	4	399	384	1	0	6	694	698	2	6	0	221	220	3	5	1	31	17

FACTEURS

DE

STRUCTURE

OBSERVES

CALCULES et

1 BROMOADAMANTANE

PHASE III

T = 253 K

H	K	L	10FO	10FC	H	K	L	10FO	10FC	H	K	L	10FO	10FC
-1	0	6	675	672	3	6	0	78	61	-3	5	1	87	77
0	0	6	644	638	4	6	0	301	316	4	5	1	92	94
0	1	6	712	716	5	6	0	39	29	-4	5	1	77	71
1	1	6	105	104	6	6	0	154	164	5	5	1	118	116
-1	1	6	545	534	7	6	0	109	130	-5	5	1	75	80
2	1	6	553	550	6	1	1	231	197	-6	5	1	62	65
-2	1	6	462	435	-6	1	1	488	468	-7	5	1	130	135
3	1	6	84	67	7	1	1	379	363	-8	5	1	20	29
-3	1	6	554	536	-7	1	1	356	339	-6	6	1	154	160
2	2	6	260	239	8	1	1	90	84	-5	6	1	178	186
-2	2	6	63	48	-8	1	1	269	261	-4	6	1	287	273
1	2	6	183	166	9	1	1	258	262	-3	6	1	241	244
-1	2	6	27	20	-9	1	1	57	63	-2	6	1	338	326
0	2	6	156	127	10	1	1	74	66	6	0	2	665	655
2	1	7	117	119	-10	1	1	143	146	-6	0	2	410	362
-2	1	7	220	197	11	1	1	114	123	7	0	2	94	51
1	1	7	563	549	-11	1	1	43	30	-7	0	2	510	508
-1	1	7	509	487	10	2	1	174	181	8	0	2	575	591
0	1	7	194	179	-10	2	1	33	11	-8	0	2	94	29
0	2	7	414	421	9	2	1	210	200	9	0	2	87	76
0	0	8	639	644	-9	2	1	337	341	-9	0	2	305	305
7	0	0	443	425	8	2	1	255	260	10	0	2	397	419
8	0	0	244	229	-8	2	1	36	28	-10	0	2	84	56
9	0	0	225	214	7	2	1	167	151	11	0	2	83	63
10	0	0	54	59	-7	2	1	433	433	-11	0	2	221	227
11	0	0	181	177	6	2	1	510	513	11	1	2	106	102
11	1	0	78	83	-6	2	1	83	53	-11	1	2	124	119
10	1	0	220	214	5	3	1	543	555	10	1	2	203	198
9	1	0	181	177	-5	3	1	310	283	-10	1	2	220	221
8	1	0	330	312	6	3	1	125	87	9	1	2	176	164
7	1	0	326	310	-6	3	1	435	419	-9	1	2	27	6
6	1	0	266	253	7	3	1	354	346	8	1	2	126	101
6	2	0	135	126	-7	3	1	232	224	-8	1	2	475	461
7	2	0	39	27	8	3	1	130	120	7	1	2	424	413
8	2	0	131	121	-8	3	1	320	315	-7	1	2	105	76
9	2	0	56	50	9	3	1	174	192	6	1	2	110	75
10	2	0	16	5	-9	3	1	75	81	-6	1	2	444	446
10	3	0	46	64	10	3	1	144	148	6	2	2	34	9
9	3	0	81	88	-10	3	1	198	201	-6	2	2	175	169
8	3	0	54	51	9	4	1	138	133	7	2	2	91	84
7	3	0	217	213	-9	4	1	99	96	-7	2	2	25	20
6	3	0	61	57	8	4	1	231	229	8	2	2	32	8
5	3	0	228	220	-8	4	1	155	153	-8	2	2	209	189
2	4	0	712	719	7	4	1	239	227	9	2	2	34	30
3	4	0	123	114	-7	4	1	108	102	-9	2	2	24	15
4	4	0	515	504	6	4	1	333	331	10	2	2	81	70
5	4	0	252	249	-6	4	1	218	217	-10	2	2	17	1
6	4	0	207	201	5	4	1	158	142	10	3	2	38	27
7	4	0	262	278	-5	4	1	175	176	-10	3	2	81	104
8	4	0	82	90	4	4	1	290	274	9	3	2	79	83
9	4	0	175	193	-4	4	1	319	294	-9	3	2	95	94
8	5	0	174	182	3	4	1	53	50	8	3	2	19	4
7	5	0	361	393	-3	4	1	198	181	-8	3	2	110	125
6	5	0	225	230	2	4	1	237	230	7	3	2	38	11
5	5	0	439	451	-2	4	1	429	390	-7	3	2	230	227
4	5	0	183	189	1	5	1	25	11	6	3	2	35	13
3	5	0	489	481	-1	5	1	142	102	-6	3	2	172	176
2	5	0	73	71	2	5	1	122	111	5	3	2	118	124
1	5	0	666	677	-2	5	1	51	17	-5	3	2	20	4
2	6	0	221	220	3	5	1	31	17	1	4	2	493	450

H	K	L	10FO	10FC	H	K	L	10FO	10FC	H	K	L	10FO	10FC
1	5	4	143	137	3	4	5	206	188	9	2	6	159	148
-1	5	4	83	73	-3	4	5	195	190	0	2	6	28	15
0	5	4	549	507	2	4	5	52	48	9	3	6	68	71
0	6	4	121	92	-2	4	5	66	58	-9	3	6	91	103
-3	6	4	126	130	1	4	5	40	34	8	3	6	223	242
-4	6	4	101	104	-1	4	5	112	110	-8	3	6	41	16
-5	6	4	138	161	0	5	5	88	80	7	3	6	54	36
-6	6	4	96	96	1	5	5	25	19	-7	3	6	190	198
5	1	5	61	36	-1	5	5	83	74	6	3	6	136	146
-5	1	5	340	319	2	5	5	59	66	-6	3	6	250	254
6	1	5	355	345	-2	5	5	93	95	5	3	6	60	43
-6	1	5	216	197	-3	5	5	78	72	-5	3	6	396	405
7	1	5	61	30	4	5	5	158	144	4	3	6	162	167
-7	1	5	314	296	-4	5	5	97	105	-4	3	6	338	328
8	1	5	204	203	5	5	5	113	106	3	3	6	214	208
-8	1	5	74	71	-5	5	5	28	30	-3	3	6	297	285
9	1	5	52	38	-6	5	5	31	26	2	3	6	271	262
-9	1	5	178	182	-7	5	5	58	69	-2	3	6	169	151
10	1	5	104	115	-5	6	5	111	106	1	3	6	33	21
-10	1	5	23	2	-4	6	5	125	142	-1	3	6	141	128
10	2	5	118	125	-3	6	5	80	82	0	3	6	144	133
-10	2	5	194	195	-2	6	5	139	124	0	4	6	608	599
9	2	5	139	145	5	0	6	546	533	1	4	6	527	516
-9	2	5	78	75	-5	0	6	150	140	-1	4	6	539	527
8	2	5	308	310	6	0	6	83	29	2	4	6	214	197
-8	2	5	234	233	-6	0	6	506	498	-2	4	6	572	573
7	2	5	255	249	7	0	6	363	348	3	4	6	464	462
-7	2	5	120	110	-7	0	6	160	152	-3	4	6	254	245
6	2	5	379	367	8	0	6	66	39	4	4	6	47	8
-6	2	5	398	395	-8	0	6	358	355	-4	4	6	271	282
5	2	5	490	496	9	0	6	259	253	5	4	6	432	441
-5	2	5	245	232	-9	0	6	156	158	-5	4	6	60	30
4	2	5	151	125	10	0	6	69	53	6	4	6	35	8
-4	2	5	531	520	-10	0	6	222	235	-6	4	6	190	215
2	3	5	582	593	10	1	6	143	156	7	4	6	256	276
-2	3	5	588	580	-10	1	6	34	18	-7	4	6	37	20
3	3	5	54	56	9	1	6	91	80	8	4	6	74	82
-3	3	5	286	283	-9	1	6	228	222	-8	4	6	176	208
4	3	5	543	540	8	1	6	280	273	-7	5	6	237	271
-4	3	5	591	592	-8	1	6	128	129	-6	5	6	103	104
5	3	5	116	111	7	1	6	62	44	5	5	6	150	156
-5	3	5	335	333	-7	1	6	383	373	-5	5	6	294	328
6	3	5	502	497	6	1	6	439	423	4	5	6	436	450
-6	3	5	433	433	-6	1	6	174	159	-4	5	6	159	160
7	3	5	124	112	5	1	6	104	95	3	5	6	332	332
-7	3	5	343	339	-5	1	6	488	467	-3	5	6	262	276
8	3	5	363	371	4	1	6	511	494	2	5	6	426	413
-8	3	5	163	163	-4	1	6	204	178	-2	5	6	141	141
9	3	5	179	173	3	2	6	305	282	1	5	6	308	298
-9	3	5	237	251	-3	2	6	254	223	-1	5	6	195	198
8	4	5	88	93	4	2	6	62	56	0	5	6	227	221
-8	4	5	152	154	-4	2	6	181	174	-2	6	6	210	230
7	4	5	120	114	5	2	6	173	165	-3	6	6	161	165
-7	4	5	77	80	-5	2	6	308	288	-4	6	6	170	200
6	4	5	35	22	6	2	6	210	208	-5	6	6	94	103
-6	4	5	96	97	-6	2	6	115	108	3	1	7	443	415
5	4	5	275	266	7	2	6	174	165	-3	1	7	421	403
-5	4	5	92	91	-7	2	6	102	98	4	1	7	264	251
4	4	5	38	17	8	2	6	131	134	-4	1	7	20	12
-4	4	5	58	54	-8	2	6	43	34	5	1	7	249	233

FACTEURS DE STRUCTURE OBSERVES et CALCULES

1 BROMOADAMANTANE

PHASE III

T = 253 K

(Suite)

H	K	L	10FO	10FC	H	K	L	10FO	10FC	H	K	L	10FO	10FC
-1	4	2	483	443	5	3	3	424	437	-9	1	4	156	159
2	4	2	385	365	-5	3	3	197	187	8	1	4	199	191
-2	4	2	212	196	6	3	3	150	145	-8	1	4	130	129
3	4	2	287	273	-6	3	3	350	359	7	1	4	384	369
-3	4	2	404	395	7	3	3	351	361	-7	1	4	190	177
4	4	2	434	438	-7	3	3	238	231	6	1	4	251	222
-4	4	2	160	148	8	3	3	45	26	-6	1	4	365	343
5	4	2	190	183	-8	3	3	205	206	5	2	4	280	259
-5	4	2	465	468	9	3	3	246	259	-5	2	4	178	167
6	4	2	494	517	-9	3	3	158	159	6	2	4	39	14
-6	4	2	217	211	10	3	3	68	54	-6	2	4	218	208
7	4	2	117	113	-10	3	3	161	163	7	2	4	312	299
-7	4	2	369	391	9	4	3	66	64	-7	2	4	300	273
8	4	2	350	384	8	4	3	100	102	8	2	4	61	53
-8	4	2	85	80	-8	4	3	82	81	-8	2	4	158	144
9	4	2	30	12	7	4	3	99	109	9	2	4	58	51
-9	4	2	190	207	-7	4	3	95	85	-9	2	4	122	104
-8	5	2	174	189	6	4	3	138	129	10	2	4	119	117
-7	5	2	42	26	-6	4	3	22	11	-10	2	4	80	71
-6	5	2	266	281	5	4	3	50	34	9	3	4	78	89
5	5	2	424	433	-5	4	3	226	214	-9	3	4	40	43
-5	5	2	68	51	4	4	3	320	309	8	3	4	234	244
4	5	2	155	130	-4	4	3	41	15	-8	3	4	211	209
-4	5	2	424	451	3	4	3	218	211	7	3	4	116	119
3	5	2	719	714	-3	4	3	203	218	-7	3	4	156	160
-3	5	2	238	211	2	4	3	515	486	6	3	4	404	403
2	5	2	318	286	-2	4	3	81	38	-6	3	4	220	212
-2	5	2	467	455	1	4	3	388	352	5	3	4	136	122
1	5	2	735	686	-1	4	3	291	269	-5	3	4	246	236
-1	5	2	453	414	0	4	3	325	288	4	3	4	276	255
0	5	2	367	320	0	5	3	296	258	-4	3	4	84	77
0	5	2	370	320	1	5	3	158	140	0	4	4	29	31
-2	6	2	218	246	-1	5	3	87	94	1	4	4	687	665
-3	6	2	248	247	2	5	3	375	350	-1	4	4	513	478
-4	6	2	127	109	-2	5	3	117	106	2	4	4	235	231
-5	6	2	168	177	3	5	3	193	195	-2	4	4	200	185
-6	6	2	39	4	-3	5	3	104	115	3	4	4	739	741
-6	1	3	80	92	4	5	3	136	134	-3	4	4	574	561
7	1	3	329	327	-4	5	3	127	89	4	4	4	258	263
-7	1	3	81	69	-6	5	3	35	15	-4	4	4	175	184
8	1	3	117	110	-7	5	3	25	32	5	4	4	389	388
-8	1	3	105	98	-8	5	3	58	55	-5	4	4	416	426
9	1	3	263	267	-6	6	3	69	66	6	4	4	233	243
-9	1	3	95	96	-5	6	3	223	261	-6	4	4	157	162
10	1	3	69	63	-4	6	3	40	31	7	4	4	110	107
-10	1	3	165	157	-3	6	3	328	341	-7	4	4	194	206
10	2	3	222	232	-2	6	3	219	210	8	4	4	206	219
-10	2	3	156	148	6	0	4	358	340	-8	4	4	202	214
9	2	3	143	145	-6	0	4	293	279	9	4	4	104	104
-9	2	3	340	368	7	0	4	285	275	-9	4	4	165	182
8	2	3	372	368	-7	0	4	394	383	-7	5	4	186	213
-8	2	3	101	78	8	0	4	396	386	-6	5	4	298	315
7	2	3	435	417	-8	0	4	303	277	5	5	4	178	182
-7	2	3	693	708	9	0	4	41	28	-5	5	4	151	148
6	2	3	555	559	-9	0	4	213	209	4	5	4	162	146
-6	2	3	89	19	10	0	4	305	315	-4	5	4	496	508
5	2	3	520	504	-10	0	4	188	182	3	5	4	186	189
-5	2	3	778	798	10	1	4	152	164	-3	5	4	32	20
4	3	3	408	374	-10	1	4	145	152	2	5	4	186	167
-4	3	3	721	740	9	1	4	183	168	-2	5	4	655	648

H	K	L	10FO	10FC	H	K	L	10FO	10FC	H	K	L	10FO	10FC
-5	1	7	375	363	0	4	7	484	481	5	2	8	112	103
6	1	7	292	281	0	5	7	46	35	-5	2	8	33	43
-6	1	7	119	108	1	5	7	269	255	6	2	8	62	50
7	1	7	120	106	-1	5	7	265	252	7	2	8	79	64
-7	1	7	310	305	2	5	7	43	39	8	2	8	109	115
8	1	7	180	184	-3	5	7	64	55	-8	2	8	84	82
-8	1	7	106	103	4	5	7	46	45	9	2	8	72	65
9	1	7	27	9	-4	5	7	66	83	-9	2	8	29	27
-9	1	7	175	183	5	5	7	52	53	8	3	8	140	166
9	2	7	318	338	-5	5	7	28	29	-8	3	8	50	62
-9	2	7	137	130	-6	5	7	52	67	-7	3	8	20	7
8	2	7	140	146	-4	6	7	290	334	6	3	8	103	121
-8	2	7	249	257	-3	6	7	28	11	-6	3	8	24	12
7	2	7	350	358	-2	6	7	348	375	5	3	8	290	293
-7	2	7	49	18	1	0	8	36	31	-5	3	8	107	95
6	2	7	241	234	-1	0	8	85	20	4	3	8	111	119
-6	2	7	439	442	2	0	8	483	475	-4	3	8	23	24
5	2	7	380	379	-2	0	8	654	649	3	3	8	338	334
-5	2	7	139	119	3	0	8	215	217	-3	3	8	101	102
4	2	7	303	299	-3	0	8	89	88	2	3	8	103	26
-4	2	7	618	615	4	0	8	569	562	-2	3	8	132	121
3	2	7	465	469	-4	0	8	586	558	1	3	8	301	302
-3	2	7	163	147	5	0	8	399	378	-1	3	8	327	323
2	2	7	303	323	-5	0	8	185	175	0	3	8	158	154
-2	2	7	584	586	6	0	8	579	584	0	4	8	284	301
1	2	7	465	458	-6	0	8	577	572	1	4	8	175	170
-1	2	7	288	269	7	0	8	382	365	-1	4	8	127	123
0	3	7	371	360	-7	0	8	172	169	2	4	8	314	322
1	3	7	468	451	8	0	8	328	315	-2	4	8	346	342
-1	3	7	474	465	-8	0	8	455	471	3	4	8	150	137
2	3	7	460	453	9	0	8	234	240	-3	4	8	63	75
-2	3	7	237	234	-9	0	8	171	166	4	4	8	192	197
3	3	7	405	396	9	1	8	82	83	-4	4	8	465	495
-3	3	7	434	437	-9	1	8	52	52	5	4	8	153	150
4	3	7	484	490	8	1	8	227	229	-5	4	8	172	189
-4	3	7	66	47	-8	1	8	173	164	6	4	8	181	188
5	3	7	189	189	7	1	8	50	44	-6	4	8	349	384
-5	3	7	328	347	-7	1	8	89	90	7	4	8	123	129
6	3	7	398	408	6	1	8	259	261	-7	4	8	132	144
-6	3	7	84	65	-6	1	8	168	158	-5	5	8	203	239
7	3	7	52	39	5	1	8	206	191	4	5	8	227	246
-7	3	7	281	292	-5	1	8	349	343	-4	5	8	96	104
8	3	7	238	245	4	1	8	276	264	3	5	8	310	337
-8	3	7	48	45	-4	1	8	148	127	-3	5	8	363	390
8	4	7	28	30	3	1	8	574	570	2	5	8	163	164
-8	4	7	48	54	-3	1	8	512	499	-2	5	8	31	33
7	4	7	119	113	2	1	8	238	225	1	5	8	463	489
-7	4	7	50	52	-2	1	8	45	26	-1	5	8	545	572
6	4	7	50	56	1	1	8	690	702	0	5	8	62	45
-6	4	7	143	151	-1	1	8	537	522	2	6	8	208	226
5	4	7	196	199	0	1	8	142	145	-2	6	8	210	258
-5	4	7	50	59	0	2	8	169	164	-3	6	8	37	40
4	4	7	85	92	1	2	8	131	120	0	1	9	178	164
-4	4	7	218	222	-1	2	8	24	15	1	1	9	610	615
3	4	7	231	234	2	2	8	48	11	-1	1	9	446	438
-3	4	7	34	8	-2	2	8	212	204	2	1	9	92	83
2	4	7	220	194	3	2	8	199	192	-2	1	9	227	213
-2	4	7	411	391	-3	2	8	53	53	3	1	9	505	497
1	4	7	225	218	4	2	8	107	89	-3	1	9	252	242
-1	4	7	122	124	-4	2	8	41	21	4	1	9	73	66

H	K	L	10FO	10FC	H	K	L	10FO	10FC	H	K	L	10FO	10FC
-4	1	9	235	223	3	0	10	234	222	-1	1	11	194	184
5	1	9	321	310	-3	0	10	431	427	2	1	11	20	22
-5	1	9	183	175	4	0	10	580	573	-2	1	11	294	288
6	1	9	185	178	-4	0	10	230	226	3	1	11	261	258
-6	1	9	159	161	5	0	10	168	169	-3	1	11	164	148
7	1	9	245	239	-5	0	10	381	391	4	1	11	79	79
-7	1	9	132	126	6	0	10	278	269	-4	1	11	358	356
8	1	9	147	149	-6	0	10	136	146	5	1	11	165	173
-8	1	9	100	109	6	1	10	103	104	-5	1	11	103	97
8	2	9	115	123	-6	1	10	292	289	4	2	11	279	274
-8	2	9	109	115	5	1	10	358	352	-4	2	11	25	16
7	2	9	139	143	-5	1	10	146	136	3	2	11	299	297
-7	2	9	274	277	4	1	10	37	28	-3	2	11	318	325
6	2	9	333	343	-4	1	10	329	314	2	2	11	274	271
4	2	9	491	508	3	1	10	248	243	-2	2	11	198	199
-4	2	9	394	393	-3	1	10	367	352	1	2	11	484	500
3	2	9	128	126	2	1	10	74	67	-1	2	11	473	483
-3	2	9	288	289	-2	1	10	366	357	0	2	11	302	296
2	2	9	481	484	1	1	10	261	252	0	3	11	243	264
-2	2	9	511	509	-1	1	10	436	423	1	3	11	244	245
1	2	9	34	23	0	1	10	172	168	-1	3	11	151	147
-1	2	9	213	208	0	2	10	39	27	2	3	11	224	243
0	2	9	487	478	1	2	10	133	128	-2	3	11	308	337
0	3	9	145	139	2	2	10	124	118	3	3	11	309	326
1	3	9	471	487	-2	2	10	32	31	-3	3	11	77	78
-1	3	9	453	469	3	2	10	33	44	0	0	12	125	122
2	3	9	20	9	-3	2	10	21	16	1	0	12	223	229
-2	3	9	174	178	4	2	10	101	98	-1	0	12	461	465
3	3	9	363	356	5	2	10	84	74	2	0	12	265	264
-3	3	9	356	353	-5	2	10	70	66	-2	0	12	31	25
4	3	9	133	134	6	2	10	65	57	3	0	12	223	222
-4	3	9	170	177	-6	2	10	65	65	-3	0	12	446	441
5	3	9	242	229	7	3	10	93	107	4	0	12	248	234
-5	3	9	251	255	-5	3	10	23	15	-4	0	12	23	13
6	3	9	160	161	4	3	10	53	45	4	1	12	236	235
-6	3	9	161	177	-4	3	10	186	193	-4	1	12	281	292
4	4	9	219	224	3	3	10	121	128	3	1	12	122	111
-4	4	9	203	227	-3	3	10	34	27	-3	1	12	24	18
-3	4	9	44	37	2	3	10	95	103	2	1	12	404	409
2	4	9	228	227	-2	3	10	163	150	-2	1	12	202	199
-2	4	9	226	240	1	3	10	113	113	1	1	12	92	80
1	4	9	151	135	-1	3	10	46	50	-1	1	12	110	102
-1	4	9	164	159	0	3	10	179	170	0	1	12	322	316
0	4	9	230	227	0	4	10	304	311	0	2	12	71	62
0	5	9	33	14	1	4	10	192	200	1	2	12	133	134
1	5	9	71	66	-1	4	10	263	284	-1	2	12	261	275
-1	5	9	35	35	2	4	10	310	325	2	2	12	123	135
0	6	10	674	688	-2	4	10	217	232	-2	2	12	31	45
1	0	10	428	416	3	4	10	180	194	3	2	12	47	37
-1	0	10	385	368	-3	4	10	237	267	-3	2	12	188	195
2	0	10	852	898	0	1	11	97	86	0	3	12	229	243
-2	0	10	343	333	1	1	11	263	254	0	1	13	236	238

FACTEURS

DE

STRUCTURE

OBSERVES

ET

CALCULES

1 BROMOADAMANTANE

PHASE III

T = 253 K

(Suite)

H	K	L	10FO	10FC	H	K	L	10FO	10FC	H	K	L	10FO	10FC
2	6	3	115	108	5	2	5	315	312	4	4	6	84	77
1	6	3	91	92	4	2	5	110	109	5	4	6	149	153
0	6	3	136	135	3	2	5	654	643	6	4	6	64	53
0	7	3	110	116	2	2	5	185	184	7	4	6	102	92
2	7	3	86	88	1	2	5	1096	1097	9	4	6	61	48
0	0	4	177	169	0	2	5	201	187	6	5	6	94	91
1	0	4	953	936	0	3	5	332	339	5	5	6	77	69
2	0	4	229	218	2	3	5	363	374	4	5	6	130	126
3	0	4	673	671	4	3	5	362	365	3	5	6	89	89
4	0	4	163	162	6	3	5	273	270	2	5	6	119	130
5	0	4	433	439	8	3	5	135	143	0	5	6	107	116
6	0	4	47	61	2	4	5	73	64	1	6	6	65	59
7	0	4	252	247	1	4	5	71	65	0	1	7	266	264
9	0	4	100	90	0	4	5	63	81	1	1	7	438	432
10	1	4	85	86	2	5	5	79	79	2	1	7	200	202
8	1	4	103	104	4	5	5	109	109	3	1	7	317	313
7	1	4	94	103	6	5	5	73	78	4	1	7	123	133
6	1	4	240	232	5	6	5	75	68	5	1	7	210	208
5	1	4	124	126	3	6	5	105	94	6	1	7	92	91
4	1	4	536	523	2	6	5	65	53	7	1	7	147	135
3	1	4	78	75	1	6	5	136	133	9	1	7	78	56
2	1	4	795	784	0	7	5	83	100	9	2	7	77	65
0	1	4	689	697	2	7	5	90	97	8	2	7	108	101
0	2	4	327	331	4	7	5	80	75	7	2	7	122	126
1	2	4	156	151	0	0	6	485	478	6	2	7	202	195
2	2	4	166	162	1	0	6	670	661	5	2	7	230	238
3	2	4	72	59	2	0	6	448	448	4	2	7	298	304
5	2	4	109	111	3	0	6	566	560	3	2	7	313	316
6	2	4	70	64	4	0	6	267	257	2	2	7	287	294
7	2	4	166	179	5	0	6	307	311	1	2	7	352	353
8	3	4	149	150	6	0	6	166	157	0	2	7	235	246
6	3	4	267	268	7	0	6	131	119	0	3	7	291	300
4	3	4	224	227	8	0	6	97	96	1	3	7	234	242
2	3	4	338	343	9	0	6	68	64	2	3	7	270	273
1	3	4	65	56	8	1	6	126	128	3	3	7	188	177
0	3	4	596	591	7	1	6	103	100	4	3	7	188	183
0	4	4	70	75	6	1	6	215	216	5	3	7	103	96
1	4	4	404	412	5	1	6	154	152	6	3	7	112	107
2	4	4	72	63	4	1	6	300	295	8	3	7	74	68
3	4	4	416	422	3	1	6	111	115	2	4	7	60	69
4	4	4	71	59	2	1	6	468	457	1	4	7	57	58
5	4	4	232	233	1	1	6	183	182	0	4	7	152	150
7	4	4	88	84	0	1	6	679	669	0	5	7	68	63
9	4	4	84	78	0	2	6	202	198	1	5	7	201	195
6	5	4	112	109	1	2	6	45	39	2	5	7	64	45
4	5	4	129	120	3	2	6	152	145	3	5	7	81	80
3	5	4	74	70	5	2	6	144	136	4	6	7	97	103
2	5	4	148	145	6	2	6	77	80	2	6	7	102	121
1	5	4	97	88	7	2	6	68	71	1	6	7	69	61
0	5	4	197	197	8	3	6	79	66	0	6	7	108	110
0	1	5	256	266	6	3	6	143	149	0	0	8	498	504
1	1	5	88	96	5	3	6	116	118	1	0	8	139	141
2	1	5	354	347	4	3	6	229	234	2	0	8	417	419
4	1	5	360	358	3	3	6	176	182	3	0	8	132	139
5	1	5	77	79	2	3	6	241	241	4	0	8	390	388
6	1	5	219	220	0	3	6	199	194	5	0	8	119	128
7	1	5	107	103	0	4	6	335	340	6	0	8	350	366
8	1	5	90	94	1	4	6	353	359	7	0	8	97	111
9	2	5	83	80	2	4	6	204	209	8	0	8	212	221
7	2	5	158	159	3	4	6	247	254	10	0	8	77	48

FACTEURS

DE

STRUCTURE

OBSERVES

ET

CALCULES

1 BROMOADAMANTANE

PHASE II

T = 295 K

H	K	L	10FO	10FC	H	K	L	10FO	10FC	H	K	L	10FO	10FC
2	0	0	1881	1956	7	3	1	182	174	0	3	2	393	383
4	0	0	347	347	8	3	1	69	69	0	4	2	309	313
6	0	0	317	323	9	3	1	57	69	1	4	2	302	306
8	0	0	203	201	8	4	1	93	94	2	4	2	231	235
10	0	0	65	28	7	4	1	63	64	3	4	2	218	225
9	1	0	133	141	6	4	1	117	117	4	4	2	222	224
7	1	0	216	214	4	4	1	98	98	5	4	2	190	193
5	1	0	634	640	3	4	1	48	30	6	4	2	227	230
3	1	0	936	949	2	4	1	98	91	7	4	2	129	123
1	1	0	184	184	0	4	1	84	78	8	4	2	124	127
0	2	0	74	72	0	5	1	70	58	9	5	2	66	45
2	2	0	178	168	1	5	1	150	140	5	5	2	112	115
4	2	0	94	89	2	5	1	88	77	4	5	2	105	100
6	2	0	64	68	3	5	1	116	101	3	5	2	240	239
8	2	0	73	62	4	5	1	74	68	2	5	2	140	141
7	3	0	147	153	5	5	1	107	99	1	5	2	286	284
5	3	0	219	225	7	5	1	94	95	0	5	2	125	124
3	3	0	202	193	9	5	1	62	35	1	6	2	87	78
1	3	0	297	296	6	6	1	96	88	2	7	2	68	56
0	4	0	523	509	4	6	1	151	154	0	7	2	105	103
2	4	0	537	528	2	6	1	199	200	0	1	3	694	705
4	4	0	373	355	1	6	1	101	96	1	1	3	485	482
6	4	0	162	157	0	6	1	209	209	2	1	3	694	680
8	4	0	81	75	1	7	1	60	66	3	1	3	285	284
7	5	0	158	162	3	7	1	61	67	4	1	3	362	349
5	5	0	210	206	0	0	2	659	626	5	1	3	175	168
3	5	0	236	233	1	0	2	348	339	6	1	3	76	66
1	5	0	324	321	2	0	2	881	857	7	1	3	113	126
0	6	0	79	67	3	0	2	772	754	9	1	3	75	74
5	7	0	80	67	4	0	2	809	803	9	2	3	149	148
3	7	0	63	53	5	0	2	517	518	8	2	3	93	96
0	8	0	62	69	6	0	2	475	463	7	2	3	382	389
0	1	1	58	61	7	0	2	184	189	6	2	3	216	219
1	1	1	908	931	8	0	2	197	199	5	2	3	513	509
2	1	1	121	114	9	0	2	129	134	4	2	3	332	331
3	1	1	595	591	10	0	2	101	107	3	2	3	500	493
4	1	1	167	166	9	1	2	78	81	2	2	3	278	282
5	1	1	481	479	8	1	2	133	129	1	2	3	553	562
6	1	1	102	99	7	1	2	191	198	0	2	3	118	123
7	1	1	279	284	6	1	2	204	212	0	3	3	578	564
8	1	1	72	73	5	1	2	228	230	1	3	3	343	346
9	1	1	111	103	4	1	2	157	155	2	3	3	520	525
10	1	1	63	33	3	1	2	364	358	3	3	3	188	188
10	2	1	91	79	2	1	2	511	499	4	3	3	351	348
8	2	1	111	112	1	1	2	765	776	5	3	3	96	102
7	2	1	106	95	0	1	2	1127	1175	6	3	3	139	138
6	2	1	225	229	1	2	2	220	219	8	3	3	71	60
5	2	1	185	181	2	2	2	163	152	10	3	3	62	58
4	2	1	590	580	3	2	2	195	194	4	4	3	81	88
3	2	1	289	281	4	2	2	79	76	2	4	3	140	146
2	2	1	908	920	6	2	2	91	81	0	4	3	156	157
1	2	1	383	384	7	2	2	58	60	0	5	3	230	233
0	2	1	965	985	8	2	2	80	74	1	5	3	86	89
0	3	1	204	211	8	3	2	75	53	2	5	3	205	208
1	3	1	456	464	6	3	2	96	95	4	5	3	119	119
2	3	1	153	152	5	3	2	91	90	6	5	3	61	19
3	3	1	354	358	4	3	2	246	241	7	6	3	61	55
4	3	1	120	114	3	3	2	337	331	5	6	3	87	88
5	3	1	287	285	2	3	2	412	414	4	6	3	67	61
6	3	1	93	92	1	3	2	351	357	3	6	3	99	92

FACTEURS DE STRUCTURE OBSERVES ET CALUCULES

1 BROMOADAMANTANE

PHASE II ; T = 295 K

H	K	L	10FO	10FC	H	K	L	10FO	10FC	H	K	L	10FO	10FC
7	1	8	61	38	1	5	8	188	188	3	1	10	200	203
6	1	8	80	71	1	1	9	396	397	1	1	10	244	241
5	1	8	165	170	3	1	9	303	305	0	3	10	106	103
4	1	8	113	114	5	1	9	188	201	0	4	10	190	179
3	1	8	359	361	7	1	9	124	123	2	4	10	174	167
2	1	8	144	149	6	2	9	147	149	4	4	10	121	133
1	1	8	396	398	4	2	9	270	271	1	1	1	915	931
0	1	8	189	194	2	2	9	349	351	1	1	11	191	197
1	2	8	65	54	0	2	9	365	368	3	1	11	176	175
3	2	8	100	97	1	3	9	234	229	3	2	11	144	150
5	3	8	78	86	3	3	9	179	175	2	2	11	183	176
4	3	8	62	66	5	3	9	121	128	1	2	11	232	236
3	3	8	173	177	1	4	9	138	125	0	2	11	231	221
1	3	8	253	268	0	0	10	506	502	1	0	12	175	168
0	3	8	66	66	1	0	10	175	174	2	0	12	157	149
0	4	8	187	184	2	0	10	455	460	3	0	12	147	145
1	4	8	153	166	3	0	10	151	147	2	1	12	143	145
2	4	8	203	199	4	0	10	295	303	0	1	12	147	146
4	4	8	183	182	6	0	10	141	145	3	2	13	159	158
6	4	8	119	133	5	1	10	151	156					

X = 1.00			PHASE PLASTIQUE			PHASE PLASTIQUE		
			T = 295 K			T = 257 K		
H	K	L	FO	FCI	FCA	FO	FCI	FCA
2	0	0	573.9	546.5	541.0	522.3	551.2	551.0
4	0	0	143.1	-143.2	-140.9	161.5	-159.5	-158.2
6	0	0	39.8	45.4	48.1	58.6	64.0	69.1
8	0	0	21.2	25.3	31.6	37.9	43.7	54.3
10	0	0	11.7	1.6	0.8	-	-	-
12	0	0	8.4	1.6	0.6	10.1	5.0	2.6
12	2	0	-	-	-	8.7	4.2	2.0
6	2	0	37.2	38.4	38.1	53.2	53.6	54.1
4	2	0	93.6	-102.9	-103.8	110.1	-114.5	-117.1
2	2	0	6.5	10.4	11.4	-	-	-
4	4	0	13.1	15.7	15.2	22.5	22.3	21.2
6	4	0	48.4	49.8	50.2	69.7	72.4	73.3
10	4	0	-	-	-	9.9	-8.4	-9.2
6	6	0	33.8	32.2	33.2	54.2	54.5	56.3
12	6	0	9.5	1.4	1.6	-	-	-
1	1	1	593.3	509.5	503.2	485.9	505.7	502.9
3	1	1	118.1	-103.8	-105.2	128.6	-118.5	-121.3
5	1	1	129.4	-134.7	-131.3	156.4	-160.8	-156.6
7	1	1	9.6	4.5	9.0	-	-	-
9	1	1	-	-	-	17.5	22.9	22.4
11	1	1	12.1	-5.8	-6.3	12.0	-12.9	-14.1
11	3	1	8.1	-3.8	-3.8	-	-	-
9	3	1	-	-	-	9.6	10.1	8.0
7	3	1	19.9	14.2	15.2	23.6	20.4	21.6
3	3	1	-	-	-	19.1	29.8	23.6
5	5	1	9.9	6.4	9.7	-	-	-
9	9	1	8.8	0.4	0.3	-	-	-
2	2	2	202.2	-167.2	-164.1	208.1	-181.6	-178.7
4	2	2	106.6	-104.7	-105.5	126.2	-122.5	-124.6
6	2	2	21.2	17.6	15.7	24.3	23.3	21.1
10	2	2	-	-	-	11.8	-13.2	-14.4
12	2	2	8.6	1.1	0.3	-	-	-
8	4	2	-	-	-	18.7	-19.3	-19.8
6	4	2	17.3	17.7	16.7	23.3	24.2	22.7
4	4	2	30.5	-25.1	-25.1	40.0	-34.2	-34.7
6	6	2	-	-	-	23.4	23.5	23.1
8	8	2	-	-	-	12.5	-5.7	-6.0
3	3	3	40.6	77.1	73.4	77.2	101.0	96.3
5	3	3	18.0	21.2	20.3	28.6	32.9	31.8
7	3	3	13.5	8.6	7.3	21.0	14.9	11.9
9	3	3	-	-	-	12.4	8.6	6.1
7	5	3	-	-	-	10.0	-8.3	-9.5
4	4	4	25.0	-22.6	-22.5	42.4	-35.8	-36.4
6	4	4	-	-	-	9.8	-6.2	-9.1
8	4	4	10.4	-7.8	-8.2	19.3	-15.7	-16.3
10	6	4	-	-	-	16.9	2.1	2.9
5	5	5	19.8	-21.2	-21.2	33.3	-38.0	-37.5
7	5	5	-	-	-	10.7	-13.9	-14.2
11	5	5	-	-	-	13.2	-0.8	0.4
6	6	6	-	-	-	13.2	8.9	7.7
10	6	6	-	-	-	12.4	3.0	4.0
7	7	7	-	-	-	9.6	2.8	3.6
8	8	8	-	-	-	10.9	-0.4	-0.2

FCI Modèle Isotrope

FACTEURS DE STRUCTURE OBSERVES ET CALCULES :

FCA Modèle Anisotrope

1 CHLOROADAMANTANE PHASE I

X = 0.00			PHASE PLASTIQUE			PHASE VITREUSE		
			T = 295 K			T = 110 K		
H	K	L	FO	FCI	FCA	FO	FCI	FCA
7	7	3	-	-	-	15.9	15.9	14.7
9	7	3	-	-	-	9.2	9.9	10.2
9	9	3	-	-	-	6.2	-4.9	-4.7
11	9	3	-	-	-	10.4	-6.0	-6.0
4	4	4	20.0	-16.5	-16.5	34.1	-27.1	-27.3
6	4	4	16.2	-19.9	-19.5	33.6	-36.4	-35.8
8	4	4	10.6	-10.2	-10.2	20.4	-21.1	-21.2
10	4	4	-	-	-	6.1	3.8	3.4
6	6	4	15.8	-17.2	-16.9	31.6	-32.4	-32.3
8	6	4	-	-	-	7.9	-4.8	-5.5
10	6	4	-	-	-	9.4	8.7	8.5
8	8	4	-	-	-	6.2	-5.1	-5.9
10	8	4	-	-	-	5.4	-4.2	-4.0
5	5	5	23.7	-26.9	-26.3	45.3	-45.5	-44.6
7	5	5	-	-	-	7.8	-4.3	-3.2
9	5	5	-	-	-	8.2	10.3	10.0
11	5	5	-	-	-	4.8	-2.4	-2.8
7	7	5	7.4	6.5	6.7	20.3	21.3	21.6
9	7	5	-	-	-	10.8	12.0	11.8
9	9	5	-	-	-	7.6	-6.2	-5.9
6	6	6	7.6	-6.4	-6.3	12.8	-12.0	-12.2
8	6	6	-	-	-	7.7	7.4	6.4
10	6	6	-	-	-	10.9	8.4	7.9
7	7	7	12.5	8.9	9.0	34.6	29.3	29.3

FACTEURS DE STRUCTURE OBSERVES ET CALCULES

FCI : Modèle Isotrope

FCA : Modèle Anisotrope

1 CYANO ADAMANTANE PHASE I

X = 0.00			PHASE PLASTIQUE			PHASE VITREUSE		
			T = 295 K			T = 110 K		
H	K	L	FO	FCI	FCA	FO	FCI	FCA
2	0	0	506.9	540.0	538.1	503.7	539.8	536.3
4	0	0	173.4	-181.2	-180.7	199.0	-194.6	-197.7
6	0	0	8.7	-10.4	-12.3	5.5	7.9	3.5
8	0	0	48.5	51.4	49.5	41.0	43.4	40.5
10	0	0	14.3	11.7	12.7	28.7	24.2	24.3
12	0	0	-	-	-	16.4	11.1	10.8
14	0	0	-	-	-	22.5	20.0	18.2
2	2	0	57.9	66.9	67.2	60.1	65.4	66.5
4	2	0	79.5	-84.0	-83.1	75.6	-80.2	-80.3
6	2	0	13.4	10.7	10.2	29.2	28.1	27.0
8	2	0	21.7	21.7	20.5	30.7	33.2	31.0
12	2	0	-	-	-	8.6	4.4	4.7
14	2	0	-	-	-	14.3	12.1	11.6
4	4	0	47.3	42.8	42.6	72.1	64.9	65.1
6	4	0	47.3	46.0	45.6	69.5	67.9	67.8
10	4	0	-	-	-	4.4	-1.5	-1.5
12	4	0	-	-	-	9.3	8.7	8.6
6	6	0	23.4	21.3	20.7	37.1	31.7	30.4
10	6	0	-	-	-	8.5	10.0	9.9
12	6	0	-	-	-	10.1	12.6	11.6
10	8	0	-	-	-	9.9	8.4	7.7
12	8	0	-	-	-	5.2	6.7	5.9
10	10	0	-	-	-	7.4	7.9	8.1
1	1	1	472.9	505.9	502.9	457.8	484.6	484.9
3	1	1	179.6	-181.7	-181.2	215.6	-211.7	-213.7
5	1	1	116.4	-125.9	-126.1	145.1	-151.1	-153.5
7	1	1	28.6	33.1	32.0	36.3	42.2	40.3
11	1	1	9.0	-9.9	-9.8	20.1	-24.3	-23.3
13	1	1	-	-	-	7.3	4.3	3.2
3	3	1	52.4	-51.1	-51.0	56.5	-57.3	-57.4
5	3	1	13.5	11.4	11.4	19.0	15.3	15.8
7	3	1	33.7	32.7	32.9	42.9	43.4	44.2
9	3	1	9.2	-7.9	-8.2	14.0	-15.1	-15.5
11	3	1	7.1	-7.0	-7.1	15.0	-15.8	-16.3
13	3	1	-	-	-	4.5	4.0	4.1
5	5	1	33.5	35.9	35.5	43.5	44.4	44.1
7	5	1	14.0	13.3	13.4	18.4	16.1	16.3
9	5	1	11.1	-9.8	-9.8	20.7	-18.3	-17.9
11	5	1	-	-	-	9.3	-5.6	-6.6
7	7	1	-	-	-	15.3	9.4	10.4
9	7	1	-	-	-	5.0	2.0	2.7
11	7	1	-	-	-	4.7	6.0	4.9
2	2	2	91.8	-73.6	-72.9	86.7	-72.1	-72.3
4	2	2	66.4	-61.0	-60.2	63.8	-58.0	-57.6
6	2	2	-	-	-	7.5	3.0	4.7
8	2	2	-	-	-	8.3	-6.3	-7.3
10	2	2	3.1	-5.6	-5.3	15.3	-12.8	-11.8
6	4	2	8.3	8.0	8.3	10.2	8.9	9.6
8	4	2	10.8	-11.3	-11.5	23.7	-24.0	-24.2
10	4	2	-	-	-	9.7	-7.6	-7.6
6	6	2	-	-	-	7.6	-9.9	-10.1
8	6	2	7.5	-7.8	-7.9	16.7	-17.7	-17.8
8	8	2	-	-	-	10.2	-12.4	-12.5
3	3	3	-	-	-	6.5	14.0	15.9
5	3	3	13.8	18.0	18.3	16.4	23.2	24.0
7	3	3	16.6	15.5	16.4	25.4	23.2	25.2
9	3	3	9.2	-7.6	-7.7	10.6	-9.7	-9.9
11	3	3	-	-	-	6.3	-8.4	-9.2
5	5	3	-	-	-	8.3	-6.5	-6.0
9	5	3	-	-	-	5.1	-1.1	-1.0